

**DEVELOPMENT OF TARGETED
THERAPIES FOR MELANOMA –
SYNTHETIC AND ANALYTICAL STUDIES
OF DUOCARMYCIN-PROTEIN
CONJUGATES**

Issa Jyamubandi

A thesis submitted for the degree of Doctor of Philosophy

September 2021
School of Pharmacy
University of East Anglia

© This copy of the thesis has been supplied on condition that anyone who consults it is understood to recognise that its copyright rests with the author and that no quotation from the thesis, nor any information derived there-from may be published without the author's prior, written consent.

Declaration

This thesis is submitted to the University of East Anglia for the Degree of Doctor of Philosophy and has not been previously submitted at this or any university for assessment or for any other degree. The work described in this thesis is original, except where stated, referenced or acknowledged.

Issa Jyamubandi

Acknowledgements

I would like to start by thanking my supervisors, Prof. Mark Searcey, Prof. Maria O'Connell and Dr Andrew Roberts for all their continued support and advice throughout my PhD, especially Prof. Mark Searcey for being very patient with me while I was getting up to speed with my chemistry and providing me an opportunity to work on emerging and interesting subject area.

Thank you to all my fellow lab members Dr Marco Commineti, Dr Andrew Beekman and Dr Ryan Tinson for their advice and support over the past 7 years. Thank you to Dr Lesley Howell for the initial supervision and help to get through my initial PhD years. Thank you to all my colleagues Dom, Olly, Muayyad, Zoe and Chris. I thoroughly enjoyed working with everyone and nothing beats a Friday meeting with lovely home baked cake.

I would like to thank my wife Khadija and my family for their unwavering support from the start to the end especially when I needed it most and for all those endless weekends and evenings that I had to put PhD first.

I would like to especially thank and dedicate this PhD to my father 'Rucamukibatsi' who passed away on the 23rd Feb 2019. He has always been my light at the end of a tunnel and encouraged me throughout but unfortunately will never be able to see me finish.

Finally, I would also like to thank LGC for sponsoring this PhD and all my colleagues at LGC for being flexible.

Abstract

Peptide-Drug Conjugates (PDCs) and Antibody-Drug Conjugates (ADCs) are compounds that aim to specifically deliver a high concentration of the cytotoxic agent to the tumour target. This project was designed to develop new PDCs based upon the potent cytotoxic agent CBI, to target melanoma.

Chapter 1 provides an overall introduction to melanoma with particular emphasis on current treatments, the involvement of the melanocortin 1 receptor (MC1R) in cancer progression and how MC1R can be used as a potential target.

Chapter 2 describes the synthesis of CBI analogues, ultrapotent cytotoxic agents that belong in the same family as CC-1065 and yatakeycin. CBI binds in the AT rich minor groove of the DNA causing their cyclopropyl group ring to open followed by adenine alkylation and then triggering a cascade of events that subsequently lead to cell apoptosis. These class of compounds are considered more effective as they can induce activity at any stage of the cell cycle. Herein, we describe the synthesis of a CBI analogue that can potentially be used in solid phase synthesis. The target compounds, which consist of an Fmoc-protected glutamic acid analogue carrying a CBI alkylating subunit on the side chain, were successfully synthesised and characterised.

Off target toxicity is a crucial factor to consider when developing PDCs and ADCs with ultrapotent payloads. Therefore, Chapter 3 explores the solid phase synthesis of melanocyte stimulating hormone (MSH) as the targeting peptide to MC1R and its conjugation with the CBI analogues. The successful synthesis of several peptide conjugates was confirmed by mass spectrometry and represents the first description of this class of PDC.

Preliminary studies of the biological activity of the CBI-MSH conjugates are described in chapter 4. The activity of the conjugates was compared with scrambled and protected versions of the active compounds and, while the activity was lower than expected, demonstrated an anti-proliferative effect in various assays. Flow cytometry also gave a preliminary indication that the peptide was binding to its target.

Access Condition and Agreement

Each deposit in UEA Digital Repository is protected by copyright and other intellectual property rights, and duplication or sale of all or part of any of the Data Collections is not permitted, except that material may be duplicated by you for your research use or for educational purposes in electronic or print form. You must obtain permission from the copyright holder, usually the author, for any other use. Exceptions only apply where a deposit may be explicitly provided under a stated licence, such as a Creative Commons licence or Open Government licence.

Electronic or print copies may not be offered, whether for sale or otherwise to anyone, unless explicitly stated under a Creative Commons or Open Government license. Unauthorised reproduction, editing or reformatting for resale purposes is explicitly prohibited (except where approved by the copyright holder themselves) and UEA reserves the right to take immediate 'take down' action on behalf of the copyright and/or rights holder if this Access condition of the UEA Digital Repository is breached. Any material in this database has been supplied on the understanding that it is copyright material and that no quotation from the material may be published without proper acknowledgement.

Table of Contents

List of Tables	8
List of Abbreviations.....	15
CHAPTER 1: INTRODUCTION	18
1.1 Skin Cancer Histology	19
1.2 Aetiology and incidence	20
1.3 Risk Factors and Genetic Susceptibility	21
1.4 Management and Treatment.....	24
1.4.1 Therapeutic Approaches.....	24
1.4.2 Surgery	24
1.4.3 Targeted therapy.....	24
1.4.4 Immunotherapy.....	28
1.4.5 Cytokines.....	28
1.4.6 Checkpoint inhibitors.....	29
1.4.7 Antigen-based active immunotherapy.....	32
1.4.8 Adoptive cell therapy.....	32
1.4.9 Radiotherapy and chemotherapy	34
1.4.10 Melanoma targeted drug delivery strategies.....	35
1.4.11 Cytotoxic payload.....	41
1.4.11.1 CC-1065, the duocarmycins and yatakemycin.....	43
1.4.11.2 CC-1065, the duocarmycins and yatakemycin mode of action.....	44
1.4.11.3 DNA alkylation selectivity	46
1.4.11.4 Development of Duocarmycins into therapeutic agents	49
1.4.12 Peptide Drug Conjugates (PDC)	54
CHAPTER 2: SYNTHESIS OF THE CBI-GLUTAMIC ACID CONJUGATE FOR SOLID PHASE SYNTHESIS	60
2.1 Chapter 2 Aims.....	61
2.2 Overview of the CBI building block.....	62
2.3 The synthesis of the CBI analogue	65
2.3.1 Synthesis of the CBI alkylating unit	65
2.3.2 Proposed synthesis of the CBI alkylating unit (3)	68

2.3.3	Stobbe Condensation followed with ester hydrolysis	69
2.3.4	Sulphuric acid promoted intramolecular cyclisation	73
2.3.5	Benzyl protection and ester hydrolysis.....	75
2.3.6	Curtius rearrangement.....	77
2.3.7	Iodination	82
2.3.8	N-Alkylation	84
2.3.9	Radical cyclisation.....	86
2.4	CBI conjugation to carboxylic acid side chain of glutamic acid.	90
2.5	Non-alkylating DNA binding unit	95
2.6	Conclusion	99

CHAPTER 3: MSH SOLID PHASE SYNTHESIS AND INCORPORATION OF THE CBI-WARHEAD BUILDING BLOCK FOLLOWED BY ON THE RESIN BENZYL DEPROTECTION... 100

3.1	Chapter 3 Aims.....	101
3.2	α -Melanocyte-stimulating hormone(α -MSH)	102
3.3	Introduction to the solid phase synthesis	105
3.3.1	Boc Solid Phase synthesis.....	106
3.3.2	Fmoc Solid Phase synthesis	107
3.4	MSH peptide synthesis	108
3.5	[Nle ⁴ ,dPhe ⁷] α -MSH Peptide drug conjugated library	112
3.6	Benzyl deprotection.....	115
3.7	Scrambled MSH peptide synthesis.....	123
3.8	Peptide Drug Conjugate Solubility	125
3.9	Incorporation of the DNA binding subunit.....	131
3.10	Conjugation of labels.....	133
3.10.1	Biotin label conjugation on the solid phase	133
3.10.2	FITC label conjugation on the solid phase	135
3.11	Conclusion	137

CHAPTER 4: BIOLOGICAL ACTIVITY OF SYNTHESISED PEPTIDE DRUG CONJUGATES 138

4.1	Chapter 4 Aims.....	139
4.2	Expression of MC1R in melanoma	140

4.3	Materials and methods	142
4.3.1	Materials	142
4.3.2	Methods	144
4.4	Result and discussion.....	156
4.4.1	Cell seeding density assessment	156
4.4.2	xCELLigence PDC biological assay assessment	158
4.4.3	MTS PDC biological assay assessment	160
4.4.4	CellTitre-Glo® PDC biological assay assessment.....	162
4.4.5	Flow Cytometry assessment.....	165
4.5	Conclusions and proposed future work.....	167
CHAPTER 5: EXPERIMENTAL.....		168
5.1	Materials and reagents.....	169
5.1.1	Reagents and Solvents	169
5.1.2	Solid Phase peptide synthesis	169
5.1.3	Physical Characterisation and Spectroscopic Techniques.....	169
5.1.4	Chromatographic Techniques.....	170
5.2	Synthesis of CBI alkylating subunit 3	172
5.2.1	Synthesis of 22	172
5.2.2	Synthesis of 23	173
5.2.3	Synthesis of 24	174
5.2.4	Synthesis of 25	175
5.2.5	Synthesis of 26	176
5.2.6	Synthesis of 27	177
5.2.7	Synthesis of 3.....	178
5.3	Synthesis of CBI alkylating subunit conjugated to the DNA binding unit.....	179
5.3.1	Synthesis of 4	179
5.3.2	Synthesis of 5.....	180
5.4	Synthesis of warhead library.....	181
5.4.1	Synthesis of 6	181
5.4.2	Synthesis of 7.....	183
5.4.3	Synthesis of 8	185

5.5	Solid Phase synthesis	187
5.5.1	Table of peptides and peptide drug conjugates synthesised.....	187
5.5.2	Synthesis of P1, P2 and P3.....	187
5.5.3	Synthesis of peptide drug conjugates (PDC): PDC1, PDC2, PDC3 and PDC4.....	190
5.5.4	Synthesis of biologically active benzyl deprotected peptide drug conjugates (PDC): PDC6, PDC7, and PDC8.....	194
5.5.5	Incorporation of the DNA binding subunit into peptide drug conjugates (PDC). PDC10	196
5.5.6	Synthesis of tagged peptide and peptide drug conjugates (PDC): PL1, PDCL1 and PDCL2.....	198
6	Reference.....	201

List of Tables

Table 1: SKMEL-28 cells proliferation assessment after 72 Hours incubation using the Celltitre-Glo	157
Table 2: Cytotoxic activity of PDC6, PDC7 and sPDC6 against SKMEL-28	161
Table 3: Cytotoxic activity of peptide P1, P2, PDC 6, sPDC7, PDC7 and PDC8 against SKMEL-28 cell line	163

Figures

Figure 1: Skin Layer showing the epidermis cell types where common skin cancers begins. ³	19
Figure 2: The four subtypes of malignant melanoma	20
Figure 3: Amino acid code sequence that corresponds to transcript MC1R-001 (ID number ENST00000555147), MC1R-002 (ID ENST00000555427) and MC1R-350. ²⁷	22
Figure 4: Signalling pathways triggered by MC1R agonists	23
Figure 5: MAPK Pathway	25
Figure 6 : Structure of Vemurafenib (a) and Dabrafenib (b)	26
Figure 7: Structure of Trametinib (a) and binimetinib (b).....	26
Figure 8: Resistance to BRAF and MEK inhibitors.....	27
Figure 9: A, T-cell activation:	31
Figure 10: The Process of Adoptive T cell Immunotherapy.	33
Figure 11: Decarbazine (DTIC) metabolism Pathway leading to guanine alkylation.....	34
Figure 12: Structure of antibody-drug conjugates.....	35
Figure 13: ADC mechanism of action. ⁸⁰	36
Figure 14: Cleavable linkers. ⁷⁹	39
Figure 15: Lysine amide coupling	41
Figure 16: BR96 Doxorubicin.....	42
Figure 17: Auristatin and maytansine structures.....	42
Figure 18: Structure of the anti-B4-DCI 'Payload and linker' ¹⁰⁰	43
Figure 19: Structure of CC-1065, the duocarmycins and yatakemycin.....	44
Figure 20: DNA alkylation mechanism of action. The reactive cyclopropane ring can be generated in situ at physiological pH from non-cyclised <i>seco</i> -analogues via the Winstein-cyclisation (Figure 21), such property can allow the development of pro drug.....	45
Figure 21: Mechanism for <i>seco</i> -CPI Winstein Cyclisation.	45
Figure 22: Depurination process to identify DNA selective alkylation	46
Figure 23: N-Boc-DSA structure.....	46
Figure 24: Structures of CBI with and without the amide linkage.....	47

Figure 25: Comparison stick of (+)-duocarmycin SA (Left) and ent-(-) duocarmycin SA (Right)	48
Figure 26: Structure of adozelesin and bizelesin	49
Figure 27 Structure of duocarmycin prodrug carzelesin	50
Figure 28: Analogues of the alkylating subunits	51
Figure 29: SYD985 linker cleavage mechanism.....	52
Figure 30: Structure of MDX-1203.....	53
Figure 31: (a) Macropinocytosis, (b) clathrin-mediated endocytosis (CME) and (c) caveolae-mediated endocytosis (CvME) mechanisms. ¹²⁵	55
Figure 32: Zoptarelin Doxorubicin also known as AN-152 or AEZ-108 drug structure. ¹²⁹	57
Figure 33: iRGD structure ¹³⁶	58
Figure 34: Multistep Binding and Penetration Mechanism of iRGD: First, the iRGD peptide accumulates at the surface and bind to αv integrin-expressing endothelial and other cells in tumours. Second, the iRGD peptide is cleaved by a cell surface- associated protease(s) to produce CRGDK which then expose the cryptic CendR motif, RXXK/R, at the C terminus (red dotted line). Lastly the CendR element then triggers binding to neuropilin-1, resulting in cell penetration. Adapted from Ref. 118. ¹³³	59
Figure 35: Schematic of the iRGD activated transcytosis mechanism for nanocarriers delivery in tumor. ¹³⁶	59
Figure 36: Structure of the CBI alkylating unit (3) and CBI alkylating unit bearing a DNA binding unit (4 and 5).....	62
Figure 37: Structure of the CBI alkylating unit conjugated to glutamic acid (6) 63	
Figure 38: Structure of the CBI alkylating unit bearing a DNA binding unit conjugated to glutamic acid (7 and 8).	64
Figure 39: Synthesis of tert-butyl (4-(benzyloxy)-1-bromonaphthalen-2-yl) carbamate.....	65
Figure 40: Post- functionalisation of CBI pyrrolidine ring.	67
Figure 41: Synthesis of the CBI alkylating unit 3.....	68
Figure 42: Claisen condensation.....	69
Figure 43: Mechanism for Stobbe condensation	70
Figure 44: Mechanism for Ester hydrolysis.....	71

Figure 45: Mass spectrometry data for compound 22 also showing corresponding fragments	72
Figure 46: Carboxylic acid resonance.....	73
Figure 47: Mechanism for acid catalysed intramolecular cyclisation.....	74
Figure 48: Mechanism for benzyl protection	76
Figure 49: a) IR spectrum data for compound 24 and of (b) the crude mixture post failed rearrangement reaction showing the azide peak.....	79
Figure 50: Mechanism for Isocyanate formation	80
Figure 51: Mechanism for Isocyanate reaction with alcohol (butanol)	80
Figure 52: Mechanism for Isocyanate reaction with H ₂ O	81
Figure 53: Mechanism for Isocyanate reaction with amine product resulting from the presence of water	81
Figure 54: Iodination Mechanism	82
Figure 55: Alkylation Mechanism	84
Figure 56: Radical cyclisation Mechanism.....	87
Figure 57: Mass spec data for compound 3 and corresponding fragment	89
Figure 58: CBI boc deprotection mechanism.....	90
Figure 59: HATU reaction mechanism	92
Figure 60: Tert-butyl acid deprotection mechanism	93
Figure 61: Fmoc protection mechanism.....	94
Figure 62: Nitro reduction mechanism.....	96
Figure 63: Condensation mechanism for possible reaction between the amine and the nitroso intermediate	97
Figure 64: Boc protection mechanism using DMAP as a catalyst	98
Figure 65: ACTH, α -, β -, and γ -MSH natural production ¹⁴⁹	102
Figure 66: Fmoc deprotection mechanism.....	107
Figure 67: [Nle ⁴ ,dPhe ⁷] α -MSH structure, showing in red the amide resulting from cleavage from the resin	108
Figure 68: Structure of HBTU and HATU	109
Figure 69: Amide coupling reaction using HBTU as a coupling agent.....	110
Figure 70: Analytical HPLC trace of [Nle ⁴ ,dPhe ⁷] α -MSH	111
Figure 71: Mass Spectrometry data for [Nle ⁴ ,dPhe ⁷] α -MSH.....	111

Figure 72: [Nle ⁴ ,dPhe ⁷]α-MSH conjugated to CBI analogue shown in blue and then acetylated.....	112
Figure 73: Analytical HPLC trace of [Nle ⁴ ,dPhe ⁷]α-MSH conjugated to Glutamic-CBI.....	113
Figure 74: [Nle ⁴ ,dPhe ⁷]α-MSH conjugated to two CBI analogue shown in blue and then acetylated.....	114
Figure 75: [Nle ⁴ ,dPhe ⁷]α-MSH conjugated to three CBI analogue shown in blue and then acetylated.....	114
Figure 76: Benzyl deprotected 6.....	115
Figure 77: Benzyl deprotected Glu-CBI coupled to [Nle ⁴ ,dPhe ⁷]α-MSH.....	116
Figure 78: Pd/C benzyl deprotection mechanism.....	116
Figure 79: BBr ₃ benzyl deprotection mechanism.....	118
Figure 80: PDC6, MSH conjugated to benzyl deprotected Glutamic acid-CBI complex. Mass spectrometry demonstrates multiple charge state from 2+ to 3+.....	120
Figure 81: PDC7, MSH conjugated to three arginine residues and to benzyl deprotected Glutamic acid-CBI complex. Mass spectrometry demonstrates multiple charge state from 2+ to 4+.....	121
Figure 82: PDC8, MSH conjugated to three glutamic acid residues and to Benzyl deprotected Glutamic acid-CBI complex. Mass spectrometry demonstrates two charge state with 2+ to 3+.....	122
Figure 83: The amino acid property of a) MSH peptide and b)the first scrambled MSH peptide P4 synthesised (http://pepcalc.com/)	123
Figure 84: The amino acid property of a) MSH peptide and b)the second scrambled MSH peptide P5 synthesised (http://pepcalc.com/)	124
Figure 85: P2, MSH conjugated to three arginine residues. Mass spectrometry demonstrates two charge state with 2+ and 3+.....	126
Figure 86: PDC2, MSH conjugated to three arginine residues and to benzyl protected Glutamic acid-CBI complex.....	128
Figure 87: PDC3, MSH conjugated to three glutamic acid residues and to Benzyl protected Glutamic acid-CBI complex.....	130
Figure 88: PDC9, benzyl deprotected MSH conjugated to three arginine residues and to Glutamic acid-DNA Binding unit-CBI complex..	131

Figure 89: PDC10, benzyl protected MSH conjugated to Glutamic acid-DNA Binding unit-CBI complex.....	132
Figure 90: PL1, Biotinylated [Nle ⁴ ,dPhe ⁷]α-MSH showing the Biotin added in green	134
Figure 91: FITC conjugated [Nle ⁴ ,dPhe ⁷]α-MSH showing FITC in green (PL2), FITC conjugated of compound PDC3 and benzyl deprotected CBI in blue and also showing FITC in green (PDCL1), FITC conjugated of compound PDC2 and benzyl deprotected CBI in blue and also showing FITC in green (PDCL2).....	136
Figure 92: MC1R receptor expression on various cell lines ¹⁷²	141
Figure 93: Intermediate electron acceptor phenazine methyl sulfate (PMS) transfers electron from NADH in the cytoplasm to reduce MTS in the culture medium into an aqueous soluble formazan. ¹⁷⁸	148
Figure 94: Reaction between Luciferase enzyme in the presence of Luciferin Mg ²⁺ , molecular oxygen and ATP released from lysed viable cells. ¹⁷⁹	150
Figure 95: Simplified diagram that demonstrate xCELLigence Real-Time Cell Analyzer (RTCA) System. In this assay example, the target cells are initially seeded in the E-plate and allowed to attach and grow overnight. The effector cells (e.g. NK cells) are then added into the same well. Cytotoxicity is proportional to the concentration of effector cells. ¹⁸¹	152
Figure 96:Flow cytometry General Principles.....	154
Figure 97: SKMEL-28 cells proliferation assessment after 72 Hours incubation using the Celltitre-Glo	157
Figure 98: Cytotoxic assessment of synthesised PDC1, PDC4 and PDC6 against A375 using the xCELLigence Real-Time Cell Analysis system	159
Figure 99: Cytotoxic assessment of synthesised PDC1, PDC4 and PDC6 against SKMEL-28 using the xCELLigence Real-Time Cell Analysis system	159
Figure 100: Cytotoxic activity of PDC6, PDC7 and sPDC6 against SKMEL-28.....	161
Figure 101: Cytotoxic activity of peptide P1, P2, PDC 6, sPDC7, PDC7 and PDC8 against SKMEL-28 cell line	163

Figure 102: Cytotoxic activity of P1 sPDC7, PDC7 and PDC8 against SKMEL-28 cell line at lower seeding density of 1×10^4 cells/mL.	164
Figure 103: SKMEL-28 receptor occupancy assessment using PDCL1 referred to as MSH-Glu3-GLUCBI (a) and PDCL2 referred to as MSH-Arg3-GLUCBI (b)	165
Figure 104: HUVEC receptor occupancy assessment using PDCL1. HUVEC primary cell line Unstained and stained with PDCL1	166

List of Abbreviations

Abbreviation	Description
ADC	Antibody drug conjugate
AML	Acute myeloid leukemia
Antp	Antennapedia
APC	Antigen-presenting cells
ARF-1	ADP-ribosylation factor 1
BAP1	Breast cancer associated protein 1
BCC	Basal cell carcinoma
Bcl-2	B-cell lymphoma 2
Bcl-XL	B-cell lymphoma-extra large
BN	Bombesin
BRCA1	Breast cancer gene 1
cAMP	Cyclic adenosine monophosphate
CBI	1,2,9,9a-tetrahydro-1H-cyclopropa[c]benz[e]inden-4-one
CD28	Cluster of Differentiation 28
CDKN2A	Cyclin-dependent kinase inhibitor
CME	Classical clathrin-mediated endocytosis
CPI	Cyclopropa[c] pyrrolo[3,2-e]indole
CPP	Cell penetrating peptides
CPT	Camptothecin
CREB	Camp response element-binding protein
CTLA-4	T-lymphocyte-associated antigen 4
CTP	Cell targeting peptides
CvME	Caveolae-mediated endocytosis
DAR	Drug : antibody ratio
DNA	Deoxyribonucleic acid
DOX	Doxorubicin
DSA	The alkylation subunit of duocarmycin SA
DTIC	Dacarbazine
ERK1/2	Extracellular signal-regulated protein kinases 1 and 2

Abbreviation	Description
FDA	Federal drug administration
GNR	Gold nanorods
GO	Gemtuzumab ozogamycin
GSK	Glaxosmithkline plc
G α	G-Protein α -Subunit
HER2	Human epidermal growth factor receptor 2
IFN- α	Interferon alfa
IL-2	Interleukin-2
ITIM	Immunoreceptor tyrosine-based inhibitory motif
LAK	Lymphokine-associated killer
LHRH	Luteinizing Hormone-releasing Hormone
MAGE	Melanoma-associated antigens
MAP	Mitogen-activated protein
MAPK	Mitogen-activated protein kinase
MC1R	Melanocortin 1 receptor
MHC	Major histocompatibility complex
MHD	MAGE homology domain
MITF	Microphthalmia-associated transcription factor
MTD	Maximum tolerated dose
MTIC	3-methyl-(triazene-1-yl) imidazole-4-carboxamide
NK	Natural killer
NRP	Neuropilin-1
PABC	P-Aminobenzyloxycarbonyl
PBL	Peripheral blood lymphocytes
PD	Pharmacodynamics
PD-1	Programmed cell death protein 1
PDC	Peptide drug conjugate
PD-L1/2	Programmed cell death ligand protein 1/2
PEG	Poly ethylene glycol
PGC1 α	Peroxisome proliferator-activated receptor gamma coactivator 1-alpha

Abbreviation	Description
PK	Pharmacokinetics
PKA	Protein kinase A
PLD	Phospholipase D
POT1	Protection of telomeres 1
PP2A	Protein phosphatase 2A
RGD	Arginine-glycine-Aspartic Acid
RHC	Red hair colour
RNA	Ribonucleic acid
SCC	Squamous cell carcinoma
SHP-1	Src homology region 2 domain-containing phosphatase-1
SMCC	Succinimidyl 4-(N-maleimidomethyl) cyclohexane-1-carboxylate
STAT	Signal transducer and activator of transcription
TAA	Tumour-associated antigens
TAT	Trans-activating transcriptional activator
TCR	T-Cell receptor
T-DM1	Trastuzumab emtansine
TERT	Telomerase reverse transcriptase
TIL	Tumour-infiltrating lymphocytes
UV	Ultraviolet
V600E	Substitution at the 600 th amino acid from a valine to a glutamic acid
α MSH	Alpha-Melanocyte stimulating hormone

CHAPTER 1: INTRODUCTION

1.1 Skin Cancer Histology

Skin cancers are subdivided into non melanoma and melanoma cancers. Non melanoma constitute two main types which are named based on the type of skin cells where the cancer originates from, namely squamous cell carcinoma (SCC) and basal cell carcinoma (BCC) (Figure 1).¹ Squamous cell carcinoma (SCC) develops from uncontrolled growth of squamous cells which are keratinocyte cells that migrate to the outer part of the skin. Basal cell carcinoma (BCC) on the other hand develops from uncontrolled growth of basal cells which constitute the deepest layer of the epidermis.²

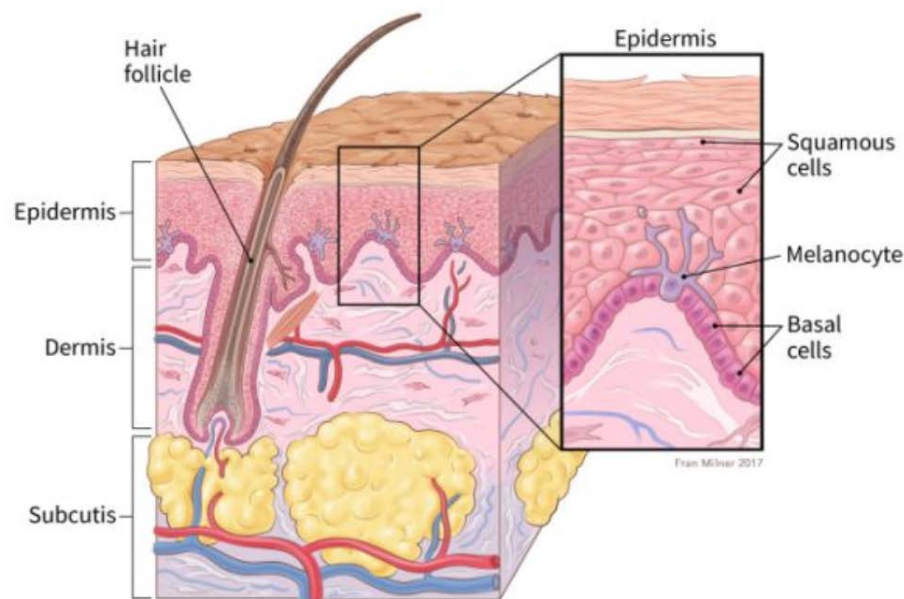


Figure 1: Skin Layer showing the epidermis cell types where common skin cancers begins.³

Malignant melanomas constitute one of the most dangerous types of skin cancer with 15970 new cases between 2014 and 2016 in the UK.⁴ Malignant melanoma results from abnormal growth of melanocytes and can occur anywhere in the body, including internal organs. Melanocytes constitute a heterogeneous group of cells that originate from the neural crest cells (NCC) and have a shared characteristic of producing melanin.⁵ There are four main histological subtypes which include superficial spreading (constituting the majority of cases), nodular, lentigo maligna melanoma and acral lentiginous (Figure 2).⁶ Superficial spreading, as can be depicted from the name starts by spreading along the epidermis before penetrating deeply in the skin. Nodular melanoma is the most aggressive type as it grows and spreads quickly and

deeply into the skin without necessarily spreading along the top layer of the skin. Lentigo maligna melanoma is easily mistaken as a benign age related spot and can go undetected for years as it grows very slowly before turning into an invasive tumour. Acral lentiginous melanoma generally develops in sole of the feet and the palms of the hand. It was named based on the Greek word akron, meaning extremity. This type of cancer predominantly occurs in black and Asian populations and may be mistaken for an injury leading to a later diagnosis compare to other subtypes.⁷

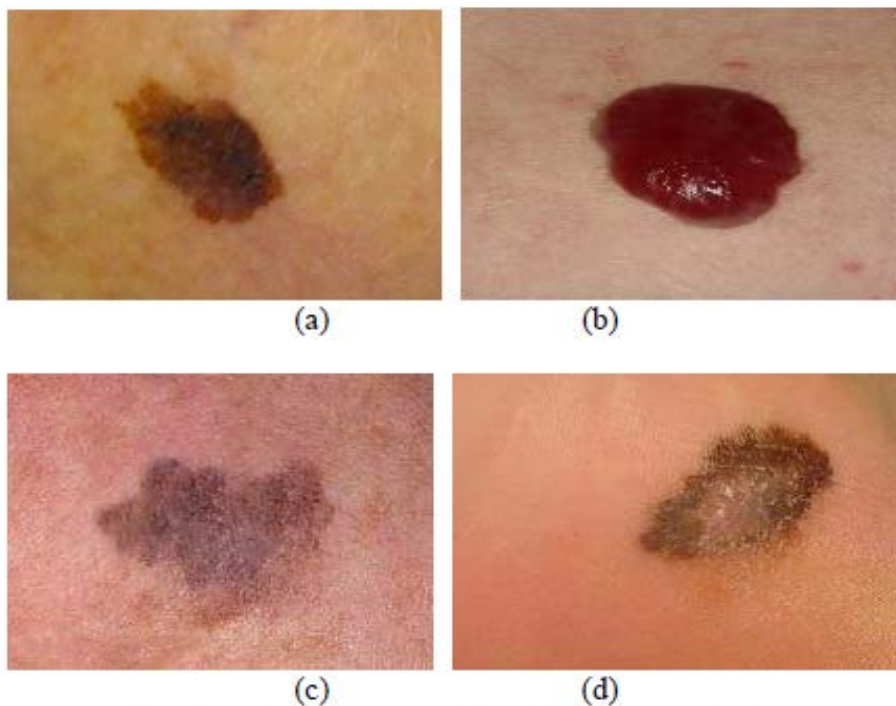


Figure 2: The four subtypes of malignant melanoma

(a) superficial spreading melanoma; (b) Nodular Melanoma; (c) Lentigo maligna Melanoma and (d) Acral Lentiginous Melanoma.⁷

1.2 Aetiology and incidence

Skin cancers have been found to be caused by both internal and external factors. One prevalent external risk factor extensively defined in the literature is UV radiation exposure which is estimated to cause approximately 65-86% and 90% of melanoma and non-Melanoma skin cancers respectively.⁸ Higher prevalence of non-Melanoma skin cancers is attributed to the use of artificial UV sources such as sunbed⁹ and an increase in UV radiation from 1979 to 2008

due to a decrease of ozone; however, recent data demonstrated ozone stability with some indication of recovery.¹⁰

Melanoma incidences have steadily risen over the last decade worldwide,¹¹ reaching an annual increase of up to 7% in some regions such as Australia and New Zealand where fair skinned individuals are reported to be at higher risk compared to darker skinned individuals.¹² The increased risk in fair skinned individuals has been attributed to the lack of melanin resulting in reduced UV protection.¹³ The incidence of melanoma has been suggested to increase significantly with age, especially in men of 65 years of age and over where the increase has been reported to be by 5-fold from the 1969 to 1999.¹⁴ However, when it comes to adult individuals, women have been described to be at higher risk mainly due to the use of indoor tanning.¹⁵

1.3 Risk Factors and Genetic Susceptibility

Melanoma development depends on several risk factors including genetics,¹⁶ UV exposure¹⁷ and age.¹⁸ Exposure to these factors does not necessarily mean that it would result in melanoma; however, it increases the risk. For example, lighter skinned Chinese individuals, are twice as likely to develop skin cancer as darker skinned individuals.¹⁹ UV is essential for vitamin D production;²⁰ however, irregular exposure to strong sunlight, such as being on holiday in a hot country, can increase the risk of melanoma compared to people with regular sunlight exposure.²¹

Some Genetic mutations, such as those in cyclin-dependent kinase inhibitor 2A (CDKN2A), have been linked with familial melanoma. Cyclin-dependent kinase inhibitor 2A (CDKN2A) was one of the first high-risk genes to be identified over 20 years ago.²² The CDKN2A gene encodes two tumour suppressor genes, p14ARF and p16INK4A, which encode proteins that lead to cell cycle arrest in the G1 phase and favour apoptosis via the P53 pathway. Mutations in Exon 2 of the CDKN2A gene were identified in the majority of tumours and were demonstrated to alter the function of p14ARF and p16INK4A proteins.²³ Other genes such as protection of telomeres 1 (POT1), Breast cancer 1 (BRCA1), breast cancer associated protein 1 (BAP1), CXC genes, telomerase reverse transcriptase (TERT),

CXC genes, ACD, TERF2IP, microphthalmia-associated transcription factor (MITF) and melanocortin 1 receptor (MC1R) have also been linked to melanoma.²² This thesis will focus on MC1R, a highly polymorphic gene (Figure 3)²⁴ that has been reported to increase the risk of melanoma.²⁵ MC1R has been suggested to be included as part of the melanoma risk prediction model, following demonstration that its inclusion increased the accuracy of detection.²⁶

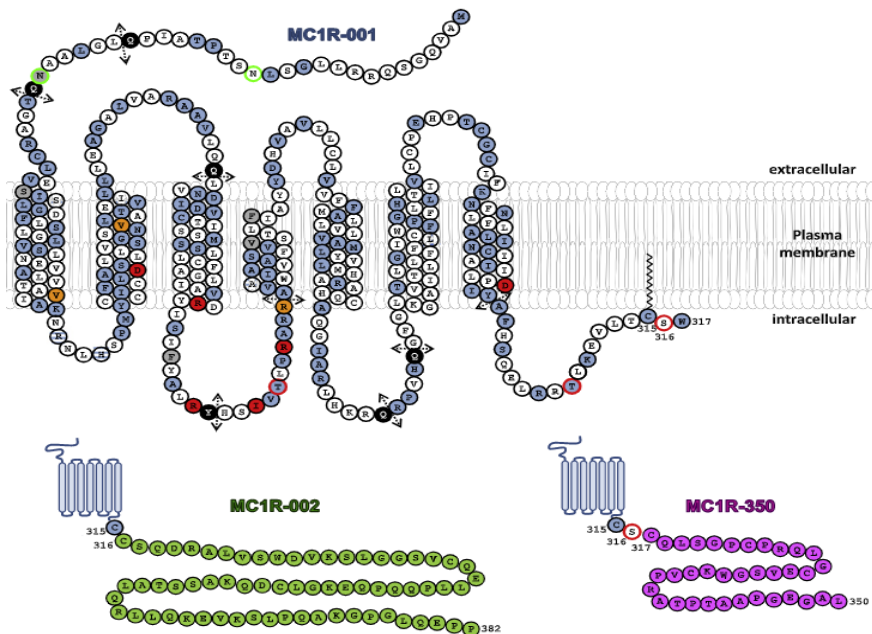


Figure 3: Amino acid code sequence that corresponds to transcript MC1R-001 (ID number ENST0000055147), MC1R-002 (ID ENST0000055427) and MC1R-350.²⁷

Demonstrating polymorphisms and possible arrangement of transmembrane regions in MC1R. Isoforms, polymorphic positions for which no reliable association studies are available, are indicated in blue. Positions of R and r variants are shown in red and orange, respectively. Residues shown in grey correspond to indels (insertion or deletion) and black circles with white lettering followed by broken arrows to premature stop codons. Positions where both an indel and a point mutation have been found are shown as blue circles hatched in white. Ser/Thr residues presumably phosphorylated are highlighted with a red border. Two Asn residues glycosylated in WT MC1R-001 are indicated with a green border. The sequence of the three proteins is identical up to Cys315. For MC1R-350 and MC1R-002, only the sequence of their specific cytosolic extensions is shown (pink and green, respectively).²⁷ Source: MC1R signalling. Intracellular partners and pathophysiological implications, page:2451.²⁷

MC1R is a G protein that activates multiple signalling pathways including the cAMP pathway, the p38 MAP kinase pathway and the extracellular signal-regulated protein kinases 1 and 2 (ERK1/2) pathway as illustrated in Figure 4.²⁷ MC1R is classified into two variants according to the red hair colour (RHC) phenotype, the strong allele form “R” and the weak allele form “r”. The R variant has been linked to approximately two fold more susceptibility to melanoma compare to the r variant.²⁸

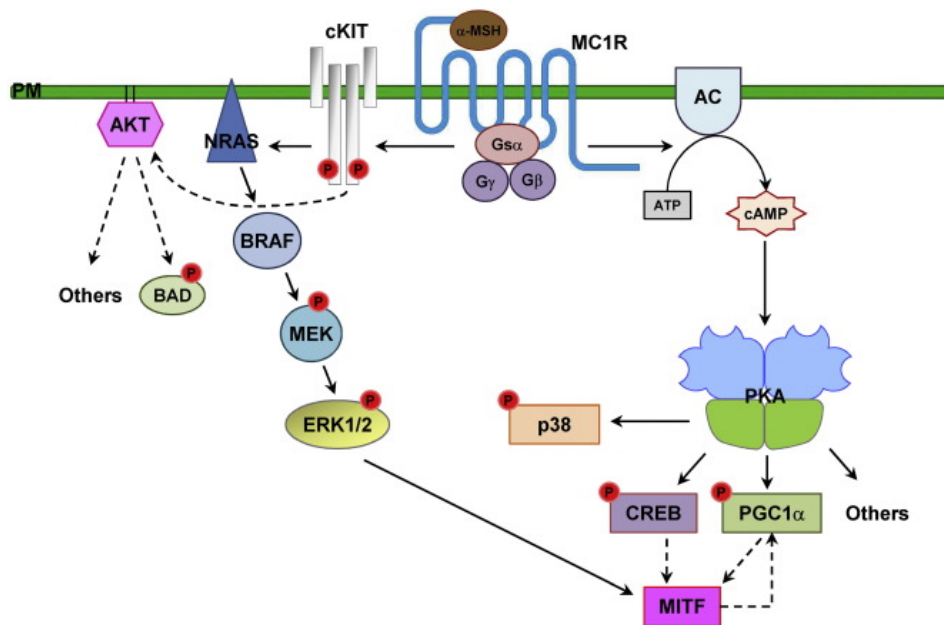


Figure 4: Signalling pathways triggered by MC1R agonists

Upon agonist binding, MC1R activates Adenylyl Cyclase (AC) via the G α protein, thus triggering cAMP synthesis and Protein Kinase A (PKA) activation. Active PKA catalytic subunits phosphorylate and activate multiple targets, such as the transcription factors cAMP response element-binding (CREB) and Peroxisome proliferator-activated receptor gamma coactivator 1-alpha (PGC1 α), which leads to an increase of the rate of transcription of the MITF gene. In turn, the Microphthalmia-associated transcription factor (MITF) protein stimulates PGC1 α expression. cAMP signalling also leads to activation of p38 kinase. Agonist-activated MC1R also transactivates cKIT (receptor tyrosine kinase) to trigger the NRAS-BRAF-MEK-ERK cascade. Active ERKs can phosphorylate MITF to increase its transcriptional activity and its proteasome-dependent degradation. In addition, Protein kinase B (PKB or AKT) activation downstream of α MSH has been demonstrated via cKIT.²⁷ Source: MC1R signalling. Intracellular partners and pathophysiological implications, page:2451.²⁷

1.4 Management and Treatment

1.4.1 Therapeutic Approaches

Therapeutic approach to melanoma depends on the type and its potential future development. Current treatment options include surgery, chemotherapy, radiotherapy, immune therapy and targeted therapy.²⁹

1.4.2 Surgery

The standard treatment for primary cutaneous melanoma is surgical removal of the melanoma with a safety margin which aims to extend beyond visible edge of the primary tumour to minimise the risk of melanoma cells that might have spread into the surrounding skin.³⁰ Distant metastatic melanoma are not usually treated with surgery; however, may be considered in case by case basis such as the removal of an obstructive metastasis.

1.4.3 Targeted therapy

The increase in understanding of the molecular pathogenesis of melanoma over the years has helped in the development of more targeted therapy. In 2000, Sorafenib was introduced as the first molecular RAF inhibitor for the treatment of RAS-mutant cancers and was approved for the treatment of renal and thyroid cancer but was demonstrated not to be an effective BRAF inhibitor for melanoma.³¹ Fifty percent of melanomas have demonstrated a mutation in the BRAF gene of a substitution at the 600th amino acid from a valine to a glutamic acid (V600E). BRAF is a kinase that is part of the MAPK (mitogen-activated protein kinase) pathway of cell proliferation (Figure 5). The V600E mutation leads to a constitutively active BRAF which, in combination with other oncogenic factors that prevent recognition of other defective pathways, results in unregulated cell proliferation.³²

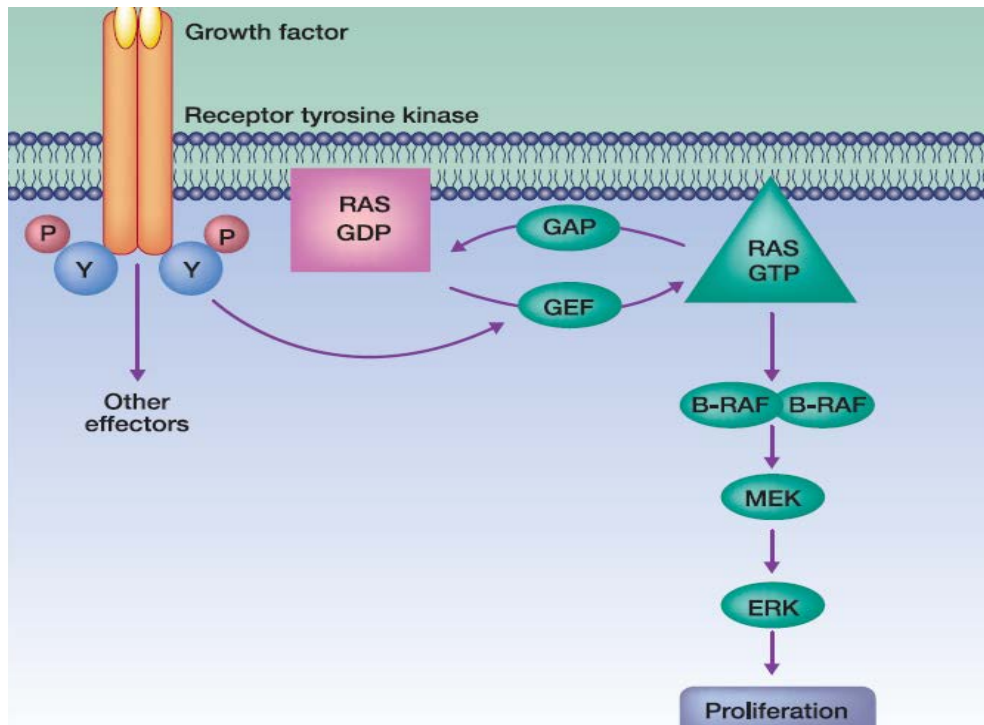


Figure 5: MAPK Pathway

The MAPK pathway involves a chain of signals that start at the surface of the cell membrane via a stimuli such as a cytokine, and leads to a series of intracellular phosphorylations that are specific to serine and threonine. The later chain of phosphorylation results in cell division/proliferation.³²

The latter understanding that BRAF mutation was harboured in approximately 50% of melanoma cases lead to the development of the first BRAF inhibitor (BRAFi), vemurafenib. Vemurafenib (**Figure 6**) recognises and binds the BRAF proteins in an active enzyme conformation caused by the V600E mutation. Due to the specificity of this treatment, the approval of Vemurafenib in 2011 was accompanied with the Cobas® 4800 BRAF V600 Mutation Test to detect if the patient had the V600E mutation before treatment.³³ In 2013 Dabrafenib (**Figure 6**) was subsequently also developed and approved as another inhibitor for BRAF with V600E mutation.³⁴

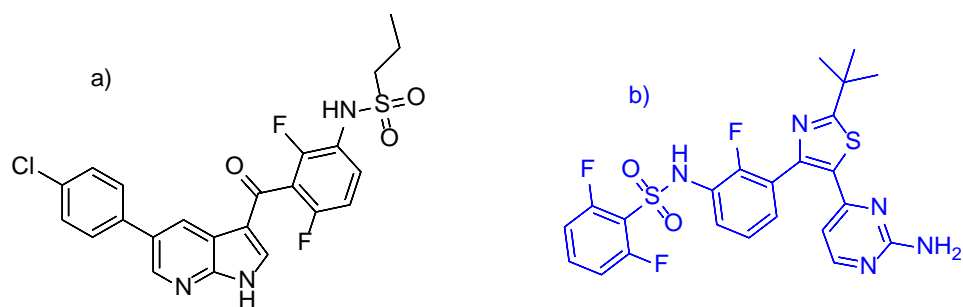


Figure 6 : Structure of Vemurafenib (a) and Dabrafenib (b)

While the focus was to target the BRAF gene mutation that accounted for the majority of mutations (>50%), other treatments targeting downstream signalling such as MEK inhibition (eg: trametinib and binimetinib in Figure 7) were also being investigated. The combination of BRAF and MEK inhibitors such as Encorafenib and binimetinib are generally recommended as standard treatment as this combination has been demonstrated to improve the patient outcome compared to a single treatment.³⁵ However, data shows that patients are subsequently prone to resisting both inhibitors within a month via the reactivation of the MAPK pathway. The resistance is achieved via alternative mechanisms such as the amplification of BRAF or upregulation of receptor tyrosine kinases (RTKs), secondary NRAS mutation or the PI3K–Akt pathways³⁶ (Figure 8).

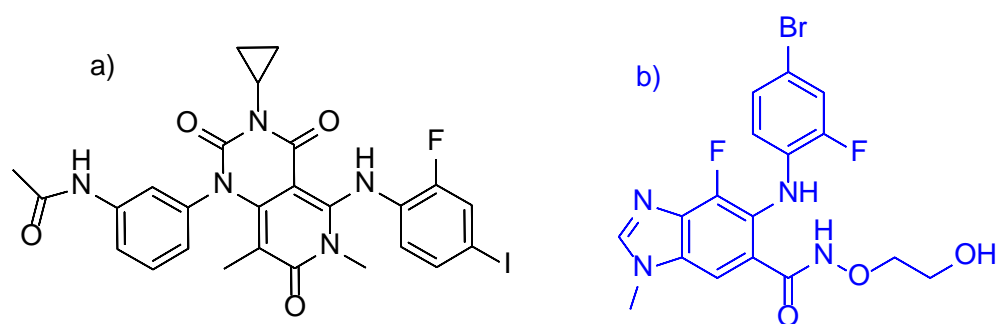


Figure 7: Structure of Trametinib (a) and binimetinib (b)

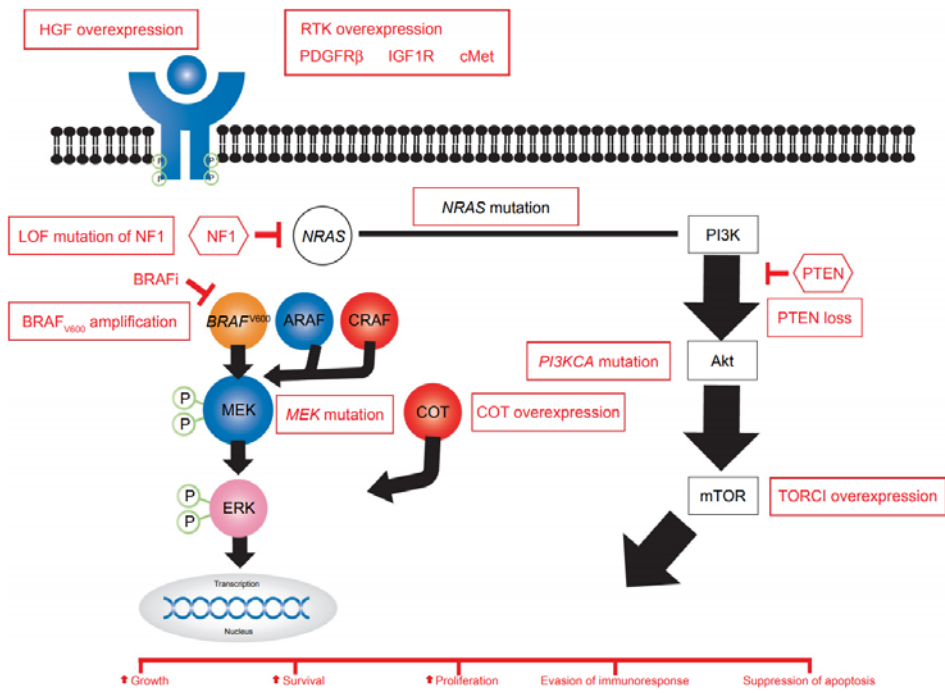


Figure 8: Resistance to BRAF and MEK inhibitors

Illustration of the genetic mutation which subsequently lead to resistance of BRAF and MEK inhibitors such as BRAF amplification, MEK mutations and NRAS mutation.³⁶

1.4.4 Immunotherapy

1.4.5 Cytokines

Cytokines are a range of proteins that exert various important roles in cell signalling, which includes regulation of the immune response and protection against infection and other disease.³⁷ Cytokines provide several advantage as therapeutic agents such as their high specificity to malignant cells, hence the FDA approved the use of IL-2 and IFN- α as drugs for the treatment of melanoma.³⁸

Interleukin-2 (IL-2) is a 15-Kda glycoprotein cytokine that functions as a growth factor stimulator for natural killer (NK) cells and T cells. IL-2 and other members of the γ -chain cytokines activate several pathways including the Ras–MAPK pathway, the Jak-signal transducer and activator of transcription (STAT) pathway and the PI3K pathway; however, their mechanism in mediating an anti-tumour effect is not well understood.³⁹

IL-2 administration stimulates the generation of lymphokine-associated killer (LAK) cells which in turn detect and lyse tumour cells. The use of recombinant IL-2 also known as aldesleukin in the USA since 1998 for the treatment of metastatic melanoma has demonstrated durable and improved outcomes in up to 10% of treated patients.⁴⁰

Interferons constitute a family of proteins produced by white blood cells as a response mainly to viruses. Interferon was first approved in 1995 for the use in patients with malignant melanoma.⁴¹ Interferons had been previously described as having both a positive and negative effect on tumour growth. Some of the negative effects include down-regulating cell cycle activity, increasing the expression of tumour antigens, activating T-lymphocytes and inducing apoptosis.⁴² In 2001, the FDA approved a pegylated version of interferon α -2b with brand name Sylatron™. The use of the PEG moiety was designed to protect the interferon protein from proteolytic activity and therefore prolong its biological half-life.⁴¹

1.4.6 Checkpoint inhibitors

In order for the immune system to target cancer cells, tumour associated antigen has to be processed and displayed on the MHC of the antigen presenting cell. This allows it to interact with the T cell receptor alongside costimulatory CD28 located on the T cell and B7 located on the antigen presenting cell. However, the expression of T-lymphocyte-associated antigen 4 (CTLA-4) and Programmed cell death protein 1 (PD-1), the two immune checkpoint inhibitors, can lead to the attenuation of this activity (Figure 9).⁴³ The discovery of CTLA-4, a checkpoint inhibitor, in 1987 by Brunet *et al.*, and additional work carried out in Allison's group to target this mechanism, led to the development of three initial anti-CTLA-4 antibodies (tremelimumab and ticilimumab by Pfizer, Ipilimumab by Bristol-Myers Squibb/Medarex, Princeton, NJ) that went into clinical trials. Ticilimumab was the parent compound of tremelimumab and both compounds have not yet been approved due to thrombocytopenia observed in the first human clinical trial. Ipilimumab, on the other hand was demonstrated to reinstate anti-tumor T-cell immunity and received approval from the FDA and EMA in 2011 and 2012 respectively.⁴⁴

Another checkpoint inhibitor extensively studied is programmed cell death 1 (PD-1). PD-1's mode of action is not exerted via the inhibition of CD28/B7 interaction but through inhibition of activated T cells in the peripheral tissue at a later stage. PD-1 interacts with PD-L1 and PD-L2, which have been demonstrated to have overlapping functions.⁴⁵ PD-L1 and PD-L2 are constitutively expressed on various immune cells and can be found on some tumour cells; however, PD-1 is only expressed on T-cells when activated.⁴⁶ PD-1 plays a crucial role in T-cell inhibition via binding to PD-L1/PD-L2. The binding of PD-1 triggers phosphorylation of the intracellular domains of immunoreceptor tyrosine-based inhibitory motif (ITIM) and immunoreceptor tyrosine-based switch motif (ITSM). These two intracellular phosphorylations lead to the recruitment of the Src homology region 2 domain-containing phosphatase-1 (SHP-1) and phosphatase-2 (SHP-2), which in turn dephosphorylate proteins involved in TCR-signalling complex, thus inhibiting T-cell activation and TCR-induced proliferation.⁴⁷

Subsequent to the discovery of PD-1 involvement in T-cell inhibition, two anti-PD-1 monoclonal antibodies, nivolumab and pembrolizumab were developed by Bristol Meyers Squibb and Merck⁴⁸ respectively and were demonstrated to have superior advantages compared with chemotherapy.⁴⁹ Studies conducted to compare anti-PD-1 monotherapeutic (nivolumab) against anti-CTLA-4 monotherapeutic (ipilimumab) in melanoma have demonstrated anti-PD-1 to have superior potency.⁵⁰ On the other hand, the combination of nivolumab and ipilimumab demonstrated improved clinical potency and is currently recommended.^{51,52}

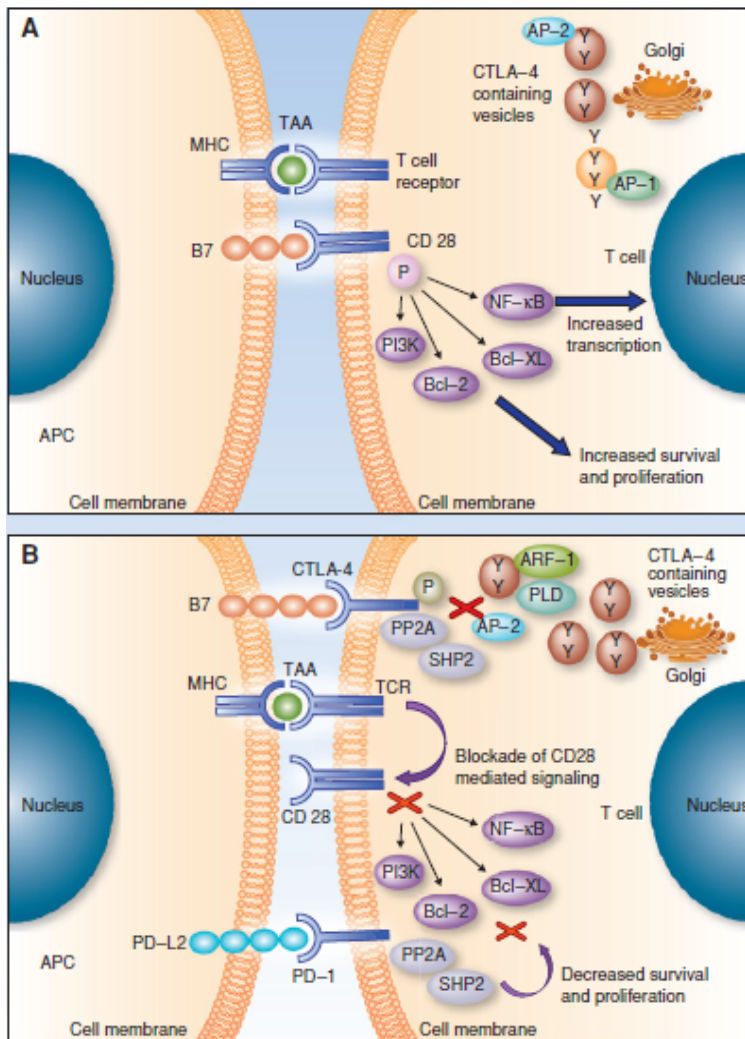


Figure 9: A, T-cell activation:

T-cell priming in response to a specific antigenic epitope requires coordination of multiple signals. The initial signal is created when a full-length peptide is processed and presented on the surface of an APC. The resulting fragments, or tumour-associated antigens (TAA), are bound to MHC molecules present on the surface of the APC. This MHC/TAA complex then allows for detection and binding of the TAA by the TCR. A) second costimulatory signal, however, is necessary to complete T-cell activation and expansion. The binding of CD28 on the T cell with B7 on the APC creates this second signal, which leads to activation of the PI3K/AKT pathway, upregulation of the anti-apoptotic proteins Bcl-2 and Bcl-XL, and an increase in the nuclear transcription factor NF- κ B. This collectively leads to increased cellular proliferation, cytokine production, and prolonged survival. Initially, regulatory proteins like CTLA-4 are primarily inactive and remain complexed with AP-2 within the intracellular compartment. B) Upregulation of CTLA-4 and maintenance of immune tolerance: TCR activation induces upregulation of CTLA-4 via a number of mechanisms. ARF-1 and PLD bind to enhance the exocytosis of CTLA-4-containing vesicles as they exit the Golgi apparatus. Phosphorylation of the cytoplasmic tail of CTLA-4 prevents binding of AP-2, which normally functions to promote receptor internalization, resulting in an increase in CTLA-4 surface expression. CTLA-4 is then capable of directly competing with CD28 for binding of B7. CTLA-4 may also exert a direct negative effect on CD28 signalling, mediated by the binding of the phosphatases PP2A and SHP-2. Additional regulatory molecules, including PD-1, are also important in limiting T-cell activation and may also inhibit TCR-mediated signalling via blockade of specific downstream effectors. The resultant decrease in pro-survival signalling serves to limit T-cell activation and expansion.⁴³

1.4.7 Antigen-based active immunotherapy

In 1991, the first melanoma-associated antigens (MAGE) were established by Terry Boon's laboratory⁵³ who also established a method of detecting new MAGEs. Following additional discoveries MAGEs were classified based on their expression patterns in subgroups I or II.⁵⁴ Both subgroups contain the 170 amino acid sequence MAGE homology domain (MHD) that is conserved in approximately 46% of cases. Among other functions MAGE has been demonstrated to be involved in the regulation of protein ubiquitination, which subsequently results in altered cellular processes leading to tumorigenesis.⁵⁵

The effectiveness of MAGE immunotherapy was mainly assessed focussing on MAGE-A3 recombinant protein with and without adjuvant (AS15) conjugation. The use of AS15 as an immunostimulator was demonstrated to trigger a robust immune response against the host antigen⁵⁶ but despite original promising data, it was later demonstrated to be ineffective.⁵⁷

1.4.8 Adoptive cell therapy

Adoptive cell therapy or ACT is used to treat many different types of cancer including melanoma. This treatment is carried out by initially harvesting tumour-specific T-cells from the patient, followed by in vitro culturing and expansion of the T-cell clones, and then reinfusion back into the cancer patient (Figure 10).⁵⁸

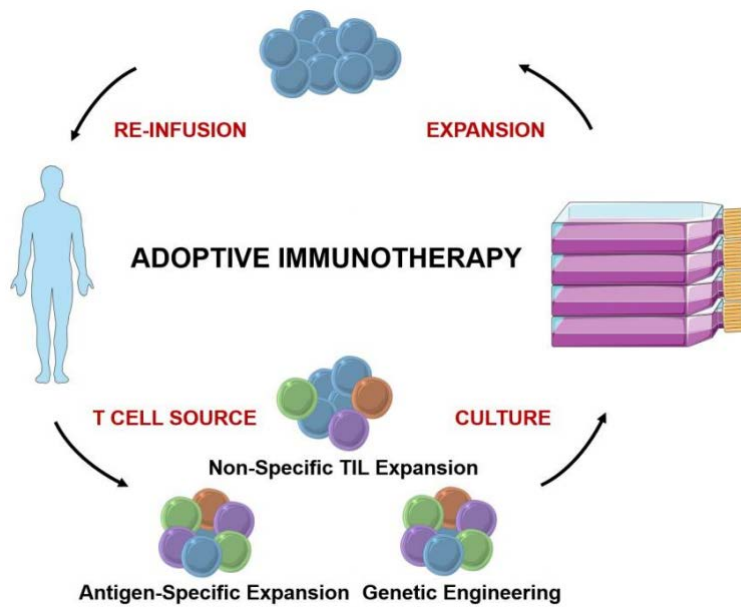


Figure 10: The Process of Adoptive T cell Immunotherapy.

T cells are harvested either from tumour (tumour-infiltrating lymphocytes, TILs) or peripheral blood (peripheral blood lymphocytes, PBLs). TILs can be expanded non-specifically since they are preferentially tumour-specific prior to culture. In contrast, tumour specificity must be induced in PBLs, either through antigen-specific expansion or genetic engineering. After several weeks of expansion in culture, tumour-specific T cells can be reinfused into the cancer patient.⁵⁸

Adoptive cell therapy has demonstrated clinical benefit; however, one of its limiting factors is the requirement for high-doses of IL-2 after treatment, which results in severe toxicity; hence, in a recent study conducted by Nguyen *et al.*, an assessment of lower doses of IL-2 was carried out and was demonstrated to be feasible.⁵⁹ In addition to the extensive research carried out to demonstrate the role of the immune system to control cancer,⁶⁰ adoptive cell therapy has also demonstrated promising outcomes, but remains challenging as a treatment due to many factors including the production of the final product that meets a certain specification given that the starting material is not always the same, not to mention the resources required for this to be achieved.⁶¹

1.4.9 Radiotherapy and chemotherapy

Radiotherapy for melanoma has traditionally been considered as only palliative care⁶² as melanoma has generally been regarded as radio resistant.⁶³ However, recent data have demonstrated improved outcome when radiotherapy was used in combination with checkpoint inhibitors.⁶⁴

Prior to all therapeutic advances described above, chemotherapy was the standard treatment for advanced metastatic melanoma.⁶⁵ For more than 4 decades, the only chemotherapy drug against melanoma approved by the FDA in 1975 is Dacarbazine (DTIC).⁶⁶ Dacarbazine is a DNA alkylating agent that exerts its mode of action by alkylating guanine (G) bases (Figure 11), subsequently leading to cell death. Dacarbazine was originally developed as an antimetabolite given its structural similarity with 5-aminoimidazole-4-carboxamide. However, in spite of this structural similarity dacarbazine was later demonstrated to be extensively metabolised in the liver by cytochrome P450 to generate a diazomethane via 3-methyl-(triazen-1-yl) imidazole-4-carboxamide (MTIC) that ultimately decomposes to generate the active methyl cation.⁶⁷ This latter group alkylates guanine preferentially at the N-7 and O-6 position, where the O-6 methylation is perceived to be the main cause of cytotoxic activity.⁶⁸ So far Dacarbazine has not demonstrated any evidence of improvement of survival rate, mainly due to resistance to apoptosis, with metastatic melanoma patients response ranging from 10 to 20%.⁶⁹

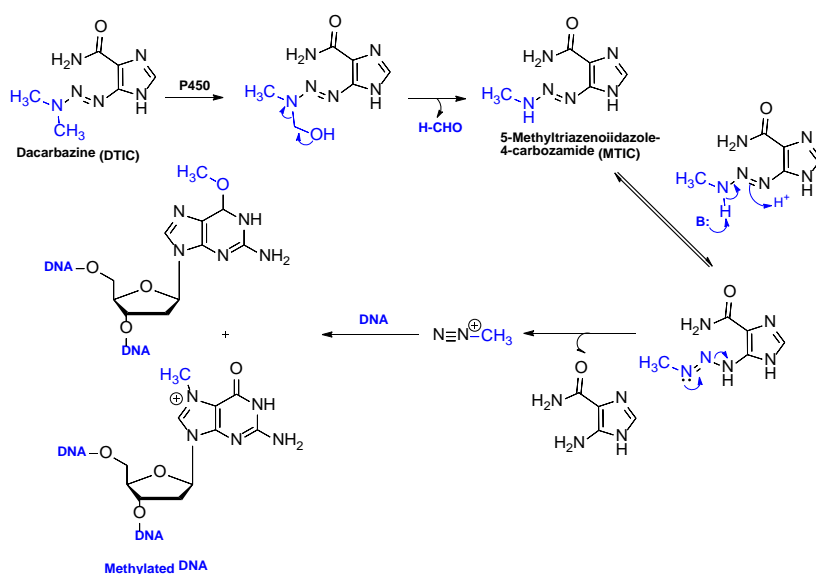


Figure 11: Dacarbazine (DTIC) metabolism Pathway leading to guanine alkylation.

1.4.10 Melanoma targeted drug delivery strategies

One of the major limitations of untargeted cancer drugs is that they are used at higher concentration near the maximum tolerated dose (MTD) in order to reach clinical relevance, which, in turn, results in off-target toxicity.⁷⁰ One of the approaches extensively described in the literature to overcome this, is the use of targeted therapeutics such as antibody drug conjugates (ADC) and peptide drug conjugates (PDC) that recognise overexpressed tumour specific antigens.⁷¹ ADCs and PDCs are highly potent therapeutic drug that are made up of an antibody or a peptide respectively coupled to a cytotoxic drug via a linker (Figure 12).⁷² For targeted drug delivery such as an ADC and PDC to be successful, they need to be able to retain the cytotoxic drug up to the tumour site and then be able to release it at site of action.⁷³

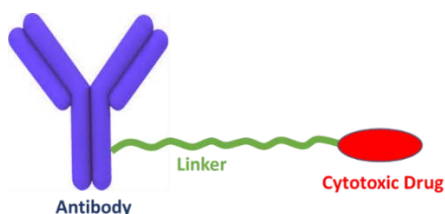


Figure 12: Structure of antibody-drug conjugates

1.4.10.1 The Antibody

Over the past three decades a number of antibody therapeutics such as Herceptin, and Avastin have been developed for the treatment of breast cancer and colorectal cancer respectively.⁷⁴ Monoclonal antibody therapeutics have revolutionised cancer treatment due to a range of functions exerted by antibodies including promoting apoptosis, increasing the host immune response and inhibiting angiogenesis and metastasis.⁷⁵

Antibody tumour targeting relies on the ability to differentiate between antigen expressed on normal cells compared to malignant cells or overexpression of the antigen on the tumour cells in comparison to normal cells.⁷⁶

Monoclonal therapeutic antibodies and cytotoxic drugs used alone have a small tumour cell-killing window and as a result are often not considered extremely effective on their own. Hence, the use of an ADC, which combines

the use of a cytotoxic agent such as duocarmycin, that kills tumour cells but which lacks that discrimination property, with monoclonal antibodies, which are specific to the tumour cells, provides a more effective drug.⁷⁷ ADCs are very complex compounds and provide more challenges before and after they reach the tumour target cell. Some of the challenges include the ability for an ADC in circulation to avoid clearance and any premature release of the cytotoxic agent. The latter requires sufficient investigation in an appropriate linker to use. Once at the target cell, the drug attached via the linker should not interfere with the antibody specificity and selectivity to the target antigen. Antigen recognition is generally followed by ADC internalisation and subsequent degradation in the lysosome to release the free drug, which finally induces cell apoptosis via a specific mechanism (Figure 13).⁷⁸ Since the initial proposal of targeted delivery of toxic agent by Paul Ehrlich in 1913 followed with the first anti-carcinoembryonic antigen antibody-vindesine conjugate in 1983, ADCs have come a long way.⁷⁹

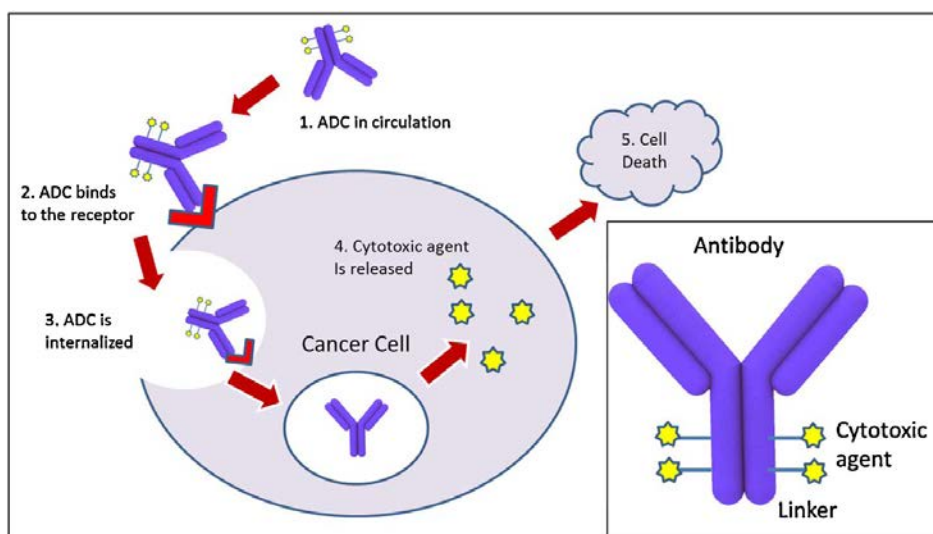


Figure 13: ADC mechanism of action.⁸⁰

1.4.10.2 Antibody Drug Conjugates (ADC) generations

Gemtuzumab ozogamycin (GO/Mylotarg), the first generation of approved ADC, is constituted with an anti-CD33 antibody conjugated to a DNA minor groove binder calicheamicin derivative.⁸¹ Mylotarg was approved in 2000 by the FDA for the treatment of acute myeloid leukemia (AML); however, its success was short lived and it was later withdrawn from the market in 2010 and later reintroduced in 2017.⁸² Although the first generation ADC had several issues, Mylotarg's initial failure was mainly attributed to an instability in the linker, which relied upon pH change for drug release.⁸³ The other component of an ADC that required additional understanding to increase its potency is the cytotoxic payload. An example of another failed first generation ADC is SGN-15, which was developed by Seattle Genetics ADC, and was made up of antibody against the Lewis Y antigen and doxorubicin as the cytotoxic payload linked using a hydrazone linker via cysteine coupling on the antibody. The failure of SGN-15 was attributed to the lack of doxorubicin potency.⁸⁴ Hence the focus of the second and next generation of ADC was on the improvement of the linker and cytotoxic agents with improved potency.

1.4.10.3 The Linker

A stable linker for an ADC is crucial to avoid premature release of the cytotoxic payloads,⁸⁵ which would cause unnecessary side effects as a result of damaging healthy tissue.⁸⁶ Premature payload release also reduces the efficacy of the ADC compound as the concentration of cytotoxic compound reaching the tumour site is reduced.⁸⁷ Once at the tumour site, intracellular or extracellular cleavage of the linker to deliver the payload should also be taken into consideration and should only happen in the tumour environment.⁸⁸ Linker evolution constitutes one of the vital parameters that has evolved from the first generation to the new generation of ADCs.⁸⁹

Linkers are classified in two groups, cleavable and non-cleavable linkers (Figure 14). The majority of ADCs in clinical trial explore the use of a cleavable linker, which exploits the target tumours inherent property as a mechanism of action to release the cytotoxic payload.⁹⁰ Cleavage mechanisms at the tumour site include, but are not limited to; protease sensitivity such as in the

case of brentuximab vedotin (Adcetris®) which uses a valine-citrulline linker that is cleaved by the high concentration of cathepsin B in the lysosome; glutathione sensitive linkers also known as disulfide linker such as that used in the case of Mylotarg; Mylotarg's linker also demonstrates pH sensitivity.⁷⁹ Non cleavable linkers on the other hand rely on complex degradation in the lysosomal pathways, for example in the case of trastuzumab emtansine where a noncleavable thioether linker was used and relied upon lysosomal enzymatic degradation to release the payload.⁹¹ The use of non-cleavable linkers is preferred as they are more stable and only rely on complete intracellular degradation to release the potent cytotoxic agent and as a result lead to lower off target toxicity.⁹² The use of a non-cleavable linker such as succinimidyl 4-(N-maleimidomethyl) cyclohexane-1-carboxylate (SMCC) has been successfully demonstrated in the case of trastuzumab emtansine (T-DM1, or Kadcyra®).⁹³

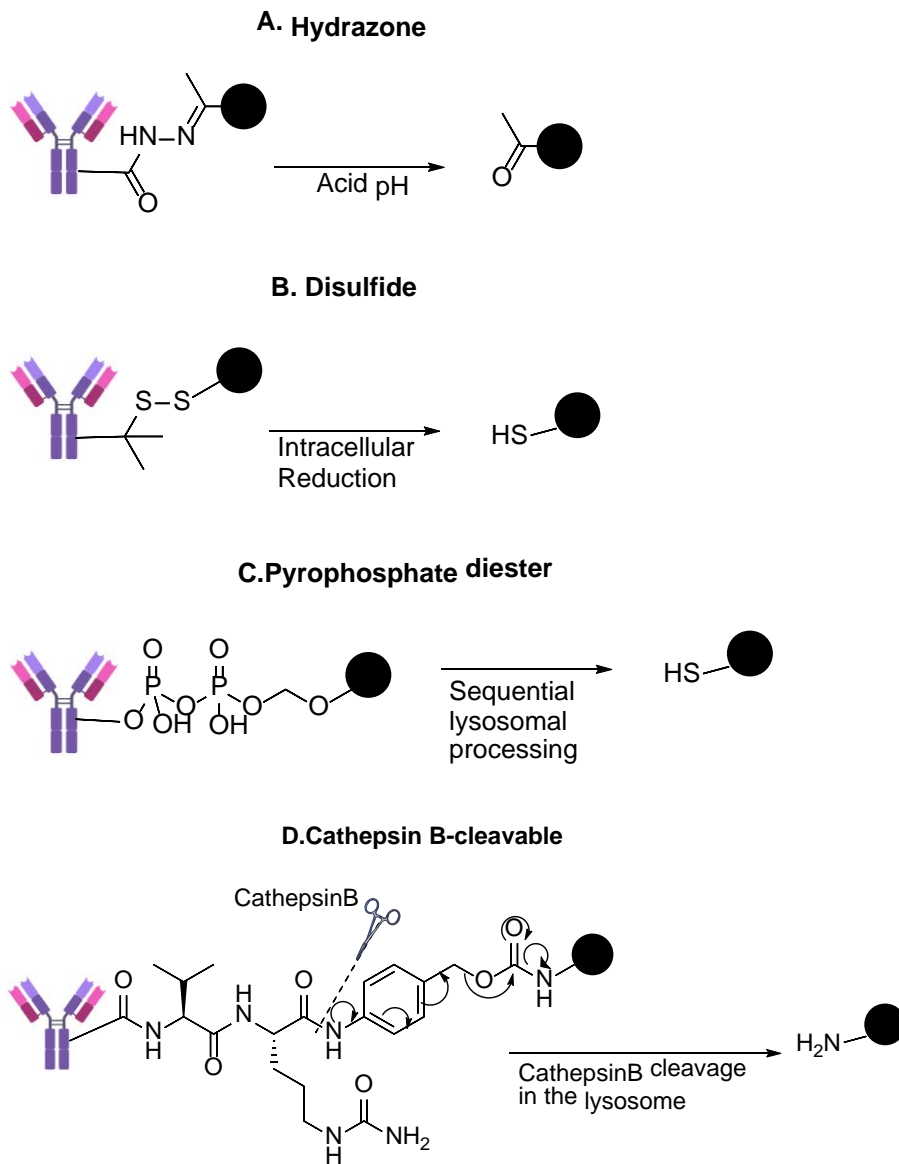


Figure 14: Cleavable linkers.⁷⁹

(A) Hydrazone linker which is cleaved in an acidic environment such as in the lysosome; (B) Disulfide linkers cleaved by intracellular glutathione (C) Pyrophosphate diester cleaved in the lysosome (D) Cathepsin B cleavable peptide linker such as in the case of Valine citrulline and alanine-p-Aminobenzyloxycarbonyl (PABC).

1.4.10.4 Chemical conjugation

As ADC developments continue to evolve, the chemical conjugation strategy is very important because the decision on where the payload is conjugated to the antibody influences the drug: antibody ratio (DAR). The choice of conjugation that leads to higher DAR may not necessarily imply more potency as the latter may also have other negative effects such as the increase of the ADC clearance rate, aggregation⁹⁴ and potential premature release of the toxic payload. Therefore, it is important to choose the site of conjugation carefully to achieve the optimum ADC activity. A well described method is the use of lysine amine coupling (Figure 15), which uses an activated carboxylic from the linker to couple with the amine on a lysine forming an amide bond. One of the major limitations of this technique is the abundance of lysine residues on the antibody leading to a high proportion of DAR species and potential conjugation in the antigen-binding domain, which may also have PK/PD effect.⁷⁹ An alternative conjugation relies on the antibody cysteine residues reacting with an active thiol on the payload to form a disulfide bridge. An antibody possesses four interchain and twelve intrachain disulfide bonds that can be exploited for this conjugation.⁹⁵ However, the preference is to use the four interchain thiols as they are not crucial in the maintenance of antibody structure stability. Mild antibody reduction may be sufficient to up to eight free thiols keeping the twelve intrachain disulfide bonds intact. Such conjugation is superior to the lysine conjugation as it achieves more controlled DAR. This conjugation idea was further explored with the generation of Thiomab, which are antibodies with two newly introduced cysteines. Thiomab provides new thiol site of conjugation and therefore improves ADC homogeneity and avoids unwanted conjugation such as in the antibody binding site. Other conjugations such as the use of enzyme and the incorporation of non-natural amino acid in the antibodies sequence are also described in the literature but have yet to be used in a clinically approved ADC.⁷⁹

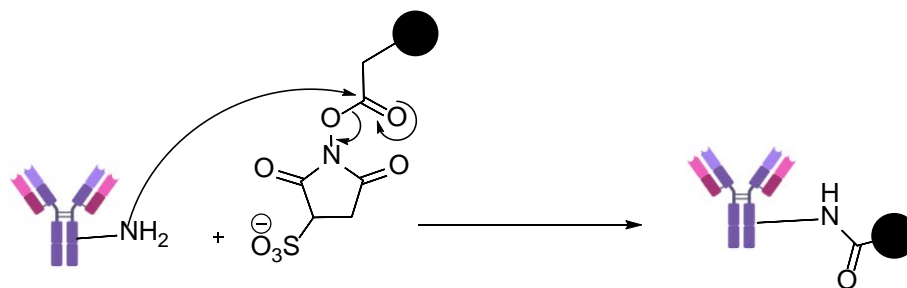


Figure 15: Lysine amide coupling

1.4.11 Cytotoxic payload

As described above the cytotoxic payload of an ADC needs to be effective at killing the tumour upon delivery at the tumour site. Therefore, some of the critical aspects to consider when selecting an appropriate cytotoxic payload include parameters such as the mode of action. To date there are two main modes of action that have been investigated: DNA damage or anti-mitotic activity. Other general considerations include parameters such as stability, solubility, potency and the ability to be able to conjugate onto the targeting antibody.⁹⁶

Solubility is one of the initial considerations as this is required to be able to conjugate the payload to the antibody. While lipophilic (hydrophobic) cytotoxic payloads may be advantageous inside the cell due their ease of being able to pass through cell membrane, they are harder to conjugate to an antibody because a higher concentration of organic solvent is required to dissolve the cytotoxic payload and such solvent would denature the antibody. Therefore, most lipophilic payloads may require additional modification prior to conjugation such as the addition of hydrophilic linkers. Commonly used hydrophilic linkers include PEG (poly ethylene glycol) or sulfonate.⁹⁷ A large proportion of cytotoxic payloads described in the literature require additional modification to enable them to be used directly for conjugation and such modifications require careful consideration as it may have an impact on the payload potency.⁹⁶

Payload potency is critical in order to get an effective ADC. For example the first generations of ADCs, used clinically approved chemotherapy such as doxorubicin and methotrexate as payload, such as in the case of BR96-

doxorubicin, a humanised monoclonal anti-Lewis Y antigen antibody conjugated to doxorubicin. BR96-doxorubicin (Figure 16) was one of the first ADCs and later demonstrated to be ineffective as the dose required was found to be higher because of low payload potency.⁹⁸

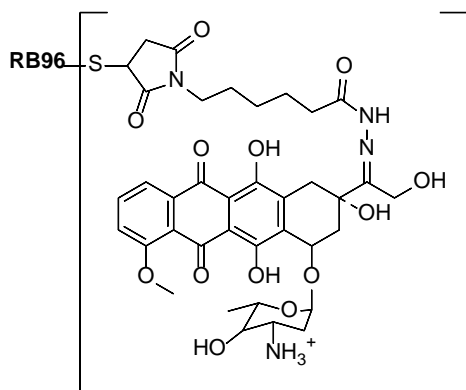


Figure 16: BR96 Doxorubicin

As a result of this initial finding, researchers were focused on the use of ultrapotent cytotoxins, such as mitotic agents, auristatin and maytansinoid (Figure 17), and DNA binding agent such as duocarmycins.^{70,99} One of the initial ADCs that used ultrapotent cytotoxic payload was the anti-B4-DC1 conjugated to the DNA minor groove binder adozelesin (CC-1065 analogue), incorporating a highly stable and synthetically more accessible CBI unit as the alkylating unit instead of CPI alkylating unit. Anti-B4-DC1 (Figure 18) demonstrated ultrapotency in picomolar range in vitro against CD19-positive cell lines; however, its clinical development was later halted as a result of poor solubility and general instability at physiological condition.^{100,101}

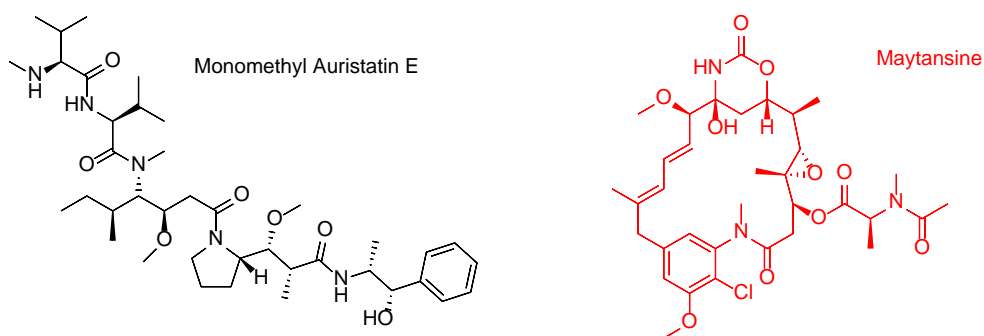


Figure 17: Auristatin and maytansine structures

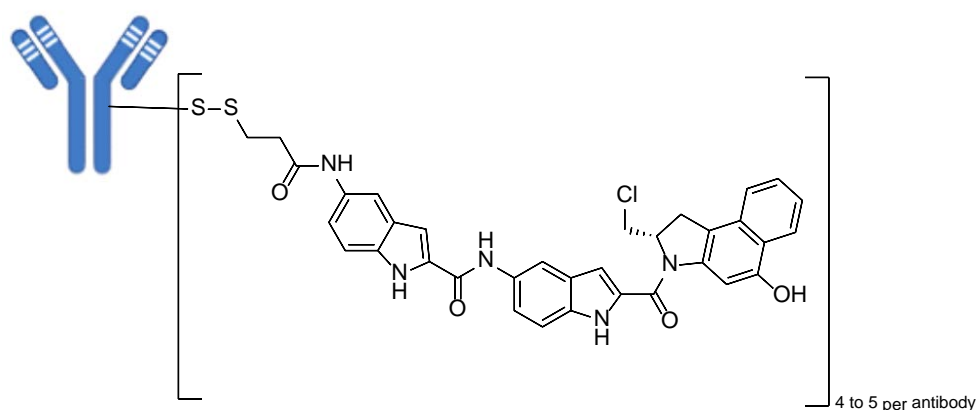


Figure 18: Structure of the anti-B4-DCI 'Payload and linker'¹⁰⁰

1.4.11.1 CC-1065, the duocarmycins and yatakemycin

CC-1065, the duocarmycins and yatakemycin (Figure 19) are anti-tumour antibiotics that belong to the same family and were all isolated from *Streptomyces* species culture broth. They are ultrapotent cytotoxic agents that possess a DNA minor groove binder and a DNA alkylating unit.¹⁰² Their use as chemotherapy alone has proven impossible due to their ultra-potency, for example when CC-1065 was administered as a single dose in healthy mice, it resulted in delayed deaths related to hepatotoxicity.¹⁰³

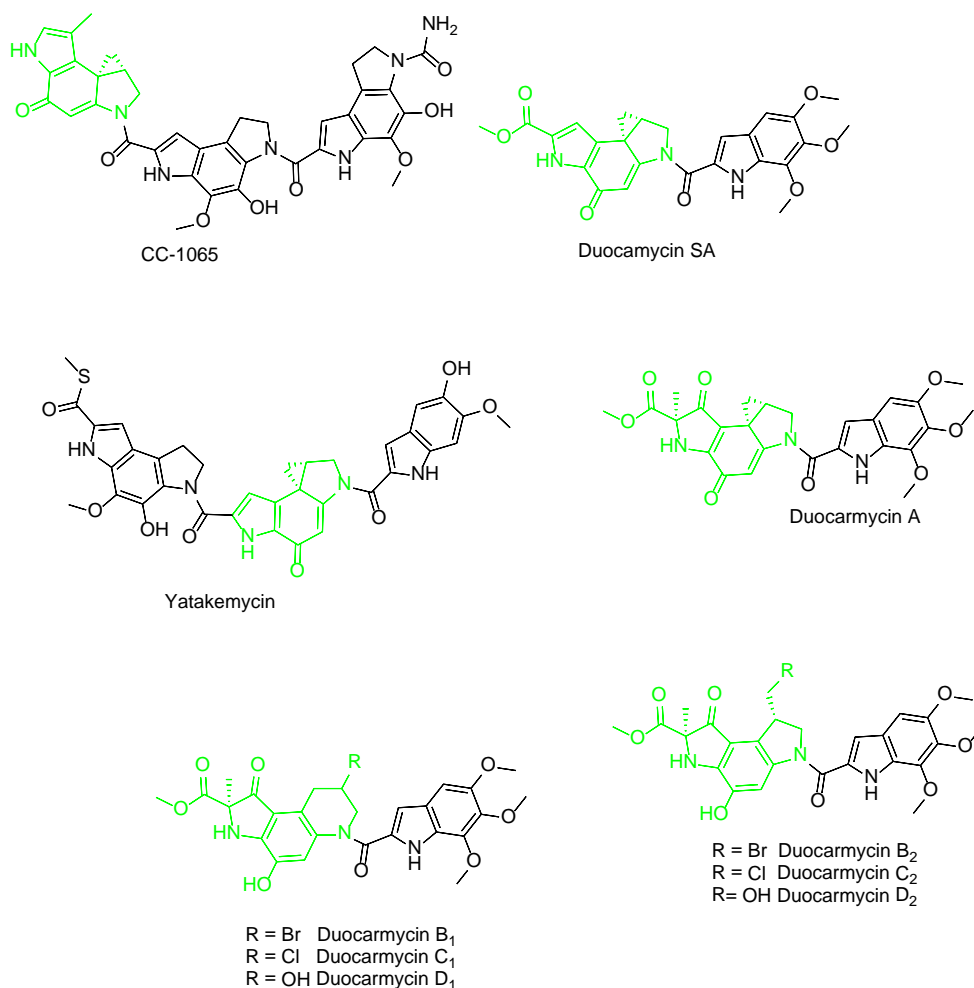


Figure 19: Structure of CC-1065, the duocarmycins and yatakemycin

1.4.11.2 CC-1065, the duocarmycins and yatakemycin mode of action

CC-1065, yatakemycin, and the duocarmycins bind in AT rich minor groove of DNA and then alkylate the DNA at the N3 position triggering a cascade of events that subsequently lead to cell apoptosis. The non-alkylating subunits play a crucial role of helping the payload bind to the DNA, *via* hydrophobic interactions and van der Waals forces. The binding triggers a twist in the payload allowing closer proximity and initiation of attack by N3 to the least substituted carbon of the cyclopropane ring, which subsequently leads to the ring opening and further electron movement forming an aromatic phenol drug-DNA adduct (Figure 20).

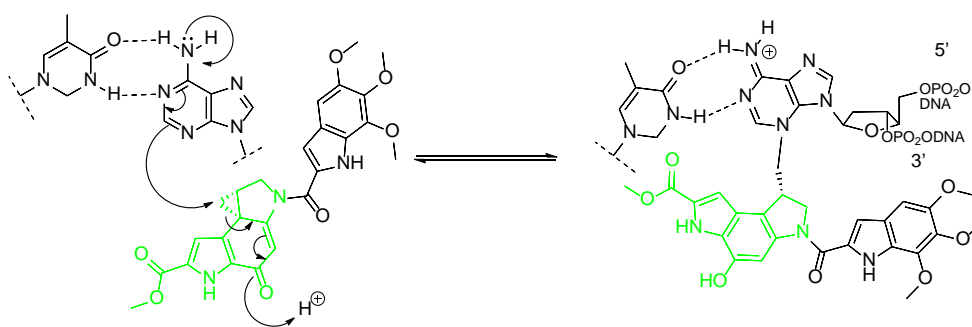


Figure 20: DNA alkylation mechanism of action. The reactive cyclopropane ring can be generated in situ at physiological pH from non-cyclised seco-analogues via the Winstein-cyclisation (Figure 21), such property can allow the development of pro drug.

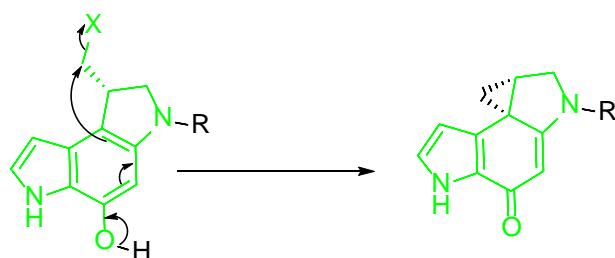


Figure 21: Mechanism for *seco*-CPI Winstein Cyclisation.

The biological and chemical impact of CC-1065 has been extensively studied on multiple cell lines and demonstrated to significantly inhibit DNA synthesis in comparison to RNA and protein synthesis. CC-1065 assessment on L1210 leukaemia cells and B16 melanoma cell lines demonstrated a similar pattern in terms of DNA, RNA and protein inhibition and more importantly CC-1065 was demonstrated to be more lethal during exponential growth phase compared to the plateau phase.^{104,105} Inhibition of DNA synthesis following alkylation was demonstrated to subsequently lead to apoptosis, the latter was observed by examining the Molt-4 leukaemia cell line under the microscope following duocarmycin exposure and lacked any cell lysis but revealed characteristics associated to apoptosis such as blebbing and shrinkage of the cells. Assessment by flow cytometry further confirmed that the cytotoxicity of duocarmycin was associated with H_2O_2 production upon binding to the DNA, which induced caspase-3 activation and apoptosis.^{106,107}

1.4.11.3 DNA alkylation selectivity

The understanding of the site selectivity of alkylation was derived by exposing labelled DNA with (+)-duocarmycins, followed with heat induced depurination and labelled DNA cleavage (Figure 22).

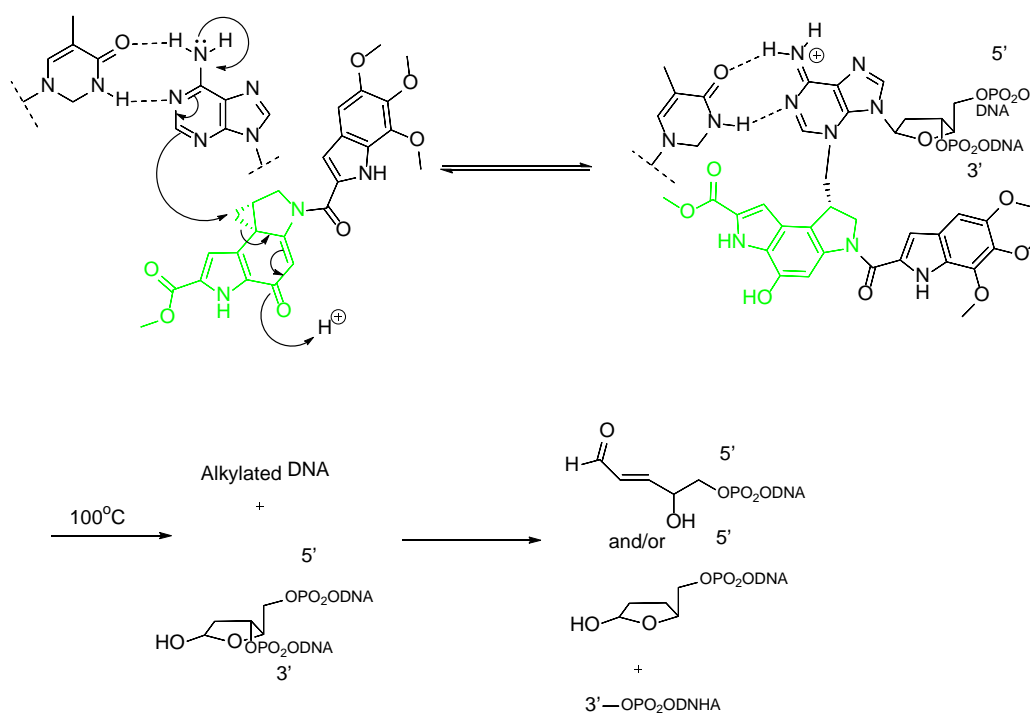


Figure 22: Depurination process to identify DNA selective alkylation

DNA alkylation selectivity is aided by the non-covalent binding of the (+)-duocarmycins in the minor groove of AT-rich regions of the DNA, and the penetration depth of the DNA alkylating agent. Hence, simpler structures such as N-Boc-DSA (Figure 23) can only exert their activity when the adjacent 5' is A or T.

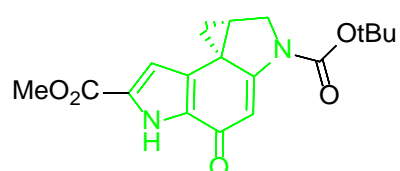


Figure 23: N-Boc-DSA structure.

Upon binding of the (+)-duocarmycins to the DNA, they undergo a conformational change which is aided by rotation of the linking amide to allow a conformation that is complementary to the helical rise of the minor groove. This highlights the importance of the amide bond presence in the structures of this natural anti-tumour antibiotics. To further elucidate the importance of the amide bond an investigation was carried out where 1,2,9,9a-tetrahydro-1H-cyclopropa[c]benz[e]inden-4-one (CBI_n) (Figure 24), a CBI without the vinylogous amide nitrogen was compared to the amide containing CBI. It was demonstrated that the CBI_n was 3200 times less stable than CBI containing amide at pH 3 and also reactive at pH 7, while CBI containing the amide was stable. The importance of the amide linkage was further assessed by substituting it with a rigid methylene bond which resulted in a compound with more solvolysis and a half-life of 3.6 years at pH 3 compared to 230 hours for the CBI-TMI. However, despite stability improvement against solvolysis, which should equate to increase in cytotoxicity, the lack of the amide linkage resulted in reduced alkylation efficiency and cytotoxic potency by >106 times and 105 fold respectively.¹⁰⁸ Other considerations such as the use of a more electron-withdrawing thioamide and amidine has also been assessed and demonstrated to cause disruptions of the vinylogous amide and subsequently lead to increased solvolysis reactivity; however, the alkylation efficiency and the cytotoxicity effect was reduced substantially compared to CBI-TMI containing the amide linkage. The later emphasized the role of the amide linkage in DNA alkylation and the fact that multiple factors are required to be considered not only solvolytic reactivity and stability to generate an effective and potent analogue.¹⁰⁹

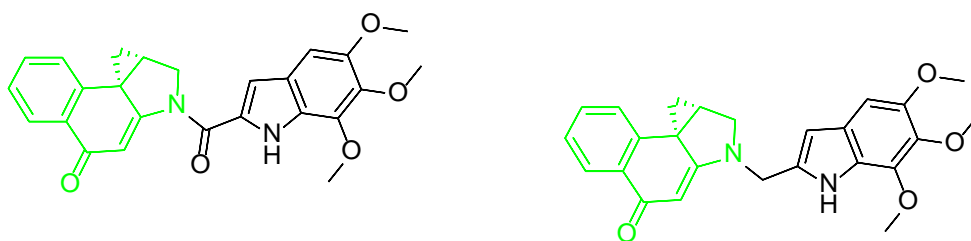


Figure 24: Structures of CBI with and without the amide linkage

CC-1065 and the duocarmycins have both been demonstrated to alkylate DNA at the adenine N3. However, their alkylation properties were demonstrated to be slightly different where CC-1065 alkylated the DNA irreversibly while the duocarmycins DNA alkylation was reversible. Natural enantiomers for CC-1065 and the duocarmycins were demonstrated to bind to adenine in the 3' → 5' direction across adjacent bases while unnatural enantiomers (-) were demonstrated to alkylates the DNA in 5' → 3' direction (Figure 25).¹¹⁰ Natural and unnatural enantiomers do not necessarily present the same alkylating potency as (-)-duocarmycin SA requires 10 × the concentration to exert the same activity as the natural enantiomer. However, the natural and unnatural enantiomers of CC-1065 have been demonstrated to alkylate DNA at comparable rate and efficiency. The order of sequence alkylation preference for the (+)-duocarmycins and (+)-CC-1065 has been demonstrated to be 5'-AAA > 5'-TTA > 5'-TAA > 5'-ATA (where the underlined base is the site of alkylation). The duocarmycins bind over 3.5 base pairs whilst CC-1065 binds over 5 base pairs.¹¹⁰

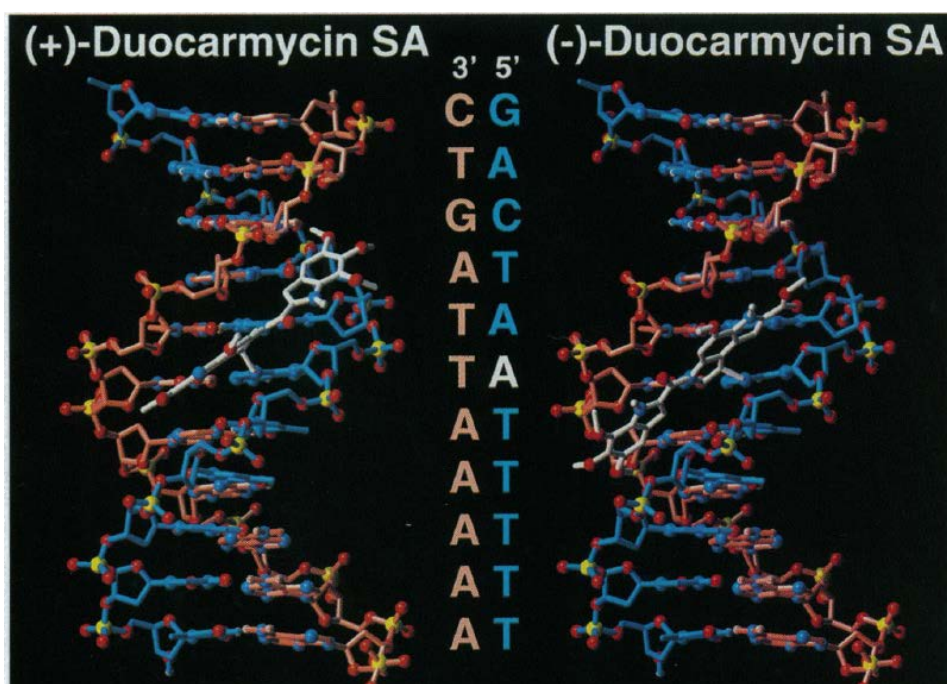


Figure 25: Comparison stick of (+)-duocarmycin SA (Left) and ent-(-) duocarmycin SA (Right)

1.4.11.4 Development of Duocarmycins into therapeutic agents

CC-1065 and the duocarmycins are ultra-potent natural products and as a result of their extreme potency their standalone use as therapeutic drug for the treatment of malignant tumour have had many major challenges. Early preclinical trial assessment of CC-1065 analogues incurred severe hepatotoxicity in animal models leading to delayed death.¹¹¹ Subsequent investigation carried out to establish the root cause of this delayed death, suggested that it was due to the fact that CC-1065 was binding to DNA irreversibly, which is not seen with the duocarmycins. Further assessment were carried out using CC-1065 analogues which led to the development of two therapeutic drug candidates adozelesin and bizelesin (Figure 26) with the hope of better clinical profile; however, they also exhibited severe toxicity and were halted from clinical trial progression.¹¹²

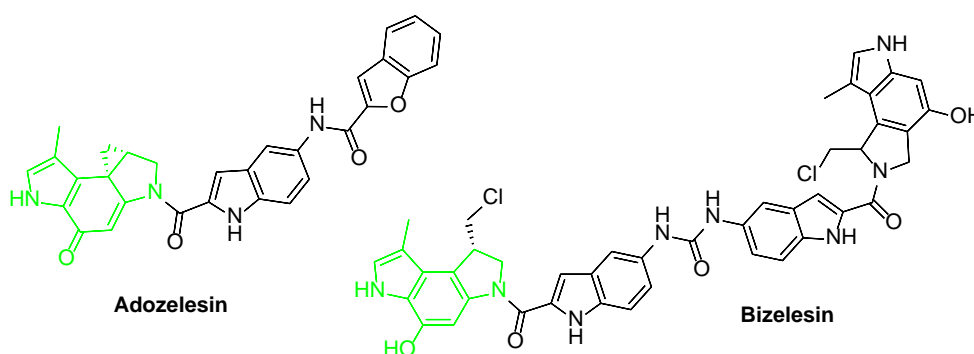


Figure 26: Structure of adozelesin and bizelesin

Despite the setbacks observed from CC-1065, the duocarmycins are still considered as a promising candidate due to having reversible alkylating characteristics and the ability to alkylate the DNA selectively over other biological nucleophiles. However; still like all classical alkylating agents, the natural products of this family are incapable of discriminating malignant cells from those of healthy tissue causing dose limiting toxicities apparent with all non-selective cytotoxins. One of the approaches used to minimize toxicity of this class of duocarmycins is the protection of the phenolic oxygen with a labile protecting group that would be specifically cleaved at the tumour site. This was initially attempted in Carzelesin (Figure 27) where the phenol was protected with phenylurethane. Such protection led to a prodrug that required two step

activation with the first one being the hydrolysis of phenylurethane followed with the formation cyclopropyl ring formation.

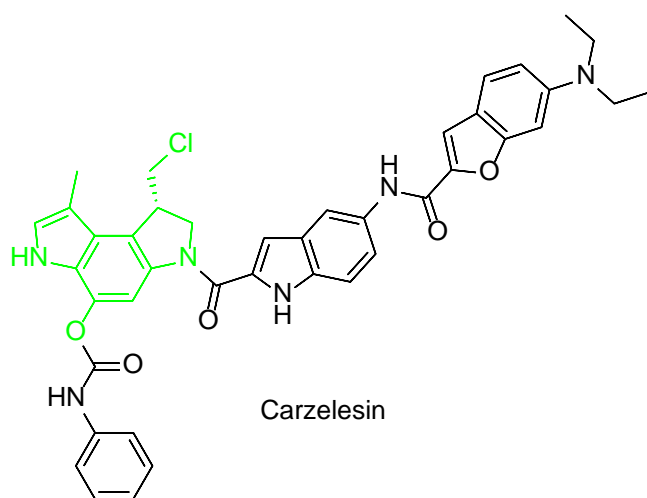
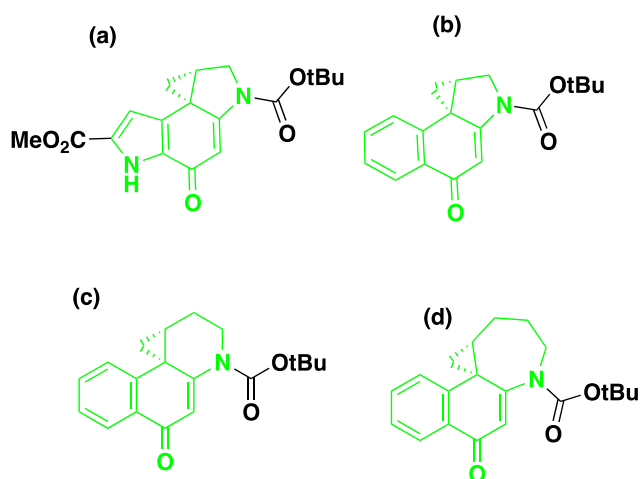


Figure 27 Structure of duocarmycin prodrug carzelesin

The discovery of this family of utrapotent cytotoxic compounds was accompanied with their extreme structure complexity and difficulty to be synthesised. Several attempts were made to understand structure activity relationships and improve the structure to obtain compounds with optimal toxicity and solubility. This thesis will discuss a more synthetically accessible 1,2,9,9a-Tetrahydrocyclopropa[c]benz[e]indole-4-one (CBI). Based on the data collected, CBI has been reported to be four times more stable to acid-catalysed solvolysis, and up to four times more biologically potent than the natural CPI alkylation subunit. The increase in potency was attributed to the increase in stability of the CBI (Figure 28).



Compounds	$t_{1/2}$	k	$t_{1/2}$	k	IC ₅₀
	(h,pH 3)	(S ⁻¹ ,pH 3)	(h,pH 7)	(S ⁻¹ ,pH 7)	
(a)	177	1.08×10^{-6}	Stable	Stable	6
(b)	133	1.45×10^{-6}	Stable	Stable	80
(c)	2.1	9.07×10^{-5}	544	3.54×10^{-7}	2000
(d)	0.03	6.90×10^{-3}	2.1	9.16×10^{-5}	5000

Figure 28: Analogues of the alkylating subunits

Given the improved stability and potency of CBI, its use was implemented in novel compounds including SYD985 (Figure 29) and MDX-1203 (Figure 30). SYD985 is a HER2-targeting ADC that is being developed by Synthron and is currently in Phase III clinical trial. SYD985 combines multiple sophisticated strategies to avoid undesired toxicity, including the attachment of the CBI analogue via the phenol group to avoid early activation. SYD985 also possesses a linker consisting of a dipeptide that is cleaved upon internalisation, minimising off-target toxicity. Cleavage of the dipeptide linker and the removal of two self-eliminating spacers leads to the release of the seco-CBI that subsequently undergoes the Winstein cyclisation to form the active CBI analogue (Figure 29).^{113,114}

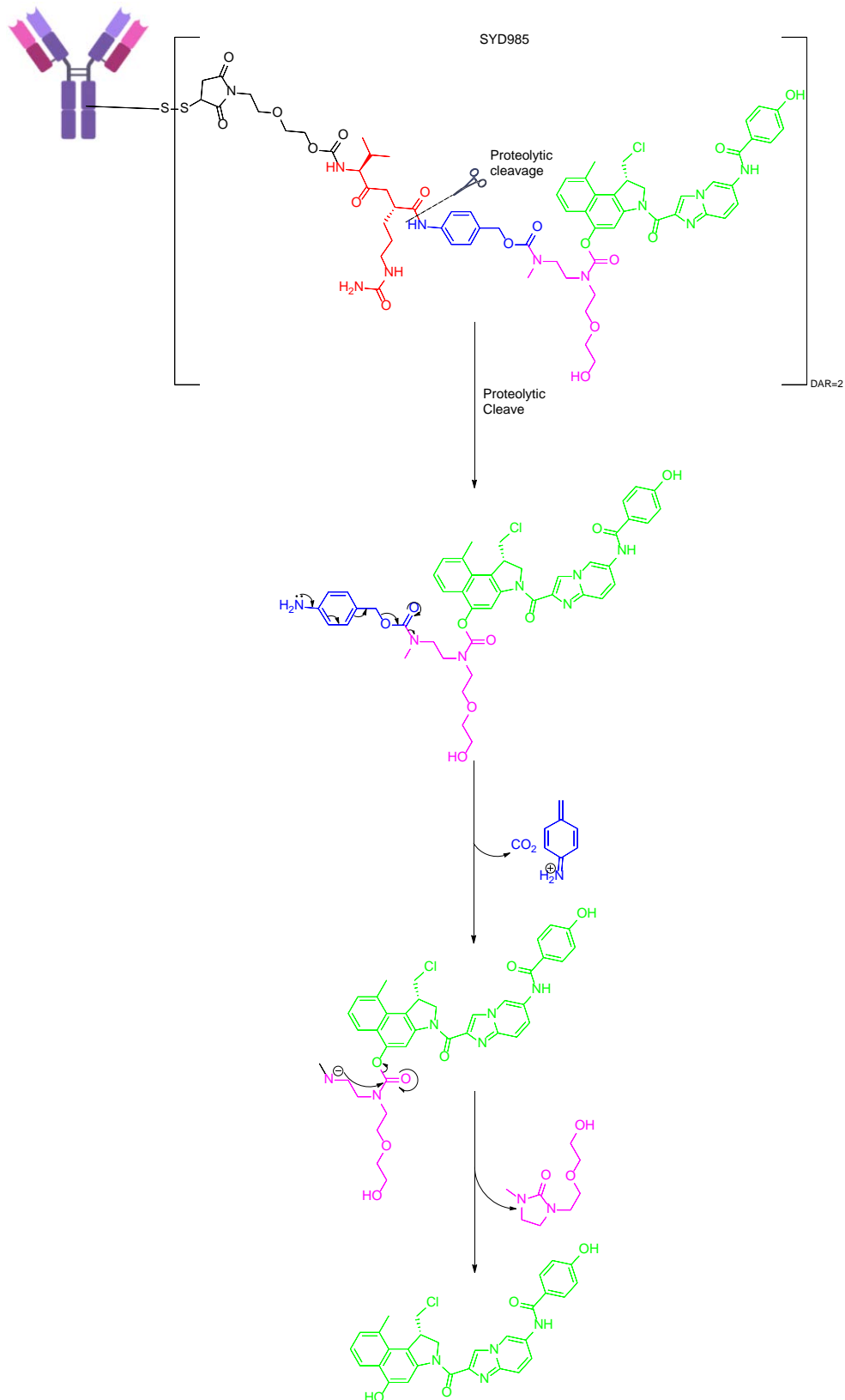


Figure 29: SYD985 linker cleavage mechanism

MDX-1203 (Figure 30), developed by Bristol-Myers Squibb was later discontinued as a result of observed toxicity. MDX-1203 was constituted of an

anti-CD70 fully human monoclonal antibody conjugated to a CBI analogue through cysteine sulfhydryl group via a protease cleavable linker. In contrast to SYD985 where the linkage is performed via the phenol of CBI analogue, MDX-1203 coupling was performed via aniline of the CBI analogue. The phenol of the CBI analogue in MDX-1203 was protected as a carbamate to also minimise off-target toxicity. The activation of MDX-1203 was also designed to be carried out in two steps, where the initial step was to enzymatically cleave the linker at the tumour site followed by the removal of the carbamate protecting group by carboxyesterases to give another level of safety and limit off target toxicity.

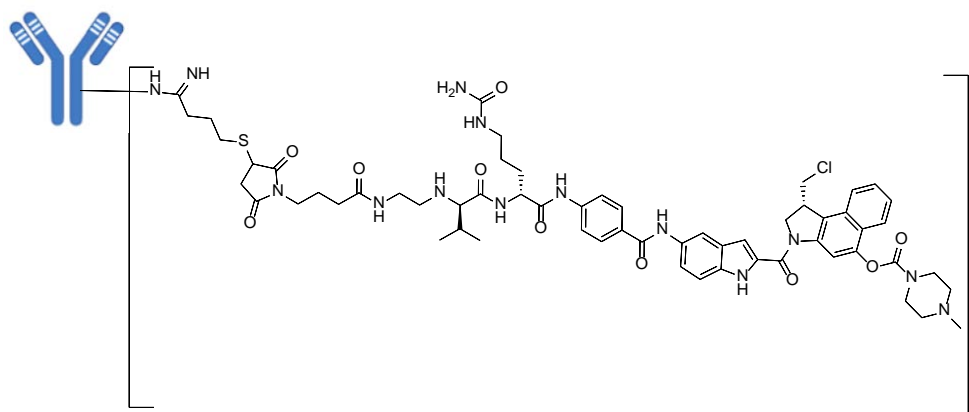


Figure 30: Structure of MDX-1203

1.4.12 Peptide Drug Conjugates (PDC)

As discussed above, the use of chemotherapy alone can be limited by the fact that dose escalation may not be possible due to related toxicity. The latter may be overcome by the use of a more selective delivery system of the cytotoxic agent such as the use of peptide drug conjugate and consequently allow the escalation with reduced systemic toxicity. Peptides continue to play an increasing role in the treatment of various disease such as cancer, viral and bacterial infections and autoimmune diseases¹¹⁵. The presence of peptide receptors on tumour cells is of increased interest as they can be used to target tumours selectively if the peptide involved can be conjugated with a cytotoxic agent. Some of the advantages associated with the use of peptides instead of an antibody in the delivery of cytotoxic agents include the fact that they are synthetically accessible, can reach the interior of large tumour, and can be cell permeable due to their small size in comparison to large antibodies. Antibodies may also be taken up non-specifically by the liver.¹¹⁶

To be able to generate an effective PDC, the choice of the peptide used is crucial. So far peptides used as part of PDCs can be subdivided into 3 parts based on their mode of action: cell targeting peptides (CTPs), cell penetrating peptides (CPPs) and micropinocytosis.¹¹⁷ CTPs are designed to bind to the receptor of the target cell followed with subsequent mode of action while CPPs are designed to take the drugs internally through the cell membrane.

A range of CPPs have been documented in the literature, such as trans-activating transcriptional activator (TAT), Antennapedia (Antp),¹¹⁸ transportan,¹¹⁹ polyarginines,¹²⁰ and model amphipathic peptide MAP.¹²¹ CPPs mechanism of action are not well elucidated ; however, the two described approaches are caveolae-mediated endocytosis (CvME) and classical clathrin-mediated endocytosis (CME) as illustrated in Figure 31. TAT peptide is derived from transcriptional activator protein encoded by HIV-1 and it is so far the most used CPP according to the literature.¹²² A study demonstrated that the use of doxorubicin-TAT was eight to ten times more potent than the use of doxorubicin against drug-resistant cells MCF-7/ADR due to resistance from energy-dependent drug efflux pump which pumps doxorubicin out of the cell.¹²³ Additional studies were conducted to try to understand the exact mechanism of action of TAT and demonstrated that

several cationic amino acids (6 arginine and 2 lysine) contained in the peptide played an important role. Later studies demonstrated that peptides with arginine rich residues had similar translocation property compared to TAT. To illustrate these findings further, an arginine oligomer conjugated to cyclosporine A was demonstrated to aid transport across the cutaneous barrier.¹²⁴

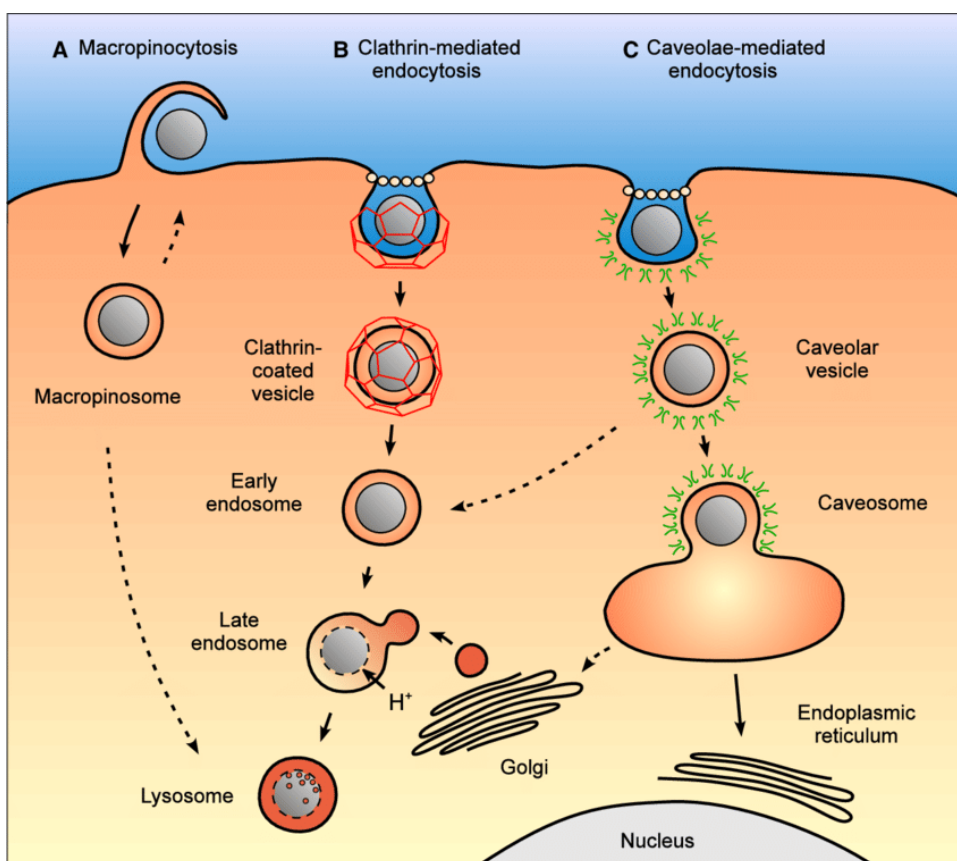


Figure 31: (a) Macropinocytosis, (b) clathrin-mediated endocytosis (CME) and (c) caveolae-mediated endocytosis (CvME) mechanisms.¹²⁵

Intracellular nanocarrier trafficking following macropinocytosis, clathrin-mediated endocytosis and caveolae-mediated endocytosis. a Macropinocytosis leads to the formation of a macropinosome, which is thought to eventually fuse with lysosomes or recycle its content to the surface. b Clathrin-mediated endocytosis of a nanocarrier leads to the formation of an early endosome, which is acidified and fuses with prelysosomal vesicles containing enzymes (in red) to give rise to a late endosome and finally a lysosome, an acidic and enzyme-rich environment prone to nanocarrier and drug degradation. Unless a lysosomal delivery is desired, strategies for a cytosolic drug delivery by this route will focus on the drug escape from the endosome as early as possible. c Caveolae-mediated endocytosis of a nanocarrier gives rise to a caveolar vesicle that can be delivered to caveosome, avoiding a degradative acidic and enzyme-rich environment.¹²⁵ Source: Nanocarriers' entry into the cell: relevance to drug delivery, Page:2881.

The focus of this thesis will be on CTPs, which have a mechanism comparable to that of ADCs that involves the peptide binding to the target receptor followed with PDC endocytosis to release the cytotoxic drug. Some of the well-

documented peptides used as CTPs include Bombesin analogues, Luteinizing Hormone-releasing Hormone (LHRH) Analogue Peptides, Somatostatin Analogue Peptides and Arginine-glycine-Aspartic Acid (RGD) Peptides.

Bombesin (BN) is a 14 amino acid peptide that is structurally homologous to gastrin-releasing peptide and neuromedin B. BN was originally isolated from the skin of *Bombinator bombina*, a European fire-bellied toad. BN has a related mode of action to gastrin-releasing peptide to stimulate G cells to release gastrin. The BN receptor has been associated with various types of cancers including prostate, pancreatic, breast and small cell lung cancer where an overexpression has been reported.¹²⁶ One of the initial assessments to demonstrate that BN can be used to build an effective PDC was carried in 2015 where a BN analogue (KGGCDFQWAV- β Ala -HFNIe) was conjugated to gold nanorods (GNR) and PEG.¹¹⁶ It was subsequently demonstrated that the BN conjugated peptide (GNR-BN-PEG) was more effective (ca. 99% decrease in tumour growth) compared to unconjugated GNR-PEG (ca. 50% decrease in tumour growth). Further assessment looked to assess a truncated C-terminal sequence of BN agonist RC-3095 and antagonist RC-3094 conjugated DOX and pyrrolino-DOX retrospectively using a glutamic acid spacer. Both PDCs demonstrated higher potency compared to Dox alone by 2-3 fold, against multiple cells expressing BN receptors such as MKN45 (human gastric cell lines) and PC3 (human prostate cell line).

Overexpression of the Luteinizing hormone-releasing hormone (LHRH) receptor on various cancers including ovarian, prostate and breast cancer attracted interest in the investigation of LHRH hormone. LHRH is a peptide that controls the release of luteinizing hormone (LH) and follicle-stimulating hormone (FSH) from the pituitary gland.¹²⁷ A PDC made of LHRH conjugated to camptothecin(CPT) (CPT-PEG-LHRH) was investigated on a human ovarian cancer cell line A2780 and demonstrated an increase in potency from nanomolar range to picomolar range when compared against CPT or CPTPEG alone.¹²⁸ Another LHRH PDC that was progressed as far as the phase III is the AEZ-108 also known as Zoptarelin Doxorubicin (Figure 32), made of [D-Lys6]LHRH conjugated to doxorubicin. AEZ-108 was assessed on multiple various cancers including ovarian, prostate, endometrial, breast and bladder cancers; however, despite hope of success, in 2017 AEZ-108 was demonstrated

motif (R/KXXR/K) at the C-terminal end followed with the binding to neuropilin-1 (NRP-1). Such binding results in cell/tissue penetration. Since the discovery of this process, iRGD peptide has been assessed for the delivery of cytotoxic agents such as doxorubicin to tumour cells and has been demonstrated to be effective in improving the tumour inhibitory effect and reduction of off-target toxicity.¹³⁴ Later studies compared the effect of conjugated iRGD-SSL-DOX against SSL-DOX on B16-F10, murine melanoma cells and demonstrated that iRGD-SSL-DOX had superior activity.¹³⁵

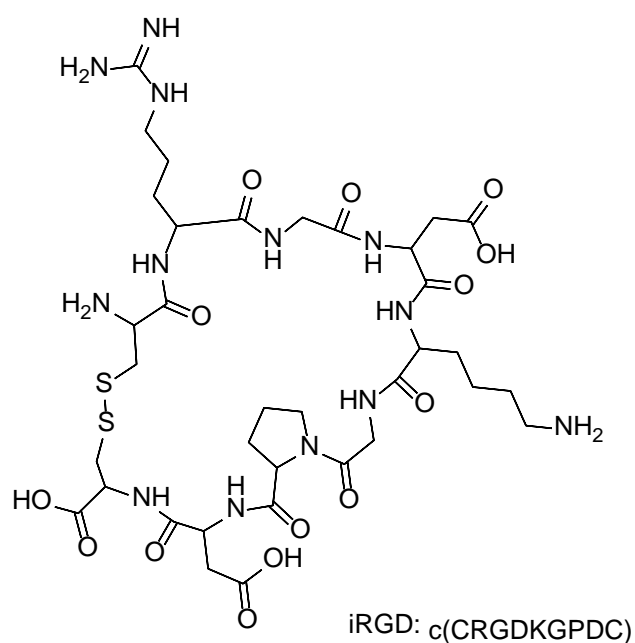


Figure 33: iRGD structure¹³⁶

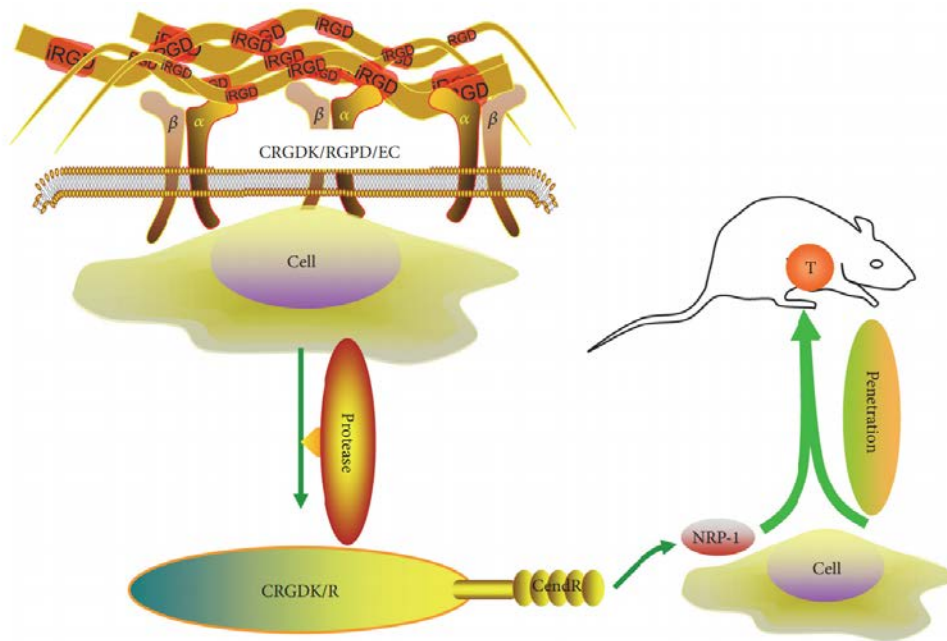


Figure 34: Multistep Binding and Penetration Mechanism of iRGD: First, the iRGD peptide accumulates at the surface and binds to $\alpha_5\beta_1$ integrin-expressing endothelial and other cells in tumours. Second, the iRGD peptide is cleaved by a cell surface-associated protease(s) to produce CRGDK which then exposes the cryptic CendR motif, RXXK/R, at the C terminus. Lastly, the CendR element then triggers binding to neuropilin-1, resulting in cell penetration. Adapted from Ref. ^{118,133}

The discovery of this mechanism has also revealed another pathway whereby the binding to the NRP-1 receptor triggers endocytic transcytosis and trans-tissue transport pathway which is believed to assist small molecule drug and nanoparticle delivery as demonstrated in (Figure 35).¹³⁶

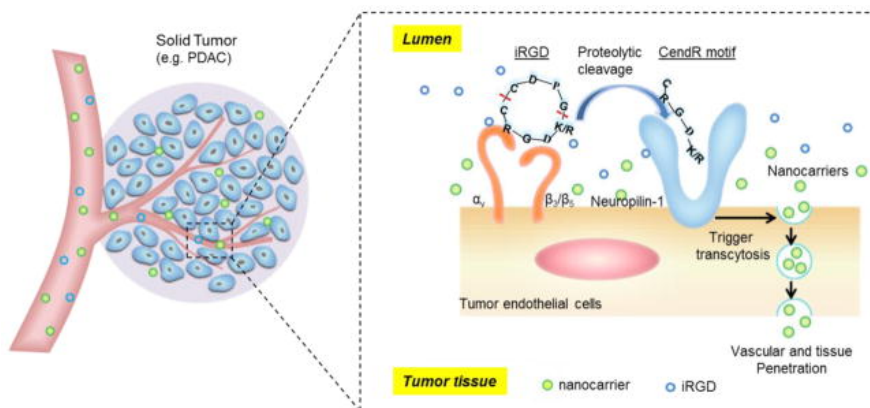


Figure 35: Schematic of the iRGD activated transcytosis mechanism for nanocarriers delivery in tumor.¹³⁶

**CHAPTER 2: SYNTHESIS OF THE CBI-GLUTAMIC ACID
CONJUGATE FOR SOLID PHASE SYNTHESIS**

2.1 Chapter 2 Aims

As part of the overall aim of this project, which is to selectively deliver highly potent cytotoxic CBI analogue warheads to melanoma tumours, Chapter 2 will describe approaches taken to synthesise CBI ready to be used as a building block during the Fmoc solid phase synthesis. This was achieved through the following steps:

- Synthesis of the CBI unit and subsequent conjugation to the carboxylic acid side chain of glutamic acid. This is to facilitate the incorporation of the complex as a building block anywhere in the solid phase.
- Synthesis of the DNA binding unit to be coupled to the CBI alkylating unit prior to coupling to glutamic acid. The inclusion of the DNA binding unit was designed to increase the potency.

2.2 Overview of the CBI building block

The first objective of this thesis was to synthesise a CBI alkylating unit that could be incorporated into Fmoc solid phase synthesis as a building block. Incorporation of the CBI alkylating unit into a peptide via an amide linkage is an important consideration as it allows the ability to maintain the amide linker. As discussed in the introduction, replacement of the amide with an alkene demonstrated a significant reduction of the potency by approximately 100 fold.¹⁰⁸ The CBI alkylating unit and the DNA binding unit both contain an amine that can be used as part of the conjugation; initial assessments were therefore carried out using the CBI alkylating unit without the DNA binding unit, followed by the use of the CBI conjugated to the DNA binding unit.

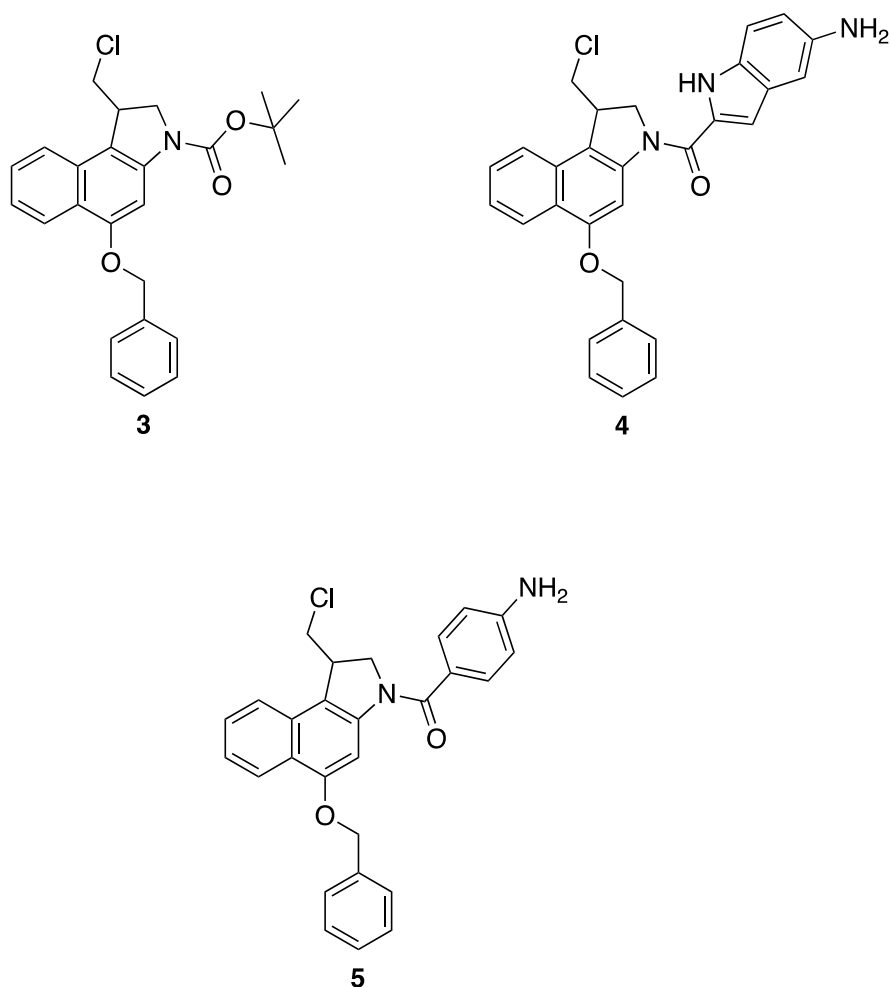


Figure 36: Structure of the CBI alkylating unit (3) and CBI alkylating unit bearing a DNA binding unit (4 and 5).

Coupling the CBI alkylating unit to a peptide on the solid phase directly is limited by the fact that its addition can only be carried out at the end of each peptide. Therefore, its coupling to glutamic acid via the carboxylic acid side chain increases diversity particularly as the CBI-Glutamic acid complex (Figure 37) would then behave like any other amino acid in solid phase synthesis.

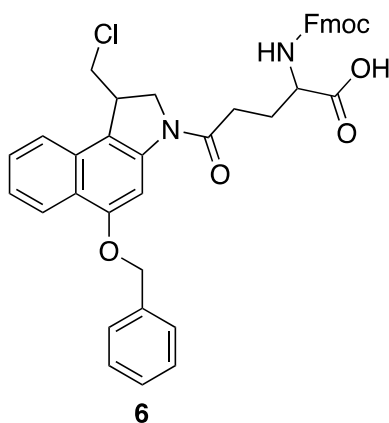


Figure 37: Structure of the CBI alkylating unit conjugated to glutamic acid (6)

In addition to this, the glutamic acid-CBI complex **6** can also be used in conjunction with added terminal valine-citrulline on the targeting peptide to make a more stable Glutamic acid-valine-citrulline linker. This linker has previously been reported to offer more stability against extracellular carboxylesterase and prevent premature release of the warhead compared to the use of valine-citrulline, preventing undesired side effects.⁸⁷ The synthesis of the warhead coupled to glutamic acid makes it easier to be incorporated anywhere as part of a peptide sequence and also offers the ability to potentially add more of such complex in one peptide sequence, potentially making the final compound more cytotoxic.

Chapter 2 also describes the synthesis and coupling of two DNA binding units, namely 5-amino-1H-indole-2-carboxylic acid and 4-aminobenzoic acid to glutamic acid. Both DNA binding unit were coupled to the CBI alkylating unit to assess if improvement of biological activity can be achieved. Coupling of the CBI alkylating unit to the DNA binding unit was followed with coupling of the complex to glutamic acid via the carboxylic acid side chain to achieve the same advantages as described above, generating **7** and **8** (Figure 38).

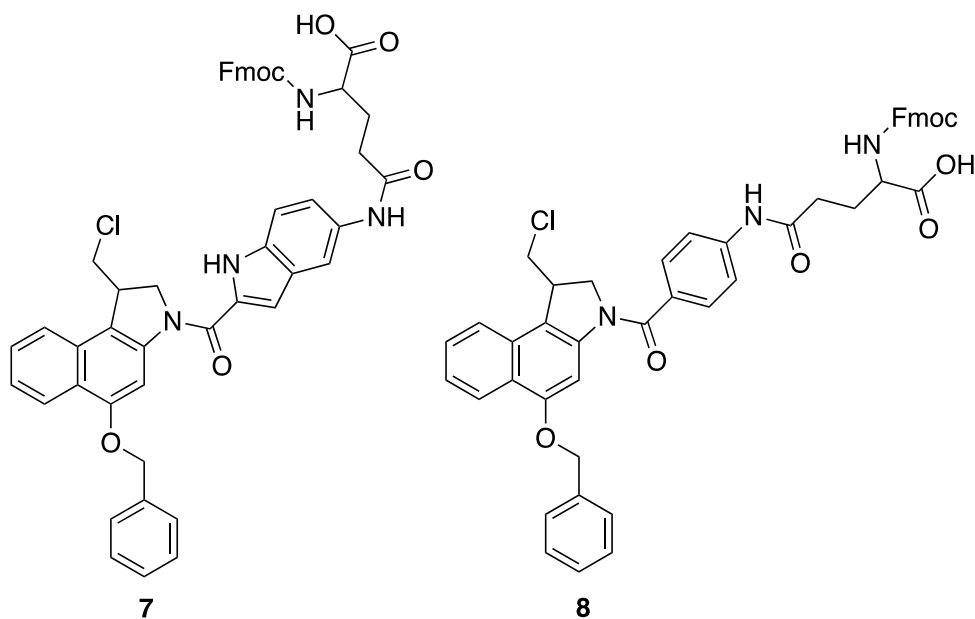


Figure 38: Structure of the CBI alkylating unit bearing a DNA binding unit conjugated to glutamic acid (**7** and **8**).

2.3 The synthesis of the CBI analogue

Several different approaches have been reported in the literature for the synthesis of the CBI analogues. Most approaches described for the synthesis of the whole CBI analogue have been subdivided into two parts, whereby the synthesis of the CBI DNA alkylating unit and the synthesis of the DNA binding unit were carried out separately followed by coupling both units together.

The approach of subdividing the entire synthesis into two parts, was also adopted here as it provided ease of synthesis and also allowed the ability to test the DNA alkylating unit alone before coupling to various DNA binding units to assess if activity can be improved.

2.3.1 Synthesis of the CBI alkylating unit

The synthesis of the CBI alkylating unit analogue has previously been described by Boger *et al.* using commercially available 1,3-dihydroxynaphthalene **9** as the starting material. Reaction of compound **9** with ammonia gave 1-hydroxy-3-naphthylamine, which after Boc-protection afforded Boc-protected amine **10**. This was subsequently benzyl protected at the hydroxyl group using benzyl bromide, followed by electrophilic bromination to afford compound **11**.¹³⁷

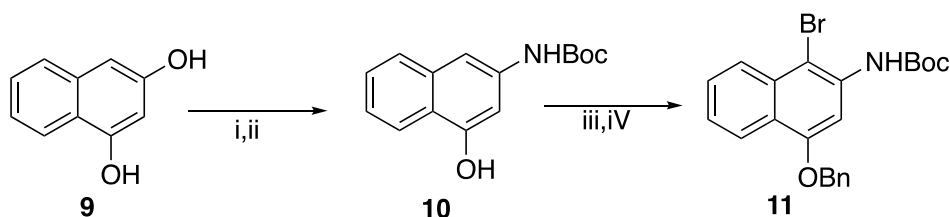


Figure 39: Synthesis of tert-butyl (4-(benzyloxy)-1-bromonaphthalen-2-yl) carbamate

Reagents and conditions: i. liquid NH₃, -78°C → 130°C, 1100 psi, 16 h; ii. Boc₂O, dioxane, 100°C, 4 h, iii. BnBr, K₂CO₃, n-Bu₄NI, dry DMF, N₂, 23°C, 8 h; iv. NBS, conc. H₂SO₄, THF, N₂, -60°C, 5 h.

After the above steps, various nitrogen alkylation approaches were assessed to synthesise the hydroxymethylindoline, initially reacting compound **11** with sodium hydride in the presence of propargyl bromide which was subsequently followed with radical cyclisation in the presence of

azobisisobutyronitrile (AIBN) and tri-butyltin hydride to afford compound **13**. Compound **13** was found to be unstable and subsequent hydroboration-oxidation gave the hydroxymethylindoline **14**. There was a complication encountered with this initial synthetic route relate to the synthesis of **13** as chromatographic purification afforded partial or complete isomerisation of methylenebenzindoline to 1-methylbenz[e]indole. In addition to this, the cyclisation reaction was demonstrated to be dependent on the concentration of tri-butyltin hydride and reaction time.

An alternative synthetic route to make hydroxymethylindoline was designed to overcome some of the initial challenges encountered as part of the functionalisation of the alkylating group. Compound **11** was alkylated with 1-bromo-3-methyl but-2-ene to afford compound **15**. Ozonolysis of **15** followed with mild reductive workup provided the aldehyde **16**. Wittig reaction of **16** with [(2-tetrahydropyranyloxy)-methylene] triphenylphosphorane afforded **17**; however, the reaction was very problematic and generated poor yields. Tri-butyltin hydride and AIBN were used to carry out the free-radical cyclisation of the vinyl ether to afford **18**. The deprotection of tetrahydropyranyloxy group gave the hydroxymethylindoline **14** which was subjected to substitution reaction to replace the hydroxy group with chlorine to afford **19**. In addition to a problematic Wittig reaction explained above, this synthetic route also requires careful adhesion to reaction condition during the ozonolysis step. Both synthetic routes require a final substitution of the hydroxy group with chlorine to afford the final alkylating product **3**.¹³⁸

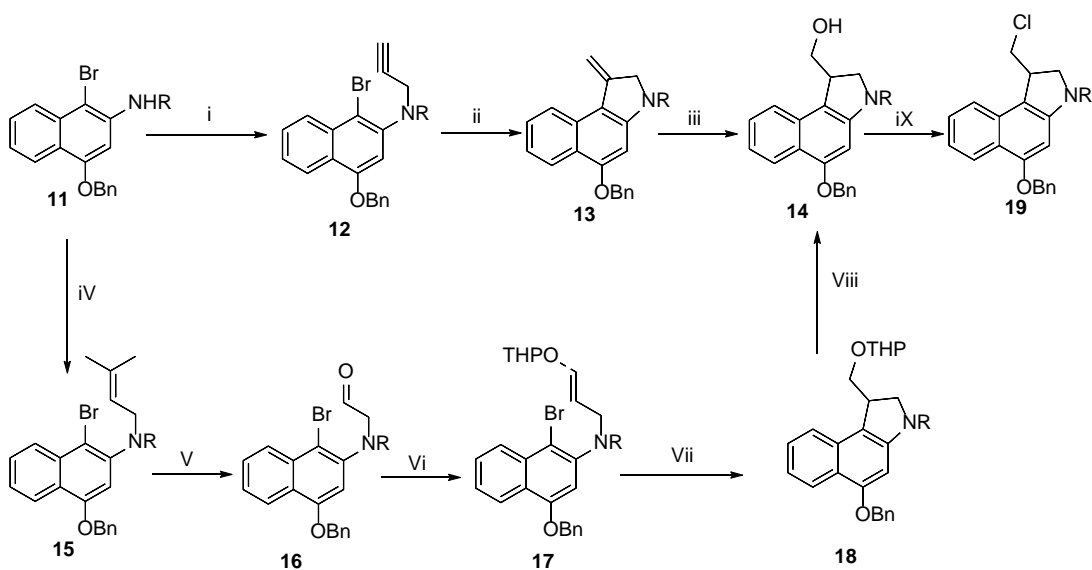


Figure 40: Post- functionalisation of CBI pyrrolidine ring.

Reagents and conditions: i. NaH, HC≡CCH₂Br, THF / DMF, N₂, 24°C, 3 h; ii. Bu₃SnH, AIBN, benzene, N₂, 80°C, 1 h; iii. BH₃.SMe₂, THF, Ar, 0-24°C, 3 h then H₂O₂, NaOH, 0→45°C, ~1 h; ix. Ph₃P, CCl₄, CH₂Cl₂, Ar, 24°C, 10 h. Pre- functionalisation of CBI pyrrolidine ring;; iv. BrCH₂CH=CMe₂, NaH, DMF, Ar, 0→24°C, 8 h; v. 3% O₃/O₂, Me₂S, CH₂Cl₂ / MeOH, -78 → 24°C, 3 h; vi. Ph₃PClCH₂OTHP, THF/HMPA, -78°C → 24°C, n-BuLi, 24 h; vii. Bu₃SnH, AIBN, benzene, Ar, reflux, 1 h, viii. MeOH, Amberlyst 15, 45°C, 6 h.

Given complications associated with described synthetic route various other alternative synthetic routes to make **19** were evaluated as one of the routes described in this thesis.

2.3.2 Proposed synthesis of the CBI alkylating unit (3)

The method described in this thesis was designed to overcome some of the challenges described with methods above including pre- or post-cyclisation functionalisation to introduce the hydroxy group. Figure 41 describes the proposed synthetic route.^{139,140}

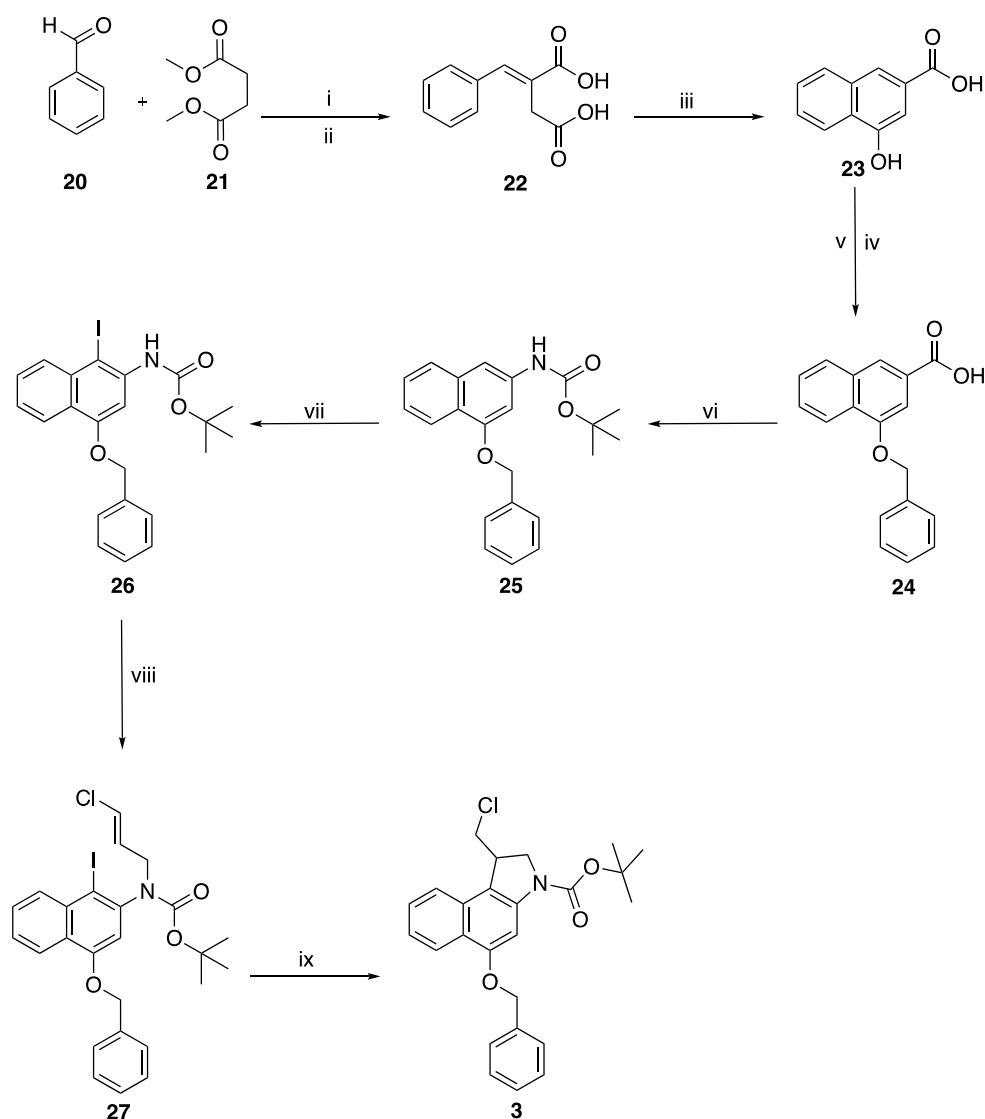
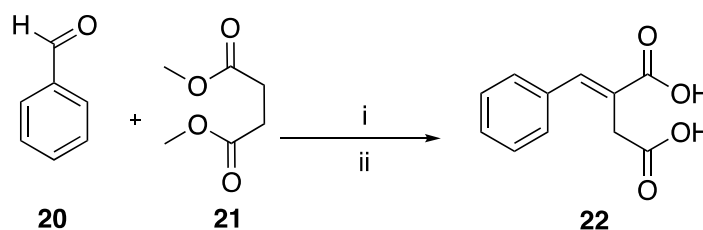


Figure 41: Synthesis of the CBI alkylating unit 3.

Reagents and conditions: i. tBuOK, tBuOH, 120°C, 3 h; ii. NaOH, MeOH, 80°C, 12 h; iii. H₂SO₄, RT, 3 h; iv. BnBr, K₂CO₃, RT, 12 h; v. NaOH, MeOH, 80°C, 5 h; vi. DPPA, Et₃N, PhMe, 4 h, 120°C→ RT; tBuOH, 10 h, RT→85°C; vii. NIS, H₂SO₄, DMF, 3 h, RT; viii. NaH, (E/Z)-1,3-dichloropropene, DMF, 1 h, 0°C→RT; ix. TTMSS, AIBN, PhMe, 90°C, 1 h.

2.3.3 Stobbe Condensation followed with ester hydrolysis



The synthesis of **3** began with two low cost commercially available starting materials. Benzaldehyde (**20**) and dimethyl succinate (**21**) were subjected to the Stobbe condensation reaction followed by ester hydrolysis to afford Benzylidenesuccinic acid (**22**).

The Stobbe condensation reaction was discovered by Hans Stobbe in 1893 while he was attempting to react acetone with diethyl succinate treated with sodium ethoxide. Stobbe did not obtain a diketo compound as expected through a previously described Claisen condensation but instead the main product was teraconic acid.¹⁴¹ The Claisen condensation mechanism shown in Figure 42, is initiated by the deprotonation of the α -proton by a strong base, forming an enolate anion. The enolate subsequently undergoes a nucleophilic attack on the carbonyl of the ester leading to the elimination of the alkoxy group. Eliminated alkoxide goes on to remove the newly formed α -proton to afford another enolate anion, which is later neutralised by the addition of the aqueous acid.

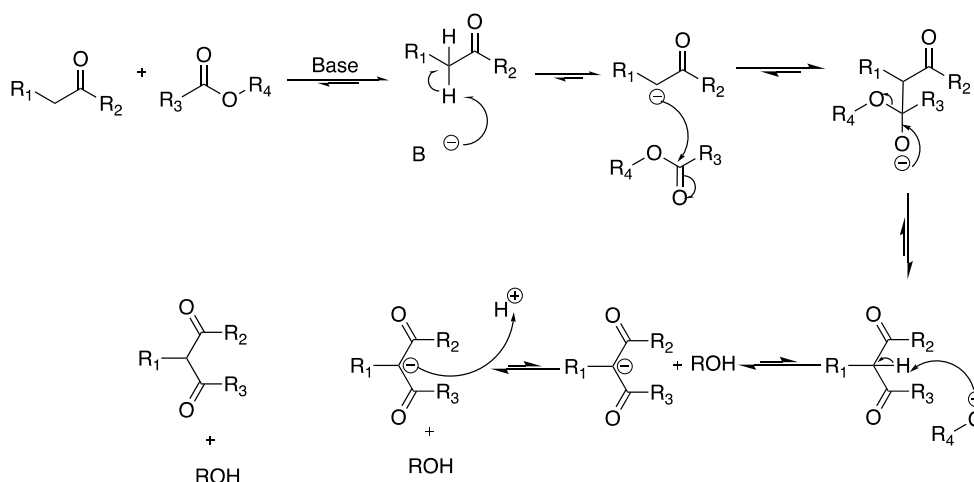


Figure 42: Claisen condensation

In contrast to the Claisen condensation, the Stobbe condensation does not require a strong base and furthermore it has been reported to not be solely driven by the α -carbon deprotonation but also the juxtaposition of a carbethoxy group facilitating the formation of the intermediate ring. However, similarly to the Claisen condensation, the Stobbe condensation is also initiated by the deprotonation of the α -proton of the dimethyl succinate using a base such as potassium tert-butoxide to afford the dimethyl succinate enolate anion. The enolate anion subsequently attacks the carbonyl of benzaldehyde leading to the formation of an active oxocarbon anion which goes on to attack the carbonyl of the dimethyl succinate forming a less restrained five membered ring and the elimination of the methoxy group. The eliminated methoxy group further acts as a base to remove a proton from the alpha carbon leading to the ring opening and the formation of desired paraconic ester **22**¹⁴¹.

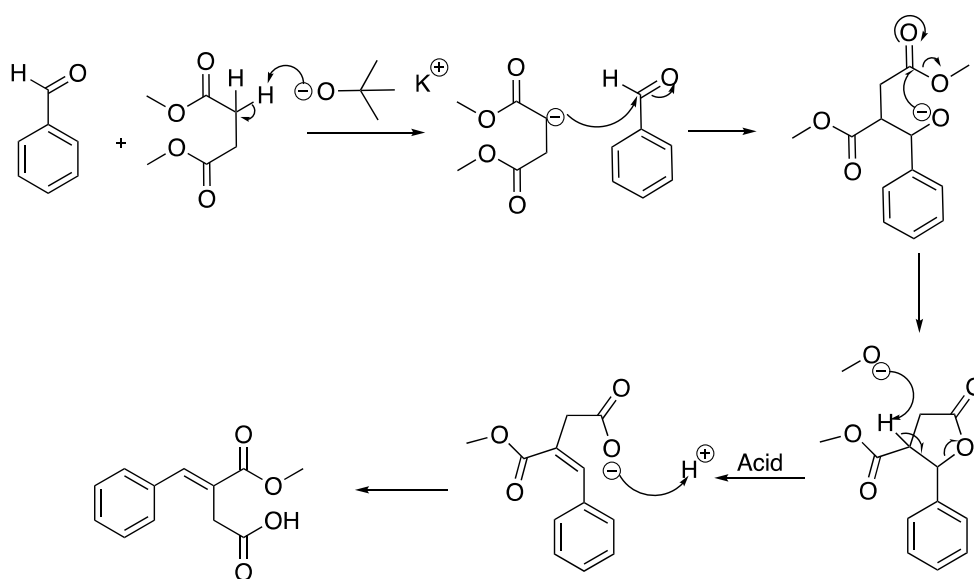


Figure 43: Mechanism for Stobbe condensation

In order to achieve the desired benzylidenesuccinic acid product, the ester was hydrolysed using NaOH in methanol. The mechanism of this hydrolysis is initiated by the attack of the hydroxide ion on the carbonyl, breaking the π bond to form a tetrahedral intermediate with an anionic oxygen. The collapse of the intermediate driven by the anionic oxygen reforms the carbonyl and leads to the loss of the methoxide ion. The methoxide ion acts as a base to

further deprotonate the newly formed carboxylic acid, which is later restored through the acid work up.

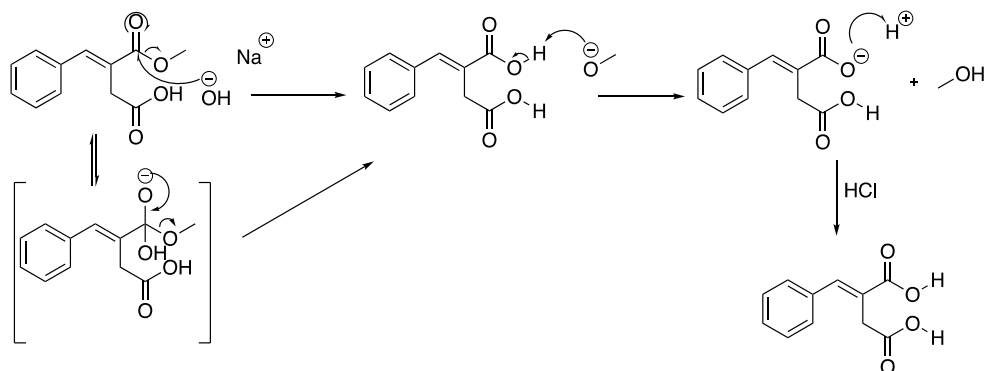


Figure 44: Mechanism for Ester hydrolysis

The final product was confirmed by ¹H NMR whereby the 5 aromatic protons corresponding to benzyl were observed overlapping at 7.38-7.44 ppm and a singlet proton downfield at 7.74 ppm corresponded to the carbon between the benzyl and succinic acid. This proton is further downfield because of the π bond interaction with the aromatic benzyl and the deshielding effect of the neighbouring carboxylic acid. A singlet corresponding to two protons from the aliphatic carbon of the succinic acid were also observed up field at 3.37 ppm due to the electron withdrawing effect of the neighbouring carboxylic acid. The two acidic protons corresponding to the succinic acid were at 12.55 ppm. Mass spectrometry assessment was also used to confirm this product where the parent product was seen mainly as a sodium adduct ([M+Na]⁺) with m/z of 229.05 and in addition to this other molecular fragments corresponding to the loss of a hydroxyl (189.05), the loss of one carboxylic acid (161.06), the loss of both carboxylic acids (117.07) were also observed (Figure 45). The yield of this two-step reaction was relatively poor at 44% which was partially attributed to the final crystallisation step where the final benzylidenesuccinic acid product was perhaps lost in the solvent used during crystallisation (hexane/ethyl acetate). This was further confirmed by leaving the solvent longer which allowed for additional recovery of the benzylidenesuccinic acid and improving the yield slightly to 52%.

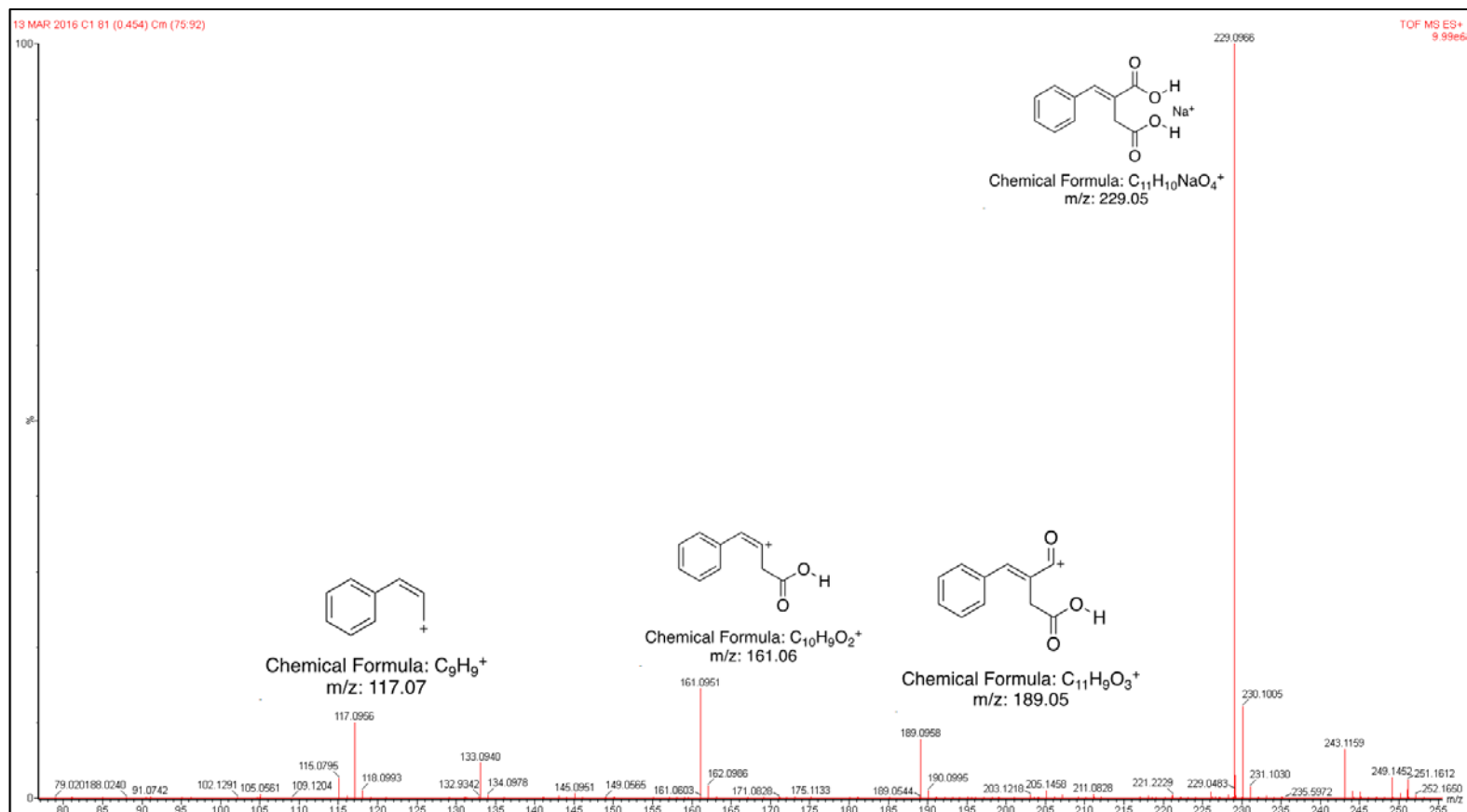
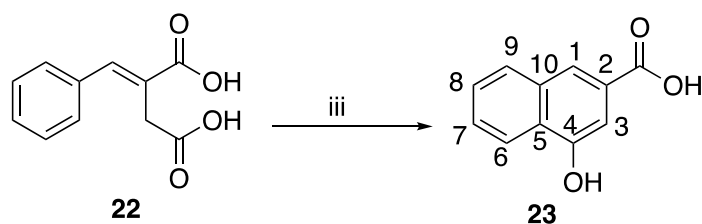


Figure 45: Mass spectrometry data for compound 22 also showing corresponding fragments

2.3.4 Sulphuric acid promoted intramolecular cyclisation



The next step of this synthesis involved intramolecular cyclisation catalysed by sulphuric acid to make the hydroxyl naphthalene carboxylic acid. As this reaction was only catalysed by sulphuric acid any impurity in the reaction could have potentially generated many other side reactions, therefore, in order to avoid this, the starting material had to be pure and also dry to achieve good yields. The mechanism of this reaction as depicted in Figure 47 is initiated with the protonation of the oxygen of the carbonyl instead of the hydroxyl oxygen because the C=O oxygen is more basic due to its partial negative charge generated from its resonance (Figure 46).

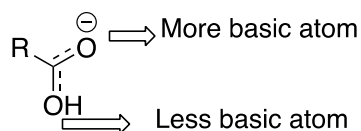


Figure 46: Carboxylic acid resonance

Protonation of the carbonyl makes it a much better electrophile for the Pi bond to attach forming a carbocation intermediate in the aromatic ring which requires stabilisation. Deprotonation of the benzene ring by hydrogen sulfate anion leads to the restoration of the aromaticity and stabilisation. Further protonation of the oxygen and removal of a proton by sulfate anion leads to the elimination of water and formation of naphthalene (Figure 47).

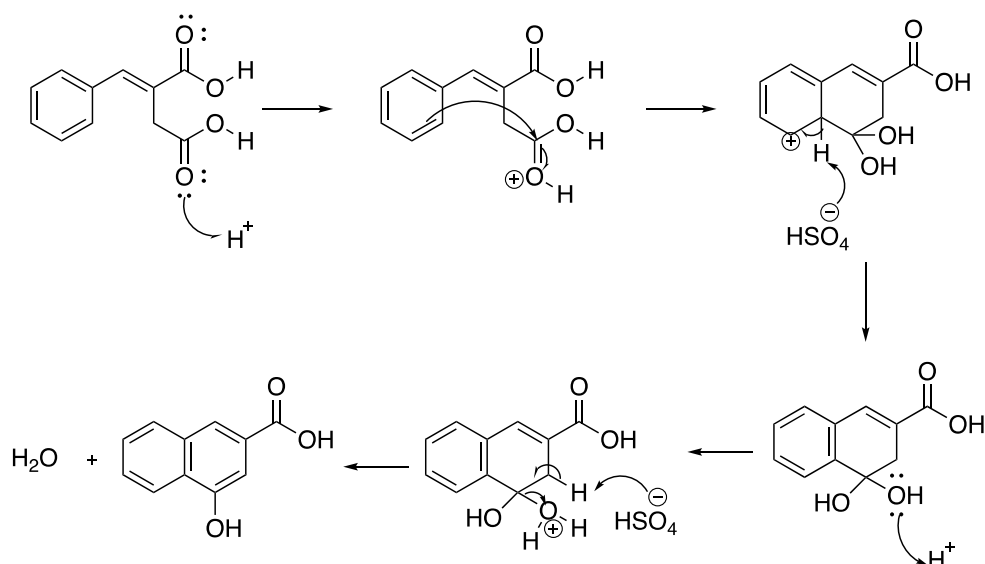
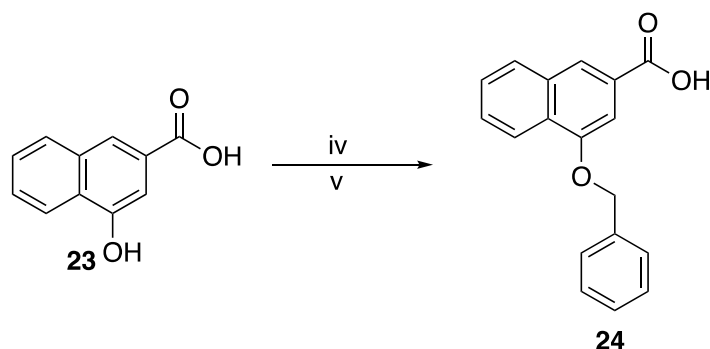


Figure 47: Mechanism for acid catalysed intramolecular cyclisation

Successful synthesis of hydroxyl naphthoic acid product was confirmed by 1H NMR, where the aliphatic protons at 3.37 ppm corresponding to the carbon C3 of succinic acid in the starting material were no longer present and a new signal for an aromatic proton at 8.61 ppm was apparent, corresponding to the C3 proton. The aromatic proton at C1 is also deshielded by neighbouring carboxylic acid and it is observed at 8.08 ppm. The proton on the C6 is also deshielded by the oxygen and is observed at 8.02 ppm. The remaining three aromatic protons are observed in the aromatic region 7.35-7.58 ppm. Mass spectrometry assessment was also used to confirm this product which revealed the desired m/z of 189.06 and an additional fragment at 171.04 corresponding to the loss of a hydroxyl group. This reaction afforded a very good yield of 92%.

2.3.5 Benzyl protection and ester hydrolysis.



The previous cyclisation as depicted in section 2.3.4 led to the formation of **23** with a free carboxylic acid and the hydroxyl group. The presence of the free hydroxyl group would have resulted in interference in the Curtius rearrangement reaction as will be explained in the next section 2.3.6. Therefore, protection of the hydroxyl group with benzyl followed by the Curtius rearrangement was carried out. On the other hand, benzyl protection was also not selective to the hydroxyl group as it also protected the acid by forming an ester, which was subsequently hydrolysed with sodium hydroxide to reform the acid ready for the next step.

Benzyl protection of the starting material occurred both on the carboxylic acid and the phenol via S_N2 nucleophilic substitution reaction. This protection is initiated by the deprotonation of the acid in the presence of K_2CO_3 as the carboxylic acid is more acidic than the phenol. Generated carboxylate acts as a nucleophile to attack the electrophilic centre of the carbon linked to the bromine triggering the loss of bromide as a good leaving group. Benzyl bromide was added in 2 equivalents in this reaction step to make sure that the phenol is also protected. In this case K_2CO_3 also acts as a base to deprotonate the phenol, generating the phenoxide ion. The phenoxide also subsequently acts as a strong nucleophile to attack the electrophilic centre of the carbon linked to bromide triggering the loss of the halogen as a good leaving group. Following the benzyl protection of both phenol and carboxylic acid, the newly formed ester bond between the acid and benzyl was cleaved to reform the carboxylic acid ready for the next step. The mechanism of this hydrolysis proceeded as described in section 2.3.3, Figure 44.

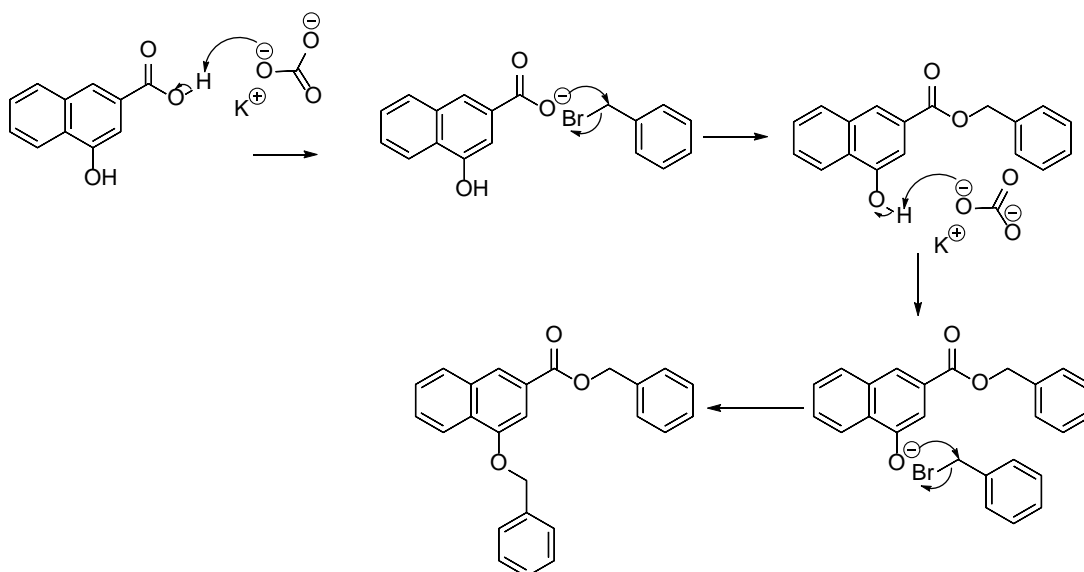
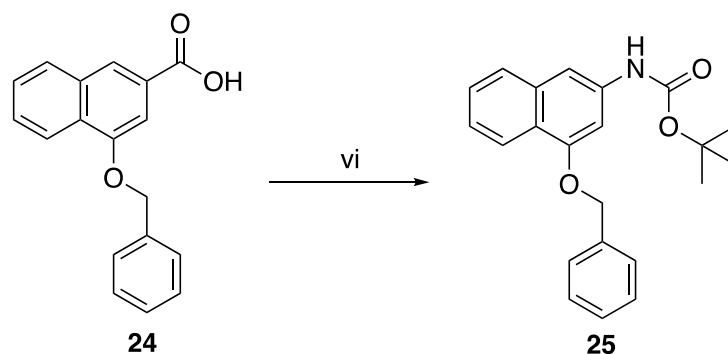


Figure 48: Mechanism for benzyl protection

Completion of this reaction to make the benzyloxy-naphthoic acid, a pale yellow solid, was confirmed by ^1H NMR. The benzyl was confirmed by an additional five protons in the aromatic region in addition to the six aromatic naphthalene protons making eleven protons from 7.33 ppm to 8.28 ppm in comparison to the starting material. An addition crucial singlet that correspond to the two aliphatic hydrogens of the benzyl was observed at 5.38 ppm. These two protons are further downfield due to the electron-withdrawing effect of the neighbouring naphthoxide.

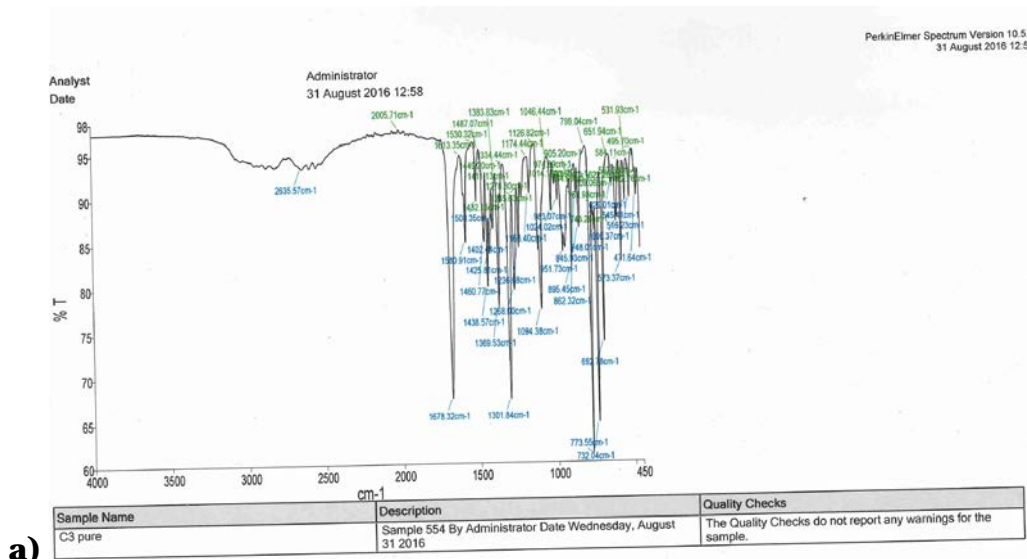
2.3.6 Curtius rearrangement



The Curtius rearrangement reaction to form a Boc protected amine from a carboxylic acid was initially attempted on the hydroxyl naphthoic acid **23**. However, the product of this reaction generated a poor yield and other side products. This may have been as a result of the phenol reacting with the isocyanate to make other side products. After this attempt the reaction was repeated using benzyl protected naphthol **24**.

The Curtius rearrangement has been extensively studied following its discovery by Julius Wilhelm Theodor Curtius in 1885, who demonstrated that acyl azides derived from the reaction between carboxylic acids and sodium azide underwent decomposition at higher temperature to afford isocyanates and nitrogen. The isocyanate intermediate has since been demonstrated to generate a range of functionalities including amines, carbamates and ureas by reacting with water, alcohol and amine respectively. One safer method that avoids the isolation of explosive acyl azide is to directly convert the carboxylic acid to the isocyanate using diphenylphosphoryl azide (DPPA) in a one pot reaction. The mechanism of this reaction (Figure 16) starts with the deprotonation of the acid by the base. The carboxylate acts as a nucleophile to attack the DPPA and form the anhydride of carboxylic acid/phosphoric acid intermediate and eliminate the azide. Eliminated azide anion in turn acts as nucleophile and reacts with the carbonyl of the anhydride eliminating phosphoric acid and affording an acyl azide. The acyl azide undergoes rearrangement at higher temperature to make the isocyanate and eliminate nitrogen gas. This reaction was initially carried out as previously

described by Zhang¹⁴² and also by Elgersma et al¹¹⁴. In our hands, however, starting with compounds **24**, when the reaction was checked on TLC it revealed multiple products and upon assessment of the product mixture using IR it was noticed that there was a peak at 2142.75 cm⁻¹ (Figure 49) which corresponded to the acyl azide that had failed to undergo the rearrangement to make the isocyanate. This was possibly due to either a faulty thermocoupling device and therefore not achieving the required temperature for the rearrangement to take place or this may have been due to the fact that the temperature may have not been evenly distributed throughout the whole flask. This reaction was successfully repeated on a smaller scale making sure to reach the desired temperature of 85°C.



b)

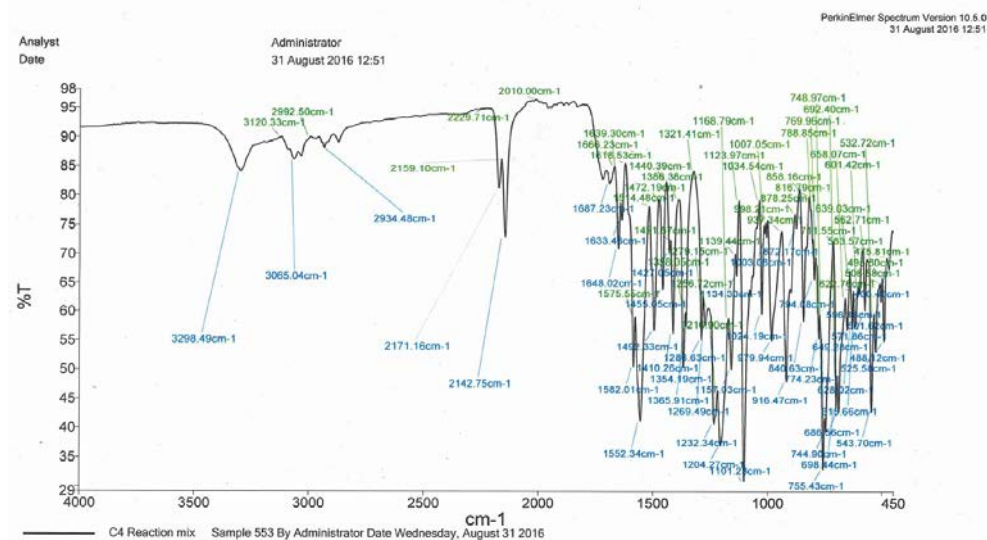


Figure 49: a) IR spectrum data for compound **24** and of (b) the crude mixture post failed rearrangement reaction showing the azide peak

The mechanism for this Curtius reaction to form either the carbamate, urea or amine is initiated by the positive charge on the NCO carbon of the isocyanate, which is generally enhanced in the presence of electron-withdrawing substituents. In the example described here, the negative charge is delocalized into the π electron of the naphthol ring system leading to the increase of the positive charge on the NCO carbon atom. The positively charged NCO carbon of the isocyanate group is attacked by the nucleophilic oxygen of the alcohol

group or nitrogen in the case of an amine. The negatively charged nitrogen of NCO also subsequently removes a proton from the alcohol or the amine leading to the formation of carbamate or urea respectively. In the presence of water, isocyanate groups react to form unstable carbamic acid intermediates which subsequently decompose to amine releasing carbon dioxide. The amine product can further react with excess isocyanate to form urea. The latter emphasize the importance of making sure that this reaction is carried out in a dry environment to avoid undesired side products.

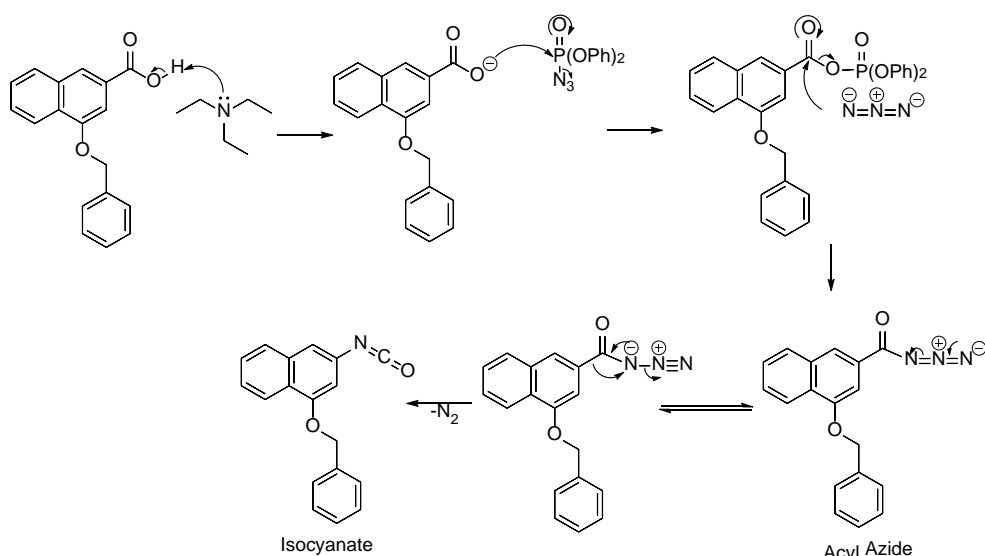


Figure 50: Mechanism for Isocyanate formation

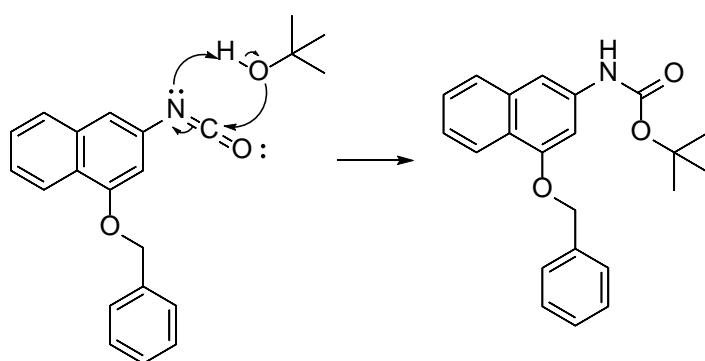


Figure 51: Mechanism for Isocyanate reaction with alcohol (butanol)

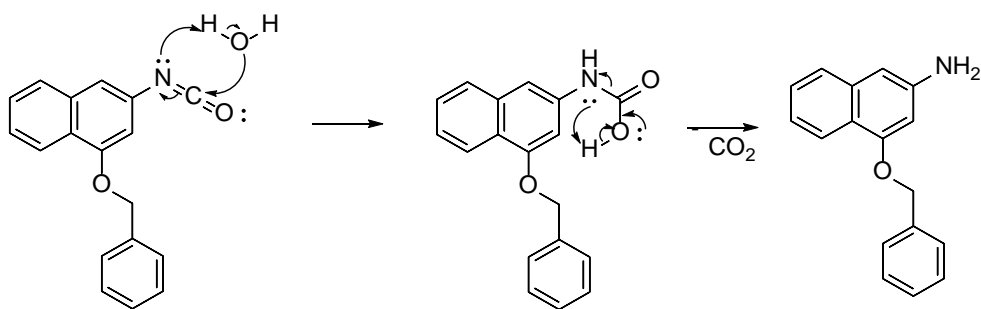


Figure 52: Mechanism for Isocyanate reaction with H₂O

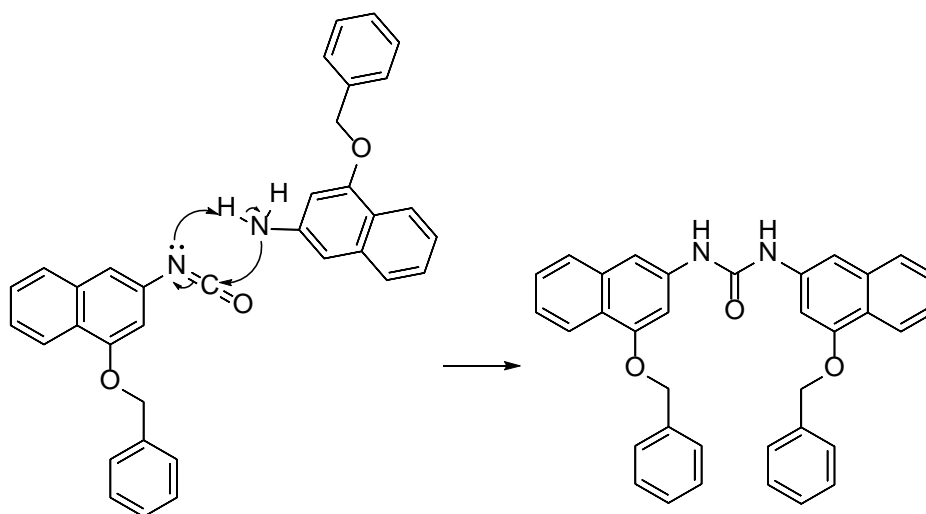
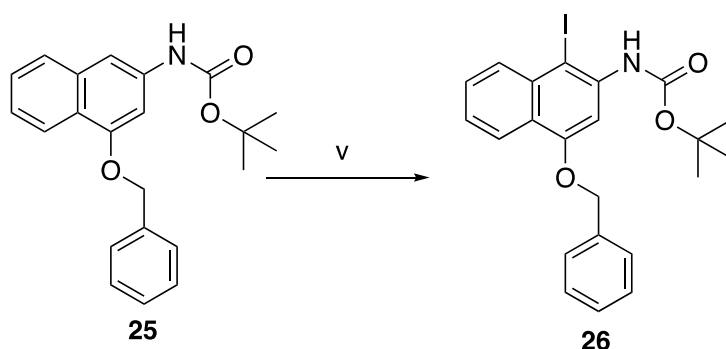


Figure 53: Mechanism for Isocyanate reaction with amine product resulting from the presence of water

This reaction step was also demonstrated to generate improved yield of 46% only when using less than 6 g of the starting material, scaling up the reaction to 12 g decreased the yield significantly to less than 20% yield. This step was adapted from the paper published by Tietze et al. where less than 6 g of starting material was used and the yield was comparable to the yield obtained here using 6 g (52%).¹⁴⁰

The tert-butyl (4-(benzyloxy) naphthalen-2-yl) carbamate product **25** was confirmed by ¹H NMR, whereby the broad singlet at 13.01 ppm in the starting material corresponding to the acid proton was no longer present. This was substituted by the appearance of a new nine protons singlet downfield at 1.55 ppm corresponding to Boc protecting group and another broad singlet at 6.59 ppm corresponding to the amine proton. The product was also assessed by mass spectrometry, which revealed the expected mass as a sodium adduct and potassium adduct with m/z of 372.15 and 388.12 respectively.

2.3.7 Iodination



The tert-butyl (4-(benzyloxy) naphthalen-2-yl) carbamate **25** was subsequently iodinated to facilitate the following 5 exo-trig-cyclisation step. The iodine carbon bond is the weakest bond in comparison to other carbon-halogen bonds in the order of $\text{F} > \text{Cl} > \text{Br} > \text{I}$. Therefore, the use of iodine would be preferred compared to the earlier use of bromine as described in the synthesis by *Boger et al.*¹⁴³ which was later substituted with the use of iodine in subsequent methods.^{137,144} The iodination was achieved by treating the starting material with N-iodosuccinimide (NIS) in DMF, catalysed by H_2SO_4 at room temperature to afford the product with 75% yield.

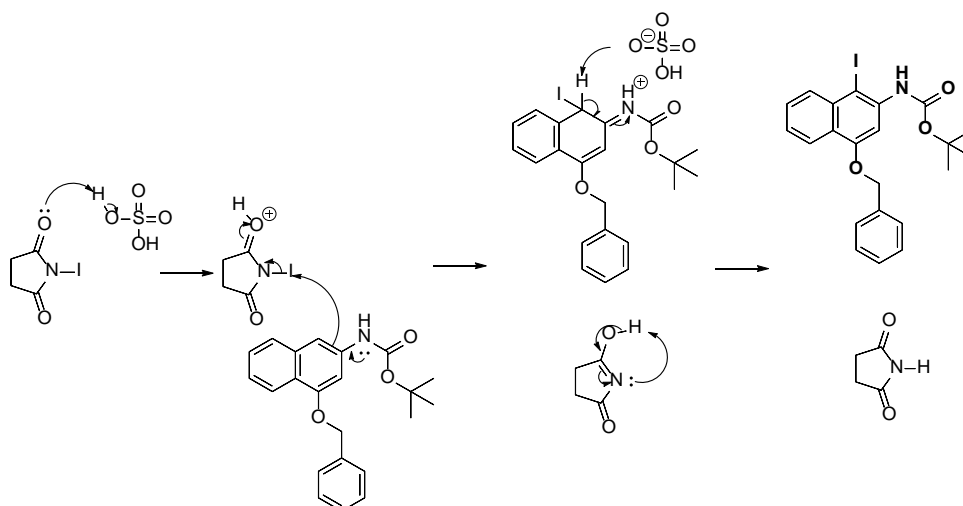


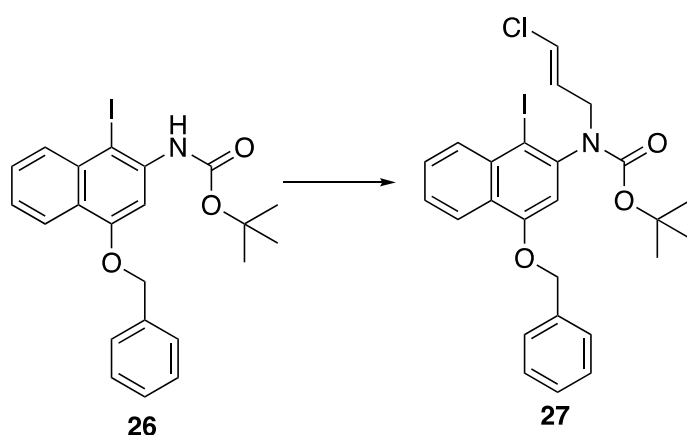
Figure 54: Iodination Mechanism

The mechanism of this reaction as described in the Figure 54 is an electrophilic aromatic substitution where NIS serves as a source of electrophilic iodine. The activation of NIS by acid catalyst such as H_2SO_4 leads to the protonation of the

carbonyl oxygen, consequently resulting in the cleavage of the nitrogen iodine bond and the loss of electrophilic iodine. The electrophilic iodine is subsequently attacked by the nucleophilic aromatic electrons in the ring. The lone pair from the nitrogen of the carbamate is donated to the ring resulting in increased nucleophilicity of the ortho position and also favouring the regioselectivity of iodination at this position. In order to restore the naphthalene aromaticity the bisulfate anion removes a hydrogen, reforming sulphuric acid to catalyse the next reaction and also form the desired iodinated product. One may argue that the carbon C3 is more nucleophilic than the C1 carbon as it is between two electron donating groups, oxygen from the ether and nitrogen from the amine. However, the iodination at this position may be prevented by steric hindrance due to the presence of the benzyl group and the Boc protecting group.

The iodination was confirmed by the disappearance of one proton in the aromatic region corresponding to C1 and a downfield shift of the neighbouring protons including the proton corresponding to the carbamate due to the electron withdrawing effect of the iodine. The product was also assessed by mass spectrometry which revealed the expected mass as a sodium adduct and potassium adduct with m/z of 498.05 and 514.02 respectively.

2.3.8 N-Alkylation



In order to synthesize the required indoline ring, the next step was the alkylation of the carbamate, which was achieved using 1,3-dichloropropene in the presence of a strong basic solution such as sodium hydride to deprotonate the amine. Prior to the use of NaH, potassium tert-butoxide was used but produced poor yields. The reaction proceeded more efficiently with the use of NaH.

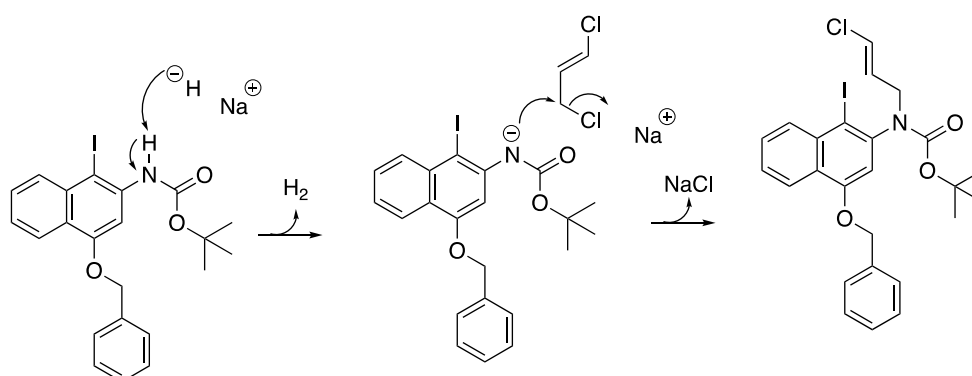
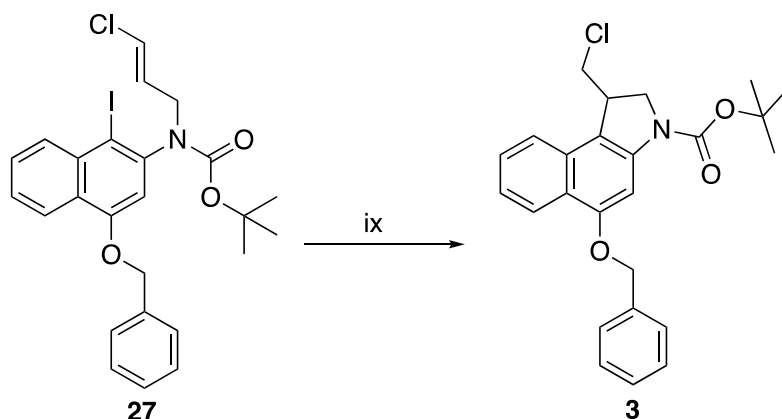


Figure 55: Alkylation Mechanism

This alkylation reaction proceeded via an S_N2 nucleophilic substitution whereby deprotonation of the amine by sodium hydride provides the nucleophile that subsequently attacked the electrophile – the polarised sp³ hybridised carbon of the C-Cl bond releasing the chloride. The first step deprotonation reaction of the carbamate was carried out on ice due to the thermal instability hazard associated with the use of NaH, especially when carrying out the reaction at a large scale.^{145,146} Proton removal by NaH is evident in the reaction due to H₂ gas release. This step was followed by a dropwise addition of 1,3-dichloropropene. The reaction temperature was slowly increased to room

temperature. This reaction used a mixture of *E*- and *Z*- 1,3-dichloropropene because following the radical cyclisation in the next step to form the indole the double bond is removed. Hence, the product of this alkylation reaction was observed as two spot on the TLC. The crude product was purified using automated flash chromatography, which was unable to separate the two isomers as they eluted very close together. The consequence of this was that the proton NMR was difficult to interpret but the product was further confirmed using mass spectrometry, where the mass corresponding to desired product was obtained and in addition a chloride isotope pattern was observed.

2.3.9 Radical cyclisation



Following the previous iodination and N-alkylation reactions, the 5-*exo-trig* radical cyclisation was ready to be performed. This radical cyclisation was carried out using AIBN and TTMSS in toluene. This reaction was performed in dry conditions under nitrogen, also making sure to degas the reaction mixture to remove any reactive oxygen as it can interfere with radical reaction. This reaction was also carried out at a dilute concentration to favour intramolecular reaction instead of intermolecular reaction.

The mechanism of this 5-*exo-trig* radical cyclisation (Figure 56) is initiated by AIBN radical. After degassing, the reaction mixture is heated causing decomposition of AIBN leading to the release of nitrogen and the formation of two isobutyronitrile radicals that acts as radical initiators. These isobutyronitrile radical can either react with themselves to form tetramethylsuccinonitrile, while other isobutyronitrile radicals go on to serve as radical initiators for the 5-*exo-trig* radical cyclisation. This initiation phase is followed by the propagation phase whereby the isobutyronitrile radical removes a hydrogen from TTMSS forming a silane radical. The silane radical subsequently removes the iodide from the starting material and this iodide removal is enhanced by the weakness of the iodide-carbon bond, to make the aryl radical. The aryl radical initiates the intramolecular cyclisation by attacking the less substituted carbon of the alkene. The attack to the less substituted carbon is favoured by the fact that the formation of a new radical is more stable at the most substituted carbon due to induction

hyperconjugation, hence the selectivity for the 5-exo-trig cyclisation. The resulting radical attacks TTMSS in the termination phase to remove a hydrogen and form the desired final product but also make additional silane radical, to further the radical propagation phase.

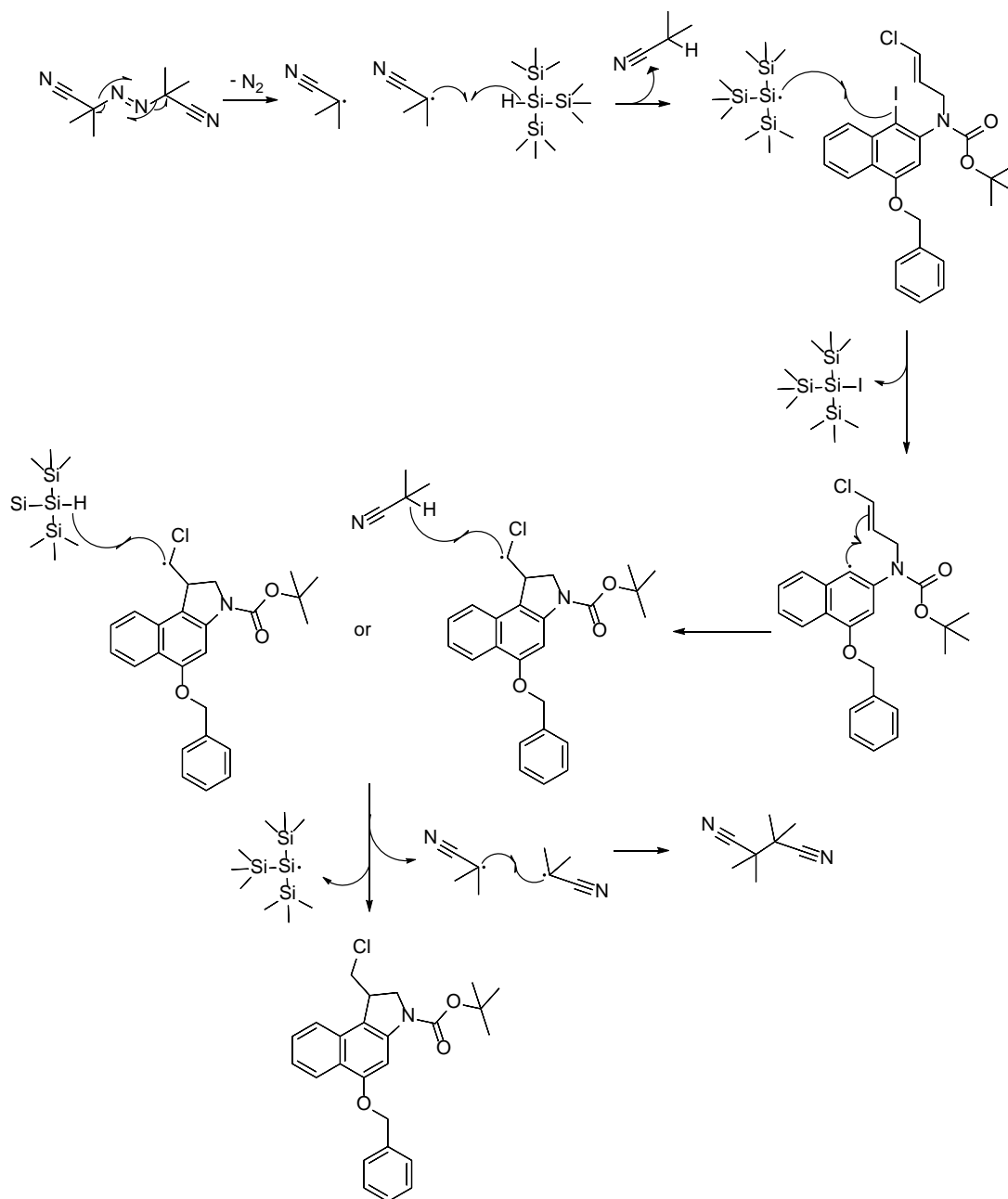


Figure 56: Radical cyclisation Mechanism

The desired product was confirmed by both the ^1H NMR spectrum and mass spectrometry. As discussed in section 2.3.8; having a mixture of E and Z isomers made it very hard to interpret the ^1H NMR, but this would be

simplified following radical cyclisation as the alkene carbons have been reduced to sp³. However, chirality in the final product was maintained as the aryl radical can attack either face of the alkene forming a racemic mixture. ¹H NMR were compared to that reported by Tietze et al.¹³⁹ and demonstrated to be comparable. This product was also assessed by mass spectrometry, where the mass corresponding to desired product was obtained as a sodium adduct and in addition a chlorine pattern was observed. Further assessment of the mass spectrum data also demonstrated fragments from the parent compound (Figure 57) which enhanced confirmation that desired compound **3** was synthesised.

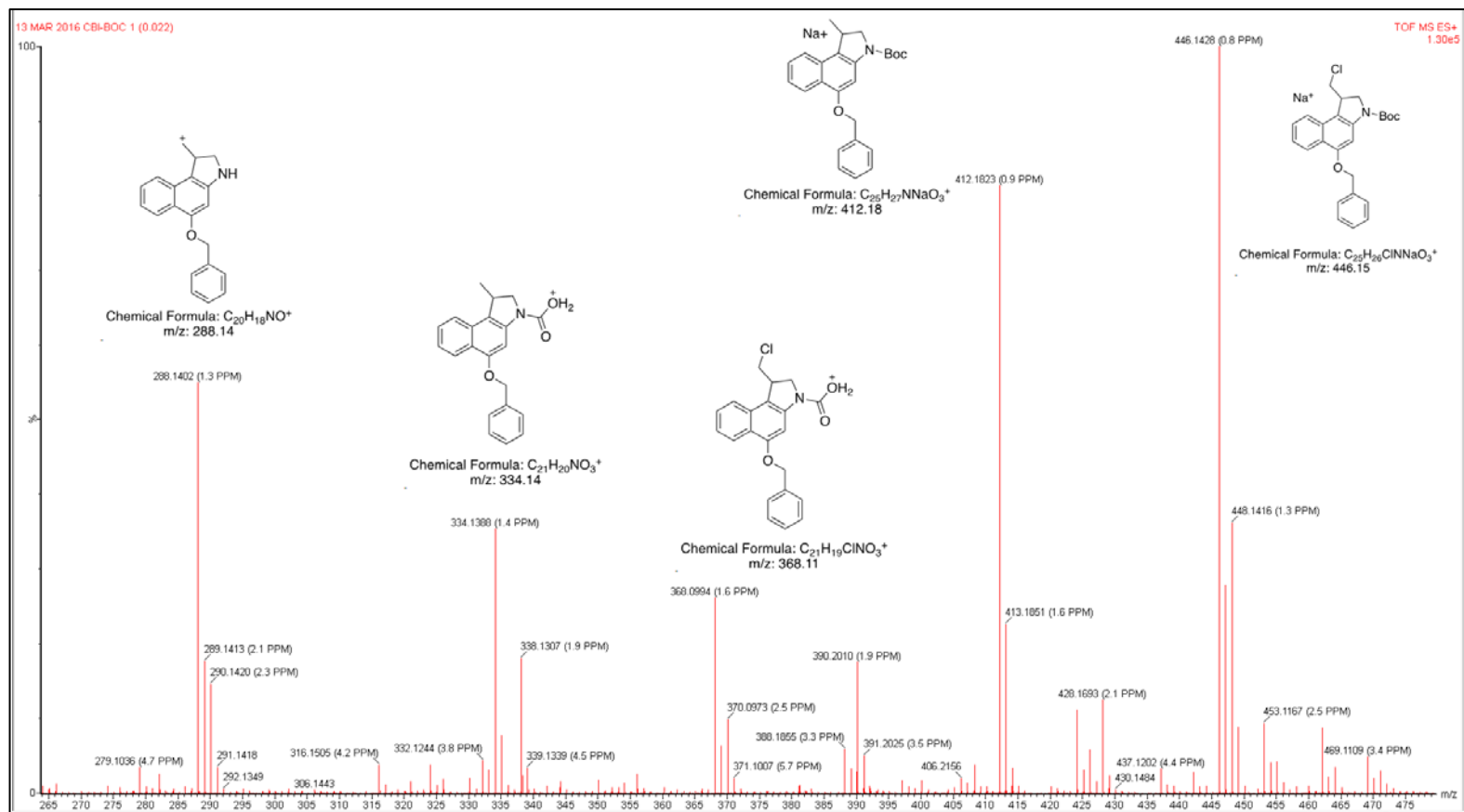


Figure 57: Mass spec data for compound 3 and corresponding fragment

2.4 CBI conjugation to carboxylic acid side chain of glutamic acid.

Completion of the CBI synthesis led to the question of how it would be incorporated into the targeting peptide or protein. As previously discussed conjugating CBI to the carboxylic acid side chain of the glutamic acid provided several advantages including the ability to behave as an amino acid following conjugation and the ability to be incorporated anywhere in the peptide chain.

The Boc deprotection reaction was carried out using commercially available 4 M HCL in dioxane. Boc deprotection mechanism of the indoline proceed by initially protonating the carbamate which leads to the formation of an unstable carbamic acid and releasing the tert-butyl cation. The unstable carbamic acid subsequently collapses releasing CO₂ and then forming a secondary amine which is subsequently protonated to afford a salt.

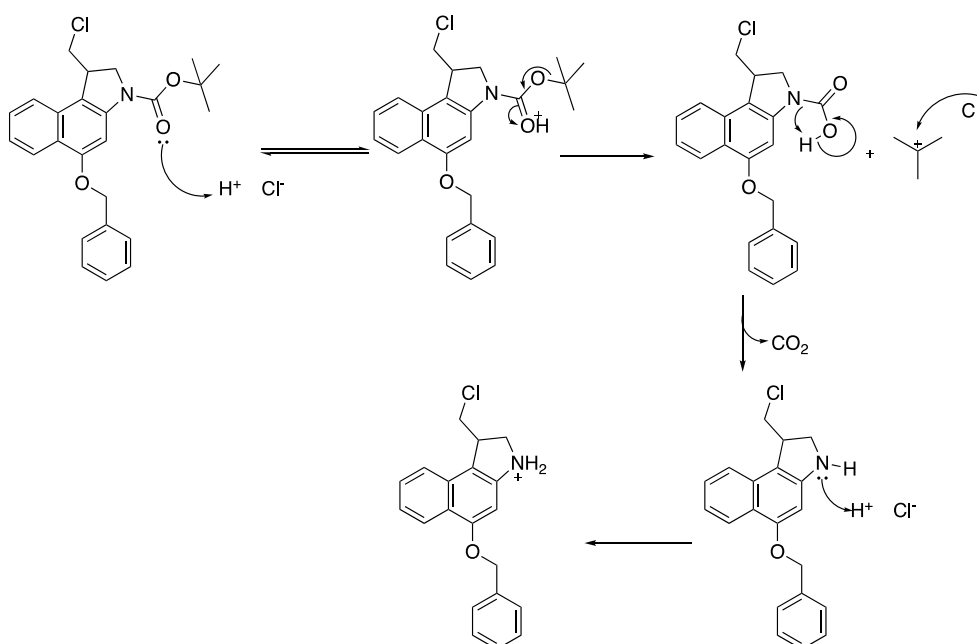


Figure 58: CBI boc deprotection mechanism

HATU was assessed as a coupling agent for this reaction. HATU has been reported to improve coupling efficiency and reacts at fast rates due to increased stability of the amine nitrogen resulting from hydrogen bonding with the pyridine nitrogen atom to form a transitional cyclic 7-membered ring.¹⁴⁷The mechanism of HATU coupling is initiated by base such as N,N-diisopropylethylamine (DIPEA) deprotonating the carboxylic acid, which

leads to the formation of a carboxylate anion. The carboxylate anion subsequently attacks the electron deficient carbon atom of HATU to make an unstable O-acyl(tetramethyl)isouronium salt intermediate and release the oxyazabenzotriazole (OAt). The OAt reacts with the carbonyl of the O-acyl(tetramethyl)isouronium salt releasing the tetramethylurea to afford the OAt active ester. The nitrogen lone pair of the amine then attacks the carbonyl of the OAt active ester forming an intermediate seven membered ring through the hydrogen bond linkage of the amine nitrogen and the pyridine nitrogen. The collapse of this cyclic intermediate releases the 1-hydroxy-7-azabenzotriazole and the desired coupled Boc-Glu(CBI)-OtBu product (Figure 59).

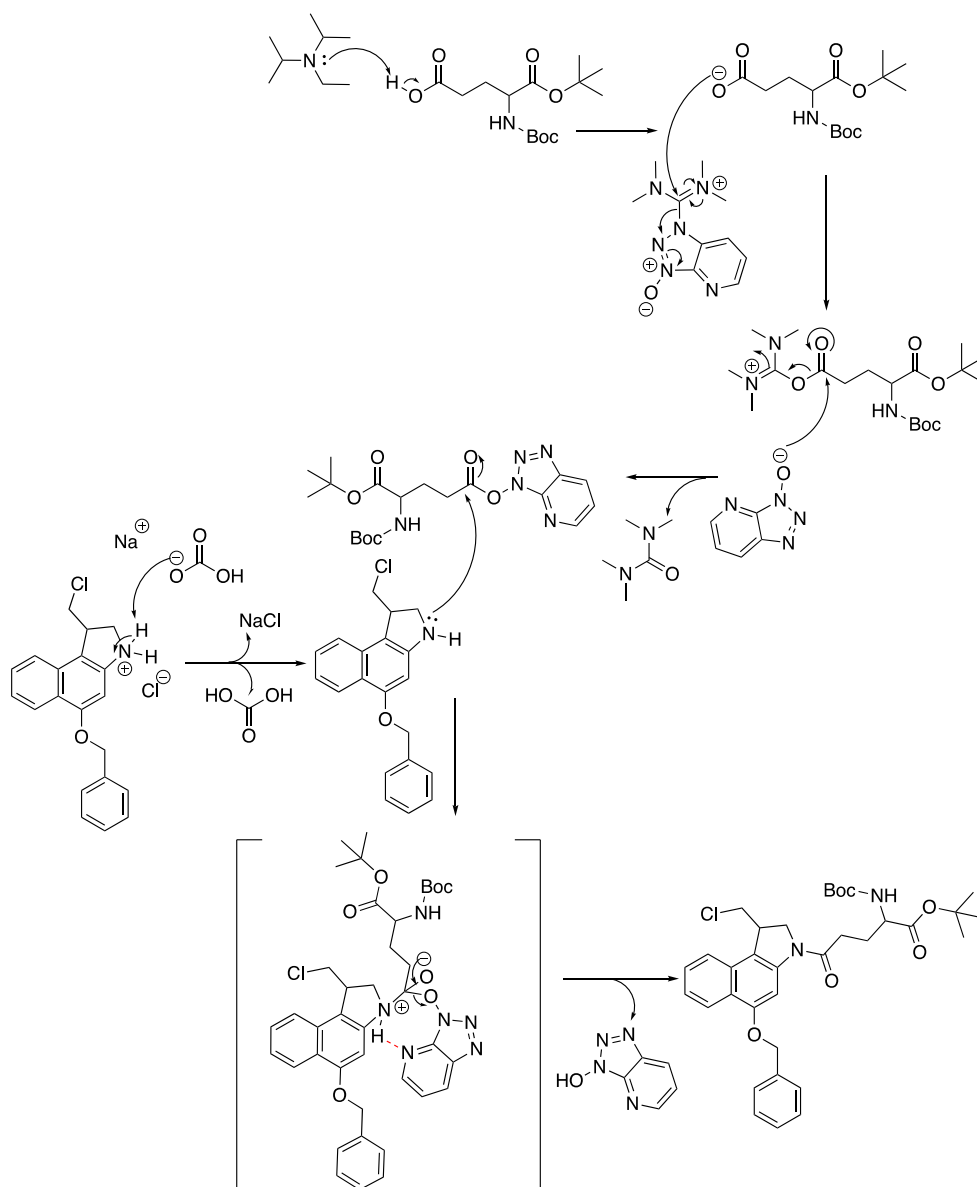


Figure 59: HATU reaction mechanism

In order for the Boc-Glu(CBI)-OtBu to be used in the Fmoc solid phase synthesis, the Boc protecting the amine had to be removed and then substituted by Fmoc and the tert-butyl protecting the alpha carboxylic acid had to be removed to obtain a free carboxylic acid. This was achieved through simultaneous deprotection of the amine and the carboxylic acid using 4M HCl in dioxane and then followed with Fmoc protection of the amine using Fmoc-Cl in the presence of sodium bicarbonate, on ice. The amine deprotection mechanism followed the same approach as described above with the indoline nitrogen Boc deprotection (Figure 58). The carboxylic acid tert-butyl deprotection on the other hand follows a closely similar mechanism whereby

the carbonyl is also protonated leading to the release of tert-butyl cation and formation of the carboxylate anion. The primary amine is subsequently protonated to afford a salt (Figure 60).

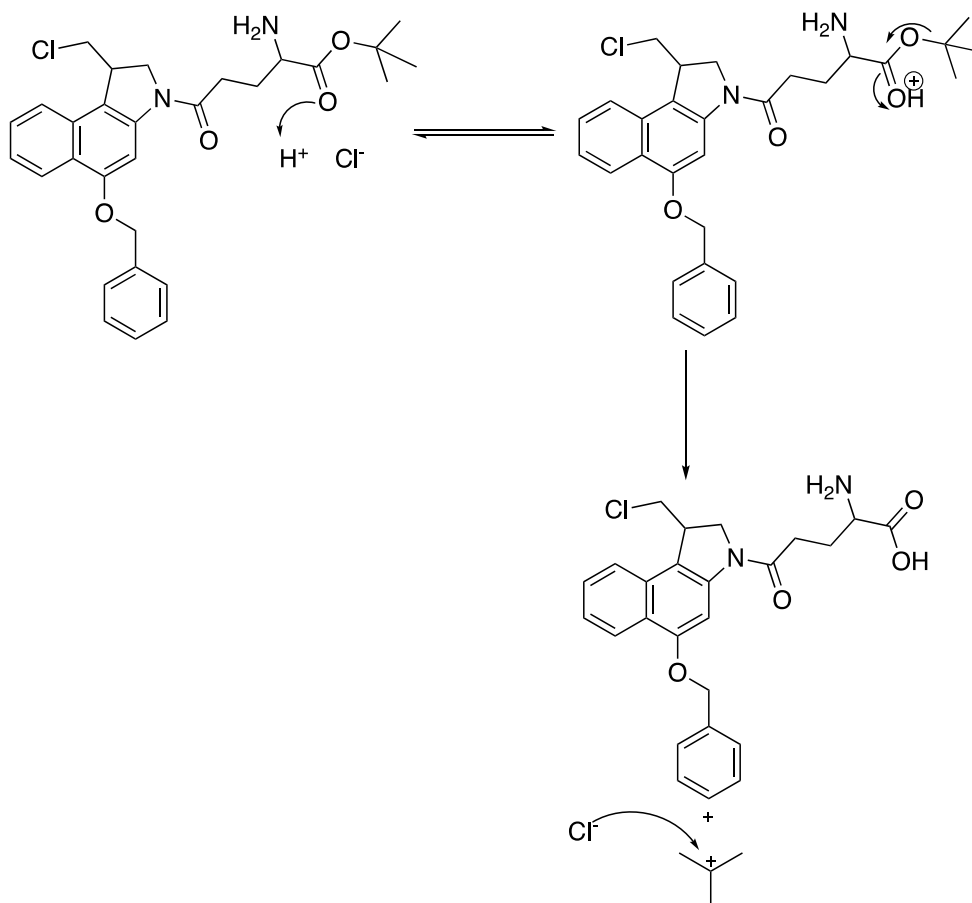


Figure 60: Tert-butyl acid deprotection mechanism

In order to achieve the desired Fmoc protected product, the resulting salt from deprotection was initially neutralised using sodium bicarbonate followed with the addition of Fmoc-Cl. The mechanism of this reaction is initiated by the nitrogen lone pair of the restored amine attacking the carbonyl of the Fmoc-Cl, leading to the release of chloride ion leaving group and the formation of desired product. The chloride anion further acts to deprotonate the carbamate forming HCl which is also subsequently neutralised by sodium bicarbonate (Figure 61).

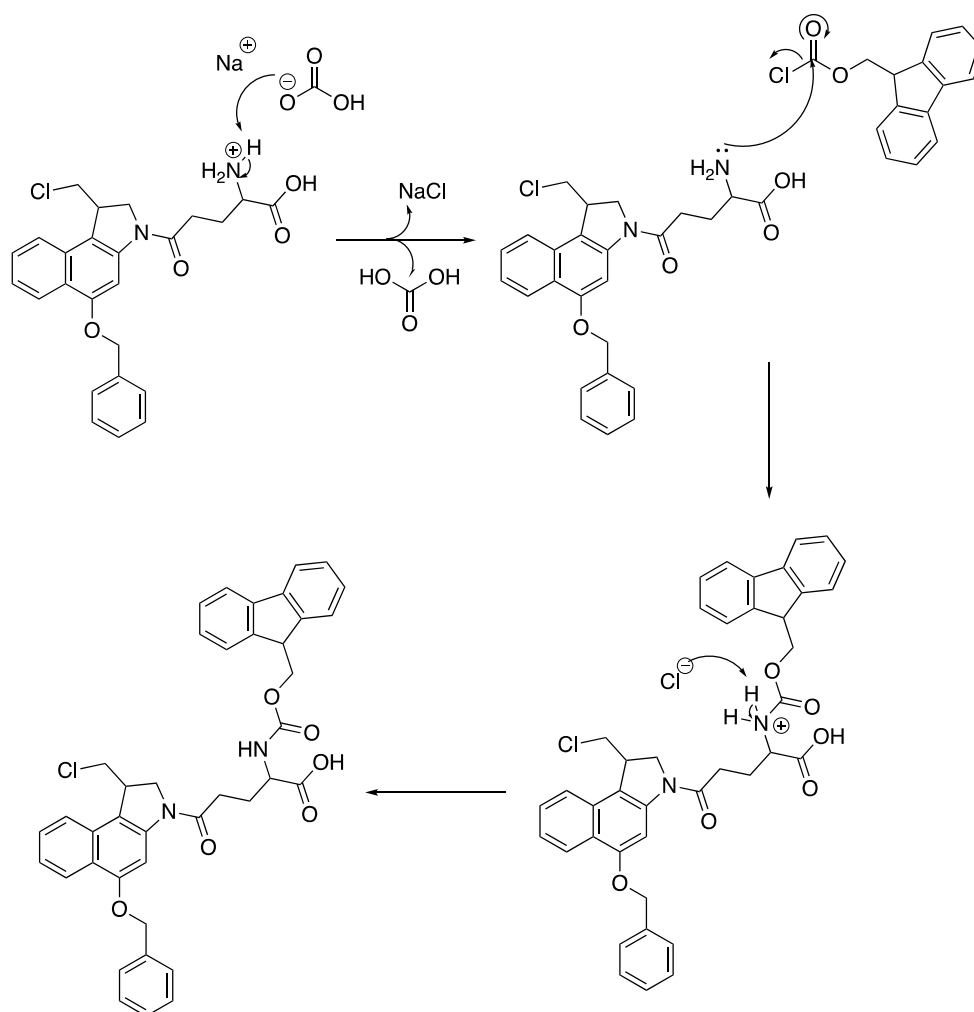


Figure 61: Fmoc protection mechanism

Successful completion of this product with 36% yield over the three steps (Boc deprotection, Glutamic acid coupling and Fmoc protection), was confirmed by mass spectrometry where the mass obtained was consistent with that of the final product and also demonstrated a chlorine isotope pattern representing the chlorine in the desired product. ^1H NMR analysis of the final product also demonstrated the lack of both tert-butyl that were characteristic of the starting material.

2.5 Non-alkylating DNA binding unit

Two different non-alkylating DNA binding units were assessed here, initially starting with the 5-amino-1H-indole-2-carboxylic acid and then assessing the use of aminobenzoic acid. As previously discussed, the non-alkylating DNA binding unit is very crucial in helping the alkylating unit have a higher affinity for DNA, consequently enhancing the cytotoxic potency.

The DNA non-alkylating units to be assessed had to have an amino at one end and a carboxylic acid on the other end in order for them to be conjugated to the DNA alkylating unit and then subsequently be coupled to the side chain of the carboxylic acid of glutamic acid due to the advantages explained in the previous section 2.4. Commercially available ethyl 5-nitroindole-2-carboxylate was used as the starting material to synthesize the 5-amino-1H-indole-2-carboxylic DNA binding unit. The first reaction step taken to achieve this was the reduction of the nitro indole to the amine using the Zn and aqueous ammonium chloride. The later method was originally employed by Boger et al. and was also subsequently repeated in our group with the only exception that both the reduction and Boc protection were combined in one reaction pot. The initial nitro reduction reaction to amine proceeds through a series of protonation and zinc electron transfer. This reduction reaction requires a source of proton such as HCl; however, the use of HCl would have interfered with the next Boc-protection step, therefore, ammonium chloride was used as an alternative source of protons. The reaction is initiated by the protonation of the nitro group followed by two electron transfers from zinc, which leads to the loss of Zn^{2+} from the bulk metal subsequently forming $ZnCl_2$ salt. This is followed by another protonation step and a subsequent loss of water to afford a protonated nitroso intermediate. Deprotonation of the protonated nitroso can lead to the formation of the nitroso intermediate. The protonated nitroso intermediate subsequently receives an additional two electrons from Zn and a proton from ammonium chloride to make the hydroxylamine intermediate. This hydroxylamine intermediate is further protonated followed with the loss of water. This loss of water is followed by receipt of two electrons from Zinc and a proton from ammonium chloride to afford the desired amine product (Figure 62).

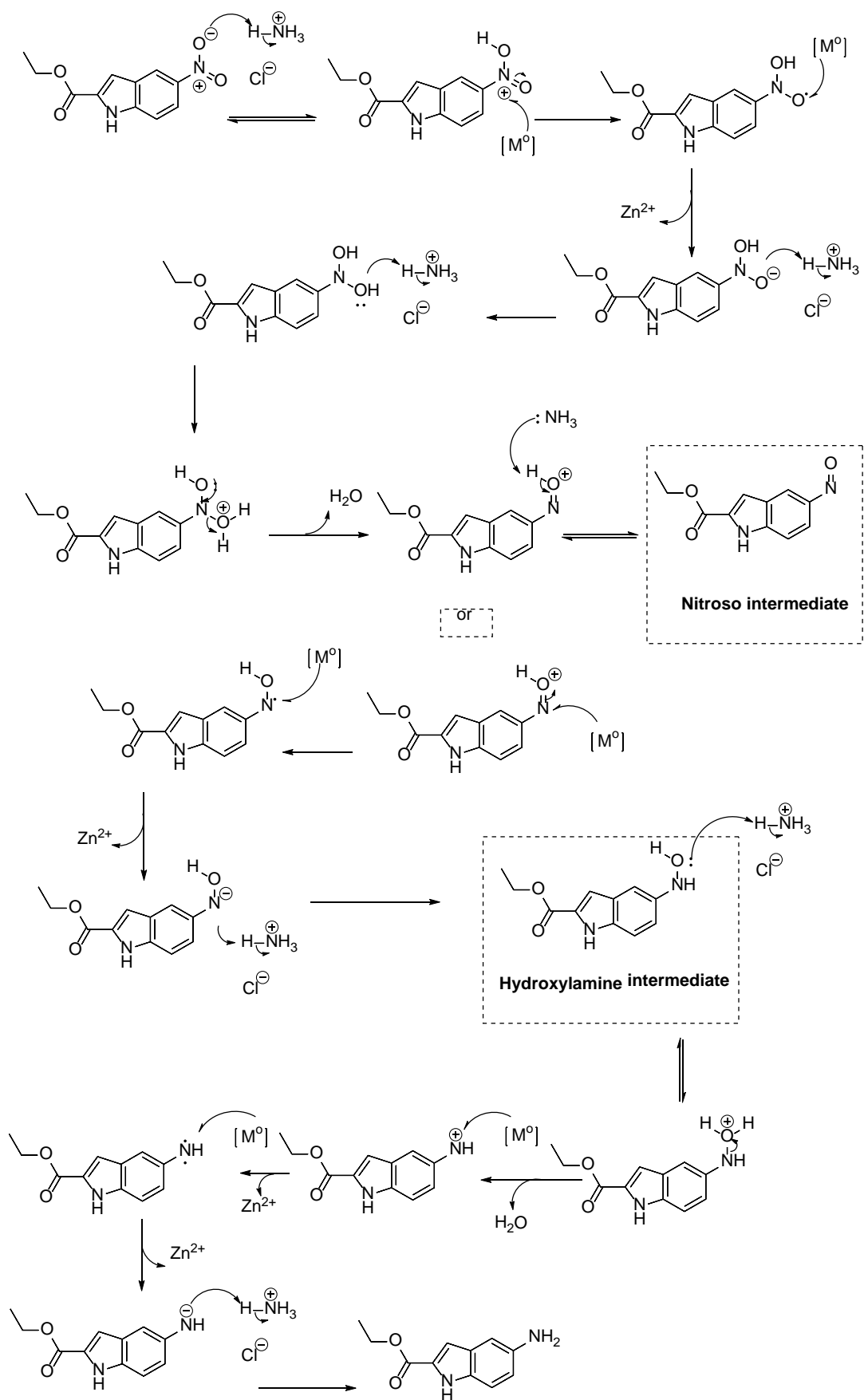


Figure 62: Nitro reduction mechanism

The amine product was immediately subjected to Boc protection and this was suggested to be an advantage as this would reduce any other side reaction resulting from the produced amine reacting with the nitroso intermediate as can be depicted in the Figure 63 to make other azo side products.

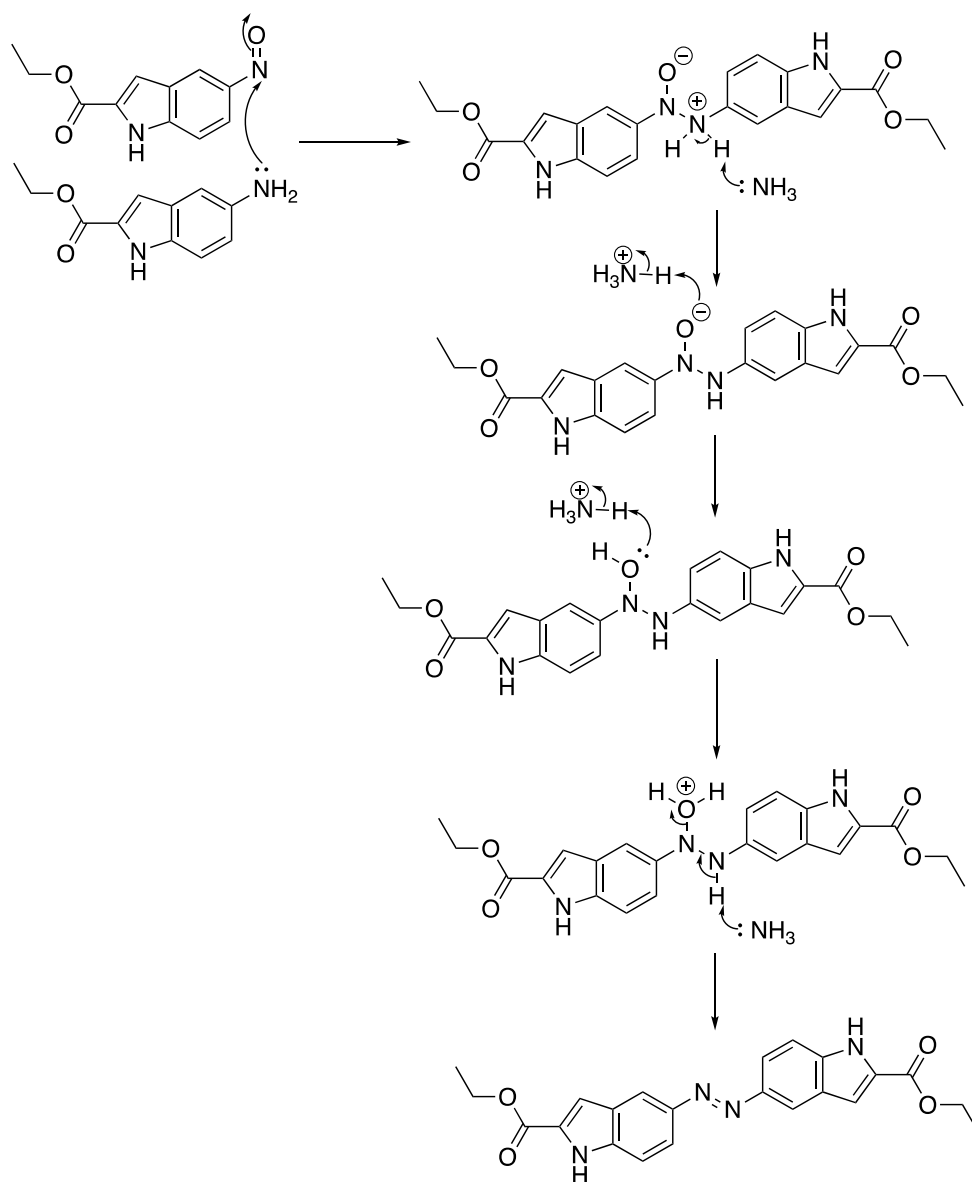


Figure 63: Condensation mechanism for possible reaction between the amine and the nitroso intermediate

Boc protection was achieved using DMAP as a catalyst whereby the most electrophilic carbonyl of Boc₂O is attacked by the DMAP nucleophilic nitrogen to form the tert-butyl carbamate pyridinium cation and the tert-butyl carbonate anion. DMAP also acts as a base to deprotonate the amine. Deprotonated nitrogen of the amine can subsequently act as a nucleophile to attach tert-butyl carbamate pyridinium cation leading to the restoration of DMAP catalyst as a leaving group and the formation of the desired Boc-protected product.

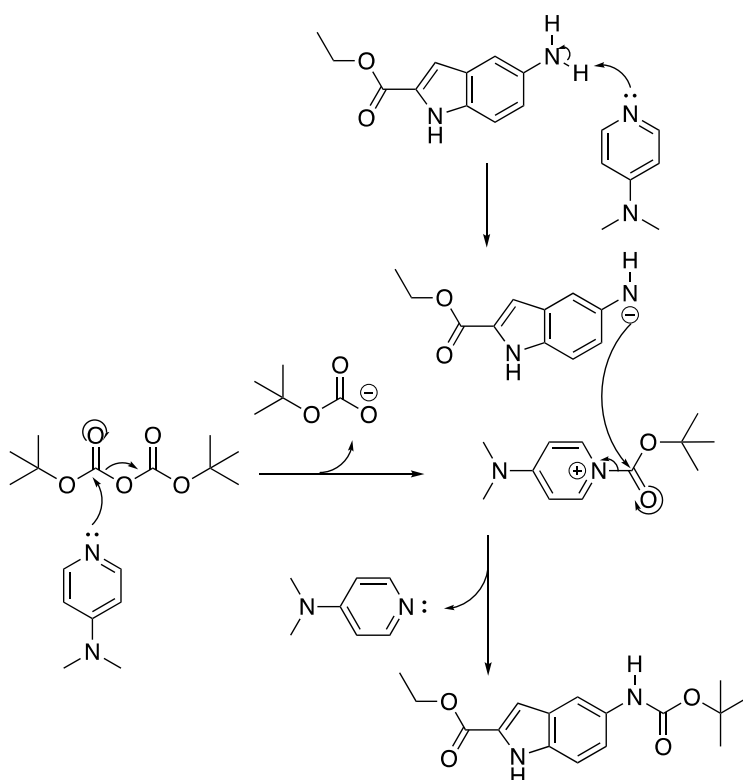


Figure 64: Boc protection mechanism using DMAP as a catalyst

The DNA binding unit was produced with an overall yield of 30% and was confirmed by ¹H NMR with a distinctive Boc peak integrating as nine protons at 1.46 ppm and the appearance of an additional broad singlet at 6.55 ppm that correspond to amine proton.

Successful production of the Boc protected amine was followed with the ester hydrolysis via the same mechanism described in section 2.3.5 to produce the desired DNA binding unit with a Boc protected amine and free carboxylic acid ready for coupling with the alkylating subunit.

2.6 Conclusion

As discussed in the introduction, the use of untargeted cytotoxic agents such as in conventional chemotherapy limits their efficiency due to associated side effects, as a result of their lack of selectivity toward tumour cells vs normal cells. This has consequently prevented the use of ultra-potent cytotoxic agents such as CBI as a treatment alone. Chapter 2 addresses some of these shortfalls by synthesizing the CBI warhead complexed to glutamic acid allowing the versatility to be conjugated to various targeting compounds and therefore increasing selectivity towards specific tumour cells.

The synthesis of the CBI alkylating unit **3** was achieved over seven steps. The only challenge encountered during this synthesis was the third and fourth step, where it was initially intended to carry out the Curtius rearrangement reaction to make the Boc-protected amine followed with the benzyl protection of the hydroxyl group, but a poor yield was achieved and many side products were observed on the TLC. This was possibly due to the hydroxyl interference in the Curtius rearrangement reaction as depicted in Figure 51. These two steps were subsequently inverted and begun by carrying out the benzyl protection of the naphthol followed by the Curtius rearrangement, which lead to the synthesis of desired product **25** with improved yield.

Conjugation of the CBI alkylating unit **3** to glutamic acid to make **6** was carried out initially using EDC coupling reagent but due to poor yield, EDC was substituted with HATU coupling reagents. Successful completion of this coupling was followed by the incorporation of DNA binding unit to make compounds **7** and **8** ready for Fmoc solid phase synthesis.

**CHAPTER 3: MSH SOLID PHASE SYNTHESIS AND
INCORPORATION OF THE CBI-WARHEAD BUILDING BLOCK
FOLLOWED BY ON THE RESIN BENZYL DEPROTECTION**

3.1 Chapter 3 Aims

Chapter 3 describes the synthesis of various peptide drug conjugates designed to target melanoma via the binding of overexpressed melanocortin 1 receptor (MC1R). Over expression of MC1R on the large majority of melanomas provides an appropriate target for delivery of ultra-potent cytotoxic agents. α -Melanocyte-stimulating hormone (α -MSH) binds to all the four subtypes of the melanocortin receptor but has been demonstrated to have higher affinity to MC1R in comparison to the other three receptors;¹⁴⁸ therefore, making an α -MSH peptide drug conjugate a good choice to target melanoma. The synthesis of α -MSH was carried out using the Fmoc solid phase synthesis, which was followed by the conjugation of various CBI ultra-potent analogue warheads synthesised as described in chapter 02.

CBI warheads conjugated to α -MSH peptide were benzyl protected and this chapter also explores various assessments carried out to remove the benzyl protecting group on the resin. Benzyl deprotection on the resin to achieve a biologically active compound was explored following complications observed when benzyl deprotection was unsuccessful in solution using H₂ and Pd/C.

Chapter 03 describes conjugation of α -MSH to biotin and FITC, which were used to confirm binding of α -MSH to MC1R on various cell lines.

Chapter 03 also describes the design and synthesis of scrambled α -MSH peptide and scrambled α -MSH peptide conjugated to CBI warhead, which was subsequently used as a control in biological assay.

3.2 α -Melanocyte-stimulating hormone(α -MSH)

α -Melanocyte-stimulating hormone (α -MSH) is a thirteen amino acid peptide hormone (Ac-Ser1-Tyr2-Ser3-Met4-Glu5-His6-Phe7-Arg8-Trp9-Gly10)-Lys11-Pro12-Val13NH₂) originally shown to be produced in the pituitary gland. α -MSH is naturally produced from its precursor proopiomelanocortin (POMC) hormone. POMC, a 31 kda protein, is proteolytically cleaved by prohormone convertases (PCs) to make ACTH, which is subsequently processed by C-terminal carboxypeptidase, α -amidating monooxygenase and N-acetyltransferase to make biologically active α -, β -, and γ -MSH (Figure 65).¹⁴⁹

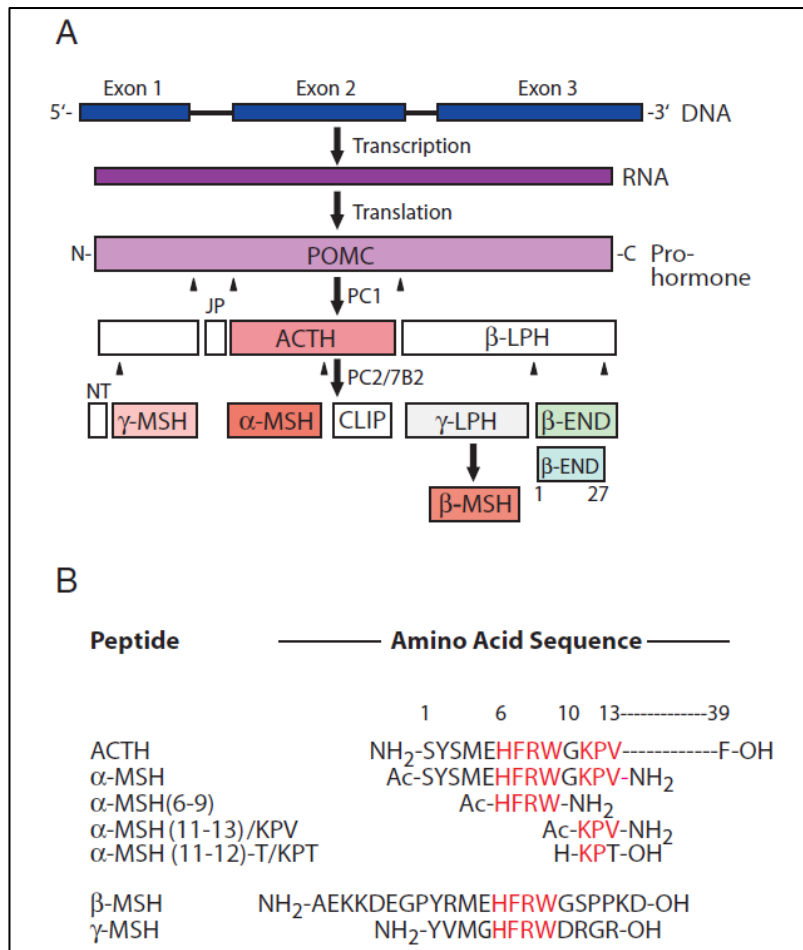


Figure 65: ACTH, α -, β -, and γ -MSH natural production¹⁴⁹

- Biosynthesis of POMC and subsequent proteolytic cleavage by PC1 to ACTH. Further cleavage of ACTH by PC2, C-terminal carboxypeptidase, α -amidating monooxygenase and N-acetyltransferase make α -, β -, and γ -MSH.
- Amino acid sequence for ACTH, α -, β -, and γ -MSH also demonstrating structure homology between all the peptides originating from POMC in red.¹⁴⁹

ACTH, α -, β -, and γ -MSH all exert their mode of action by acting on the cell surface melanocortin receptors (MC-Rs). There are five MC-Rs G protein coupled receptors (MC1R, MC2R, MC3R, MC4R and MC5R) which all share up to 61% sequence homology. ACTH, α -, β -, and γ -MSH all bind to these five MC-R receptors but with various degrees of affinity; the ability of all these four peptide to all bind to MC-Rs has been linked to the shared HFRW sequence highlighted in red in Figure 65. α -MSH binds to MC1R with more affinity compared to other receptors; however, its binding to other MC-Rs receptors has been demonstrated. Extensive research has been carried out to demonstrate the pigmentation role of α -MSH;¹⁴⁹ however, recent studies have extended this area of research showing that α -MSH is also involved in other functions ranging from its role in neurology,¹⁵⁰ to its role as an anti-inflammatory cytokine, an appetite control¹⁵¹ and finally in its role in melanoma¹⁵² which will form the basis of discussion in this chapter.

In a bid to make a more stable and physiological active analogue of α -MSH, Sawyer et al. demonstrated that the synthetic analogue of α -MSH whereby methionine at position 04 and the phenylalanine at position 7 were substituted by norleucine and D-phenylalanine respectively, increased potency twenty-six times and extended biological activity ($[\text{Nle}^4, \text{D-Phe}^7]\alpha\text{-MSH}$).¹⁵³ Further assessments into a more potent version of MSH were carried out focusing on the D-Phe7 because of previous consideration that the increase in activity was attributed to the turn conformation seen in residues 5-9. The latter hypothesis led to the synthesis of a cyclic version of MSH, $\text{cyclo}(4-10)[\text{Cys}^4, \text{Cys}^{10}]\alpha\text{-MSH}$, that was demonstrated to be highly potent in frog skin but had a very short half-life compared to $[\text{Nle}^4, \text{D-Phe}^7]\alpha\text{-MSH}$.¹⁵⁴

Further research interest has grown over the years in targeting overexpressed MC1R receptor on human melanoma cells. Most importantly recent studies have also demonstrated that MC1R receptor overexpression was also maintained in melanoma cells that had metastasized elsewhere in the body. This was demonstrated using an imaging technique where MSH was coupled to DOTA [Ga-DOTA-GGNle-CycMSH_{hex}(1,4,7,10-tetraazacyclononane-1,4,7,10-tetraacetic acid -Gly-Gly-Nle-c[Asp-His-DPhe-Arg-Trp-Lys]-CONH₂), to targets MC1Rs. This study was able to visualise melanoma that had metastasised to other parts in the patient's body, including to the connective tissues, lung, brain and small intestines.¹⁵⁵ Such a discovery was ground-breaking as it demonstrated the ability to use α -MSH as a targeting peptide to deliver various therapeutic drugs to melanoma cells. Following from this discovery Xu et al. investigated delivering radionuclides Yttrium-90 (⁹⁰Y) (⁹⁰Y-DOTA-GGNle-CycMSH_{hex}) to the melanoma as a targeted therapy which demonstrated high uptake and prolonged retention in melanoma.¹⁵⁶ These two recent publications emphasised the use of α -MSH as a targeting peptide to deliver potent anti-cancer drug to melanoma cells. This section of the thesis focused on the approaches taken to synthesize α -MSH on the solid phase synthesis, followed with coupling of the seco-CBI analogue.

3.3 Introduction to the solid phase synthesis

Solid phase synthesis was introduced in 1963 by Bruce Merrifield when it was becoming increasingly clear that despite significant improvements made in the synthesis of small peptides, it was still difficult to synthesise a long chain polypeptide due to solubility and purification complications.¹⁵⁷ Since the early years of the introduction of solid phase methods, the technique has improved significantly but the basic fundamentals have remained the same; whereby the first amino acid is bound covalently on a solid phase (Resin) that is insoluble in widely used solvents during the solid phase synthesis. Subsequent to this first amino acid, additional amino acids are added, followed by filtration and a wash step which allows the removal of excess and unbound reagents. The solid phase removes the need for a purification step following every coupling reaction and also allows the ability to add excess of reagents to help the reaction go to completion. Upon completion of the synthesis the polypeptide can be cleaved from the solid phase support (resin).^{158,159}

In the early SPPS by Bruce Merrifield Z (Benzyl) protected amino acids were used and treatment with 30% HBr in acetic acid removed the Z protecting group. The use of Z protecting group was later superseded by Boc protected amino acids a year later in 1964. Additional work was carried out to improve the SPPS and in 1970, Han and Carpino introduced the Fmoc protecting group which is now a widely used approach for peptide synthesis.¹⁵⁹

3.3.1 Boc Solid Phase synthesis

When Boc solid phase synthesis was introduced by Bruce Merrifield in the 1967 as an improvement to the use of Z-protected amino acids, the two forms of protecting group continued to be used. However, Merrifield demonstrated that the use of Boc protection was able to improve the yield and also reduced the synthesis time compared to Z protecting group. The use of both Z and Boc protecting group was important in establishing the use of solid phase; however, its use had several limitation including the fact that both protecting groups are not orthogonal as they can both be cleaved in the presence of acid and with the only difference being how sensitive the two protecting groups are. Therefore, the use of this technique require experienced analysts to avoid excessive undesired products. The other limitation of these two protecting groups is associated with the use of highly toxic hydrofluoric acid to remove the final peptide from the resin, as well as orthogonal side chain protection. However, despite these limitations Boc SPSS is still used today for some complicated peptides that suffer from poor deprotection or poor coupling during Fmoc-SPs.¹⁵⁹

3.3.2 Fmoc Solid Phase synthesis

The use of Boc solid phase synthesis has been generally superseded by the use of Fmoc solid phase synthesis in both industry and research laboratories. The deprotection of Fmoc from the N α amino group is carried out using mild basic treatment with piperidine and in order to maintain orthogonality the side chains are protected with groups that can be cleaved by acid treatment. The mechanism of removal of Fmoc is initiated by piperidine attacking and removing the acidic proton from the fluorenyl group. Deprotonation triggers an intramolecular reaction leading to the formation of a carbamic acid anion and reactive dibenzofulvene. The carbamic acid further decomposes releasing CO₂ and leading to the formation of desired amine. Piperidine is added in excess for this deprotection reaction to also play the role of scavenger where it reacts with dibenzofulvene to make the fulvene–piperidine adduct (Figure 66). The dibenzofulvene produced as part of this deprotection made the use of piperidine for Fmoc deprotection in solution-based peptide reaction unsuitable because of potential other side reaction such as that with deprotected amine.^{159,160,161}

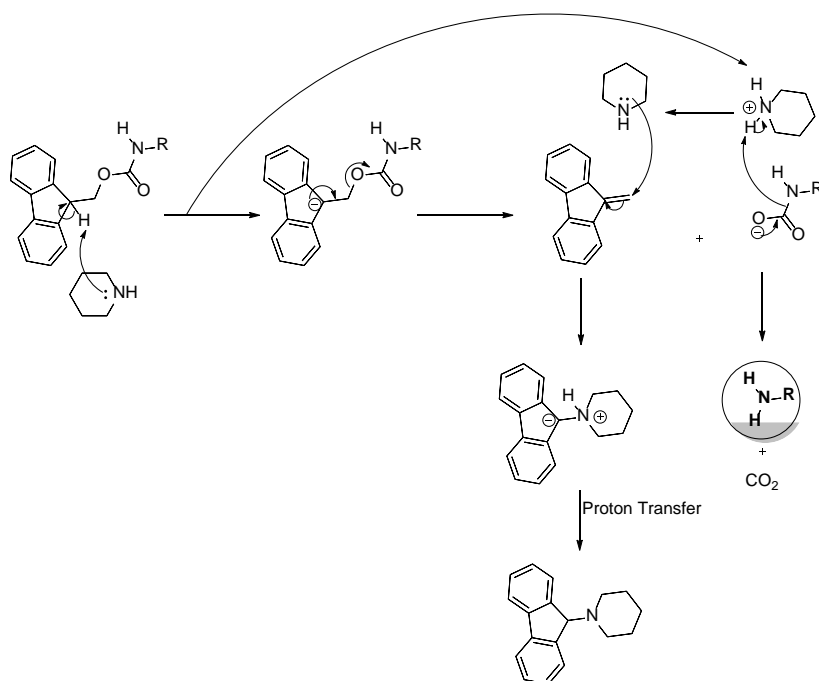


Figure 66: Fmoc deprotection mechanism

3.4 MSH peptide synthesis

α -MSH was synthesised using Fmoc solid phase synthesis and then subsequently purified and analysed using mass spectrometry and HPLC. As discussed in the introduction of this chapter, synthetic [Nle⁴,dPhe⁷] α -MSH peptide (Figure 67) was demonstrated to be 26 time more potent¹⁵³ than the parent α -MSH. Therefore, this thesis primarily focuses on the synthesis of [Nle⁴,dPhe⁷] α -MSH, which was then used for subsequent conjugation of various different warheads. As the synthesis of CBI alkylating unit analogues took longer to achieve the final product, it was therefore paramount to make sure the synthesis of the targeting peptide was optimal before conjugation of various CBI alkylating units.

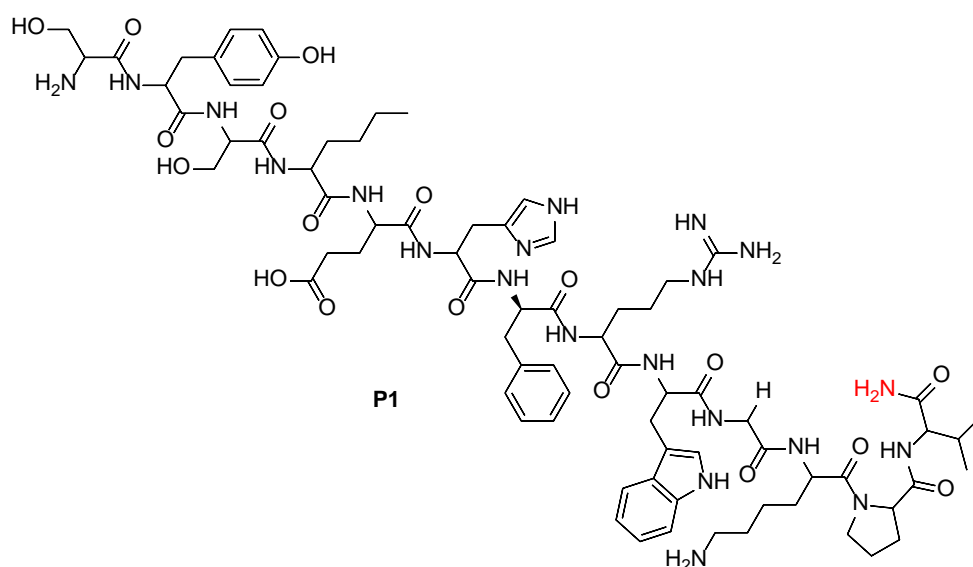


Figure 67: [Nle⁴,dPhe⁷] α -MSH structure, showing in red the amide resulting from cleavage from the resin

Prior to the initiation of amino acid conjugation, the resin was swollen by incubating in DCM for 30 min followed by a wash step with DMF and another incubation with DMF for 30 min. This is to improve access of added amino acid to already formed polymer. The coupling reagent used as part of this peptide synthesis was HBTU, which is one of the commonly used coupling agent due to its affordability. HBTU and HATU (Figure 68) are both guanidinium salts, which have in the past been classified as O-uronium salts.¹⁶²

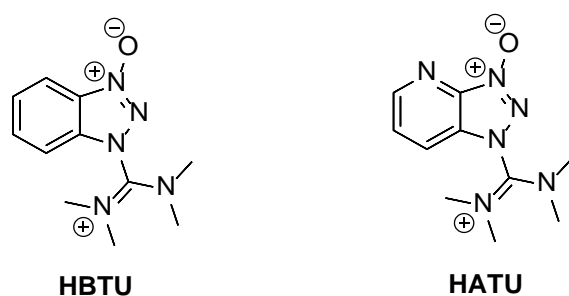


Figure 68: Structure of HBTU and HATU

The mechanism by which HBTU and HATU catalyse the amide bond formation is initiated by deprotonation of the carboxylic acid using a base such as DIPEA (Figure 5). The newly formed carboxylate anion then attacks the carbon in the guanidinium structure leading to the loss of oxybenzotriazole anion and formation of the isouronium cation. The oxybenzotriazole anion subsequently attacks the carbonyl of the newly formed ester bond in the isouronium cation causing the release of tetramethylurea and the formation of oxybenzotriazole ester. The nucleophilic nitrogen of the amine then attacks the carbonyl of oxybenzotriazole ester releasing the oxybenzotriazole anion to further catalyse other coupling reactions and then finally forming the desired amide bond after deprotonation by DIPEA. HBTU is mixed with HOBT as an additive during the preparation and HOBT is believed to increase the formation of oxybenzotriazole.

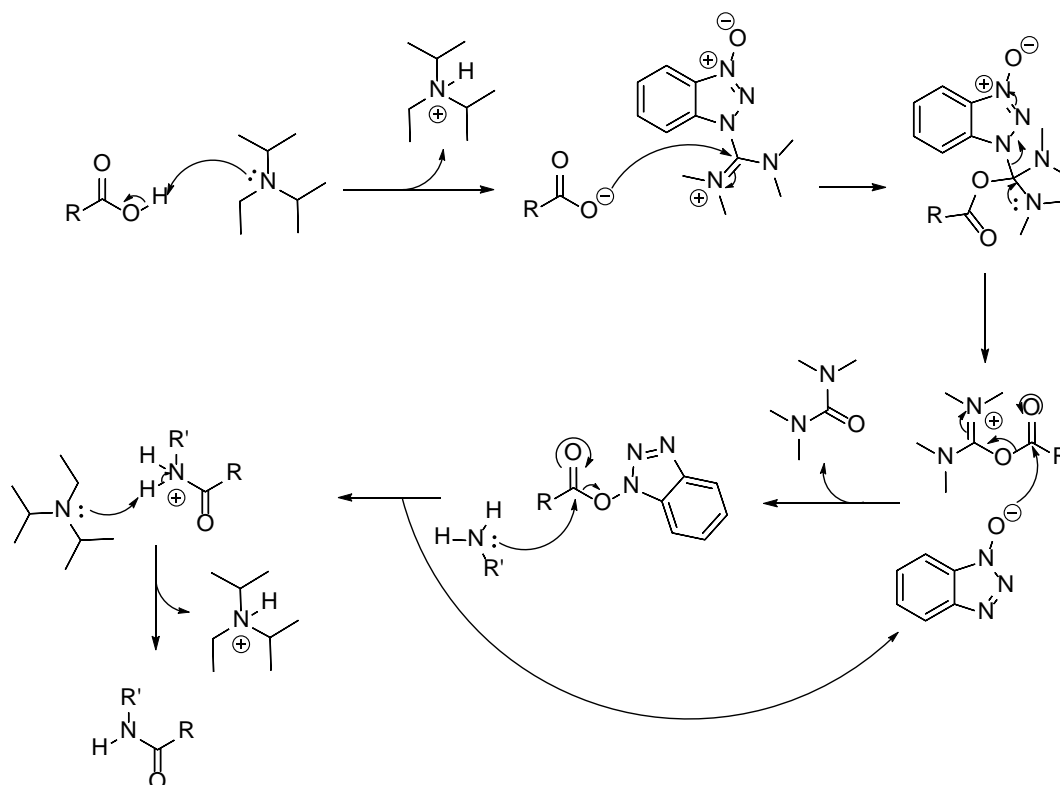


Figure 69: Amide coupling reaction using HBTU as a coupling agent

The synthesis of all the peptides described was carried out using a Syro automated peptide synthesiser, except for the addition of the alkylating unit, which was carried out manually due to limited material availability. All the amino acids were diluted in NMP except arginine and histidine, which were dissolved in DMF. At the end of the peptide synthesis, the resin was washed extensively with DMF to remove any excess followed by a further extensive wash with DCM and drying of the resin. In order to cleave the peptide, the resin was then subjected to 95 % TFA, 2.5 % TIPS, and 2.5 % water, which was filtered and dried under reduced pressure. The later was followed by another wash with Et₂O which allowed the desired peptide to precipitate.

The crude product P1 was assessed using the HPLC which revealed one major peak (Figure 70). P1 was then purified and subsequently assessed using the mass spectrometry where the correct mass of m/z of 1604.8683 and associated ion fragment (Figure 71) were observed. Successful completion of the [Nle⁴,dPhe⁷]α-MSH peptide was critical to allow further investigation into the coupling of DNA alkylating subunits.

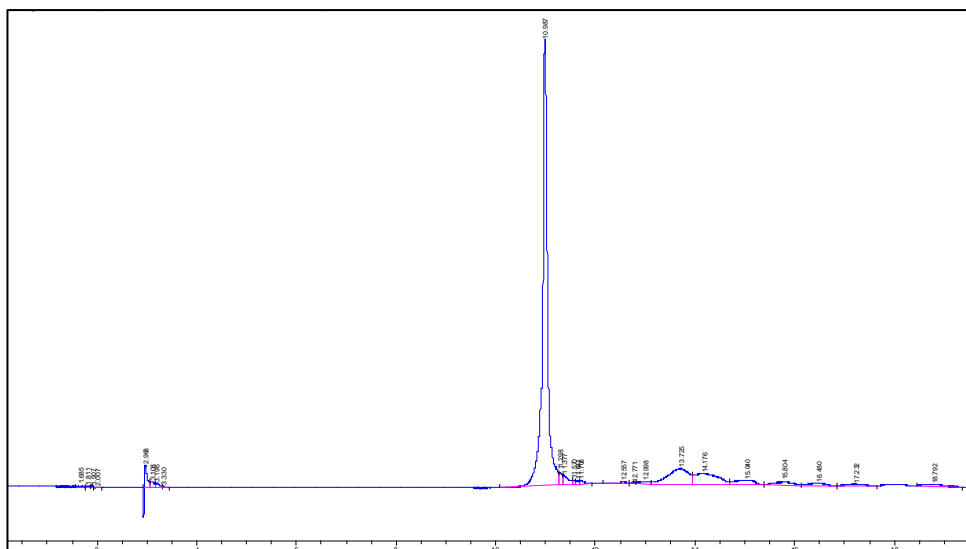


Figure 70: Analytical HPLC trace of [Nle⁴,dPhe⁷]α-MSH

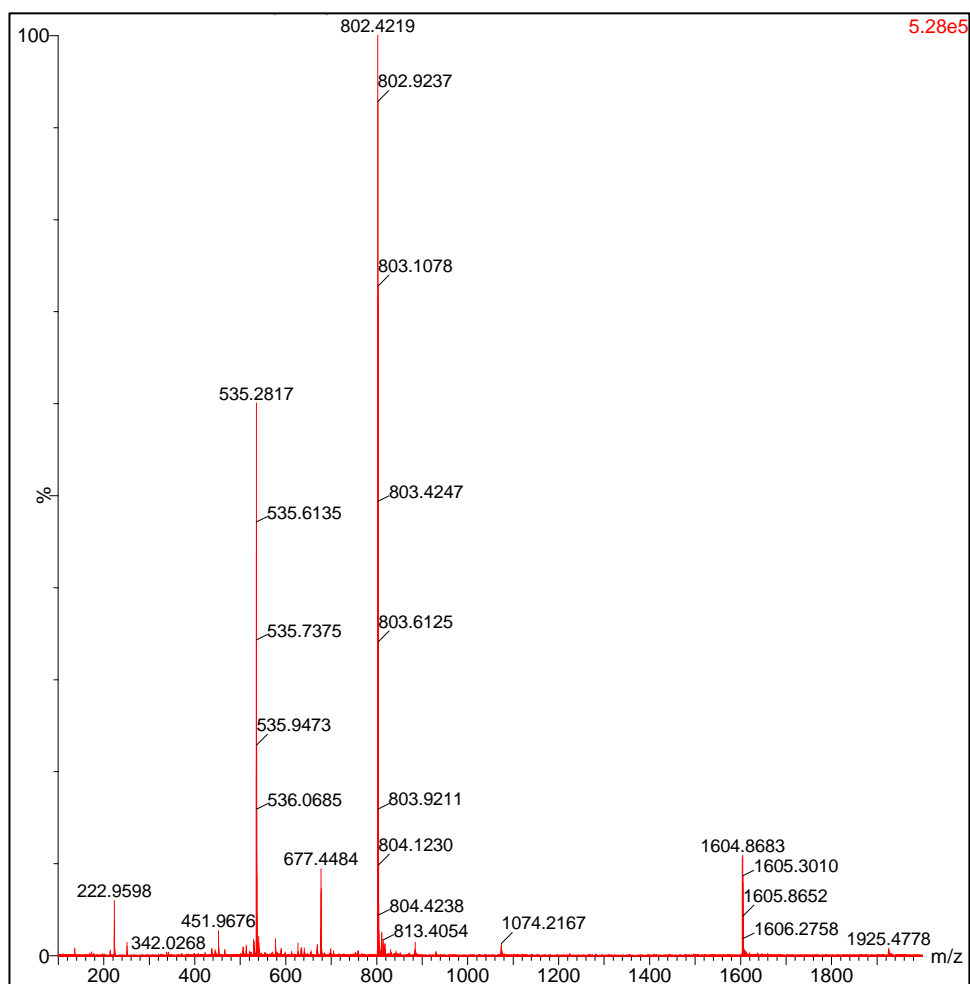


Figure 71: Mass Spectrometry data for [Nle⁴,dPhe⁷]α-MSH

3.5 [Nle⁴,dPhe⁷]α-MSH Peptide drug conjugated library

Following successful synthesis of various DNA alkylating units analogue as described in chapter 02 and [Nle⁴,dPhe⁷]α-MSH peptide, it was time to start synthesising various peptide drug conjugate. To assess feasibility, the first attempt was carried out by conjugating **6** to [Nle⁴,dPhe⁷]α-MSH peptide to afford the first peptide drug conjugate PDC1 (Figure 72).

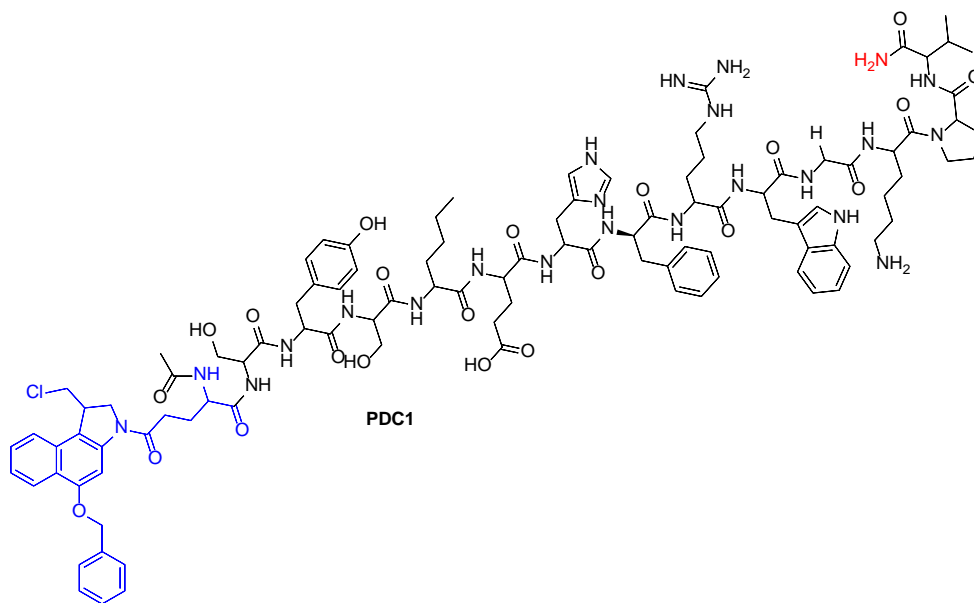


Figure 72: PDC1, [Nle⁴,dPhe⁷]α-MSH conjugated to CBI analogue shown in blue and then acetylated

Alkylating unit **6** was dissolved in DMF and conjugation was carried out on the resin using HATU coupling reagent. The cleavage of the peptide drug conjugate from the resin was affected by 95 % TFA, 2.5 % TIPS, and 2.5 % water. HPLC assessment demonstrated an intense UV absorbance peak at 254 nm which was absent in the parent [Nle⁴,dPhe⁷]α-MSH peptide and is characteristic of CBI based compounds. Higher absorbance at 254 nm gave confidence that conjugation had taken place. As the CBI analogue used to couple to MSH was a racemic mixture; two merged peaks (Figure 73) were observed following coupling which confirmed the presence of the two racemic mixture. Both peaks were purified and assessed on the mass spectrometry which corresponded to the correct mass (calculated $M + 2H)^{2+}$: 1041.00; found: 1041.10).

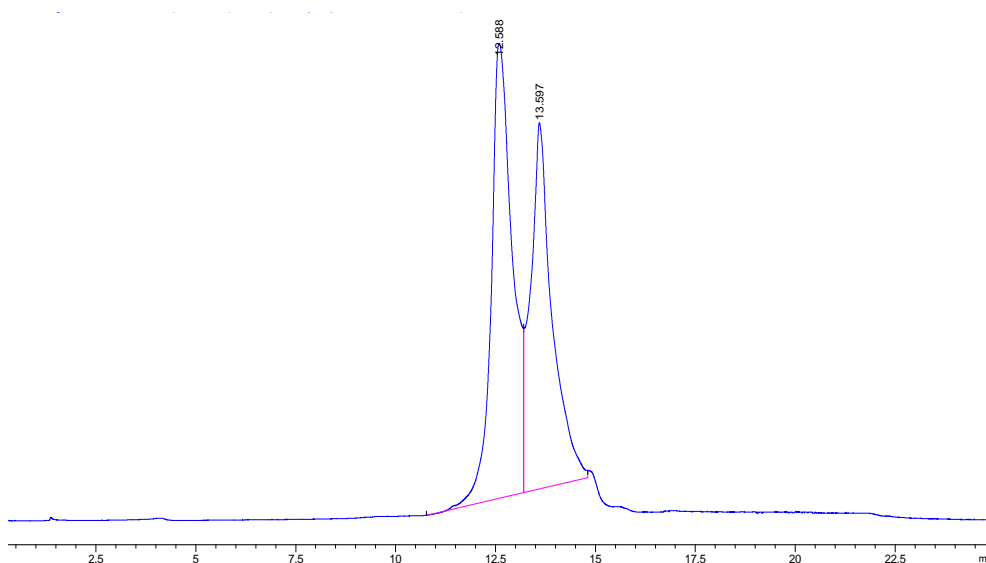


Figure 73: Analytical HPLC trace of [Nle⁴,dPhe⁷]α-MSH conjugated to Glutamic-CBI

Following successful initial conjugation of one glutamic acid CBI analogue **6** on MSH peptide, additional conjugations were also assessed with two and three glutamic acid CBI analogue **6** to afford the peptide drug conjugate **PDC4** and **PDC5** respectively. The addition of more than one warhead was assessed as this could potentially increase the potency of the peptide drug conjugate. The addition of multiple racemic mixtures of glutamic acid CBI analogue complex was complicated to assess on the HPLC. HPLC analysis produced multiple peaks that were isolated and assessed by mass spectrometry and achieved the desired mass. However, if such an approach of using multiple warheads was to be considered, recommendation would be to use only one isomer.

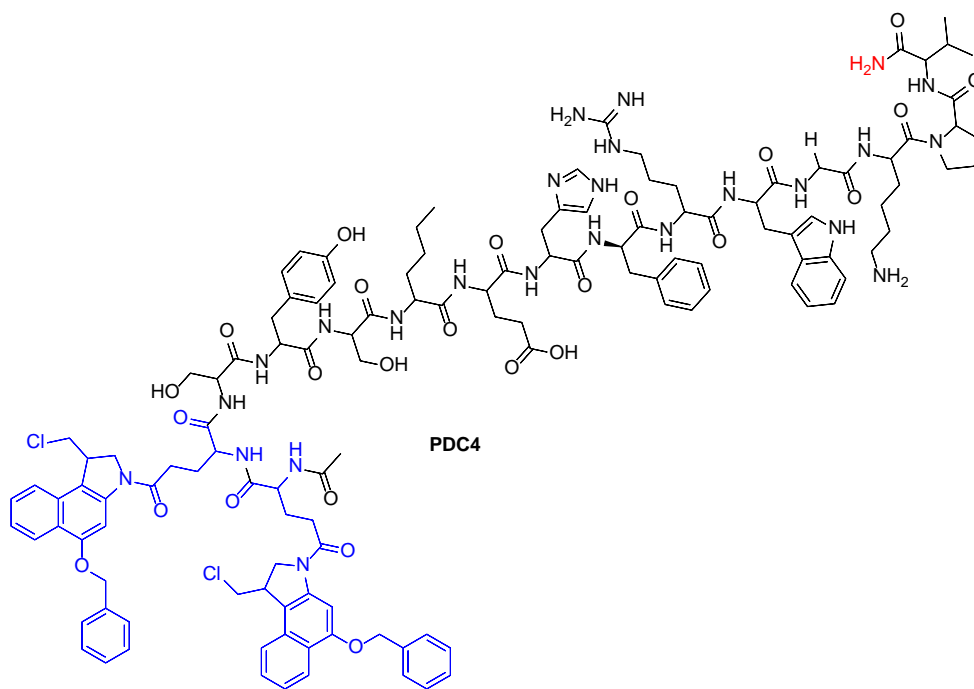


Figure 74: [Nle⁴,dPhe⁷]α-MSH conjugated to two CBI analogue shown in blue and then acetylated

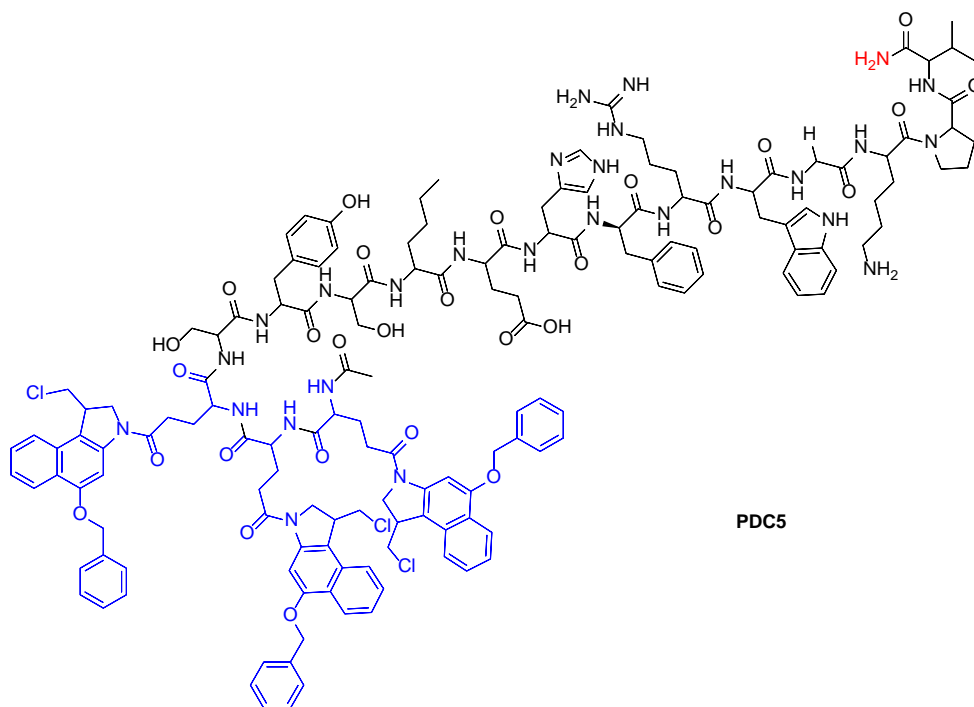


Figure 75: [Nle⁴,dPhe⁷]α-MSH conjugated to three CBI analogue shown in blue and then acetylated

3.6 Benzyl deprotection

Benzyl deprotection of the peptide drug conjugate to achieve biologically active compound was initially attempted using the classic hydrogen transfer with Pd/C as a catalyst. After multiple failed attempts where the starting material was recovered, a small amount of glutamic acid CBI analogue was then subjected to benzyl deprotection using the same hydrogen of transfer with Pd/C as a catalyst to assess if the peptide was the root cause of unsuccessful benzyl deprotection. Benzyl deprotection of glutamic acid CBI analogue complex **6** was successful and afforded biologically active compound **38**.

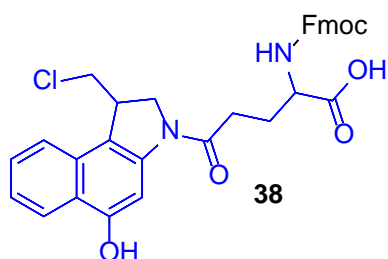


Figure 76: Benzyl deprotected **6**

38 was subsequently conjugated to [Nle⁴,dPhe⁷]α-MSH peptide to produce the active benzyl deprotected peptide drug conjugate **PDC6** (Figure 77). Benzyl deprotection of **6** prior to conjugation to [Nle⁴,dPhe⁷]α-MSH reaction was carried out in the MeOH and added aqueous ammonium formate as a hydrogen donor. The proposed mechanism by which this reaction proceeds is initiated by oxidative addition of **6** to the Pd(0) catalyst, forming a Pd(II) complex with **6**. The presence of excess hydrogen originating from ammonium formate facilitates the transfer, which leads to the formation of desired alcohol, the release of toluene and further regeneration of the palladium catalyst (Figure 78). One of the advantages of using Pd/C was the ease of purification after reaction completion as Pd/C was removed by filtration through a layer of cotton wool and celite.

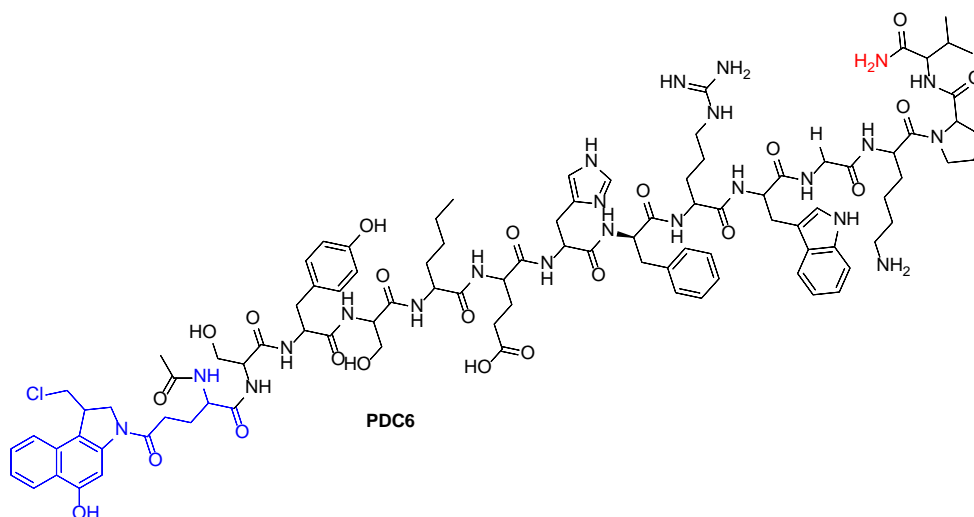


Figure 77: Benzyl deprotected Glu-CBI coupled to [Nle4,dPhe7] α -MSH

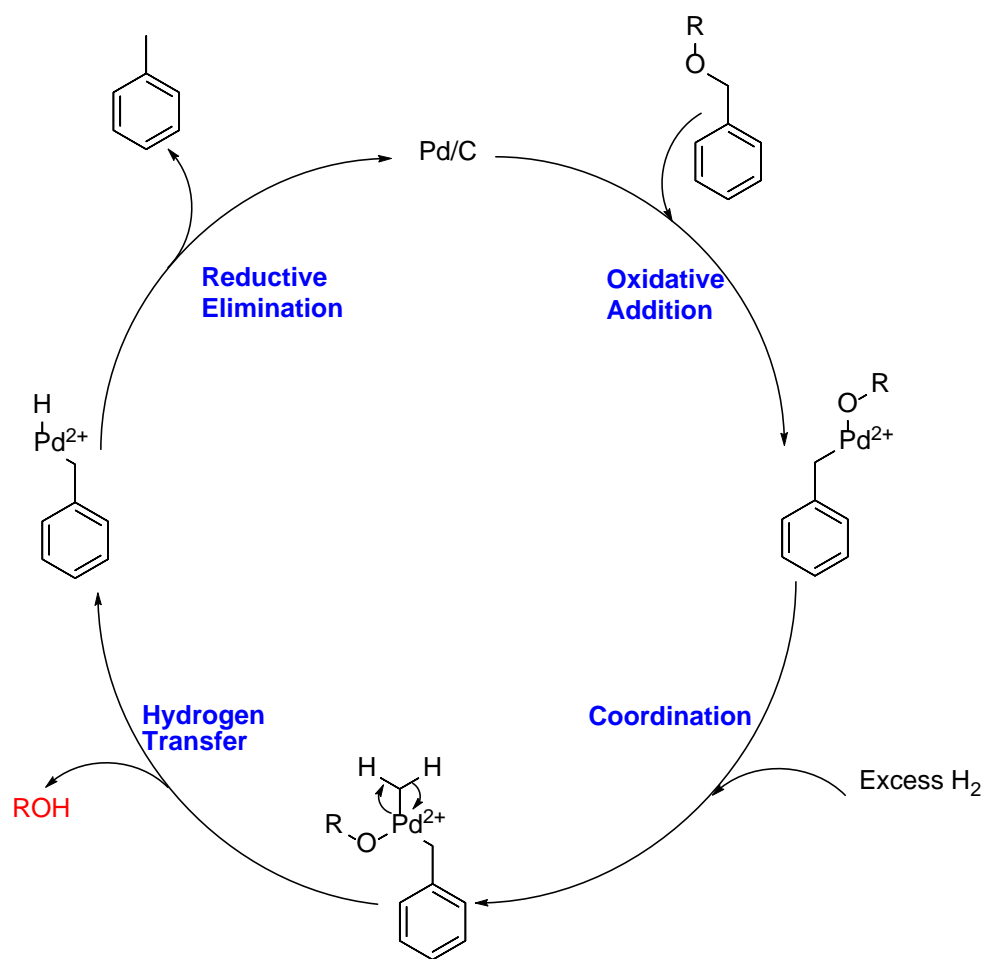


Figure 78: Pd/C benzyl deprotection mechanism

One of the limitations to carrying out benzyl deprotection of the glutamic acid CBI analogue complex prior to coupling to the solid phase was that only a small amount had to be deprotected at the time to avoid handling the cytotoxic substance. Unsuccessful benzyl deprotection using Pd/C of larger peptides and small peptides incorporating cysteine residue has also been reported in our group previously. Therefore, additional investigations were directed toward the assessment of other methodologies to benzyl deprotect on the resin. Previous attempts by our group to carry out the benzyl deprotection on the resin which were unsuccessful assessed the following conditions:

- Pd(OAc)₂ (30 mol %), Et₂SiH (25 equiv.), Et₃N (25 equiv), anhydrous DCM, N₂, overnight.

- Pd(PPh₃)₄ (25 mol %), Ph₃SiH (25 equiv), anhydrous DCM, N₂, overnight.

Following an extended literature search, there was evidence to suggest that BBr₃ in DCM can be used to remove a benzyl group in solution.¹⁶³ The use of BBr₃ to remove the benzyl group would be a preferable approach as it would potentially remove the risk of handling cytotoxic compounds and only cleave the benzyl at the end of the reaction before cleavage of the peptide drug conjugate from the resin. For the first attempt to remove benzyl on the resin, BBr₃ was added to the cleavage cocktail (H₂O/TIPS/TFA) to assess if benzyl deprotection could be carried out at the same time as cleaving the peptide from the resin. However, upon addition of BBr₃ to the cleavage cocktail it reacted with water vigorously, producing HBr acid gas. The reaction produced the desired benzyl deprotected peptide drug conjugate but with also other impurities. It was therefore decided to carry out the reaction in DCM as previously reported in the literature followed by cleaving the peptide from the resin using the cleavage cocktail (H₂O/TIPS/TFA).

The proposed mechanism by which benzyl deprotection using BBr₃ proceed is initiated by a nucleophilic attack of the oxygen atom to the boron atom of BBr₃ leading to the formation of a zwitterionic intermediate. The bromide from BBr₃ then attacks the benzyl carbon yielding an alkoxydibromoborane and benzyl bromide. The alkoxydibromoborane then subsequently breaks down in the presence of water yielding the desired benzyl-deprotected compound.¹⁶⁴

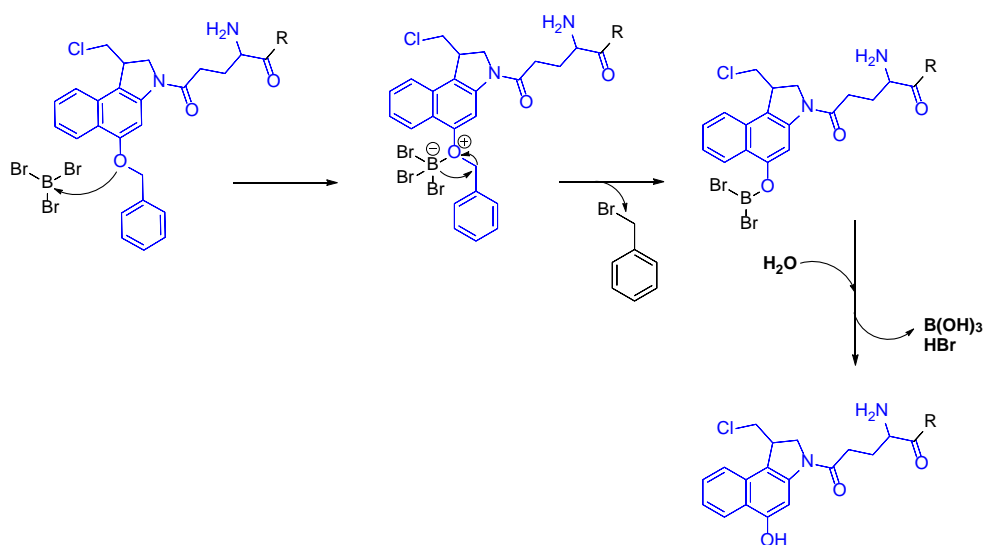


Figure 79: BBr₃ benzyl deprotection mechanism

BBr₃ benzyl deprotection on the resin was subsequently assessed on various peptides including **PDC1**, **PDC2** and **PDC3** and was demonstrated to yield desired products **PDC6**, **PDC7** and **PDC8** respectively. Peptide drug conjugates **PDC6**, **PDC7** and **PDC8** were all purified on the HPLC and then assessed on the mass spectrometry. The data obtained on the mass spectrometry revealed the correct mass for **PDC6**, **PDC7** and **PDC8**.

PDC6 demonstrated various charge state in the mass spectrometry ranging from two and three charges. Two charge state calculated $(M + 2H)^{2+}$: 995.97; found: 996.07, three charge state calculated $(M + 3H)^{3+}$: 664.31; found: 664.33) (Figure 80).

PDC7 demonstrated multiple charge state in the mass spectrometry ranging from two to four charges. Two charge state calculated $(M + 2H)^{2+}$: 1209.12; found: 1209.25, three charge state calculated $(M + 3H)^{3+}$: 806.41; found:

806.44 and four charge state calculated $(M + 4H)4+$: 605.06; found: 605.06 (Figure 81).

PDC8 demonstrated two charge state in the mass spectrometry ranging from two and three charges. Two charge state calculated $(M + 2H)2+$: 1168.53; found: 1168.65, three charge state calculated $(M + 3H)3+$: 779.36; found: 779.38) (Figure 82).

Data generated across the three PDCs confirmed successful benzyl deprotection on the resin. The use of BBr₃ was therefore considered as the preferred approach instead of benzyl deprotection prior to coupling, to minimise the risk associated with handling cytotoxic compounds.

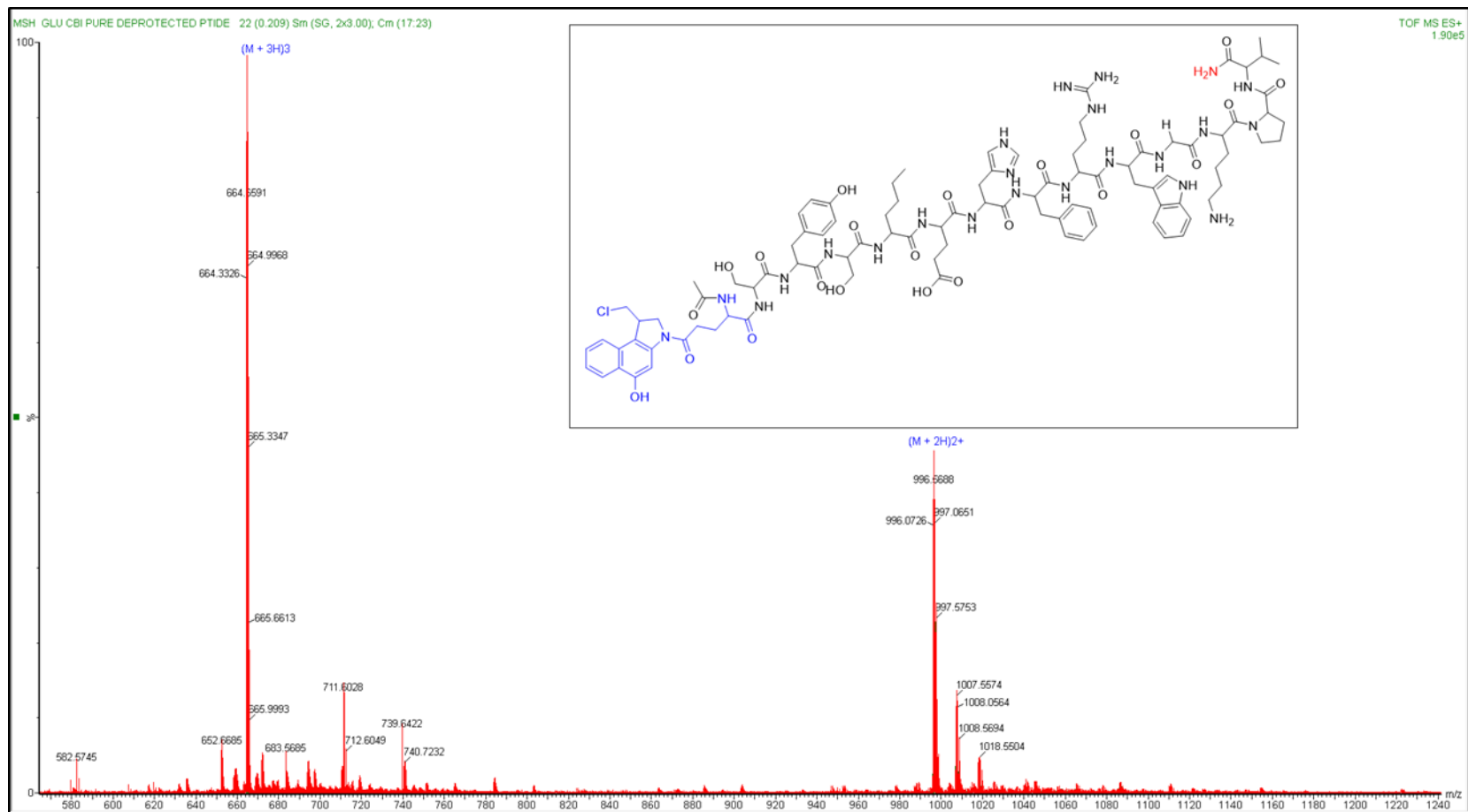


Figure 80: **PDC6**, MSH conjugated to **benzyl deprotected Glutamic acid-CBI complex**. Mass spectrometry demonstrates multiple charge state from 2+ to 3+.

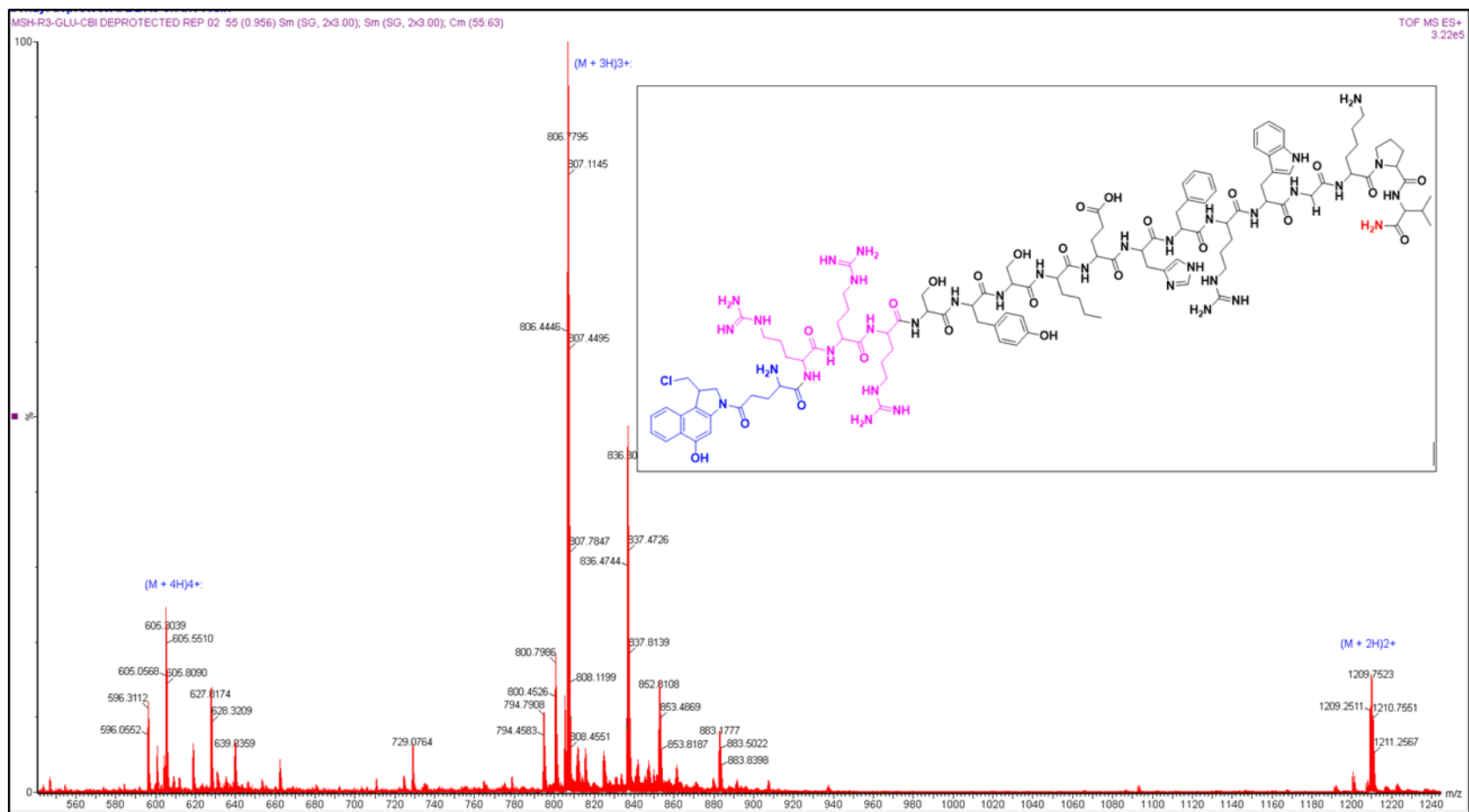


Figure 81: **PDC7**, MSH conjugated to **three arginine** residues and to **benzyl deprotected Glutamic acid-CBI complex**. Mass spectrometry demonstrates multiple charge state from 2+ to 4+.

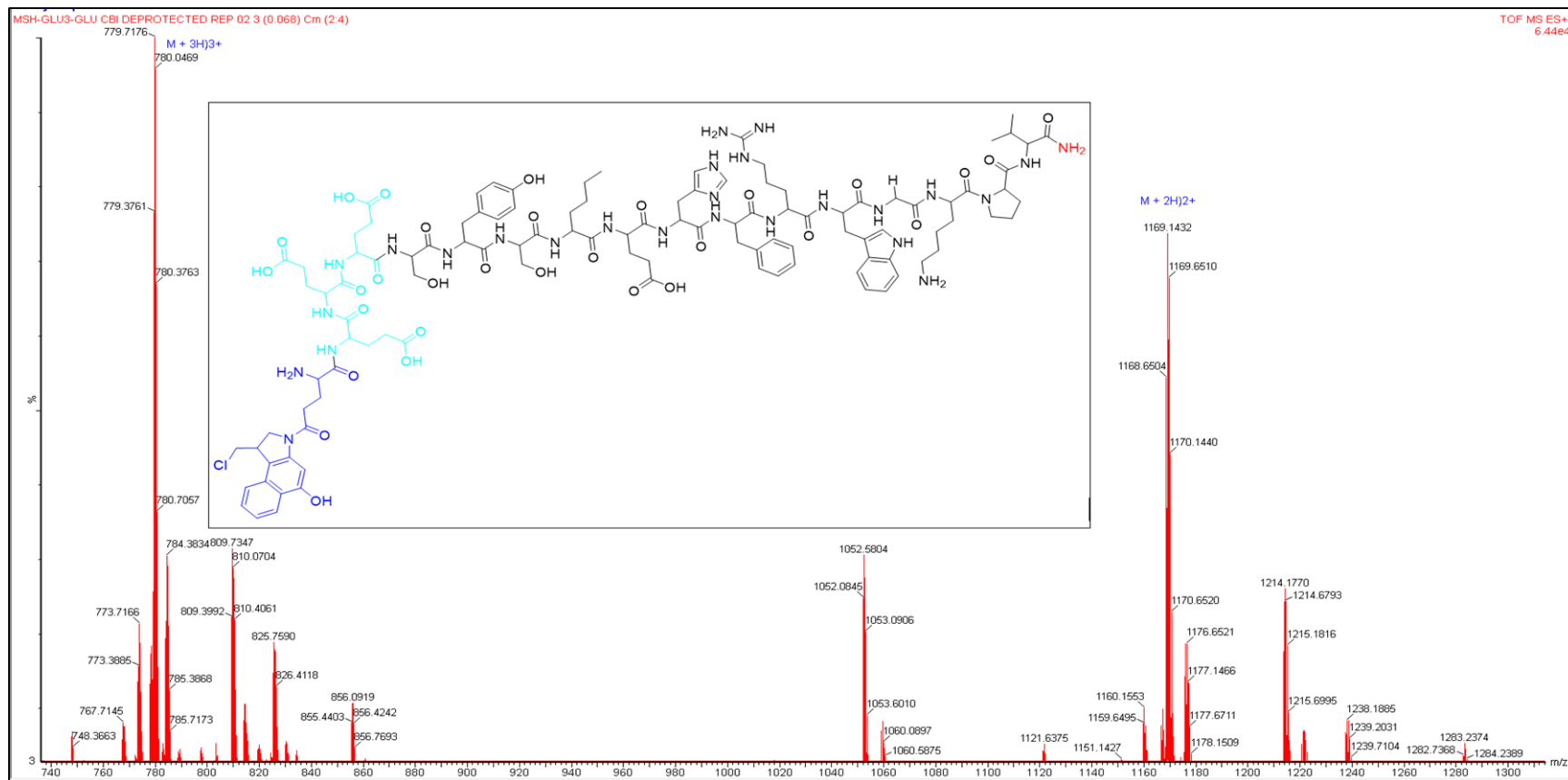
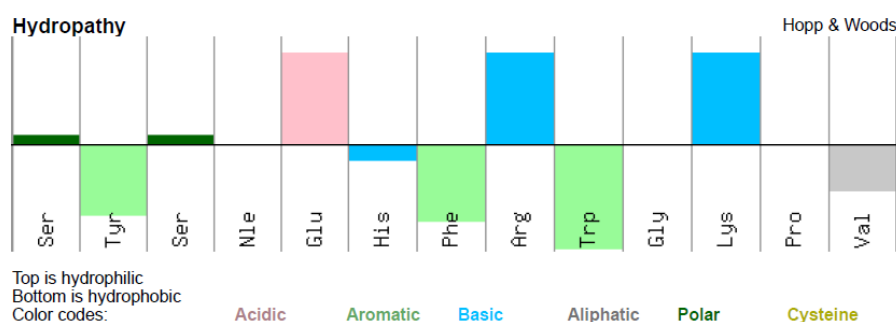


Figure 82: **PDC8**, MSH conjugated to **three glutamic acid** residues and to Benzyl deprotected **Glutamic acid-CBI complex**. Mass spectrometry demonstrates two charge state with 2+ to 3+.

3.7 Scrambled MSH peptide synthesis

In order to demonstrate the specificity of a synthesised peptide drug conjugate to the target receptor, it was initially attempted to find a cell line that does not express MC1R; however, the literature search as will be explained in chapter 04 suggested that MC1R was expressed on multiple cell lines and therefore made it difficult to find a suitable negative control. As a result of this complication, it was decided to use scrambled MSH peptide as an alternative. An initial attempt to scramble MSH was carried out randomly to afford peptide **P4**. Subsequently comparison of the parent MSH against the scrambled peptide **P4** as shown in Figure 83 demonstrated that **P4** maintained levels of similarity to the parent compound as described in Chapter 04.

a)



b)

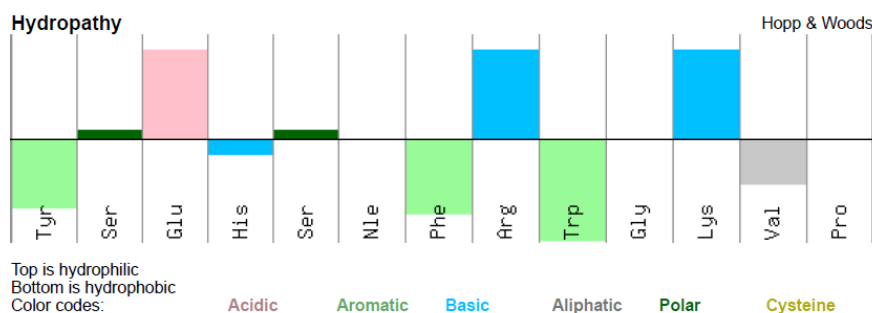
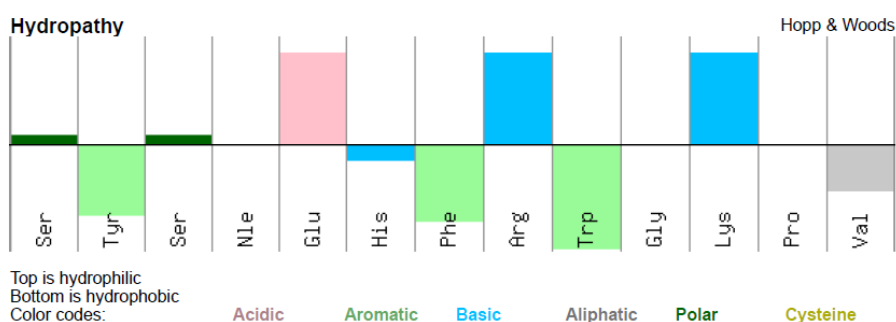


Figure 83: The amino acid property of a) MSH peptide and b) the first scrambled MSH peptide **P4** synthesised (<http://pepcalc.com/>)

Upon closer inspection it was noticed that the activity demonstrated by scrambled MSH peptide **P4** was potentially due to the fact that conserved MSH region of HFRW as explained in the introduction was not scrambled sufficiently in **P4**, where the FRW was maintained and only the H was substituted with Nle. Upon literature research it was also clear that FRW sequence was paramount in the activity of MSH and therefore in order to obtain a scrambled MSH peptide that would potentially be used as a control, extensive modification of this common region had to be considered. ^{149,165}

The second attempt to synthesise another scrambled peptide **P5** as demonstrated in Figure 84 was therefore focused on making sure that the HFRW conserved region was sufficiently substituted to assess if the activity can be significantly abolished.

a)



b)

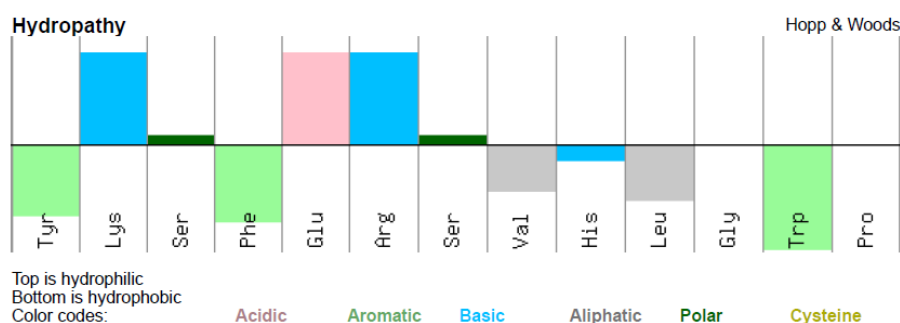


Figure 84: The amino acid property of a) MSH peptide and b) the second scrambled MSH peptide **P5** synthesised (<http://pepcalc.com/>)

3.8 Peptide Drug Conjugate Solubility

The duocarmycins and CBI are in nature very hydrophobic¹¹⁴ therefore the conjugation of these compounds onto peptide may reduce the water solubility of the final peptide drug conjugate. This was observed when the glutamic acid-CBI complex was conjugated to α -MSH where the water solubility was significantly diminished, rendering the peptide drug conjugates no longer water soluble. The large majority of the failure observed during drug development is attributed to limited water solubility¹⁶⁶ and as previously reported by Connelly et al, most of the products that demonstrate higher potency, suffer from the lack of solubility.¹⁶⁷ Therefore, additional assessments were carried out to investigate how to increase the water solubility of the peptide drug conjugate. Addition of arginine on a peptide to increase the water solubility has previously been reported¹⁶⁸ and in this case it was also decided to use three arginine as a linker to afford **P2** (Figure 85). Assessment of HPLC data and mass spectrophotometry data revealed the correct compound **P2** with $[M+2H]^{2+}$ of 1036.919 and $[M+3H]^{3+}$ of 691.61 (Figure 85).

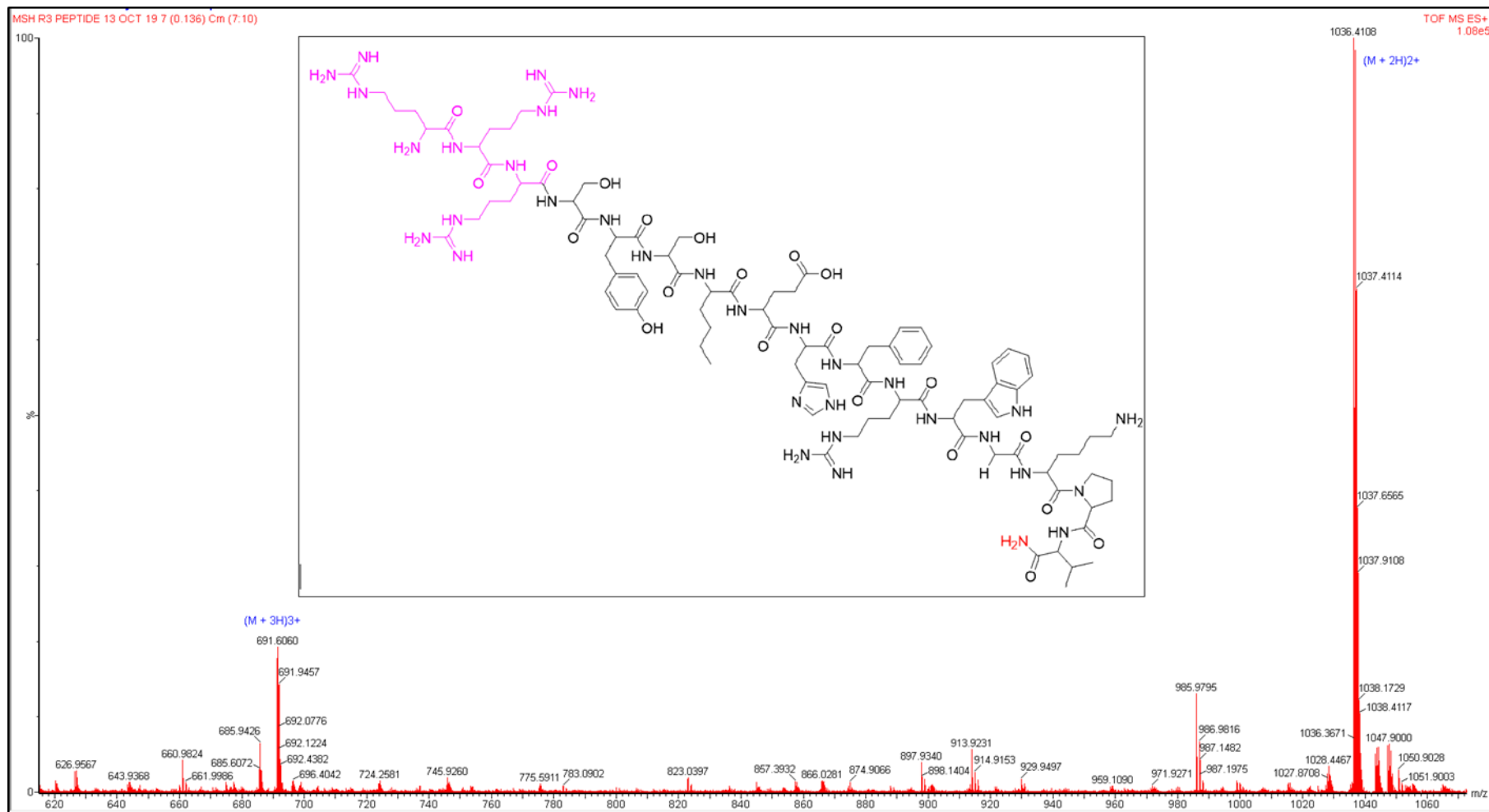


Figure 85: **P2**, MSH conjugated to three arginine residues. Mass spectrometry demonstrates two charge state with 2+ and 3+.

Following the synthesis of **P2**, the Glutamic acid-CBI complex warhead was coupled to afford **PDC2** and then subsequently benzyl deprotected using BBr₃ to afford biologically active peptide drug conjugate **PDC7**. The inclusion of three arginine linker improved the solubility of the peptide drug conjugate. The inclusion of arginine and Glutamic acid linker increase the number of organic functional group which should increase compound solubility.¹⁶⁹

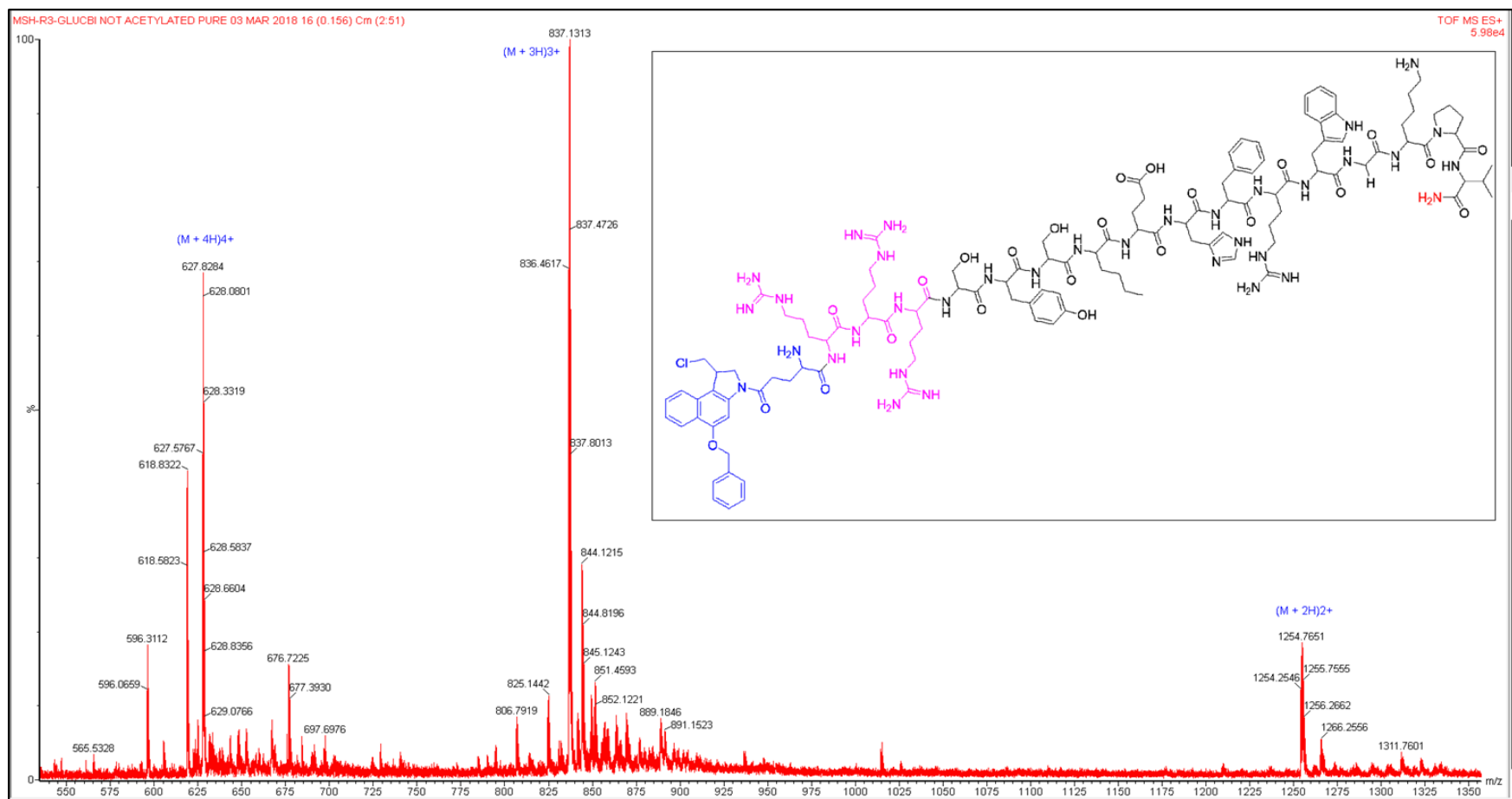


Figure 86: **PDC2**, MSH conjugated to **three arginine** residues and to benzyl protected **Glutamic acid-CBI complex**.

Three glutamic acid were also coupled to α -MSH and used as linker to synthesize peptide **P3**; followed by coupling of glutamic acid-CBI complex to afford **PDC3** (Figure 87) and then subsequently benzyl deprotected using BBr₃ on the resin to afford biologically active peptide drug conjugate **PDC8** (Figure 82). Prior to benzyl deprotection **PDC3** was cleaved off the resin and then purified using the HPLC followed by the assessment on the mass spectrometry. The data generated on the mass spectrometry confirmed that the correct compounds had been synthesised showing **PDC3** at mainly two charge states with $[M+2H]^{2+}$ calculate at 1213.55 and found 1213.66 and $[M+3H]^{3+}$ calculate at 809.37 and found 809.39 (Figure 87).

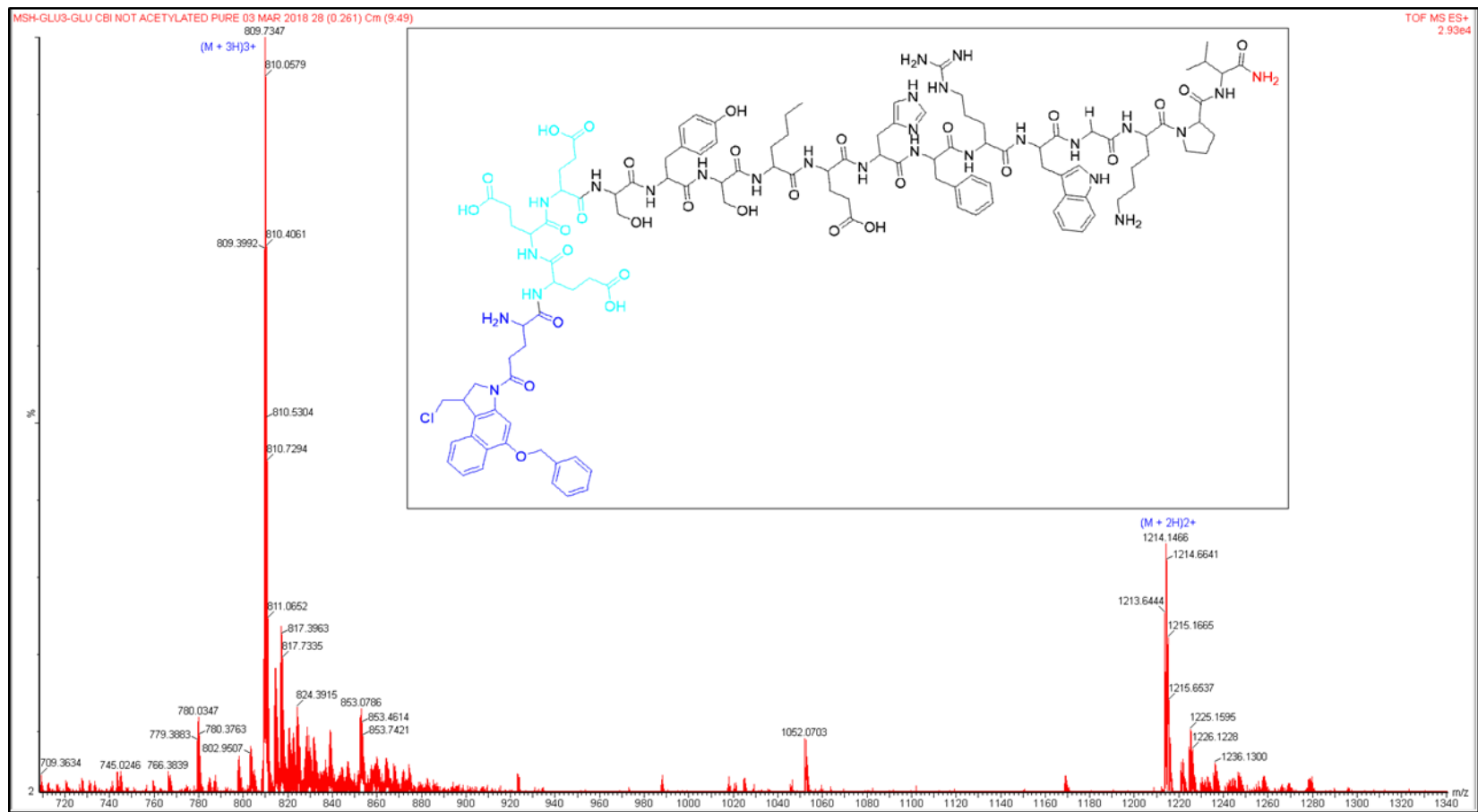


Figure 87: **PDC3**, MSH conjugated to **three glutamic acid** residues and to Benzyl protected **Glutamic acid-CBI complex**.

3.9 Incorporation of the DNA binding subunit

Following the synthesis of various peptide drug conjugates and improvement in compound solubility, the next step was to assess if there could be improved potency as will be discussed in the following chapter. One of the approaches to improve the potency was to incorporate the DNA binding subunit. The DNA binding subunit has been demonstrated to control the binding into the minor groove and to play a crucial role in enhanced DNA alkylation activity.¹⁷⁰ Tischener et al, have demonstrated that removal of the binding subunit in yatekemycin resulted in 10,000 fold activity reduction.¹⁷¹ Incorporation of the binding unit was therefore an avenue to consider for potency increase. The incorporation of the binding unit was carried out as described in chapter 02 followed by conjugation to peptide. Following demonstration that incorporation of arginine as a linker improved the solubility and activity of the peptide, it was decided to also conjugate the glutamic-DNA subunit-CBI complex to **P2** and then benzyl deprotected on the resin to afford peptide **PDC9**. The native MSH peptide **P1** without linker was used as a control to conjugate the glutamic-DNA subunit-CBI complex to afford **PDC10** which was cleaved from the resin initially to confirm successful coupling of the warhead incorporating the DNA binding unit. **PDC10** was purified on the HPLC and then assessed on the mass spectrometry which confirmed that the correct compounds had been synthesised showing **PDC10** at mainly two charge states with $[M+2H]^{2+}$ calculated at 1099.02 and found 1099.11 and $[M+3H]^{3+}$ calculate at 733.01 and found 733.03 (Figure 89).

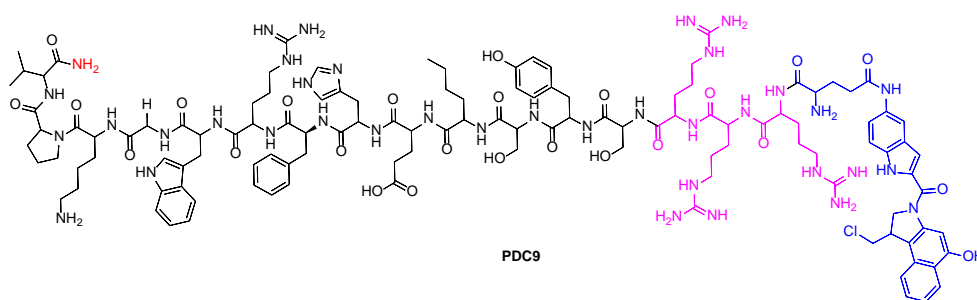


Figure 88: **PDC9**, benzyl deprotected MSH conjugated to three arginine residues and to Glutamic acid-DNA Binding unit-CBI complex.

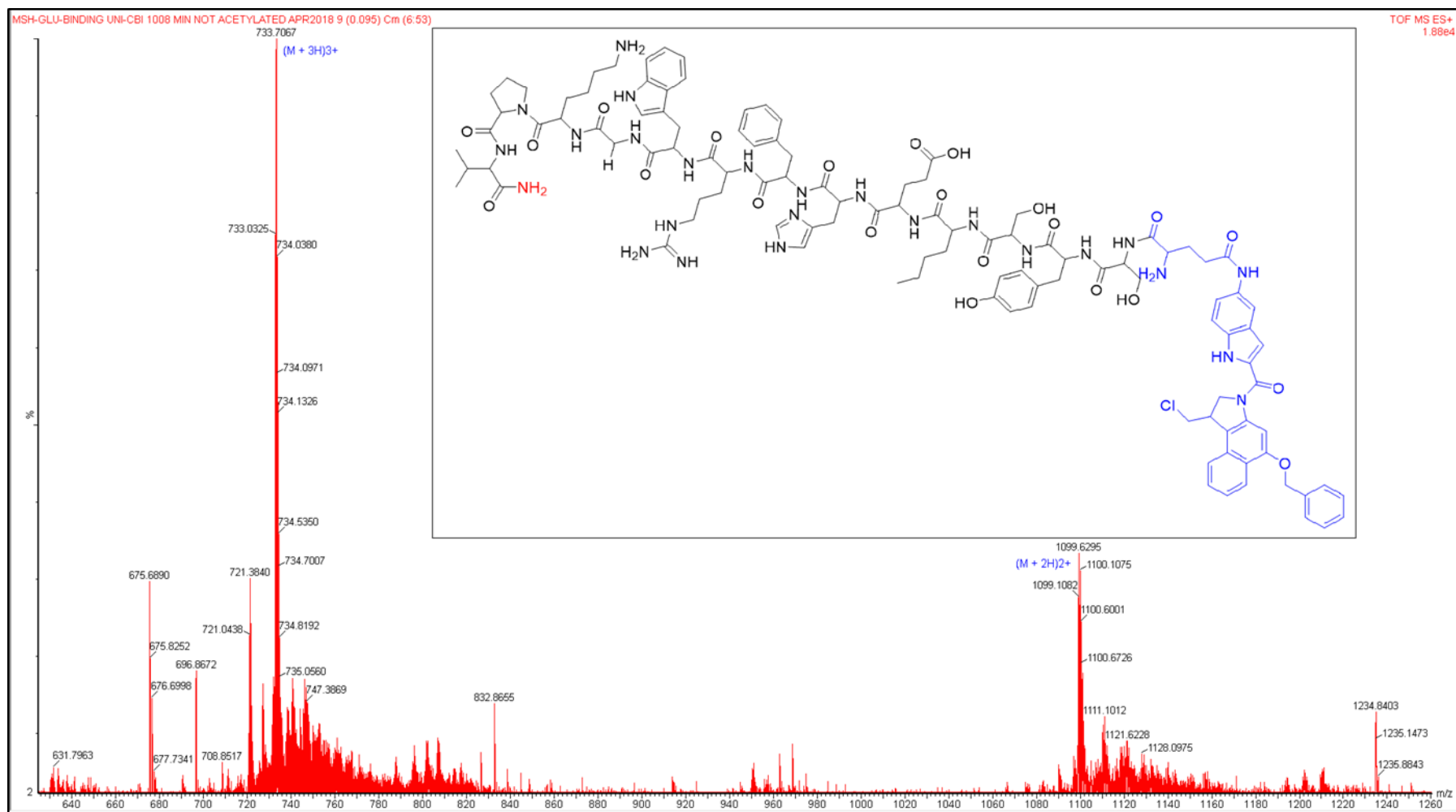


Figure 89: PDC10, benzyl protected MSH conjugated to Glutamic acid-DNA Binding unit-CBI complex.

3.10 Conjugation of labels

3.10.1 Biotin label conjugation on the solid phase

[Nle⁴,dPhe⁷]α-MSH peptide was conjugated to Biotin (Figure 90) on the resin to afford labelled **PL1**, in order to help with the assessment of cells expressing desired MC1R on the flow cytometry. Biotin was dissolved in DMF and conjugation was carried out on the resin using HATU coupling reagent. The cleavage of biotinylated [Nle⁴,dPhe⁷]α-MSH was also affected by 95 % TFA, 2.5 % TIPS, and 2.5 % water. **PL1** was purified on the HPLC and then assessed on the mass spectrometry. The data obtained on the mass spectrometry confirmed the correct mass for the peptide, showing multiple charge state of the peptide from one charge to three charge states. One charge state calculated (M + 1H)¹⁺: 1830.91; found: 1831.24; two charge state calculated (M + 2H)²⁺: 915.96; found: 916.04, three charge state calculated (M + 3H)³⁺: 610.98; found: 610.98) (Figure 82).

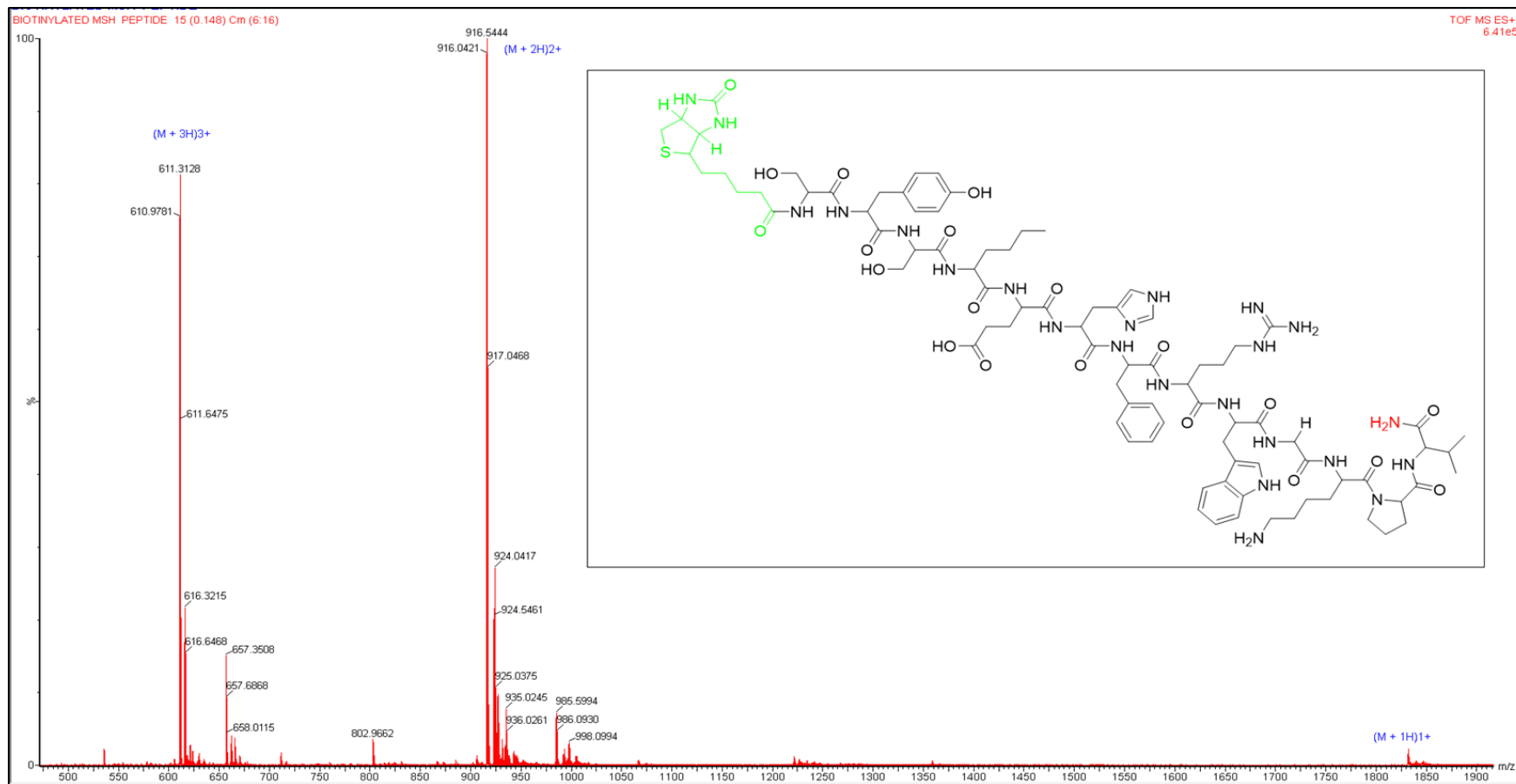
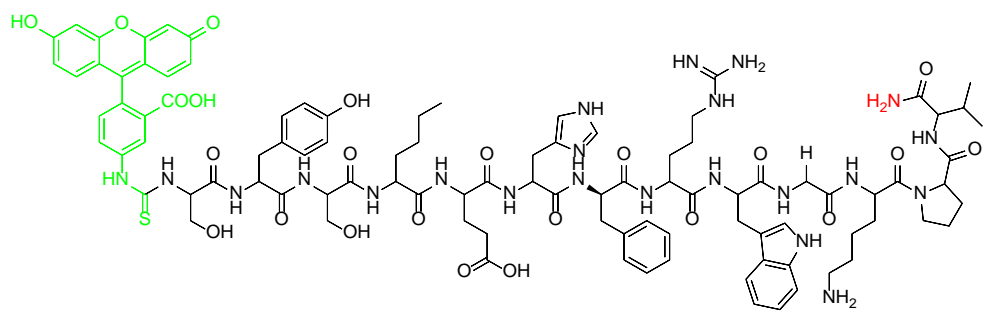


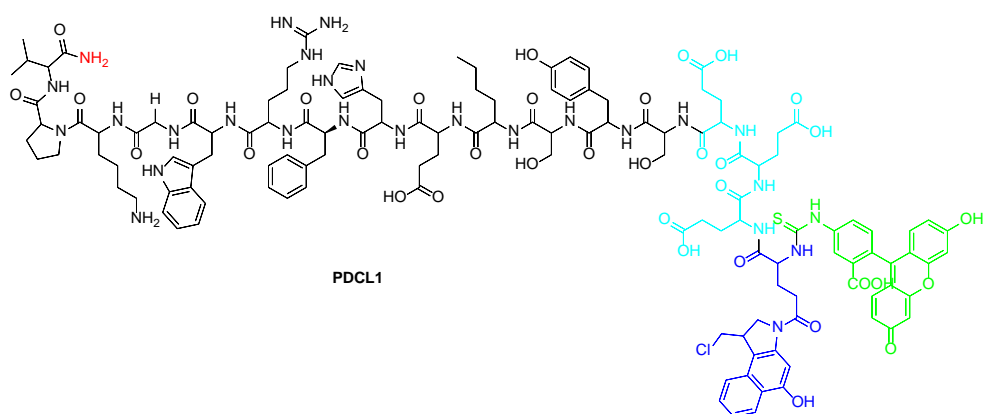
Figure 90: **PL1**, Biotinylated [Nle⁴,dPhe⁷]α-MSH showing the Biotin added in green

3.10.2 FITC label conjugation on the solid phase

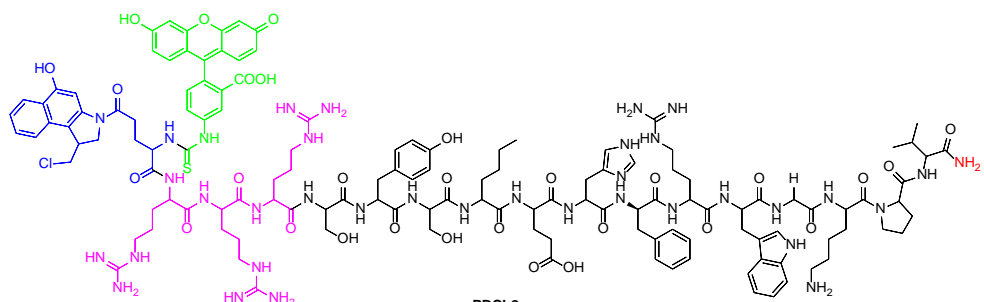
In order to assess the cell binding of [Nle⁴,dPhe⁷]α-MSH peptide conjugated to the CBI war head. **P1**, **PDC7** and **PDC8**, incorporating glutamic acid CBI complex, were all conjugated with FITC to afford **PL2**, **PDCL1** and **PDCL2** (Figure 91). This was carried out in order to obtain a direct alternative to use on the flow cytometry and assess their binding to the MC1R receptor. Peptide drug conjugates were used in this case to demonstrate that conjugation of the war head to the [Nle⁴,dPhe⁷]α-MSH peptide did not abolish the binding to MC1R receptor. FITC conjugation was carried out on the solid phase. The cleavage of FITC conjugated peptides from the resin were affected by 95 % TFA, 2.5 % TIPS, and 2.5 % water.



PL2



PDCL1



PDCL2

Figure 91: FITC conjugated [Nle⁴,dPhe⁷] α -MSH showing FITC in green (PL2), FITC conjugated of compound PDC3 and benzyl deprotected CBI in blue and also showing FITC in green (PDCL1), FITC conjugated of compound PDC2 and benzyl deprotected CBI in blue and also showing FITC in green (PDCL2).

3.11 Conclusion

Fmoc solid phase synthesis was demonstrated to be an effective tool to synthesise α -MSH and could be used for other targeting peptides as it provides ease of synthesis and many opportunities to modify the sequence at a chosen point. The latter can be very powerful when incorporating, for example, cytotoxic drugs and other modifications such as those to make the peptide more soluble as demonstrated in the case of arginine. This data also demonstrate that peptide activity does not necessarily require the full peptide sequence as the use of scrambled peptide containing the common HRFW sequence was also demonstrated to be active. This could be something to investigate in the future but highlights additional potential with peptide drug conjugates. The ability to remove the benzyl protecting group using BBr_3 on the resin demonstrated here, is the preferable approach as this removes the risk in handling cytotoxic compounds at an early stage and allows the benzyl deprotection at the end of the synthesis before removal of the peptide drug conjugate from the resin. Such an approach would allow the synthesis of larger quantity of peptide drug conjugate without the risk of handling cytotoxic compound until final cleavage from the resin.

**CHAPTER 4: BIOLOGICAL ACTIVITY OF SYNTHESISED PEPTIDE
DRUG CONJUGATES**

4.1 Chapter 4 Aims

Chapter 04 describes the assessment of biological activity of synthesised peptide drug conjugates and how their activity influenced the synthesis of additional compounds with improved activity. This chapter will be subdivided into the following parts:

- MC1R expression, the choice of cell line and culturing procedure
- Assessment of a library of synthesised peptide drug conjugates
- Assessment of cellular binding of the peptide drug conjugate
- Modification of the peptide sequence to optimize the activity
- Future considerations

4.2 Expression of MC1R in melanoma

MC1R RNA expression has previously been analysed by the Human Protein Atlas in various cell lines from their database and it was demonstrated that MC1R was expressed on multiples cell lines corresponding to various organs, but the highest expression was particularly seen in human melanoma cell line SKMEL-30 (Figure 92).¹⁷² The expression of MC1R on normal melanocytes is classified as low and it is estimated to be around 700 MC1R per melanocyte.¹⁷³ mRNA expression of MC1R has been demonstrated in a large variety of other primary cells; however, the assessment of MC1R RNA expression in primary cells is limited by the fact that culturing conditions are restricted to the type of primary cell line of interest and this is an important variable to consider, especially as certain cell culture condition can favour the expression of MC1R. The other discussion associated with reported level of MC1R expression is in regard to the functional relevance of the amount of mRNA detected, as most reported expression in some primary cells required a higher level of amplification to reach detectable levels, suggesting that these lower levels may not necessarily have any physiological relevance. The latter was further evaluated by Roberts et al. by looking at the cAMP stimulation in various cells, where MC1R mRNA expression was reported. Interestingly, this demonstrated that cells such as keratinocytes and fibroblasts, where low levels of mRNA expression were reported, did not have any detectable stimulation of cAMP while melanocytic cells did.¹⁷⁴

Overall this suggest that despite the presence of mRNA expression of MC1R in various cells, the expression may be lower and therefore not lead to protein expression and as a consequence have no physiological relevance. On the other hand overexpression of MC1R has been reported on the vast majority of melanoma making MC1R an appropriate target.¹⁷⁵

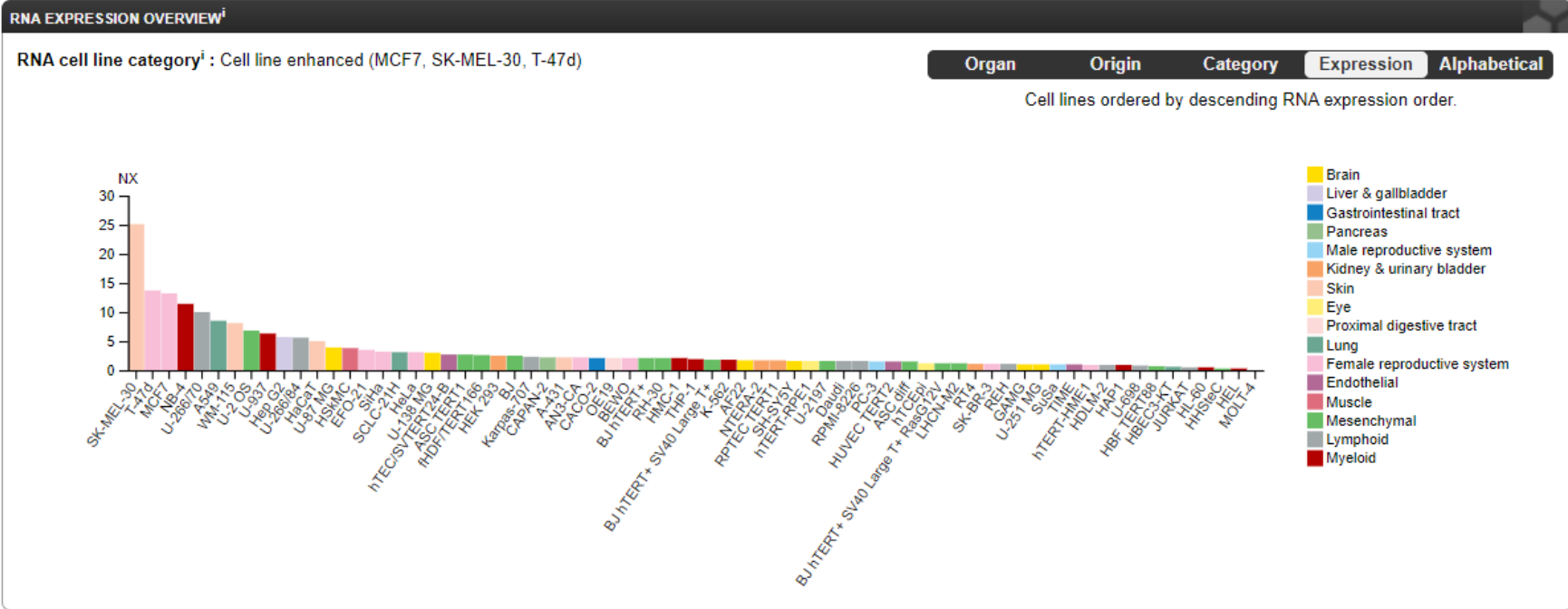


Figure 92: MC1R receptor expression on various cell lines¹⁷²

4.3 Materials and methods

4.3.1 Materials

4.3.1.1 Cells

SKMEL-28, a human melanoma cell line isolated from a 51 year-old male with malignant melanoma and A345, a melanoma cell line isolated from a 54 year-old female with malignant melanoma, were obtained from Professor Maria O'Connell's Laboratory at UEA.

4.3.1.2 Cell culture media and flasks

Roswell Park Memorial Institute (RPMI) 1640 medium, T25 and T75 were purchased from ThermoFisher Scientific.

4.3.1.3 CellTiter-Glo® Luminescent Cell Viability Assay and CellTiter 96® AQueous One Solution Cell Proliferation Assay

CellTiter-Glo® Luminescent Cell Viability Assay and CellTiter 96® AQueous One Solution Cell Proliferation Assay were both purchased from Promega UK LTD (2 Benham Road, Southampton Science Park, Chilworth Southampton, Hampshire SO16 7QJ).

4.3.1.4 Additional reagents

The following reagents were sourced from commercial suppliers and used as per manufacturers instruction:

Reagent	Supplier	Storage conditions
Dulbecco's phosphate buffered saline	ThermoFisher Scientific	2-8°C
Penicillin-streptomycin	ThermoFisher Scientific	-20°C
200 mM L-glutamine	ThermoFisher Scientific	-20°C
Dimethyl sulfoxide (DMSO)	Sigma-Aldrich	RT
Heat-inactivated fetal bovine serum (FBS)	Sigma-Aldrich	-80°C
BSA	ThermoFisher Scientific	2-8°C
0.05% Trypsin with EDTA	ThermoFisher Scientific	-20°C

4.3.2 Methods

4.3.2.1 Cell culture media preparation

Cell culture media for both SKMEL-28 and A345 were prepared in the laboratory as follows:

- 440 mL of RPMI-1640 w/o glutamine
- 50 mL heat-inactivated fetal bovine serum (FBS) (10%)
- 5 mL penicillin-streptomycin (1%)
- 5 mL 200 mM L-glutamine (1%)

Note: RPMI-1640 containing L-glutamine can be purchased from a trusted supplier. In this case, no further L-glutamine was added.

4.3.2.2 Cell thawing and culturing

- Work area was prepared before collecting the cells from their storage location. The safety cabinet was switched on a minimum of 20 min before use and thoroughly cleaned with 70% Ethanol before use.
- SKMEL-28 medium was removed from the fridge (2-8°C) and allowed to warm up at 37°C in a water before being transferred to the safety cabinet.
- The cells were collected from the liquid nitrogen storage tank or -150°C freezer and transferred the vial to the clean room using the Dewar Dilvac liquid nitrogen carrier or dry ice.
- The vial lid was slightly loosened and the cryovial placed on the benchtop at room temperature (nominally 22°C) for approximately 30 seconds. This allowed any liquid nitrogen on the surface to evaporate. The lid was then tightly closed and the vial added in the water bath set at 37°C. The vial was thawed quickly by gentle agitation in the 37°C water bath ensuring that the O-ring remains above the water level to avoid contamination.
- Working quickly, the cells were transferred into the Falcon tube containing 5 mL pre-warmed SKMEL-28 medium and then centrifuged at 500 g for 5 minutes to remove the freezing medium.

- The supernatant was carefully removed and discarded before resuspending the cellular pellet in 25 mL of fresh, pre-warmed SKMEL-28 medium.
- Diluted cells were then transferred into the pre-labelled T25 cell culture flask and placed into the 37°C CO₂ incubator.

4.3.2.3 Cell passaging

- An appropriately sized cell culture flask with vented lid was prepared by adding fresh SKMEL-28 growth medium prewarmed at 37°C.
- Cells were passaged at 80-90% confluency which was achieved approximately every 2-3 days. Confluency was assessed using an inverted light microscope.
- The medium overlaying the cells was removed and discarded before washing the cells with sterile PBS (Ca²⁺- and Mg⁺-free) twice.
- The monolayer cells were detached by adding sterile 0.05% (1X) Trypsin with EDTA and incubate the flask at 37°C in the CO₂ incubator for 5-10 minutes.
- Once the cells were detached, pre-warmed SKMEL-28 growth medium was added to the flask to neutralise the Trypsin. Cells were counted followed by seeding the cells at approximately 2-6x10³/cm² and then transferred the flask to the incubator.

4.3.2.4 Freezing cells for long-term storage

- For long term storage, cells were suspended in a freezing medium and then maintained in a liquid nitrogen storage tank or in a -150°C ultrafreezer.
- SKMEL-28 cells were frozen when they reach a confluency of approximately 85%.
- Freezing medium consisted of sterile, heat-inactivated FBS containing 10% v/v dimethyl sulfoxide (DMSO).
- Cells were washed and detached as detailed in the section 4.3.2.3 followed by Centrifugation at 500 g for 10 minutes. The supernatant

was then discarded and then resuspended the cellular pellet in the appropriate volume of freezing medium to obtain a cell density of $3-5 \times 10^6 \text{ mL}^{-1}$ and then immediately aliquot into 1 mL aliquots in the pre-labelled sterile cryovials.

- Aliquots were then placed in a Mr Frosty freezing chamber and promptly transferred to a -80°C freezer.
- After 24-48 hours, the cryovials were transferred in a liquid nitrogen tank or in a -150°C ultrafreezer for long-term storage.

4.3.2.5 Cell based assays

In order to assess the cytotoxic effect of synthesised peptide drug conjugates, various assay methods were carried out including the MTS assay, CellTitre-Glo assay and the use of real-time cell analysis using xCelligence RTCA instrument.

4.3.2.6.1 MTS assay

MTS are cell based assays that determine cell viability using tetrazolium salt reduction. Tetrazolium reduction assays are subdivided into two categories: those utilising positively charged tetrazolium salt such as MTT and those utilising negatively charged tetrazolium such as MTS used in this thesis. Positively charged tetrazolium salt suffers from the fact that the formazan product produced is not readily soluble in solution and requires an extra step to solubilise the precipitate. The use of MTS that produces a formazan product that is readily soluble is preferred. However, the negative charge on the tetrazolium salt makes it less permeable,¹⁷⁶ and as a result the MTS salt is combined with electron acceptor reagents such phenazine methyl sulfate (PMS), which can penetrate the cell and become reduced in the cytoplasm and subsequently exit the cytoplasm to reduce MTS and produce a soluble red formazan dye which absorbs at 492 nm (Figure 93). The rate at which MTS is converted to the red dye is dependent upon the number of viable cells present.¹⁷⁷

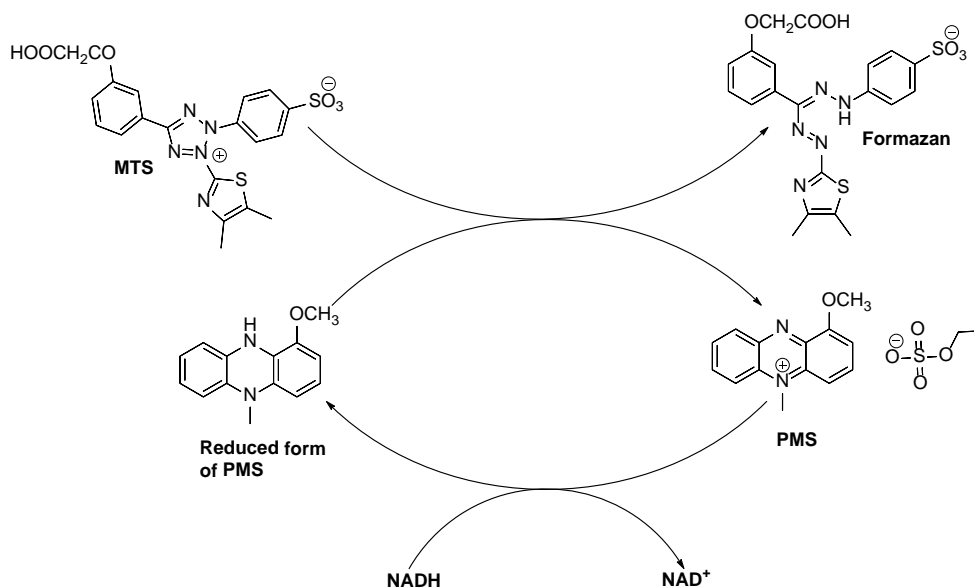


Figure 93: Intermediate electron acceptor phenazine methyl sulfate (PMS) transfers electron from NADH in the cytoplasm to reduce MTS in the culture medium into an aqueous soluble formazan.¹⁷⁸

4.3.2.6.2 MTS Analytical assay procedure

- Cell were detached as described in section 4.3.2.3, resuspended, counted and then diluted to desired seeding density (For SKMEL-28 1×10^5 cells/mL was used) with pre-warmed media.
- Cells were then plated out by adding 100 μ L of diluted cells followed by an incubation of the cells overnight at 37°C, 5% CO₂ for them to adhere to the plate.
- The next day 100 x the compounds final concentration was prepared, followed by the addition of 1 μ L to the plate containing cells and then incubated at 37°C, 5% CO₂ for the desired time period (48-72 hours).
- About 1 hour before the end of the time period, MTS reagent was taken out of the freezer and allowed to thaw on the bench.
- Once the plate had been incubated with the compound for the desired time period, the cells were checked under the microscope to determine visually which wells contain cells that are alive and which contain cells which are dead.

- 10 μ L MTS reagent was then added to each well that contains either cells or media, incubated and then read using the Optima plate reader at 492nm.
- Blank subtracted the absorbance reading against the media absorbance reading.

4.3.2.6.3 CellTitre-Glo assay

CellTitre-Glo was used as an alternative method to assess cell viability through the measurement of ATP released from viable cells. ATP is used as a cell viability marker because dead cells lose the ability to synthesis ATP and also any pre-existing cytoplasmic ATP is depleted by endogenous ATPases. In order to detect ATP, the cells are lysed by a lysis buffer, which also contains the ATPase inhibitor to prevent depletion of pre-existing ATP.¹⁷⁷ The luciferase enzyme catalyses the mono-oxygenation of luciferin in the presence of Mg^{2+} , molecular oxygen and ATP released from lysed cells, producing a stable luminescent signal (Figure 94).¹⁷⁹ In comparison to MTS assay the CellTitre-Glo presents several advantages as it is faster, more sensitive and has a larger dynamic range.¹⁷⁷

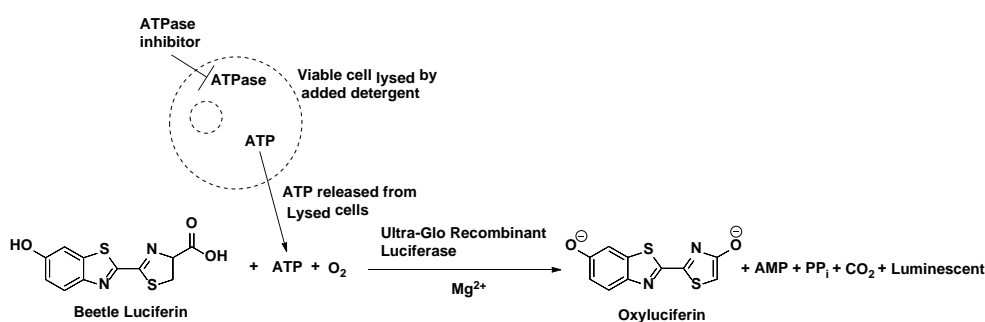


Figure 94: Reaction between Luciferase enzyme in the presence of Luciferin Mg^{2+} , molecular oxygen and ATP released from lysed viable cells.¹⁷⁹

4.3.2.6.4 CellTitre-Glo® assay analytical procedure

- Cell culturing and compound treatment were carried out as described in the MTS assay procedure section 4.3.2.6.2.
- About 1 hour before the end of the cell/compound incubation time period, the CellTitre-Glo® reagent was taken out of the freezer and allowed to thaw on the bench.
- Once the plate has been incubated with the compound for the desired time period, the cells were checked under the microscope to determine visually which wells contain cells that were alive and which contain cells which were dead.
- CellTitre-Glo® substrate vial was reconstituted with one CellTitre-Glo® buffer vial provided in the kit and mixed to make sure it was fully dissolved.
- 100 µL of reconstituted CellTitre-Glo® substrate reagent was added to each well that contained either cells or media.
- The plate was mixed for 3 minutes on an orbital shaker set at 300 rpm to induce cell lysis, followed with a 10 min incubation at RT to allow equilibration.
- The luminescence was recorded using the Perkin elmer, envision plate reader instrument.

4.3.2.6.5 xCELLigence assay

xCELLigence is a relatively new real-time cell analysis that was also used to assess the impact of synthesised compounds. The xCELLigence system uses e-plates that have gold microelectrodes in their base that allow the measurement of impedance differences that are subsequently converted to cell index within an electrical circuit (Figure 95). The cell index is affected by multiple factors such as cell attachment, number and size and as a result can provide more real-time cell functional data such as proliferation and death. The xCELLigence system is more suited for adhesion cells as the measurement of CI require cells to be attached to the electrode; however, recently additional studies have been carried to assess the use of suspension cells with an adhesion molecule such as collagen etc.^{180,181}

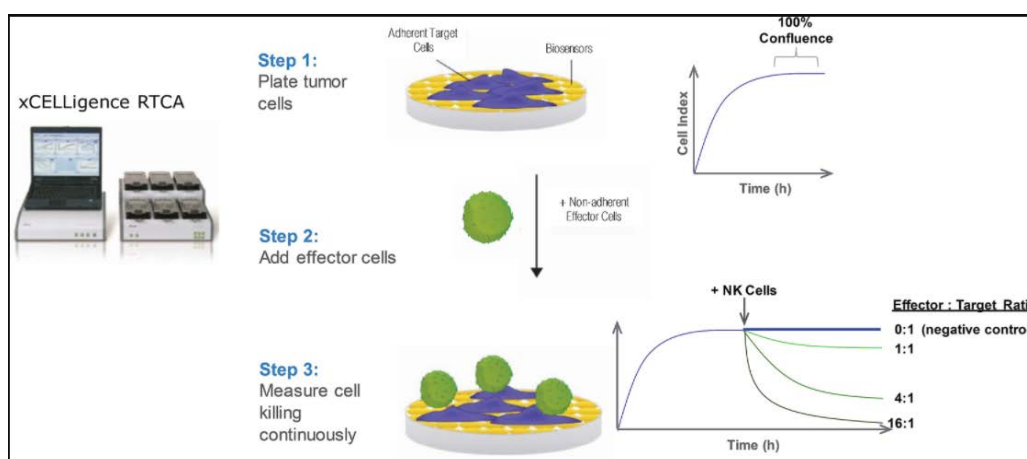


Figure 95: Simplified diagram that demonstrate xCELLigence Real-Time Cell Analyzer (RTCA) System. In this assay example, the target cells are initially seeded in the E-plate and allowed to attach and grow overnight. The effector cells (e.g. NK cells) are then added into the same well. Cytotoxicity is proportional to the concentration of effector cells.¹⁸¹

4.3.2.6.6 Xcellingence assay procedure

- Cells were cultured, detached and counted as described in section 4.3.2.3. Cells were then diluted at desired seeding density (For SKMEL-28 and A375 1×10^5 cells/mL was used) with pre-warmed media.
- Cells were plated by adding 100 μ L of diluted cells in the E-plate as indicated on the plate map.
- The E-plate was equilibrated with cells at room temperature for 30 min to allow the cells to settle evenly on the bottom of the well.
- Following the equilibration, the E-plate was brought back to the RTCA located in the incubate set at 37°C, 5% CO₂ and the measurement of impedance was initiated. The software was set to display Cell Index versus Time automatically at every 60 min.
- The cells were incubate overnight at 37°C, 5% CO₂ prior to treatment with compound stock solutions prepared at 100x the final concentration.
- Prior to adding 1 μ L of the vehicle control and the compound stocks, the RTCA acquisition was paused and the E-plate was brought in the cell culture hood.
- The E-plate was again equilibrated following the addition of compound at room temperature for 30 min and then returned the E-plate to the RTCA to resume recording the impedance.

4.3.2.7 Flow cytometry assay

The flow cytometry technique was used to assess the receptor occupancy of FITC/Biotin conjugated peptide to MC1R. Flow cytometry has been used previously to assess the binding of ligand to G protein coupled receptors.¹⁸²

The principle of the flow cytometer is as demonstrated in Figure 96. Particles including suspended cells are carried in a single file stream through a focused laser beam. Each single cells is then subsequently hit by the laser light, which excites one or more fluorophores associated with that particular cell to emit light at certain wavelength. Emitted light can be deflected as a result of multiple factors including the size/surface area and compartmentalization of the cell to produce forward scatter (FCS) and side scatter (SSC) measurement respectively. Scattered light as well as the fluorescence produced are collected and separated by mirrors and filters, and detected by a photo-multiplier tube.¹⁸³ In this thesis the flow cytometry was used to assess the receptor occupancy of synthesised PDCs. Synthesised PDCs were couple to Fluorescein isothiocyanate (FITC) and incubated with cells to allow binding to the target receptor and then the fluorescence alongside the FCS and SSC were determined to confirm binding of the compounds to the target receptor.

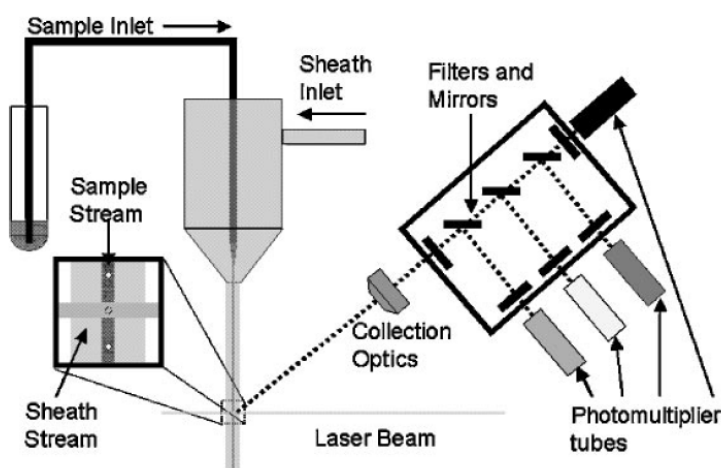


Figure 96:Flow cytometry General Principles

4.3.2.7.1 Flow cytometry assay procedure

- Cells were cultured, detached and counted as described in section 4.3.2.3. Cells were then diluted at desired seeding density (For SKMEL-28 and A375 1×10^5 cells/mL was used) with pre-warmed media.
- 1 mL of 1×10^5 cells/mL was centrifuged at 1500 rpm for 5 minutes, the supernatant was discarded and then the cells were suspended in 1 mL assay buffer (0.3% BSA, 0.02% Na-azide in 1X PBS).
- The cells were centrifuged at 1500 rpm for 5 minutes, the supernatant was discarded and then the cells were suspended in 20 μ L wash buffer then added the following amounts into micro centrifuge tubes.

	1.1. control (μ L)	1.2. stained (μ L)
cell suspension	20	20
FITC/ Biotin labelled compounds	-	5
Assay buffer	80	75

- The cells were incubated overnight at 4 °C and then washed the with 1 mL ice-cold assay buffer.
- The cells were centrifuged at 1500 rpm for 5 minutes, the supernatant was discarded and then the cells were suspended in 1 mL ice-cold assay buffer.
- The previous wash steps were repeated two more times.
- Only for biotinylated compound, streptavidin Phycoerythrin (PE) was added and incubate the tubes for 30 minutes at 4 °C in the dark.
- The cells were centrifuged at 1500 rpm for 5 minutes, the supernatant was discarded and then the cells were suspended in 1 mL ice-cold assay buffer.
- The wash steps were repeated two more times and then the cells were resuspended in 200 μ L BD Cytofix and measured within 3 days using the BD accuri C6 flow cytometry. If not analysed immediately, the cells were kept in the tube in the dark at 4°C.

4.4 Result and discussion

4.4.1 Cell seeding density assessment

Appropriate cell seeding density is crucial to obtain reliable and reproducible cytotoxicity data. As previously reported by Wu et al.¹⁸⁴ when lower seeding density was used, they observed a direct relationship between the cell viability and the cytotoxic agent ascorbic acid-2-phosphate; however, when higher cell density was assessed a relatively higher concentration was required to reduce the number of viable cell significantly.¹⁸⁴ For the work described in this thesis, cell density optimization was only carried out for the CellTitre-Glo® assay and then used the same seeding density for the MTS assay and xcelligence. The cell density used for the xcelligence may have not been optimal because adhesion cells to the gold electrode may not be comparable to clear nunc plates.¹⁸⁵ A paper published by Pasini et al. used 5×10^3 SKMEL-28 cells/mL to assess the effect of TrKA on their proliferation suggesting that the concentration that was used may have been higher.¹⁸⁶

To assess the appropriate cell seeding density, SKMEL-28 cells at various cell numbers (0.5×10^3 , 1×10^3 , 2.5×10^3 , 5×10^3 , 1×10^4 , 2.5×10^4 and 5×10^4 in well cell numbers) were incubated for 72 h with and without DMSO to also assess the effect of 1% DMSO on cell growth. This experiment demonstrated that higher numbers of cells were less affected by 1% DMSO. As can be seen in the data the CellTitre-Glo® was very sensitive and capable of detecting 500 cells/mL after the 72 h incubation, which is one of the advantages of the CellTitre-Glo® compared to MTS assay. Riss et al reported that the CellTitre-Glo® was extremely sensitive and capable of detecting as low as 15 cells.¹⁸⁷ However, because the MTS assay used 10000 cells/well it was maintained at the same density in order to maintain comparability. 10000 cells/well demonstrated sufficient level of cell proliferation after 72 hours and was less affected by DMSO and therefore was used going forward (Table 1 and Figure 97).

In well Cells number (cells)	SKMEL-28 (No DMSO)			SKMEL-28 (1% DMSO)		
50000	997072	974000	1026656	963540	932544	834456
25000	660308	699068	674504	604812	575784	573760
10000	454000	454940	459124	369864	370948	355800
5000	338104	311688	321036	243680	243944	231788
2500	205008	192684	213728	118228	122768	117392
1000	68912	65084	63312	35852	34344	33712
500	24060	24100	27064	13872	15308	13096
0	388	416	448	428	360	296

Table 1: SKMEL-28 cells proliferation assessment after 72 Hours incubation using the Celltitre-Glo

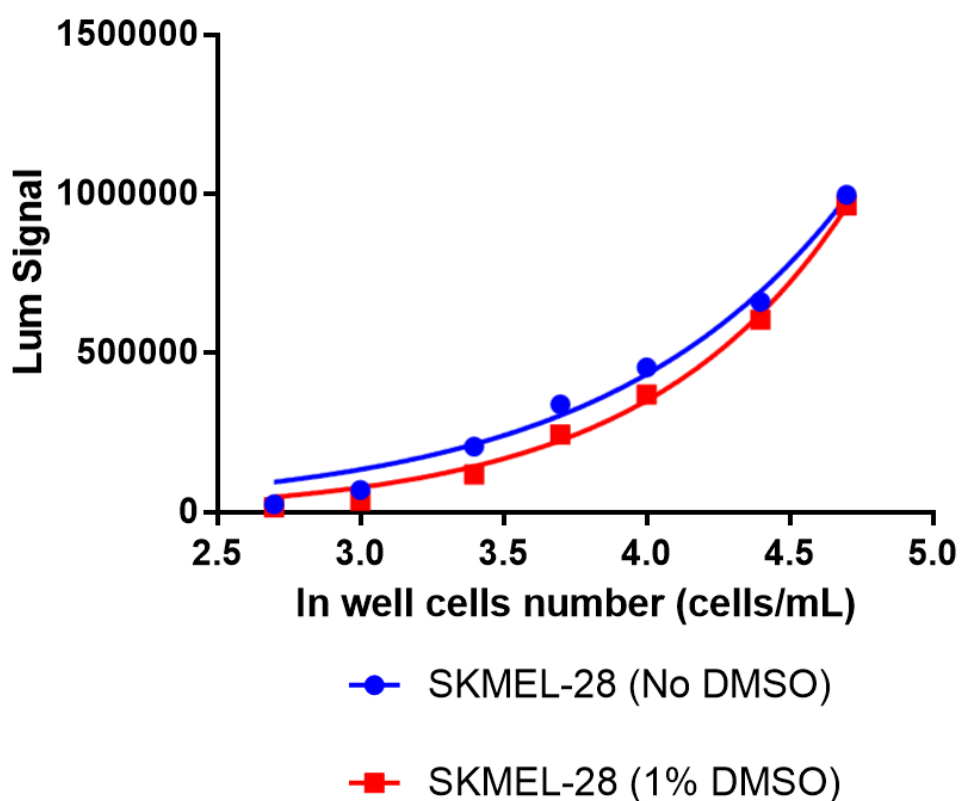
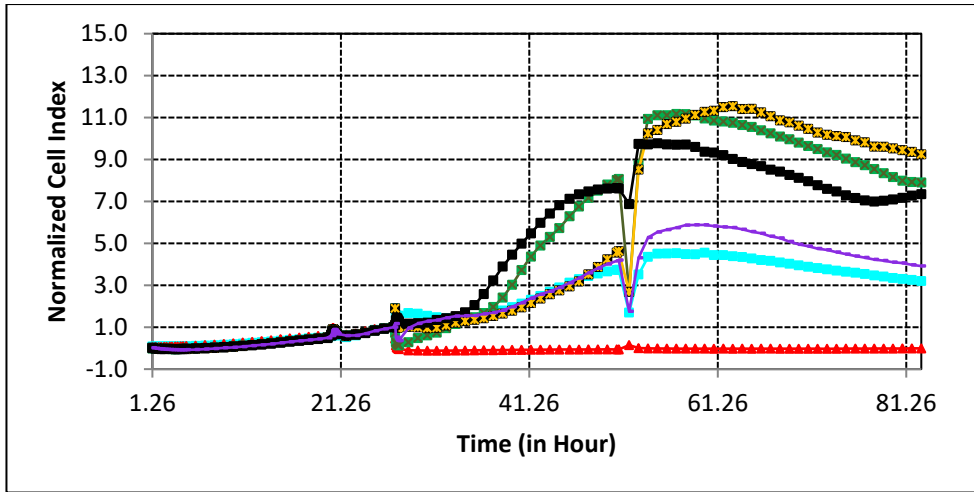


Figure 97: SKMEL-28 cells proliferation assessment after 72 Hours incubation using the Celltitre-Glo

4.4.2 xCELLigence PDC biological assay assessment

Initial cytotoxic assessment of synthesised compounds was carried out using the xCELLigence assay to analyse real time cytotoxic impact on A375 and SKMEL-28 cell lines. **PDC1**, **PDC4** and **PDC6** at the final in well concentration of 1, 10 and 100 μM were assessed alongside three control samples (two negative controls: the first control containing 1% DMSO, the other without DMSO and a positive control contain Triton X-100). All the compounds were assessed against SKMEL-28 and A375 as described in section 4.3.2.6.6. Out of all the PDCs concentrations tested only the 100 μM concentration exerted significant cytotoxic effects on both A375 and SKMEL-28 cell lines. As described in the previous section the cell number used in this experiment may have been higher and therefore requiring a higher concentration to exert desired cytotoxic effect. The data obtained for both the A375 and SKMEL-28 cell lines demonstrated that the benzyl protected PDC compound **PDC1** did not exert any cytotoxic activity as the response was comparable to that of the control. Triton X-100 which was used as a positive control to demonstrated cell death, exerted cytotoxic activity shortly after addition. Compound **PDC4** which contains two protected warhead demonstrated very low activity only in SKMEL-28 cells compared to compound **PDC6** which contains one deprotected warhead which demonstrated cytotoxic activity on both A375 (Figure 98) and SKMEL-28 (Figure 99). The data obtained in this experiment demonstrated the cytotoxic activity of the benzyl deprotected compound **PDC6**; however, the concentration required to achieve this activity was higher than expected and the next step would have been to assess lower cell seeding density but due to limited time to access the instrument this was not carried out. Further investigations were carried out using alternative end point cytotoxic cell based assays: the MTS assay and CellTitre-Glo.









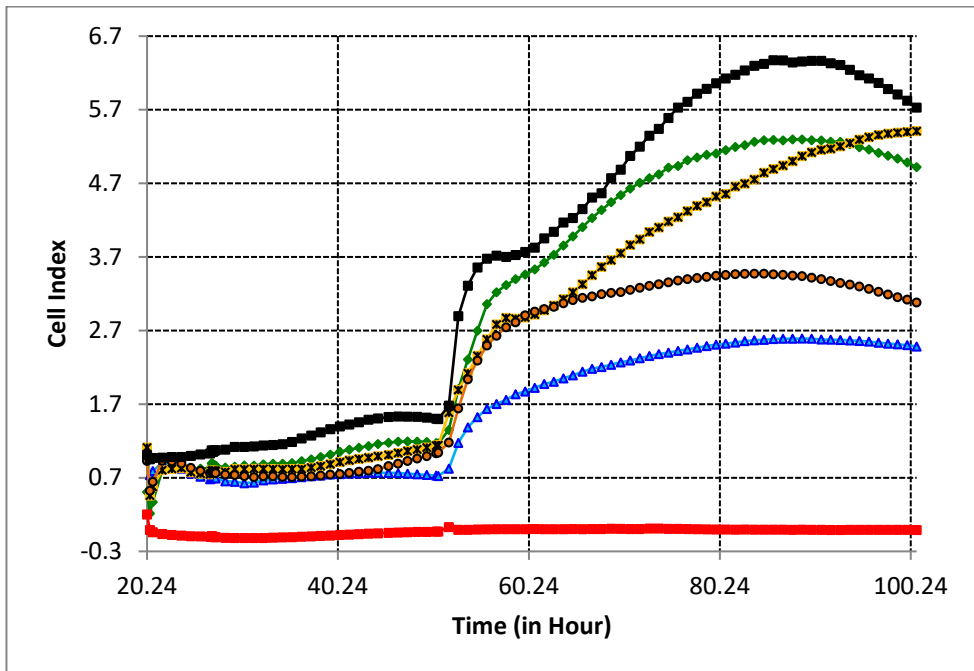
-  A375 without 1% DMSO
-  A375 plus 1% DMSO
-  Benzyl protected MSH-(Glu-CBI)1 (**PDC1**)
-  Benzyl protected MSH-(Glu-CBI)2 (**PDC4**)
-  Benzyl deprotected MSH-(Glu-CBI)1 (**PDC6**)
-  Triton

Figure 98: Cytotoxic assessment of synthesised **PDC1**, **PDC4** and **PDC6** against A375 using the xCELLigence Real-Time Cell Analysis system









-  SKMEL28 without 1% DMSO
-  SKMEL28 plus 1% DMSO
-  Benzyl protected MSH-(Glu-CBI)1 (**PDC1**)
-  Benzyl protected MSH-(Glu-CBI)2 (**PDC4**)
-  Benzyl deprotected MSH-(Glu-CBI)1 (**PDC6**)
-  Triton

Figure 99: Cytotoxic assessment of synthesised **PDC1**, **PDC4** and **PDC6** against SKMEL-28 using the xCELLigence Real-Time Cell Analysis system

4.4.3 MTS PDC biological assay assessment

The data obtained using the xCELLigence Real-Time Cell Analysis system indicated that benzyl deprotected-compound **PDC6** exerted some antiproliferative activity. The same compound **PDC6** was used to assess if comparable activity can be observed using the MTS assay. While diluting this compound in previous assay, it was observed that solubility in growth media was significantly diminished causing the PDCs to precipitate out of solution, the latter may have contributed to low potency observed with compound **PDC6**; therefore, PDCs incorporating three arginine in a linker were used to assess if this can increase the PDC solubility. The increase in solubility resulting from the addition of arginine residues has previously been reported by Paraskevopoulou et al. where they compared the addition of lysine vs arginine to a poorly soluble bovine pancreatic trypsin inhibitor and demonstrated that arginine increased its solubility significantly.¹⁶⁸ The same approach was used in this thesis to assess if increase in solubility by adding arginine linker between the peptide and the warhead can increase the PDC solubility and therefore improve the cytotoxic potency. **P4**, a scrambled MSH protein conjugated to three arginines and a deprotected warhead was considered as an alternative approach to show specificity as it was not possible to find a negative cell line that lack MC1R expression.

The data obtained from this experiment confirmed the cytotoxic activity observed for compound **PDC6** using the xCELLigence. Benzyl-deprotected **PDC7**, incorporating three arginines as a linker significantly increased cytotoxic activity compared to **PDC6** suggesting that increase solubility was beneficial. However, when scrambled **sPDC6** was used to assess specificity, it also exerted activity with an $IC_{50} = 82 \mu M$, which was comparable to that of **PDC6** with an $IC_{50} = 95 \mu M$. The potential reason for scrambled **sPDC6** to also exert cytotoxic activity was attributed to the fact that the conserved MSH region of HFRW as explained in Chapter 01 and Chapter 03 was not scrambled sufficiently to abolish the binding to MC1R. The FRW sequence was maintained in **sPDC6** and only the H was substituted with Nle, and as a consequence **sPDC6** maintained the cytotoxic activity (Figure 100, Table 2).

In Well Conc (nM)	Deprotected MSH-Glu-CBI (PDC6)			Deprotected MSH-Arg3-Glu-CBI (PDC7)			Deprotected Scrambled MSH-Arg3-Glu-CBI (sPDC6)		
1000000	0.233	0.453	0.959	0.119	0.128	0.11	0.259	0.283	0.253
500000	0.205	0.301	0.35	0.086	0.098	0.094	0.138	0.157	0.149
100000	1.179	1.172	0.983	0.185	0.151	0.107	0.903	0.66	0.88
20000	1.74	1.622	1.819	1.587	1.656	1.166	0.519	1.167	1.487
4000	1.678	1.749	1.517	1.708	1.605	1.513	1.606	1.588	1.608
800	2.038	2.112	1.914	1.919	1.138	1.594	1.307	1.659	1.488
160	2.065	1.86	1.752	2.004	1.977	1.754	1.441	1.835	1.837
32	2.12	1.936	1.645	1.862	1.987	1.959	1.619	1.902	1.978

Table 2: Cytotoxic activity of **PDC6**, **PDC7** and **sPDC6** against SKMEL-28

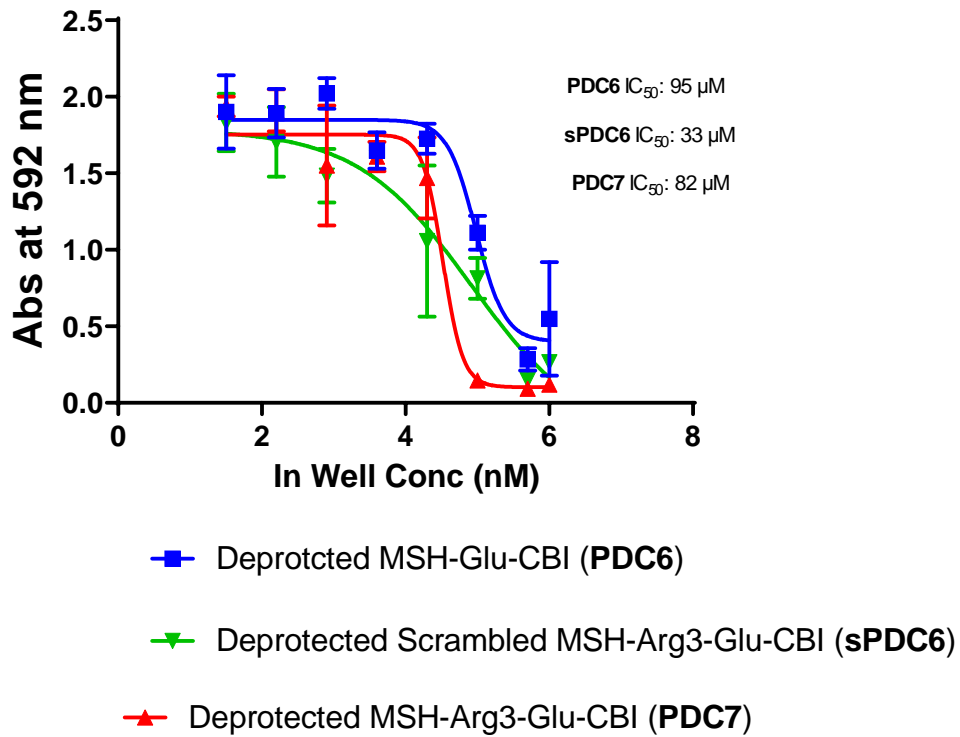


Figure 100: Cytotoxic activity of **PDC6**, **PDC7** and **sPDC6** against SKMEL-28

4.4.4 CellTitre-Glo® PDC biological assay assessment

The CellTitre-Glo® assay is very sensitive method and is able to detect very low numbers of cells compared to the MTS assay, as a consequence the IC₅₀ determined can be significantly lower compared to the MTS assay. In one of the studies conducted by Wang et al., they demonstrated that the IC₅₀ determined using the MTS assay was 120 µM of EGCG against LNCaP and 60 µM EGCG against MCF-7 cells; and when the CellTitre-Glo® was use, the IC₅₀ was determined to be 55 µM and 35 µM respectively.¹⁸⁸

As discussed previously in section 4.4.1, it is possible to use less cell density in the CellTitre-Glo; however, for consistency the same cell number (1 x10⁵ cells/mL) was initially used. All the synthesised PDCs and the parent compound α-MSH were initially analysed at the concentration of 1, 10 and 100 µM; However, due to the limited number data points the IC₅₀ was not reliable. Therefore, the assessment was repeated using more data points at the concentration of 0.16, 0.8, 4, 20, 100 and 500 µM. Overall the data obtained using the CellTitre-Glo also demonstrated that peptide incorporating three arginine amino acid linker (**PDC7**) exerted the highest level of cytotoxic activity followed by the compound **PDC8** which incorporated three glutamic acids as a linker. This data suggests that incorporation of the solubilising linker was beneficial in the increase of CBI potency. MSH peptide and MSH coupled to three arginines were also assessed in this experiment as control and were both demonstrated not to have cytotoxic impact on SKMEL-28 cells. Scrambled **sPDC7** was also demonstrate to exert cytotoxic activity although significantly diminished compared to **PDC7** (Table 3 and Figure 103).

Conc. (nM)	Log Conc. (nM)	MSH (P1)		MSH-GluCBI deprotected (PDC6)		MSH-R3 Peptide (P2)		Scrambled MSH-Arg3-GluCBI Deprotected (sPDC7)		MSH-Arg3-GluCBI Deprotected (PDC7)		MSH-Glu3-GluCBI Deprotected (PDC8)	
0	0	74204	80944	75180	79100	72592	69740	69324	67392	69008	74028	66772	63180
500000	5.699	72420	79104	34556	35212	74128	80040	2044	2832	828	760	852	648
100000	5.000	74064	77372	78344	74260	84764	86968	64956	67684	5076	8244	22396	30324
20000	4.301	71584	77664	78012	75300	76880	80936	72280	74416	65148	69376	61856	65352
4000	3.602	74448	76400	74568	78312	74516	79424	71472	68840	65960	65372	56468	65636
800	2.903	71100	71800	76036	76108	73688	76176	69696	68232	66700	58276	58840	61384
160	2.204	69276	69268	69060	73512	71836	69620	67816	70528	65480	60560	58788	57108
0	0	62256	65032	68120	67904	67828	69320	71316	67284	61368	60120	59468	53024

Table 3: Cytotoxic activity of peptide **P1**, **P2**, **PDC 6**, **sPDC7**, **PDC7** and **PDC8** against SKMEL-28 cell line

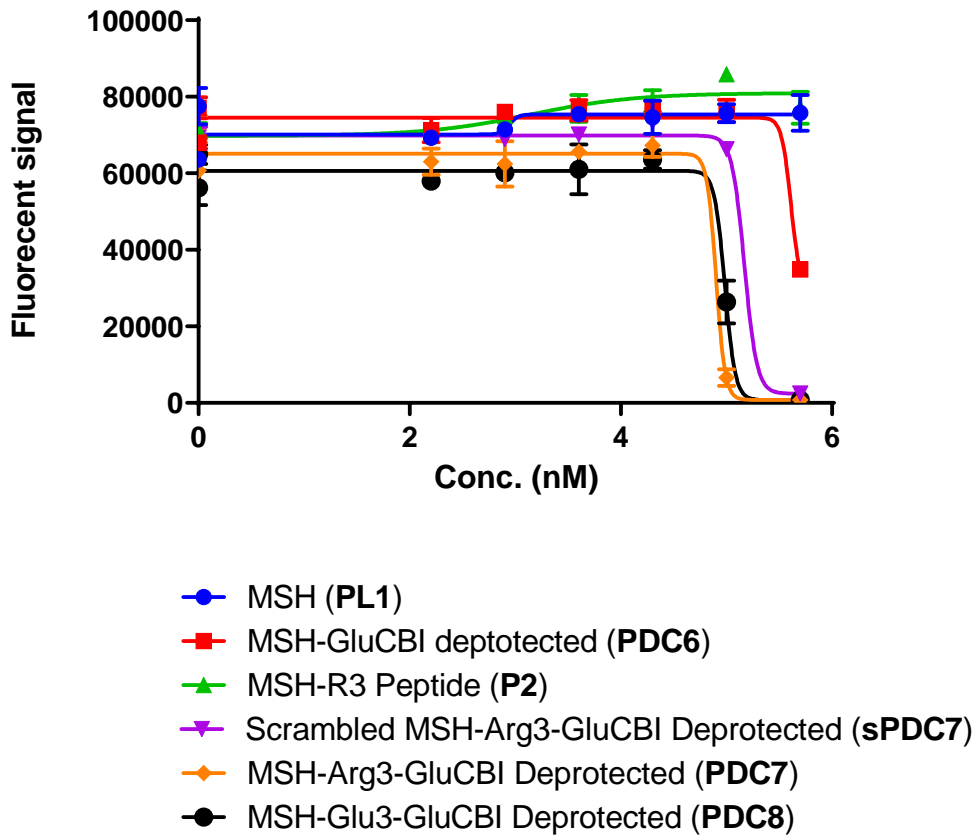


Figure 101: Cytotoxic activity of peptide **P1**, **P2**, **PDC 6**, **sPDC7**, **PDC7** and **PDC8** against SKMEL-28 cell line

To assess the impact of cell seeding density on IC₅₀ determination, another experiment was carried out where lower cell seeding density of 1 x 10⁴ cells/mL was used instead of 1x10⁵ cells/mL. This was possible using the CellTitre-Glo given the level of sensitivity demonstrated from the data in section 4.4.1. Peptide **P1** (Control) and **PDC7**, **PDC8** and **sPDC7** were analysed in the range of 0.16 to 500 μM. The data obtained demonstrated that peptide **P1** used as a control did not have any cytotoxic impact on the cells but all the three PDCs exerted cytotoxic activities. The IC₅₀ determined for PDCs assessed was lower compared to the use of higher cell seeding density emphasizing the importance of using a well optimised seeding density. The PDC incorporating the three arginine amino acid linker (**PDC7**) and the PDC incorporating three glutamic acid amino acid linker (**PDC8**) demonstrated cytotoxic activity that is five times more potent than that of the scrambled PDC incorporating the three arginine amino acid linker (**sPDC7**) (Figure 102).

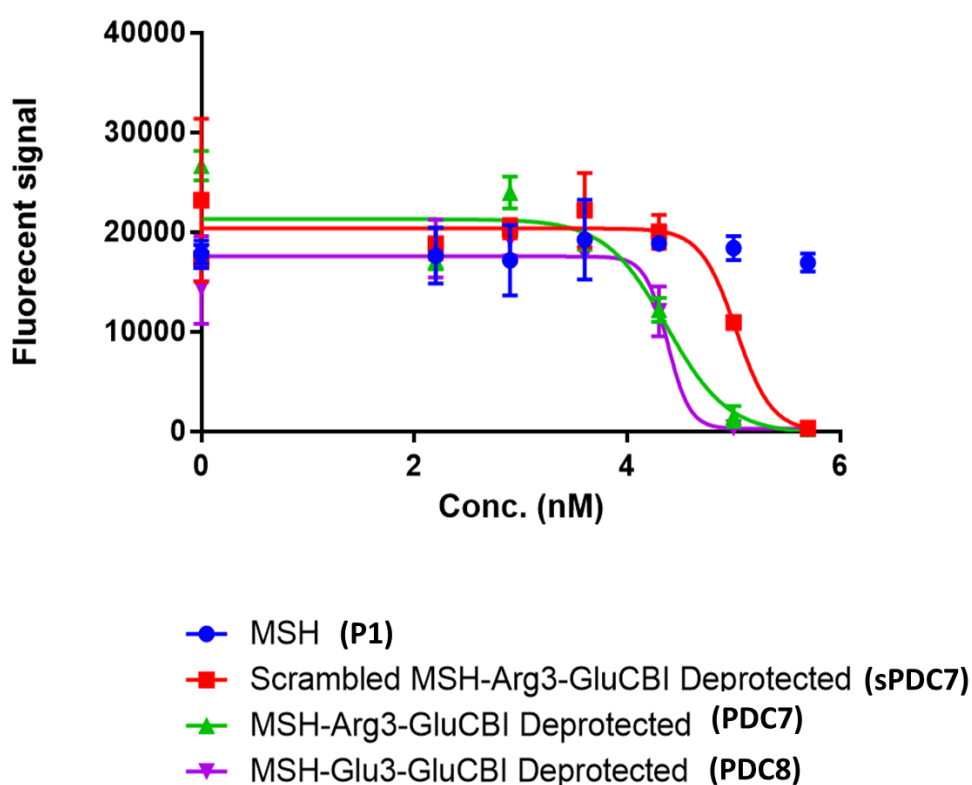
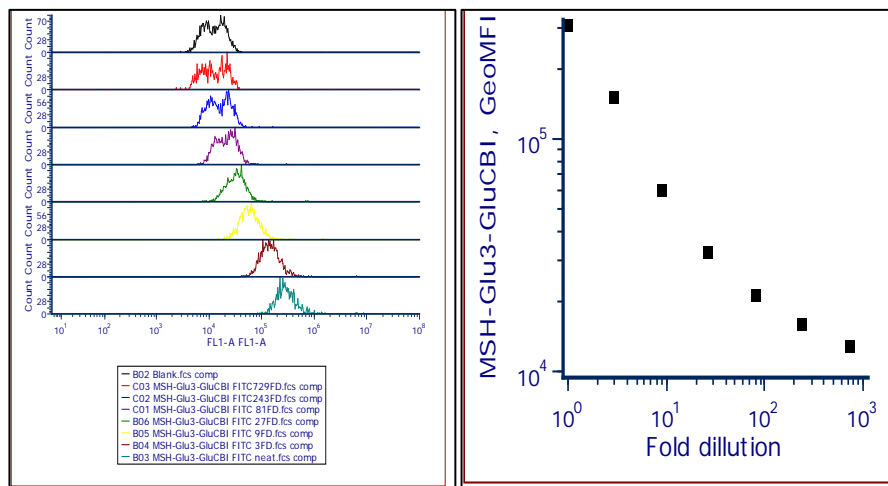


Figure 102: Cytotoxic activity of **P1**, **sPDC7**, **PDC7** and **PDC8** against SKMEL-28 cell line at lower seeding density of 1x10⁴ cells/mL.

4.4.5 Flow Cytometry assessment

Flow cytometry was used to assess the receptor occupancy of synthesised MSH and corresponding PDCs to MC1R receptor. In order to assess this, an increasing concentration of **PDCL1** (MSH-Glu3-CBI conjugated to FITC) and **PDCL2** (MSH-Arg3-CBI conjugated to FITC) with a 3 fold serial dilution (3 fold, 9 fold, 27 fold, 81 fold, 243 fold and 729 fold) of the master stock was assessed as detailed in section 4.3.2.7.1. The concentration of FITC conjugated peptides **PDCL1** and **PDCL2** were demonstrated to be directly proportional to the mean fluorescence seen confirming the binding of peptides **PDCL1** and **PDCL2** to the receptors (Figure 103).

a)



c)

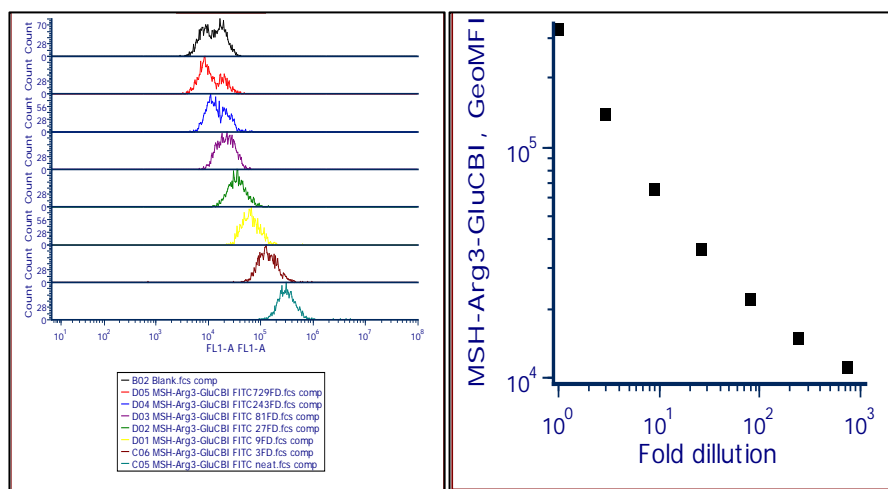


Figure 103: SKMEL-28 receptor occupancy assessment using **PDCL1** referred to as MSH-Glu3-GLUCBI (a) and **PDCL2** referred to as MSH-Arg3-GLUCBI (b)

In the bid to try and locate a negative control, **PDCL1** was also assessed against primary human umbilical vein endothelial cells (HUVEC) which were isolated from the vein of the umbilical cord. HUVEC cell line were stained with **PDCL1** at the concentration of 10 μ M and were demonstrated to express MC1R (Figure 104) but the shift in florescence observed suggest lower levels of expression which mimic data displayed in Figure 92.

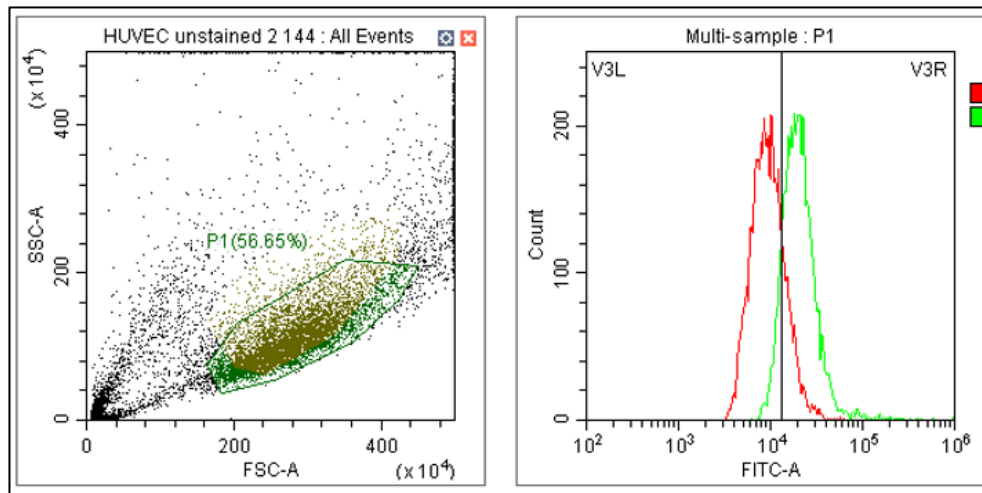


Figure 104: HUVEC receptor occupancy assessment using **PDCL1**. HUVEC primary cell line Unstained and stained with **PDCL1**

4.5 Conclusions and proposed future work

In conclusion, the xCELLigence was a suitable technique to assess when relevant activity of the drug can be observed in real-time; however, multiple data points collection with lower intervals was not very informative in the context of PDCs cytotoxicity. The data generated from the xCELLigence used the same cell seeding density as that of the MTS and CellTitre-Glo of 1×10^5 cell/ml which may have not been optimal and it would be recommended to optimise this step to get more accurate data.

The CellTitre-Glo provide a larger dynamic range compared to the MTS assay and provides a more sensitivity assay allowing the ability to use a lower cell seeding density.

The data obtained suggest that inclusion of three arginines as linker increased the PDC potency by at least three fold and this was postulated to be as a result of increased solubility. Additional considerations to increase the potency of synthesised PDCs would be to assess PDCs incorporating the DNA binding unit. **PDC9** and **PDC10** including the DNA binding unit were synthesised however, they were not assessed in a biological assay as at the time of assessment both PDCs had decomposed and were therefore not analysed. Future projects can look at resynthesizing these PDCs and assessing the biological activity.

The flow cytometry receptor occupancy assay was used to confirm the presence of MC1R receptor on SKMEL-28 cell line and HUVEC primary cell line. It was not possible to locate a negative cell line during the course of this project and future work may consider the use of MC1R knockout cell lines as a negative control to confirm specificity.

CHAPTER 5: EXPERIMENTAL

5.1 Materials and reagents

5.1.1 Reagents and Solvents

Chemical reagents were sourced from various manufacturers including Merck (Sigma Aldrich, Novabiochem), Fisher Scientific, Fluorochem and Tokyo Chemical Industry. Chemicals were reagent grade and specifications were as described by the manufacturer.

Solid phase reagents including the resins, Fmoc-amino acids and coupling reagents were sourced from Merck (Novabiochem), Fluorochem and AGTC Bioproducts. Solvents were sourced from Sigma Aldrich. HPLC Solvents used for purification were HPLC grade and were also sourced from Sigma Aldrich.

5.1.2 Solid Phase peptide synthesis

The solid phase peptide synthesis was carried out using a fully automated parallel peptide synthesiser Syro I except for the addition of the cytotoxic payload which was carried out manually.

5.1.3 Physical Characterisation and Spectroscopic Techniques

A Bruker spectrometer operating at 400 MHz for ¹H- and 100 MHz for ¹³C-NMR spectra, was used using specified deuterated solvents. NMR spectra were processed using Topspin and MestReNova software. The chemical shifts for both ¹H- and ¹³C were recorded in ppm and were referenced to the residual solvent peak.

Multiplicities in the NMR spectra were described as s = singlet, d = doublet, t = triplet, q = quartet, m = multiplet, br = broad and coupling constants were reported in Hz.

Mass spectra were recorded using Kratos Analytical Axima MALDI-TOF and Waters Synapt G2 Q-ToF HDMS (High Definition Mass Spectrometry). Accurate mass spectra were recorded using the Synapt G2 Q-ToF HDMS or sent at the EPSRC National Mass Spectroscopy Service Centre, Swansea.

Melting points were recorded using open capillary tubes on a Stuart Scientific melting point apparatus SMP3.

Infrared spectra were recorded as neat samples using the PerkinElmer Spectrum BX instrument.

5.1.4 Chromatographic Techniques

Aluminum plates coated with 0.2 mm silica gel-60 F254 were used for thin-layer chromatography and then subsequently visualized under UV light.

Flash chromatographic separations were performed manually in a glass column packed with silica gel for column chromatography (particle size 60 μm) or with the Isolera Biotage systems using pre-packed Biotage column.

Analytical Reverse Phase-HPLC was performed on an Agilent 1200 using an Agilent eclipse XDB-C18 column (4.6 x 150 mm, 5 μM and a flow rate of 1 mL/min) or on an Agilent 1100 using a phenomenex luna 3u Phenyl-Hexyl column (4.6 x 150 mm, 3 μM and a flow rate of 1 mL/min).

Analytical Reverse Phase-HPLC methods were run over 25 min with a gradient from 5% B up to 95% B over 20 minutes and then equilibration to 5%B from 20 min to 25 min. The solvent used for the Analytical Reverse Phase-HPLC were:

-Solvent A = Water + 0.05% TFA

-Solvent B = MeOH + 0.05% TFA

Preparative Reverse Phase-HPLC was performed on an Agilent 1200 using an Agilent eclipse XDB-C18 column (21.2 x 150 mm, 5 μM and a flow rate of 20 mL/min).

Preparative Reverse Phase-HPLC methods were run over 25 min with a gradient from 5% B up to 95% B over 20 minutes and then equilibration to 5%B from 20 min to 25 min. The solvent used for the Analytical Reverse Phase-HPLC were:

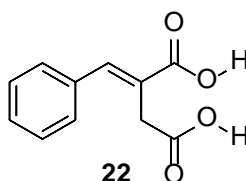
-Solvent A = 95% H₂O + 5% MeOH + 0.05% TFA

-Solvent B = 95% MeOH + 5% H₂O + 0.05% TFA

Both the analytical and preparative HPLC detection wavelength were set at 214 nm, 280 nm and 254 nm.

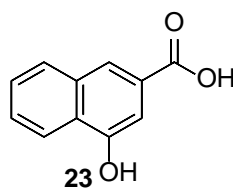
5.2 Synthesis of CBI alkylating subunit 3

5.2.1 Synthesis of 22



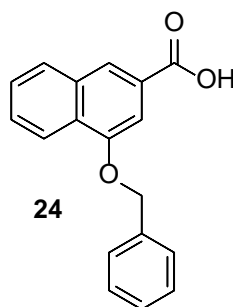
2-benzylidenesuccinic acid (22), followed^{189,190}: A solution of dimethyl succinate (47 g, 321 mmol) was combined with a solution of benzaldehyde (28.2 g, 265.7 mmol) and a solution of tert-butanol (35 mL) and then mixed at RT. Potassium tert-butoxide (32 g, 282 mmol) was subsequently dissolved in 150 ml of tert-butanol, heated to reflux until completely dissolved, and then the mixture of dimethyl succinate and benzaldehyde was added slowly dropwise. The resulting solution was heated under reflux for 3 h. The residue was dissolved in 1N HCl (300 mL) and the solution extracted with EtOAc (3 x 250 ml). The organic layers were separated, combined, dried (Na₂SO₄) and concentrated in vacuo. The residue was redissolved in hot CH₃OH (70 mL) before being added to a solution of NaOH (28 g, 700 mmol) in methanol (180 mL) that was heated to reflux and maintained at this temperature for 16h. The solution was concentrated in vacuo and then allowed to cool. H₂O (300 mL) was added and the solution was washed with EtOAc (200 mL) three times. The water phases were combined and acidified with concentrated HCl (20 mL) and the product was extracted with EtOAc (3 x 200 mL). The organic layers were combined and dried over Na₂SO₄, filtered and concentrated under reduced pressure to afford the crude product as a yellow solid. The crude product was further triturated with ether to afford 2-benzylidenesuccinic acid as a white solid (24 g, 44% yield). ¹H NMR (400 MHz, DMSO-d₆): δ 3.36 (s, 2H), 7.38–7.45 (m, 5H), 7.73 (s, 1H), 12.61 (brs, 2H). mp 181-183 °C. MS (ES+) calculated (M+Na)⁺ 229.18 found 229.13.

5.2.2 Synthesis of 23



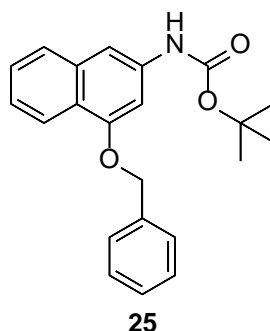
4-hydroxy-2-naphthoic acid (23), followed^{189,190}: 2-benzylidenesuccinic acid (**22**) (24 g, 116 mmol) was dissolved in conc. H₂SO₄ (200 mL) and stirred at room temperature for 5 h. The reaction mixture was then carefully poured over crushed ice and the crude product allowed to crystallise. The resulting crystals were filtered, washed with water and dried in vacuo to afford the 4-hydroxy-2-naphthoic acid as yellow solid (20 g, 92 % yield). mp 220-222°C. ¹H NMR (400 MHz, DMSO-d₆): δ 7.37-7.38 (d, J=1.63, 1H), 7.54-7.60 (m, 2H), 7.99-8.01 (m, 1H), 8.05 (s, 1H), 8.15-8.17 (m, 1H), 10.45 (brs, 1H). MS (ES⁻) calculated (M-H)⁻ 187.04 found 187.13.

5.2.3 Synthesis of 24



4-Benzyloxy-naphthalene-2-carboxylic acid (24), adapted from^{191,140}: 4-hydroxy-2-naphthoic acid (**23**) (20 g, 106.4 mmol) was dissolved in DMF (200 mL) containing K_2CO_3 (30.6 g, 223 mmol) and BnBr (38 g, 223.2 mmol) was added dropwise and stirred at RT for 16 h. The reaction mixture was then diluted with EtOAc (200 mL), washed 1N HCL (2x200 mL), 10% NH_4Cl (200 mL) and saturated brine (200 mL). Ethyl acetate was removed in vacuo and the residue was redissolved in hot CH_3OH (400 mL) before being added to a solution of NaOH (28 g, 700 mmol) in methanol (180 mL) at reflux. After 5 h, the solvent was removed in vacuo and then the residue was acidified with 5M HCl forming a precipitate. The aqueous solution was extracted with EtOAc (2 x 200 mL) and combined with the precipitate dissolved in EtOAc. The combined organic layer was washed with brine (400 mL) and then dried over $NaSO_4$. The solvent was removed in vacuo to afford a pale yellow solid 4-Benzyloxy-naphthalene-2-carboxylic acid product (18.2 g, 61 % Yield). mp 221-223 °C. 1H -NMR (400 MHz, $DMSO-d_6$): δ = 5.38 (s, 2 H), 7.35–7.47 (m, 3 H), 7.49 (s, 1 H), 7.57–7.68 (m, 4 H), 8.07–8.10 (m, 1 H), 8.23–8.26 (m, 2 H) 13.06 (brs, 1 H). MS (ES⁺) calculated $(M+Na)^+$ 301.08 found 301.08.

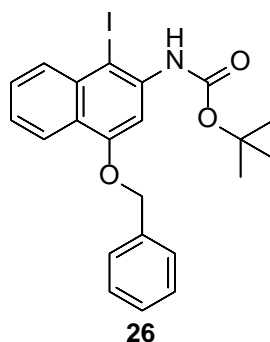
5.2.4 Synthesis of 25



Tert-butyl (4-(benzyloxy) naphthalen-2-yl)carbamate (25), adapted from ^{140,142}: 4-Benzyloxy-naphthalene-2-carboxylic acid (**24**) (6 g, 21.5 mmol) was dissolved in anhydrous toluene (300 mL) under nitrogen and stirred for 5 min, followed with the addition of NEt₃ (10.5 ml, 75 mmol) and DPPA (11.4 ml, 54 mmol). The reaction mixture was stirred at RT for 1 h followed by 3 h heating to reflux.. The reaction mixture was allowed to return to RT before adding tert-butanol (22.3 g, 301 mmol) and subsequent heating to reflux for an additional 6 h.

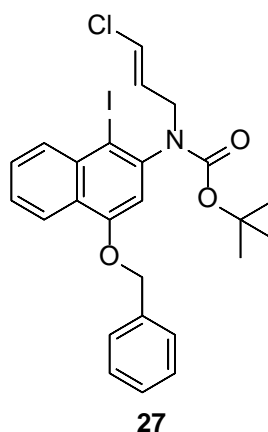
After being cooled to room temperature, EtOAc (500 mL) was added to the reaction mixture, which was then washed successively with aqueous saturated NaHCO₃ solution (2 x 600 mL) , water (600 mL) and brine (600 mL). The organic solution was dried over NaSO₄, filtered and concentrated in vacuo to afford a yellow solid. The crude product was purified by silica gel chromatography using the Isolera automated flash chromatography system. The crude was dry loaded on to a pre-packed silica column adsorbed on to silica. A linear gradient of 0 to 20 % dichloromethane in hexane was run until complete elution of the product. The solvent was removed in vacuo under reduced pressure to afford tert-butyl (4-(benzyloxy) naphthalen-2-yl)carbamate, a white solid amount (46% yield). mp 221-223 °C. ¹H NMR (400 MHz, CDCl₃): δ = 1.55 (s, 9 H), 5.25 (s, 2 H), 6.59 (brs, 1 H), 7.07 (d, *J* = 1.6 Hz, 1 H), 7.32–7.54 (m, 8 H), 7.68-7.70 (d, *J* = 8 Hz, 1 H), , 8.21 (d, *J* = 8.4 Hz, 1 H). MS (ES⁺) calculated (M+H)⁺ 350.17 found (M+H)⁺ 350.17, calculated (M+Na)⁺ 372.15 found (M+Na)⁺ 372.15.

5.2.5 Synthesis of 26



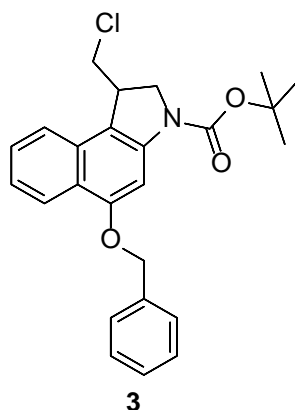
Tert-Butyl (4-(benzyloxy)-1-iodonaphthalen-2-yl) carbamate (26), adapted from ^{192,137}: Conc. H₂SO₄ (160 μ L, 3.03 mmol) was added to a stirring solution of Tert-Butyl (4-(benzyloxy)-1-naphthalen-2-yl)carbamate (**25**) (10 g, 28.62 mmol) in DMF (100 mL), followed by portion wise addition of NIS (9.6 g, 42.9 mmol) and then incubation with stirring for 4 h at RT. The reaction mixture was then poured over crushed ice and then extracted with ethyl acetate (5 x 100 mL). The organic layer was successively washed with H₂O (100 mL), sodium thiosulfate (100 mL) and saturated brine, dried over NaSO₄, filtered and concentrated in vacuo. The crude mixture was dry loaded on to a pre-packed silica column adsorbed on to silica and then purified by silica gel chromatography using the isolera automated flash chromatography system. A linear gradient of 0 to 20 % ethyl acetate in hexane was run until complete elution of the product. The solvent was removed in vacuo under reduced pressure to afford Tert-Butyl (4-(benzyloxy)-1-iodonaphthalen-2-yl) carbamate, a pale yellow solid (9.6 g, 71% yield). mp 140-142°C. ¹HNMR (400 MHz, CDCl₃): δ = 1.59 (s, 9 H), 5.29 (s, 2 H), 7.32 (s, 1 H), 7.35–7.58 (m, 7 H), 8.03-8.05 (m, 2 H), 8.22-8.25 (d, J = 9.1 Hz, 1H). MS (ES⁺) calculated for (M+Na)⁺ 498.05 found 498.05.

5.2.6 Synthesis of 27



(E/Z)-2-amino-4-benzyloxy-N-(tert-butyloxycarbonyl)-N-(3-chloro-2-propenyl)-1-iodonaphthalene (27), adapted from ^{192,139}: Tert-Butyl (4-(benzyloxy)-1-naphthalen-2-yl) carbamate (**26**) (5.00 g, 10.04 mmol) was dissolved in DMF (20 mL) and then NaH (1.69 mg, 70.44 mmol) was added and the solution was stirred for 30 min at RT. Following this incubation, the reaction was cooled to 0°C and (E/Z)-1,3-dichloropropene (4.35 mL, 47.83 mmol) was added dropwise and the mixture was stirred for an additional 3 h. The reaction was subsequently quenched with the addition of a saturated aqueous solution of NH₄Cl (10 mL), 50 % brine (60 mL), and Et₂O (100 mL), and extraction with Et₂O (3×60 mL). The combined organic layers were washed twice with 50% brine (2×100 mL) and then once with brine (100 mL), dried over Na₂SO₄ followed by the removal of the solvent under vacuo. The crude product was subsequently purified by column chromatography on the silica to afford the (E/Z)-2-amino-4-benzyloxy-N-(tert-butyloxycarbonyl)-N-(3-chloro-2-propenyl)-1-iodonaphthalene as yellow oil (3.4 g, 61% yield). ¹H NMR (400 MHz, CDCl₃): δ = 1.33 (s, 9 H), 4.25-4.30 (m, 1 H), 4.57- 4.62 (m, 1 H), 5.22-5.30 (m, 2 H), 6.03 (s, 2H), 6.71 (s, 1H), 7.36-7.52 (m, 7 H), 8.03 (s, 1 H), 8.31-8.33 (d, J = 8.4 Hz, 1H). MS (ES⁺) calculated for (M+Na)⁺ 572.05 found 572.04.

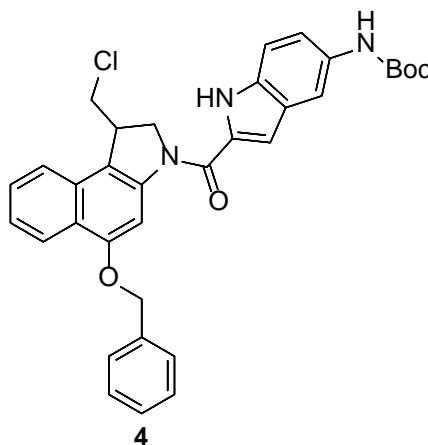
5.2.7 Synthesis of 3



3H-Benz[e]indole-3-carboxylic acid, 1-(chloromethyl)-1,2-dihydro-5-(phenylmethoxy)-, 1,1-dimethylethyl ester (3) adapted from ^{192,139}: (E/Z)-2-amino-4-benzyloxy-N-(tert-butyloxycarbonyl)-N-(3-chloro-2-propenyl) -1-iodonaphthalene (**27**) (2 g, 3.64 mmol) was dissolved in anhydrous toluene (50 mL) and degassed thoroughly for 45 min prior to the addition of tris(trimethylsilyl)silane (1.4 mL, 4.54 mmol) and AIBN (150 mg, 0.91 mmol). The reaction mixture was subsequently heated at 90 °C and stirred for 2 h. After cooling to RT, the solvent was removed under vacuo and the crude product was dissolved in EtOAc (50 mL). The EtOAc organic layer was then dried over Na₂SO₄ and the solvent was removed in vacuo and dried on silica followed by purification by column chromatography using the isolera to afford the product as an off white solid (1.4 g, 90 % Yield). mp 140-142°C. ¹H NMR (400 MHz, CDCl₃): δ = 1.33 (s, 9 H), 3.14-3.19 (t, 1 H), 3.64- 3.72(m, 2 H), 3.83-3.88 (t, 1 H), 3.98 (brs, 1 H), 4.99 (s, 2 H), 7.32-7.57 (m, 8 H), 7.36-7.38 (d, J = 8.74, 1 H), 8.01-8.03 (d, J = 8.76 Hz, 1H). MS (ES⁺) calculated for (M+Na)⁺ 446.14 found 446.14.

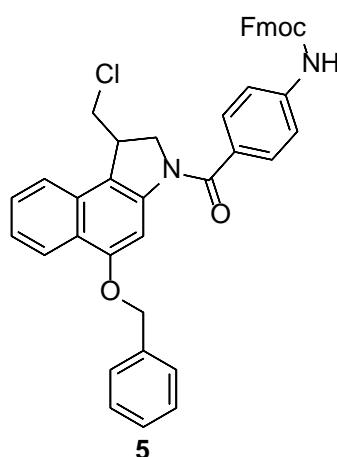
5.3 Synthesis of CBI alkylating subunit conjugated to the DNA binding unit

5.3.1 Synthesis of 4



(4): 3H-Benz[e]indole-3-carboxylic acid, 1-(chloromethyl)-1,2-dihydro -5-(phenylmethoxy)-, 1,1-dimethylethyl ester (**3**) (250 mg, 0.591 mmol) was treated with a solution of 4 M HCl in dioxane (10 mL) and then stirred for 3 h. Upon completion, N₂ gas was bubbled through the solution for 15 min and then the solvent was subsequently removed under vacuo. The Boc deprotected residues were dissolved in dry DMF (3.5 mL) and in a different flask 5-amino-1H-indole-2-carboxylic acid (244 mg, 0.885 mmol) was dissolved in DMF (1 mL) and HATU (448 mg, 1.18 mmol) and DIPEA (0.426 mL, 2.45 mmol) were added for 1 min prior addition of this solution to the Boc deprotected DNA alkylating subunit in DMF. The mixture was incubated on ice, allowing the reaction to gradually heat to RT, followed by an overnight incubation. At the end of the reaction, EtOAc (50 mL) was added to the reaction mixture and then washed with 0.1 N HCL (50 mL) and then with saturated sodium bicarbonate (2 x 50 mL). The EtOAc organic layer was then dried over Na₂SO₄, concentrated in vacuo and then adsorbed on silica followed by purification on column chromatography using the isolera to afford the product as a brown solid (62 % yield). mp 140-142°C. ¹H NMR (400 MHz, CD₃OD): δ =1.55 (s, 9 H), 3.62-3.68 (m, 1 H), 3.80- 3.87 (m, 0.5 H), 3.94- 3.97 (m, 1 H), 4.07- 4.12 (m, 1 H), 4.18- 4.29 (m, 0.5 H), 4.59- 4.67 (m, 1 H), 5.15- 5.29 (m, 2 H), 7.02- 7.04 (s, 1 H), 7.21-7.57 (m, 9 H) , 7.75-7.79 (m, 2 H), 8.23-8.26 (d, J = 8.68, 1 H). MS (ES-) calculated for (M-H)- 580.20 found 580.45.

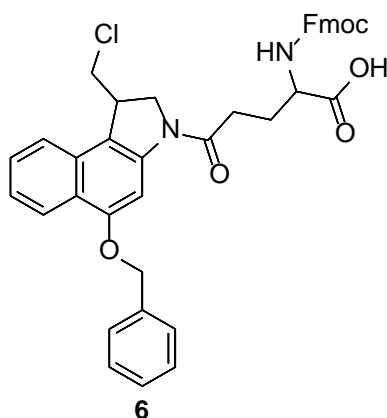
5.3.2 Synthesis of 5



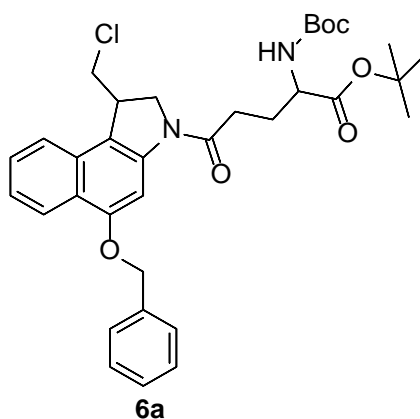
(5): 3H-Benz[e]indole-3-carboxylic acid, 1-(chloromethyl)-1,2-dihydro -5-(phenylmethoxy)-, 1,1-dimethylethyl ester (**3**) (600 mg, 1.416 mmol) was treated with a solution of 4 M HCl in dioxane (10 mL) and then stirred for 2 h. Upon completion, N₂ gas was bubbled through the solution for 15 min and then the solvent was subsequently removed under vacuo. The Boc deprotected residues were dissolved in dry DMF (3.5 mL) and in a different flask N- α -Fmoc-p-aminobenzoic acid (1.01 g, 2.81 mmol) was dissolved in DMF (1 mL) and HATU (1.06 g, 2.80 mmol) and DIPEA (1.01 mL, 5.6 mmol) were added for 1 min prior to the addition of the Boc deprotected DNA alkylating subunit in DMF. The mixture was incubated on ice allowing the reaction to proceed to room temperature followed by an overnight incubation. At the end of the reaction, EtOAc (50 mL) was added to the reaction mixture and then washed with 0.1 N HCL (50 mL) and then with saturated sodium bicarbonate (2 x 50 mL). The EtOAc organic layer was then dried over Na₂SO₄, removed in vacuo and then adsorbed on silica followed by purification on column chromatography using the isolera to afford the product as a green solid (611 mg, 65% yield). mp 140-142°C. ¹H NMR (400 MHz, CDCl₃): δ = 3.51 (s, 0.5 H), 3.68- 3.73 (m, 0.5 H), 3.88- 3.96 (m, 1 H), 4.25- 4.37 (m, 3 H), 4.60- 4.65 (m, 3 H), 5.17 (brs, 2 H), 7.19 (s, 1 H), 7.32-7.47 (m, 10 H), 7.55-7.65 (m, 5 H), 7.78-7.80 (m, 3 H), 8.18 -8.21 (d, J = 8.14, 2 H), 8.45 -8.47 (dd, J = 9.85, 1.56, 1H), 8.72 -8.73 (dd, J = 5.92, 1.56, 1H). MS (ES⁺) calculated for (M+Na)⁺ 687.20 found (M+Na)⁺ 687.23.

5.4 Synthesis of warhead library

5.4.1 Synthesis of 6

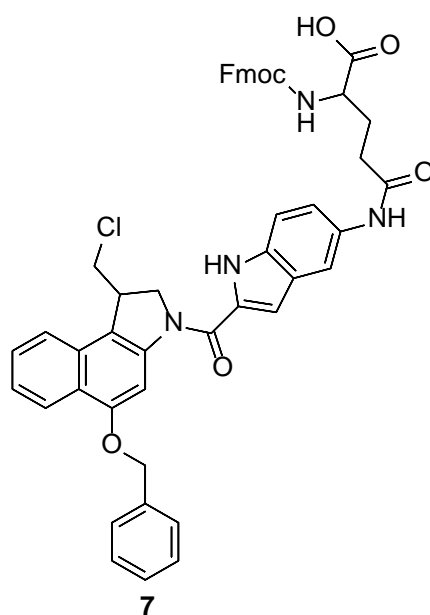


(6): 3H-Benz[e]indole-3-carboxylic acid, 1-(chloromethyl)-1,2-dihydro-5-(phenylmethoxy)-, 1,1-dimethylethyl ester (**3**) (500 mg, 1.18 mmol) was treated with a solution of 4 M HCl in dioxane (10 mL) and then stirred for 2 h. Upon completion N₂ gas was bubbled through the solution for 15 min and then the solvent was subsequently removed under vacuo. The Boc deprotected residues were dissolved in dry DMF (5 mL) and in a different flask 1-tert-Butyl N-(tert-Butoxycarbonyl)-L-glutamate (537 mg, 1.77 mmol) was dissolved in DMF (1 mL) and HATU (673 mg, 1.77 mmol) and DIPEA (0.636 mL, 3.54 mmol) were added for 1 min prior to the addition of Boc deprotected DNA alkylating subunit in DMF. The mixture was incubated on ice, allowing the reaction to gradually heat to RT followed by an overnight incubation. At the end of the reaction, EtOAc (20 mL) was added to the reaction mixture and then washed with 0.1 N HCL (20 mL) and with saturated sodium bicarbonate (2x50 mL). The EtOAc organic layer was then dried over Na₂SO₄, removed in vacuo and then adsorbed on silica followed by purification on column chromatography using the isolera. A linear gradient of 0 to 20 % ethyl acetate in hexane was run until complete elution of the product, to afford the product **6a**.

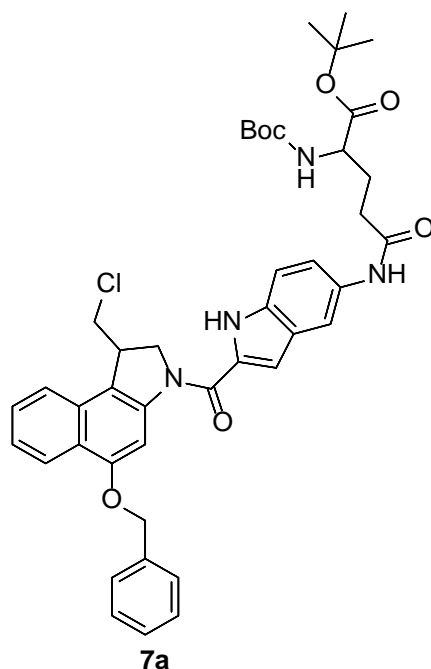


A portion of **6^a** product (365 mg, 0.600 mmol) was dissolved in 4 M HCl in dioxane (5 mL), HCl gas was bubbled through the solution for 2 h to deprotect both the amine and the carboxylic acid. Upon completion, N₂ gas was bubbled through the solution for 15 min and then the remaining solvent was subsequently removed under vacuo. The crude product was dissolved in THF (8 mL) and H₂O (4 mL) followed by the addition of 10% sodium bicarbonate (8.5 ml) solvent and cooling the reaction to 0°C on ice. A solution of Fmoc-Cl (155 mg, 0.600 mmol) in THF (8.5 mL) was then added dropwise and stirred for a further 30 min. The reaction was subsequently quenched using MeOH (10 mL) and the solvent removed under vacuo. EtOAc (50 mL) was added to the residue and then washed with 1 N HCl (3 x 50 mL). The EtOAc organic layer was then dried over Na₂SO₄, concentrated in vacuo and then adsorbed on silica followed by purification by column chromatography using the isolera. The crude was dry loaded on to a pre-packed silica column adsorbed on to silica. A linear gradient of 0 to 30 % acetone in hexane was run until complete elution of the product, to afford the product **6** as a green solid (138 mg, Overall 36% yield). mp 140-142 °C. ¹H NMR (400 MHz, DMSO-d₆): δ = 1.95 (brs, 2 H), 2.08 (brs, 2 H), 3.82-3.87 (m, 1 H), 3.98- 4.34 (m, 9 H), 5.28 (brs, 2 H), 7.32-7.45 (m, 7 H), 7.54-7.58 (m, 3 H), 7.72-7.74 (m, 3H), 8.16 -8.18 (d, J = 7.69, 2 H), 12.68 (brs, 1 H), MS (ES⁻) calculated for (M-H)⁻ 673.21 found 673.35. Another predominant mass peak observed was for compound without the Cl calculated for (M-H)⁻ 639.25 found 639.38.

5.4.2 Synthesis of 7

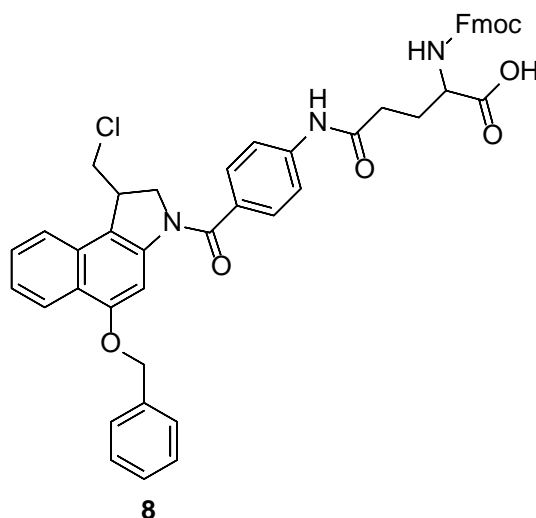


(7): **4** (200 mg, 0.34 mmol) was treated with a solution of 4 M HCl in dioxane (10 mL) and then stirred for 2 h. Upon completion N₂ gas was bubbled through the solution for 15 min and then the solvent was subsequently removed under vacuo. The Boc deprotected residues were dissolved in dry DMF (3.5 mL) and in a different flask 1-tert-Butyl N-(tert-Butoxycarbonyl)-L-glutamate (125 mg, 0.412 mmol) was dissolved in DMF (1 mL) and HATU (210 mg, 0.412 mmol), and DIPEA (185 μ L, 1.03 mmol) were added for 1 min prior to the addition of the Boc deprotected DNA alkylating subunit in DMF. The mixture was incubated on ice, allowing the reaction to gradually increase to RT followed by an overnight incubation. At the end of the reaction, EtOAc (50 mL) was added to the reaction mixture and then washed with 0.1 N HCl (50 mL) and then with saturated sodium bicarbonate (2 x 50 mL). The EtOAc organic layer was then dried over Na₂SO₄, removed in vacuo and then adsorbed on silica followed by purification on column chromatography using the isolera. A linear gradient of 0 to 20 % ethyl acetate in hexane was run until complete elution of the product, to afford the product **7a** which was used without further characterisation.

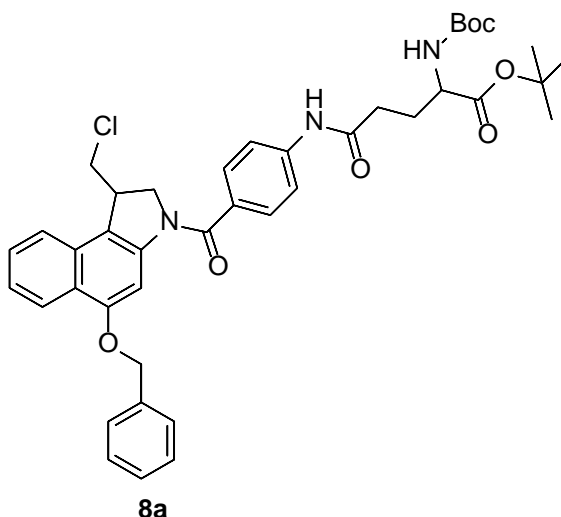


A portion of **7a** product (100 mg, 0.130 mmol) was dissolved in 4 M HCl in dioxane (5 mL), HCl gas was bubbled through the solution for 2 h to deprotect both the amine and the carboxylic acid. Upon completion, N₂ gas was bubbled through the solution for 15 min and then the remaining solvent was subsequently removed under vacuo. The crude product was dissolved in THF (8 mL) and H₂O (4 mL) followed by the addition of sodium bicarbonate (43 mg, 0.512 mmol) and cooling the reaction to 0°C on ice. A solution of Fmoc-Cl (51 mg, 0.195 mmol) in THF (1.7 mL) was then added dropwise and the solution was stirred for a further 30 min. The reaction was subsequently quenched using MeOH (10 mL) and the solvent removed under vacuo followed by the addition of EtOAc (50 mL) to the reaction mixture and then washed with 1 N HCL (3 x 50 mL). The EtOAc organic layer was then dried over Na₂SO₄, concentrated in vacuo and adsorbed on silica, followed by purification by column chromatography using the isolera. A linear gradient of 0 to 10 % methanol in DCM was run until complete elution of the product, to afford the product **7** as a brown solid (34 mg, Overall 32% yield). mp 140-142 °C. ¹H NMR: δ = 1.91 (brs, 1 H), 2.12 (brs, 1 H), 2.45 (brs, 2 H), 4.03-4.09 (m, 3 H), 4.21-4.32 (m, 3 H), 4.39-4.46 (m, 1 H), 4.54-4.62 (m, 1 H), 4.75-4.88 (m, 2 H), 5.31 (brs, 2 H), 7.03 (brs, 1 H), 7.15-7.52 (m, 10 H), 7.56-7.78 (m, 5 H), 7.83-8.16 (m, 5H), 8.20 -8.24 (d, J = 8.41, 1 H), 9.89 (brs, 1 H), 11.70 (brs, 1 H). MS (ES-) calculated for (M-H)⁻ 831.26 found 831.27.

5.4.3 Synthesis of **8**



(8): 5 (500 mg, 0.76 mmol) was treated with a solution of 40% diethylamine in ACN (20 mL) for 1 h. Removal of the solvent under vacuo and subsequent addition of acetone (2 x 50 mL) followed by removal under vacuo facilitated the removal of diethylamine through azeotropy. The Fmoc deprotected residues were dissolved in dry DMF (10 mL) and in a different flask 1-tert-Butyl -N-(tert-Butoxycarbonyl)-L-glutamate (356 mg, 1.18 mmol) alkylating unit was dissolved in DMF and HATU (456 g, 1.19 mmol), and DIPEA (430 μ L, 2.4 mmol) for 1 min prior to the addition of the Fmoc deprotected DNA alkylating subunit. The mixture was incubated on ice allowing the reaction to gradually heat to RT followed by an overnight incubation. At the end of the reaction, EtOAc (50 mL) was added to the reaction mixture and then washed with 0.1 N HCL (50 mL) and then with saturated sodium bicarbonate (2 x 50 mL). The EtOAc organic layer was then dried over Na_2SO_4 , removed in vacuo and then adsorbed on silica followed by purification on column chromatography using the isolera. A linear gradient of 0 to 10 % Methanol in DCM was run until complete elution of the product, to afford the product **8a**, which was used without further characterisation.



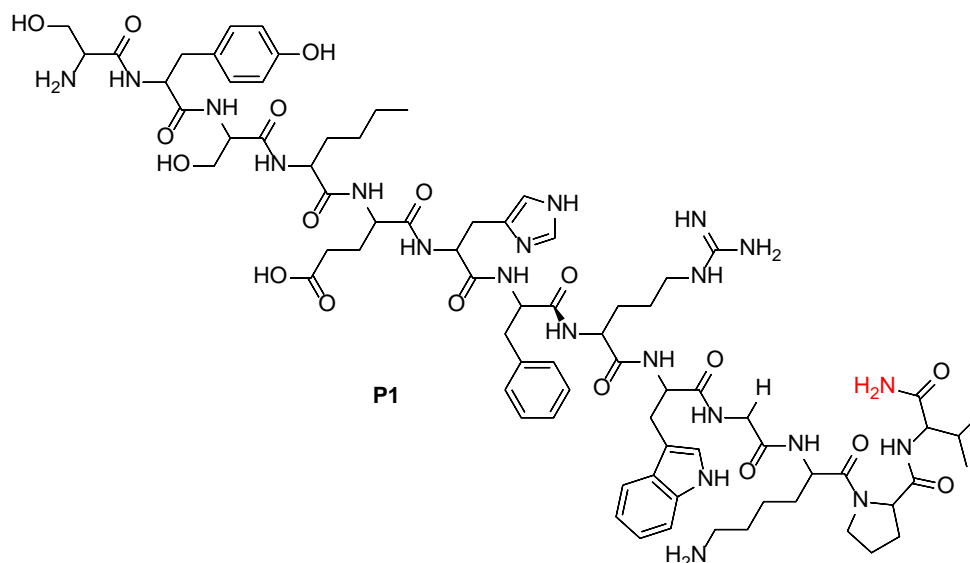
A portion of **8a** product (300 mg, 0.412 mmol) was dissolved in 4 M HCl in dioxane (5 mL) and HCl gas was bubbled through the solution for 2 h to deprotect both the amine and the carboxylic acid. Upon completion, N₂ gas was bubbled through the solution for 15 min and then the remaining solvent was subsequently removed under vacuo. The crude product was dissolved in THF (8 mL) and H₂O (4 mL) followed by the addition of sodium bicarbonate (34 mg, 0.41 mmol) and cooling the reaction to 0°C on ice. A solution of Fmoc-Cl (107 mg, 0.41 mmol) in THF (1.7 mL) was then added dropwise and stirred for a further 30 min. The reaction was subsequently quenched using MeOH (10 mL) and the solvent removed under vacuo followed by the addition of EtOAc (50 mL) to the reaction mixture and then washed with 1 N HCl (3 x 50 mL). The EtOAc organic layer was then dried over Na₂SO₄, removed in vacuo and then adsorbed on silica followed by purification on column chromatography using the isolera. A linear gradient of 0 to 10 % Methanol in DCM was run until complete elution of the product, to afford the product **8** as a brown solid (129 mg, 41% yield). mp 140-142 °C. ¹H NMR (400 MHz, DMSO-d₆): δ = 1.08 (brs, 1 H), 1.25 (brs, 1 H), 1.91 (brs, 1 H), 2.12 (brs, 1 H), 3.71 (brs, 1 H), 3.86 (brs, 1 H), 3.97 (brs, 1 H), 4.02-4.10 (m, 2 H), 4.20-4.34 (m, 3 H), 4.43 (brs, 1H), , 5.19 (brs, 2H), 7.27-7.36 (m, 3 H), 7.39 -7.43 (m, 5 H), 7.47-7.67 (m, 5 H), 7.70-7.77 (m, 5H), 7.86-7.92 (m, 3H), 8.17 -8.19 (d, J = 7.8, 1 H), 10.24 (brs, 1 H), 12.69 (brs, 1 H). MS (ES⁻) calculated for (M-H)⁻ 792.25 found 792.54.

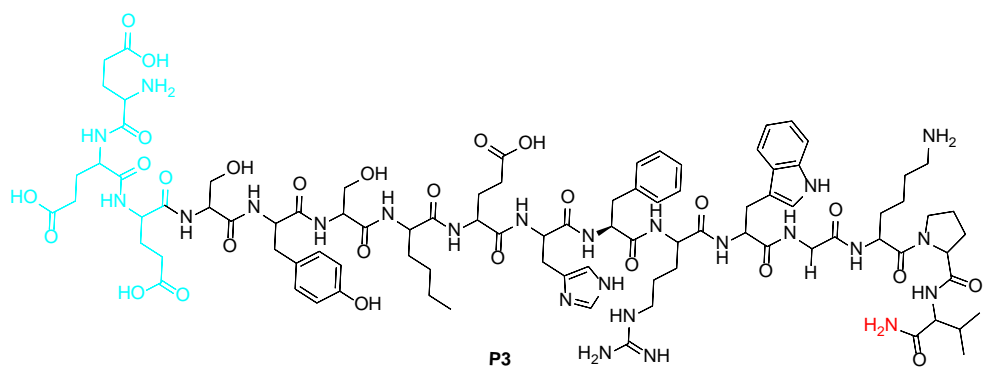
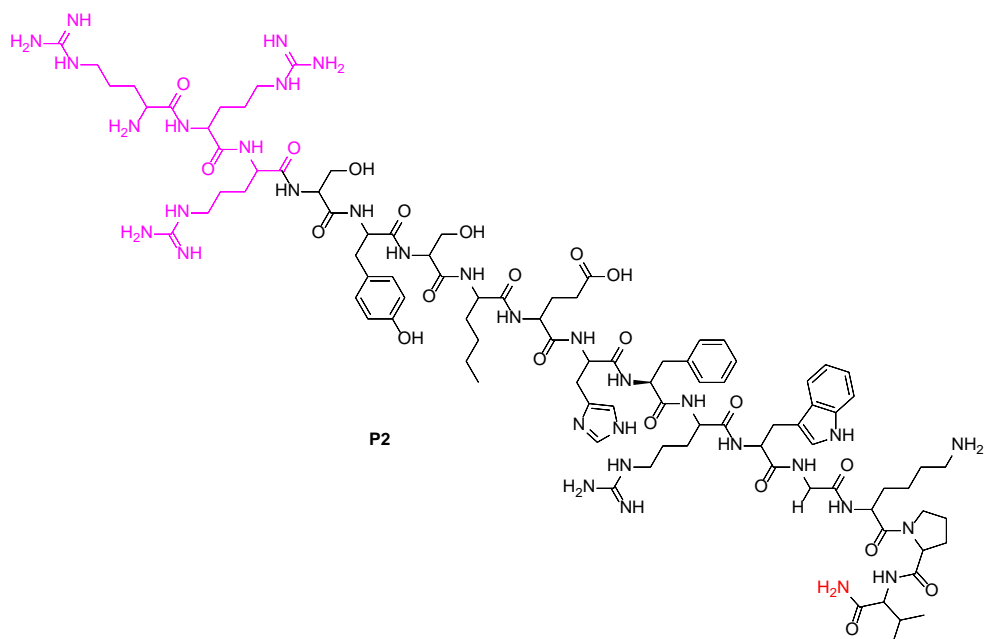
5.5 Solid Phase synthesis

5.5.1 Table of peptides and peptide drug conjugates synthesised

Compound Name	Compound ID
MSH Peptide	P1
MSH-(Arg)*3	P2
MSH-(Glu)*3	P3
Scrambled MSH peptide 01	P4
Scrambled MSH peptide 02	P5
MSH-(GluCBI)*1 Protected	PDC1
MSH-(Arg)*3-(GluCBI)*1 Protected	PDC2
MSH-(Glu)*3-(GluCBI)*1 Protected	PDC3
MSH-(GluCBI)*2 Protected	PDC4
MSH-(GluCBI)*3 Protected	PDC5
MSH-(GluCBI)*1 Deprotected	PDC6
Scrambled MSH-(GluCBI)*1 Deprotected	sPDC6
MSH-(Arg)*3-(GluCBI)*1 Deprotected	PDC7
Scrambled MSH-(Arg)*3-(GluCBI)*1 Deprotected	sPDC7
MSH-(Glu)*3-(GluCBI)*1 Deprotected	PDC8
MSH-(Arg)*3-(Glu-DNA binding unit- CBI)*1 Deprotected	PDC9
MSH-(Glu-DNA binding unit- CBI)*1 Protected	PDC10
MSH-(Glu)*3-(GluCBI)*1 conjugated to FITC	PDCL1
MSH-(Arg)*3-(GluCBI)*1 conjugated to FITC	PDCL2
MSH Conjugated to Biotin	PL1
MSH Conjugated to FITC	PL2

5.5.2 Synthesis of P1, P2 and P3

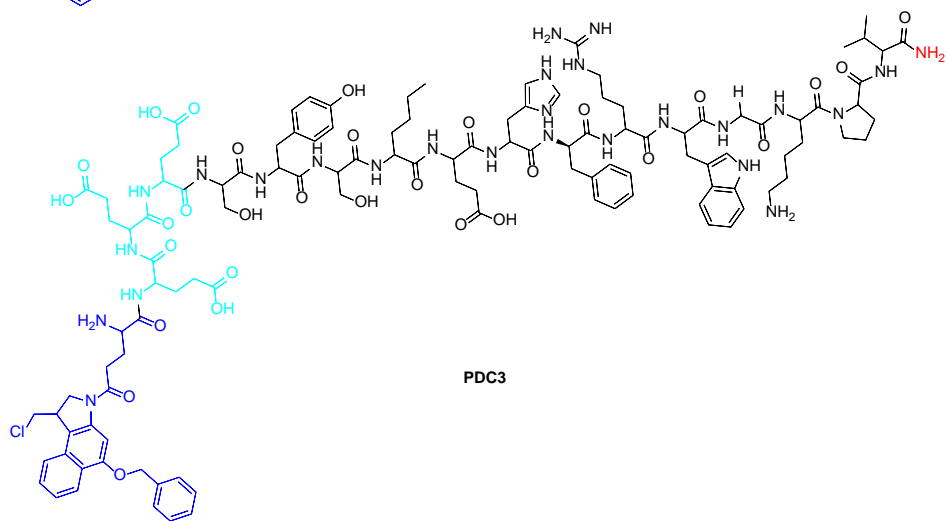
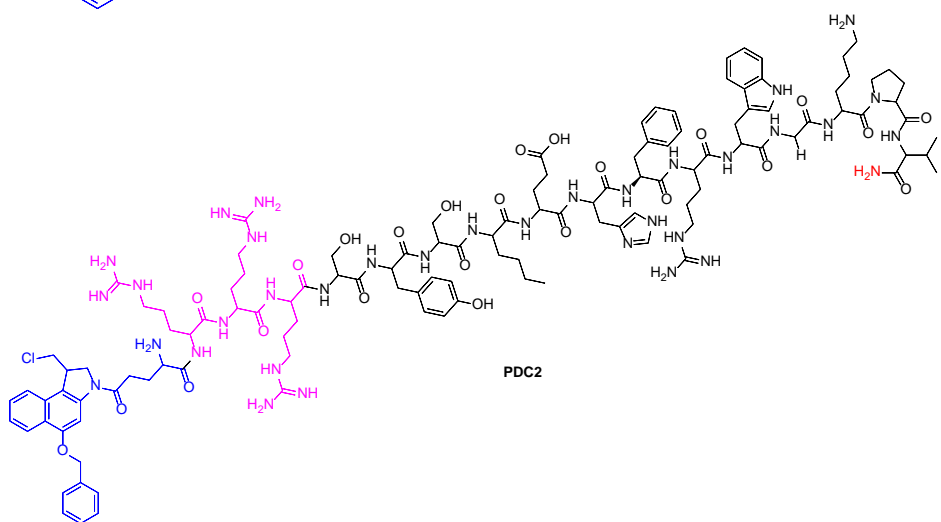
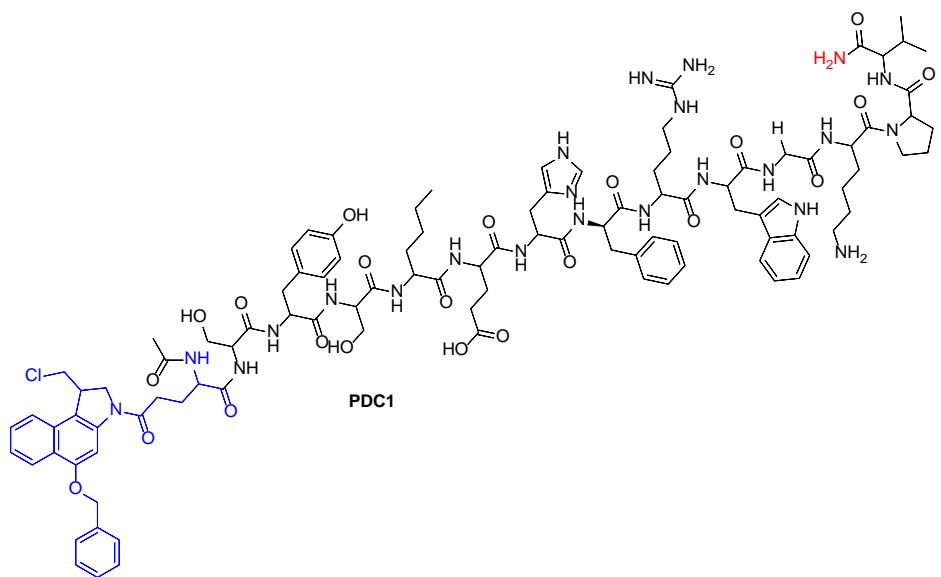




P1, P2 and P3 were prepared using the NovaPEG Rink Amide resin. 100 mg of NovaPEG Rink Amide resin (0.049 mmol based on the manufacturer's resin loading of 0.49 mmol/g) was prepared for coupling by swelling in DMF (2 mL) for 30 mins in a peptide column. DMF was drained from the peptide column and then Fmoc-Val-OH (4 equivalent) was added followed by the addition of 4 equivalent of HBTU and HOBt and 8 equivalent of DIPEA in DMF. The reaction mixture was incubated shaking for 30 min followed by draining and a wash with DMF (2 mL) three times. The coupling was repeated to ensure complete coupling and then subjected to 40 % piperidine for 10 min (2 x 2 mL) to remove the Fmoc. After Fmoc deprotection, the resin coupled to the first amino acid was washed with DMF (2 x 2 mL). subsequent amino acids were coupled following identical procedures and then after completion, the resin was drained and then washed with DMF (10 x 10 mL) followed by DCM (10 x 10 mL). The peptide was cleaved from the resin using 95% TFA, 2.5% TIPS and 2.5% H₂O and incubated mixing for 3 h. The cleaved peptide cocktail was collected and the resin was further washed with TFA (2 x 2mL). The combined washings were concentrated in vacuo. The peptide was precipitated with cold diethyl ether, which was then decanted. The precipitated peptide was dissolved in water and then purified using automated reversed phase Prep HPLC. Purified peptide was lyophilised from water to yield an off white solid for **P1, P2 and P3**.

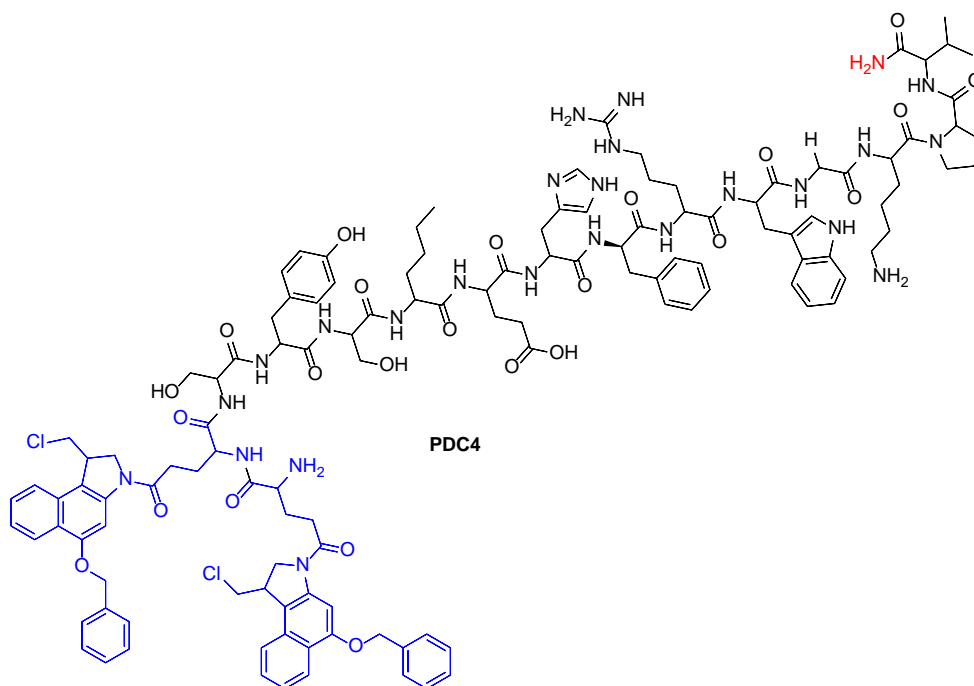
P1, P2 and P3 were subsequently analysed using RP-HPLC and had a retention time of 12.27 min, 10.52 min and 11.37 min respectively. Mass spectrometry analysis demonstrated correct mass for all the peptides; **P1** (calculated (M + 2H)²⁺ 802.92 ; found: 802.95); **P2** (calculated (M + 2H)²⁺: 1037.07; found: 1036.91); **P3** (calculated (M + H)⁺: 1993.16. ; ound: 1993.76).

5.5.3 Synthesis of peptide drug conjugates (PDC): PDC1, PDC2, PDC3 and PDC4.



PDC1, **PDC2** and **PDC3** were prepared by initially synthesising **P1**, **P2** and **P3** respectively as described in section 5.5.1. Peptides **P1**, **P2** and **P3** coupled to the NovaPEG Rink Amide resin were suspended in DMF (2 mL) for 30 min, allowing the resin to swell. DMF was drained from the peptide column and then 1.5 equivalent of **6** in DMF were added, followed by the addition of 1.5 equivalent of HATU and 3 equivalent of DIPEA in DMF. The mixture was then incubated for 2 h shaking followed by draining and washing with DMF (2 mL) three times. The coupling was repeated to ensure complete coupling and then subjected to 40% piperidine for 10 min (2 x 2 mL) to remove the Fmoc. For peptide **PDC1** which was acetylated, after Fmoc deprotection the resin coupled to the PDC was washed with DMF (5 x 10 mL) before the addition of anhydrous DMF (2 mL), DIPEA (10 equivalent), and AcCl (5 equivalent) and then incubated shaking for 1 h. The acetylation was repeated one more time to insure complete acetylation. After Fmoc deprotection and acetylation, the resin coupled to the PDC was washed with DMF (5 x 10 mL) followed by DCM (5 x 10 mL). The PDCs were cleaved from the resin using 95% TFA, 2.5% TIPS and 2.5% H₂O and incubated mixing for 3 h. The cleaved PDC cocktail was collected and the resin was further washed with TFA (2 x 1 mL). The combined washings were concentrated in vacuo. The PDC was precipitated with cold diethyl ether, which was then decanted. The precipitated peptide was dissolved in 50% methanol in water and then purified using automated reversed phase Prep HPLC. Purified peptide was lyophilised from water to yield a brown solid for **PDC1**, **PDC2** and **PDC3**.

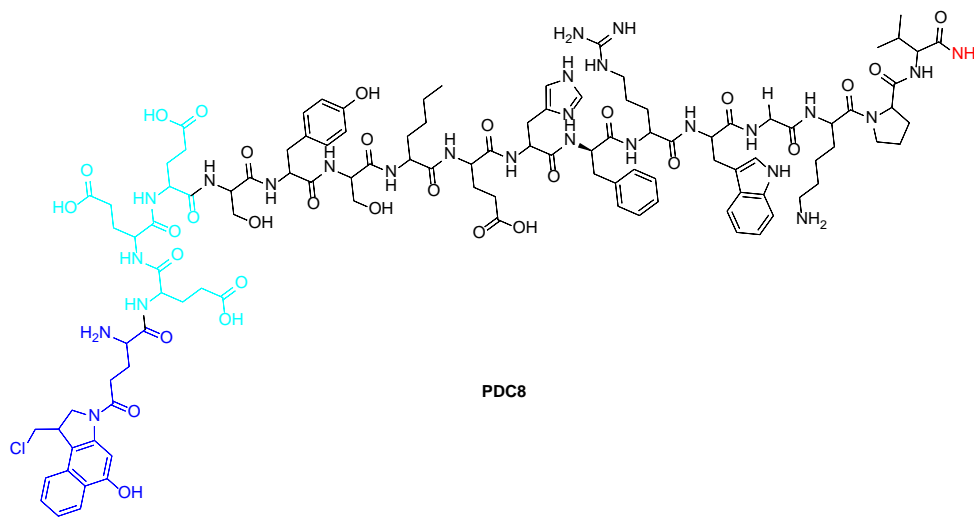
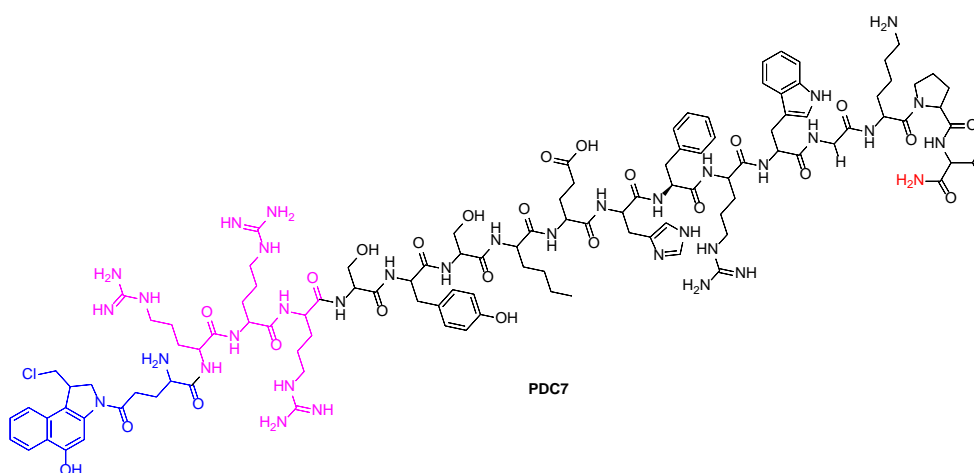
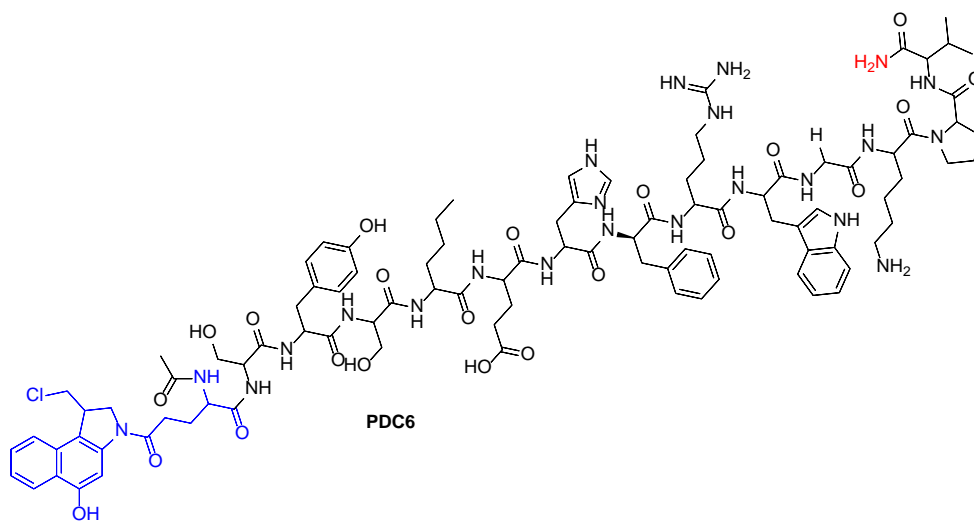
PDC1, **PDC2** and **PDC3** were subsequently analysed using RP-HPLC and had a retention time of 12.48 - 13.43 min, 11.21-12.26min and 12.06-13.05 min respectively. Mass spectrometry analysis demonstrated correct mass for all the peptides; **PDC1** calculated (M + 2H)²⁺: 1041.00; found: 1041.10; **PDC2** (calculated (M + 3H)³⁺: 836.43; found:836.43); **PDC3** (calculated (M + 3H)³⁺: 809.37 ; found: 809.34).



PDC4 coupled to two warheads **6** was prepared through the extension of peptide **PDC1** prior to acetylation. Non-acetylated peptide **PDC1** coupled to the NovaPEG Rink Amide resin was suspended in DMF (2 mL) for 30 min, allowing the resin to swell. DMF was drained from the peptide column and then added 1.5 equivalent of **6** in DMF, followed by the addition of 1.5 equivalent of HATU and 3 equivalent of DIPEA in DMF. The mixture was then incubated for 2 h shaking followed by draining and washing with DMF (3 x 2 mL). The coupling was repeated to ensure complete coupling and then subjected to 40% piperidine for 10 min (2 x 2 mL) to remove the Fmoc. After Fmoc deprotection, the resin coupled to the PDC was washed with DMF (2 x 2 mL). After completion of the synthesis of **PDC4**, the resin was drained and then washed with DMF (5 x 10 mL) followed by DCM (5 x 10 mL). The PDCs were cleaved from the resin using 95% TFA, 2.5% TIPS and 2.5% H₂O and incubated mixing for 3 h. The cleaved PDC cocktail was collected and the resin was further washed with TFA (2 x 1 mL). The combined washings were concentrated in vacuo. The PDC was precipitated with cold diethyl ether, which was then decanted. The precipitated peptide was dissolved in 50% methanol in water and then purified using automated reversed phase Prep HPLC. Purified PDC was lyophilised from water to yield **PDC4** as a brown solid.

PDC4 was subsequently analysed using RP-HPLC and had a retention time of 16.17-17.66 min. Mass spectrometry analysis demonstrated correct mass; **PDC4** calculated $(M + 3H)^{3+}$: 825.04; found: 825.04.

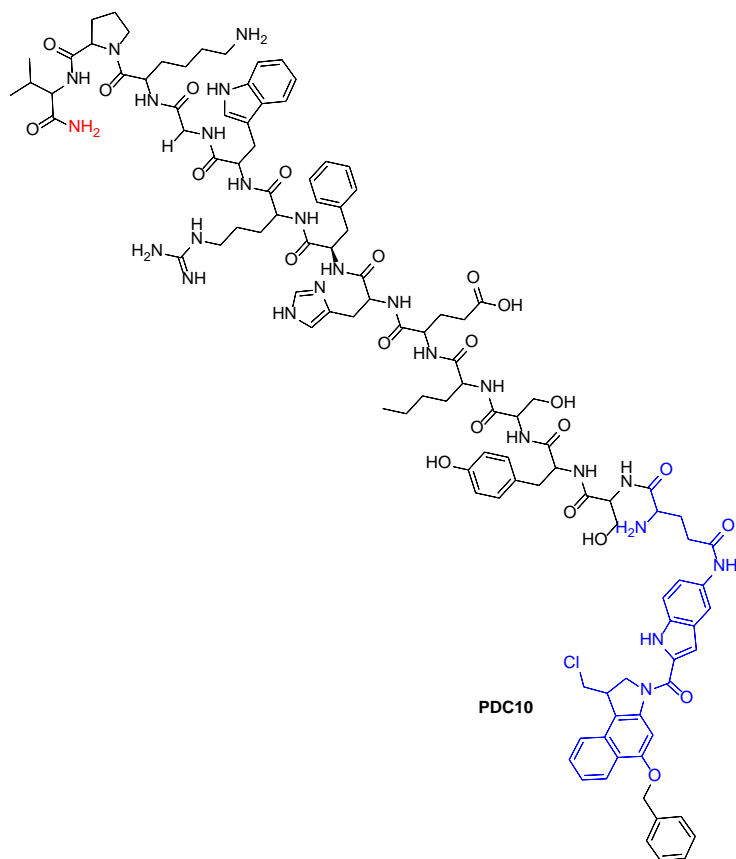
5.5.4 Synthesis of biologically active benzyl deprotected peptide drug conjugates (PDC): PDC6, PDC7, and PDC8.



Biologically active peptide drug conjugate **PDC6**, **PDC7** and **PDC8** were prepared from peptide drug conjugate **PDC1**, **PDC2** and **PDC3** coupled on the Novapeg Rink amide resin. The resin was first washed with DCM (5 x 2 mL) and then subsequently allowed to swell in anhydrous DCM (2 mL) under an atmosphere of N₂ for 30 min. Following the 30 min incubation, two equivalence of 1 M solution of BBr₃ in DCM was added and then subsequently incubated for 1 h at nominally -78°C→RT and incubated for a further 1 h at RT. The resin was subsequently washed with DCM (5 x 5 mL), followed by the addition of the cleavage cocktail using 95% TFA, 2.5% TIPS and 2.5% H₂O and incubated mixing for 3 h. The cleaved PDCs cocktail were collected and the resin was further washed with TFA (2 x 1 mL). The combined washings were concentrated in vacuo. The PDCs were precipitated with cold diethyl ether, which was then decanted. The precipitated peptide was dissolved in 50% methanol in water and then purified using automated reversed phase Prep HPLC. Purified PDC was lyophilised from water to yield **PDC6**, **PDC7** and **PDC8** as a brown solids.

PDC6, **PDC7** and **PDC8** were subsequently analysed using RP-HPLC and had a retention time of 15.31-15.97 min, 13.40-13.76 min and 14.45-14.77 min respectively. Mass spectrometry analysis demonstrated correct mass for all the peptides; **PDC6** (calculated (M + 3H)³⁺: 664.31; found: 664.33); **PDC7** (calculated (M + 3H)³⁺: 806.41; found: 806.17); **PDC8** calculated (M + 3H)³⁺: 779.36; found: 779.17).

5.5.5 Incorporation of the DNA binding subunit into peptide drug conjugates (PDC). PDC10

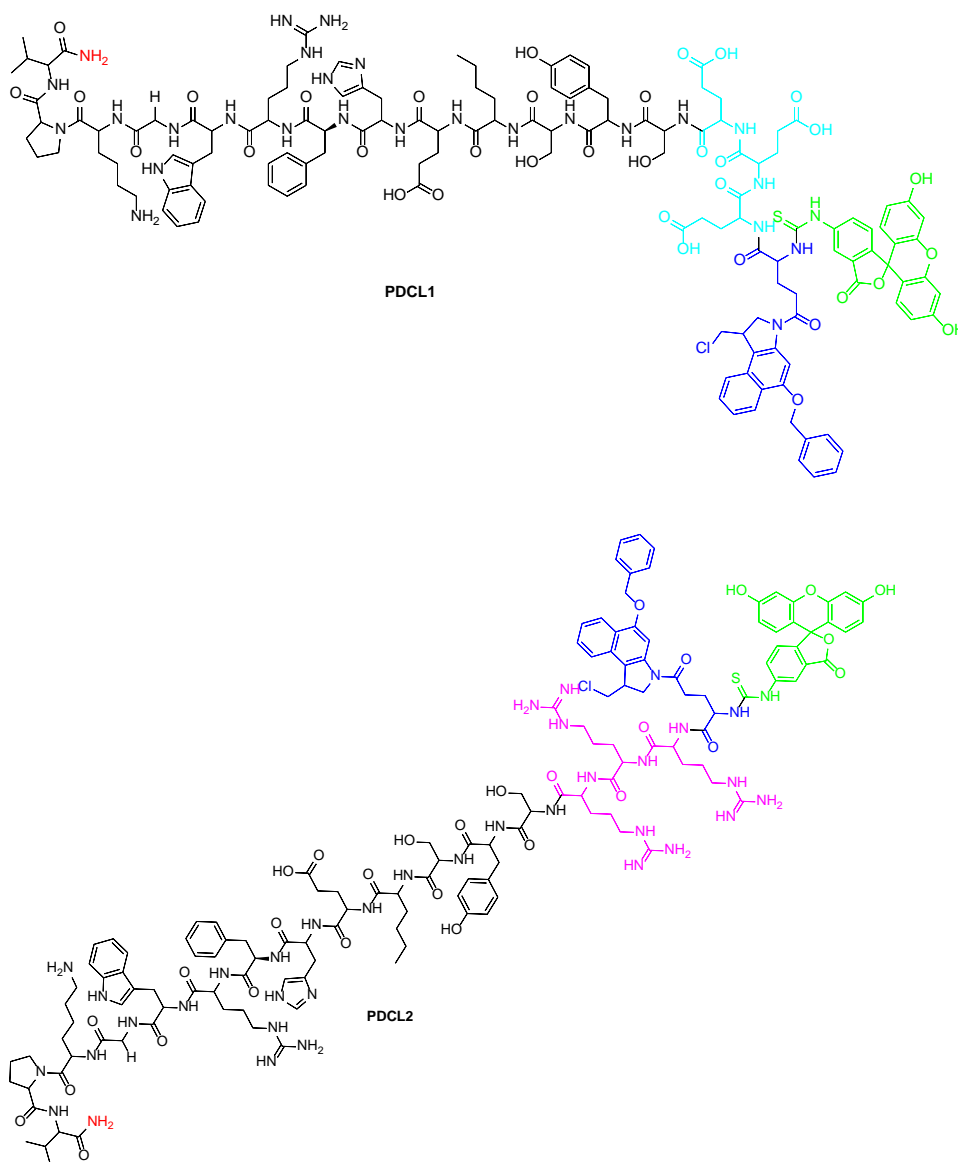


PDC10 incorporating the DNA binding unit was prepared by initially synthesising **P1** as described in section 5.5.1. Peptides **P1** coupled to the NovaPEG Rink Amide resin were suspended in DMF (2 mL) for 30 min, allowing the resin to swell. DMF was drained from the peptide column followed by the addition of 1.5 equivalent of **7** in DMF, 1.5 equivalent of HATU and 3 equivalent of DIPEA in DMF. The mixture was then incubated overnight shaking followed by draining and washing with DMF (5 x 10 mL). The coupling was repeated to ensure completion and then subjected to 40% piperidine for 10 min (2 x 2 mL) to remove the Fmoc. After Fmoc deprotection, the resin was drained and then washed with DMF (5 x 10 mL) followed by DCM (5 x 5 mL). The PDC was cleaved from the resin using 95% TFA, 2.5% TIPS and 2.5% H₂O and incubated mixing for 3 h. The cleaved PDC cocktail was collected and the resin was further washed with TFA (2 x 1 mL). The combined washings were concentrated in vacuo. The PDC was precipitated with cold diethyl ether, which was then decanted. The precipitated peptide was dissolved in 50%

methanol in water and then purified using automated reversed phase Prep HPLC. Purified PDC was lyophilised from water to yield **PDC10** as a brown solid.

PDC10 was subsequently analysed using RP-HPLC and had a retention time of 10.08 min. Mass spectrometry analysis demonstrated correct mass for all the **PDC10**, calculated $(M + 3H)^{3+}$: 733.01; found: 733.03.

PL1 was subsequently analysed using RP-HPLC and had a retention time of 9.99 min. Mass spectrometry analysis demonstrated correct mass for all the peptides; calculated $(M + 3H)^{3+}$:610.98; found: 610.98).



FITC conjugated to peptide drug conjugate **PDCL1** and **PDCL2** were prepared from peptide drug conjugate **PDC3** and **PDC2** respectively. PDCs **PDC3** and **PDC2** coupled on the Novapeg Rink amide resin were first suspended in DMF (2 mL) for 30 min, allowing the resin to swell. DMF was drained from the peptide column and then added 4 equivalent of

Fluorescein-5-isothiocyanate (FITC) in DMF respectively, followed by the addition of 4 equivalent of HATU and 4 equivalent of DIPEA in DMF. The mixture was then incubated for 2 h shaking followed by draining and washing with DMF (5 x 10 mL). The coupling was repeated to ensure completion. After the label conjugation, the resin was washed with DMF (5 x 10 mL) and then DCM (5 x 5 mL), followed by the addition of the cleavage cocktail using 95% TFA, 2.5% TIPS and 2.5% H₂O and incubated mixing for 3 h.

Cleaved peptide cocktail were collected and the resin was washed with TFA (2 x 1 mL) and the washings were combined and concentrated in vacuo. The peptide was precipitated with cold diethyl ether, followed by the removal of diethyl ether. The precipitated PDCs were dissolved in in 50% methanol in water and then purified using automated reverse phase Prep HPLC. Purified peptide was lyophilised from water to yield a bright yellow solid for **PDCL1** and **PDCL2**.

PDCL1 and **PDCL2** were subsequently analysed using RP-HPLC and had a retention time of 15.97 min and 19.93 min respectively. Mass spectrometry analysis demonstrated correct mass for all the peptides; **PDCL1** calculated (M + 4H)⁴⁺: 704.54; found: 704.13); **PDCL2** (calculated (M + 4H)⁴⁺: 724.83; found: 724.52.

6 Reference

- (1) Linares, M. A.; Zakaria, A.; Nizran, P. Skin Cancer. *Primary Care - Clinics in Office Practice*. W.B. Saunders 2015, pp 645–659. <https://doi.org/10.1016/j.pop.2015.07.006>.
- (2) Thieu, K.; Ruiz, M. E.; Owens, D. M. Cells of Origin and Tumor-Initiating Cells for Nonmelanoma Skin Cancers. *Cancer Letters*. September 10, 2013, pp 82–88. <https://doi.org/10.1016/j.canlet.2012.05.008>.
- (3) American Cancer Society. About Basal and Squamous Cell Skin Cancer. Jan 15, 2020, pp 1-13. <https://www.cancer.org/content/dam/CRC/PDF/Public/8818.00.pdf>
- (4) Cancer Research UK. Melanoma skin cancer incidence statistics <https://www.cancerresearchuk.org/health-professional/cancer-statistics/statistics-by-cancer-type/melanoma-skin-cancer/incidence#heading-Zero> (accessed Dec 20, 2019).
- (5) Cichorek, M.; Wachulska, M.; Stasiewicz, A.; Tyminińska, A. Skin Melanocytes: Biology and Development. *Postep. Dermatologii i Alergol.* **2013**. <https://doi.org/10.5114/pdia.2013.33376>.
- (6) Reed JA, Shea CR. Lentigo maligna: melanoma in situ on chronically sun-damaged skin. *Arch Pathol Lab Med*. 2011 Jul;135(7):838-41. doi: 10.5858/2011-0051-RAIR.1. PMID: 21732771.
- (7) Alasadi, A. H.; M.Alsafy, B. Early Detection and Classification of Melanoma Skin Cancer. *Int. J. Inf. Technol. Comput. Sci.* **2015**, 7 (12), 67–74. <https://doi.org/10.5815/ijitcs.2015.12.08>.
- (8) Wu, S.; Zhu, W.; Thompson, P.; Hannun, Y. A. Evaluating Intrinsic and Non-Intrinsic Cancer Risk Factors. *Nature Communications*. Nature Publishing Group December 1, 2018. <https://doi.org/10.1038/s41467-018-05467-z>.
- (9) Wehner, M. R.; Shive, M. L.; Chren, M. M.; Han, J.; Qureshi, A. A.;

- Linos, E. Indoor Tanning and Non-Melanoma Skin Cancer: Systematic Review and Meta-Analysis. *BMJ* **2012**, *345* (7877). <https://doi.org/10.1136/bmj.e5909>.
- (10) Herman, J. R. Global Increase in UV Irradiance during the Past 30 Years (1979-2008) Estimated from Satellite Data. *J. Geophys. Res. Atmos.* **2010**, *115* (4). <https://doi.org/10.1029/2009JD012219>.
- (11) Whiteman, D. C.; Green, A. C.; Olsen, C. M. The Growing Burden of Invasive Melanoma: Projections of Incidence Rates and Numbers of New Cases in Six Susceptible Populations through 2031. *J. Invest. Dermatol.* **2016**, *136* (6), 1161–1171. <https://doi.org/10.1016/j.jid.2016.01.035>.
- (12) Nikolaou, V.; Stratigos, A. J. Emerging Trends in the Epidemiology of Melanoma. *British Journal of Dermatology*. Blackwell Publishing Ltd 2014, pp 11–19. <https://doi.org/10.1111/bjd.12492>.
- (13) Brenner, M.; Hearing, V. J. The Protective Role of Melanin against UV Damage in Human Skin. *Photochemistry and Photobiology*. May 2008, pp 539–549. <https://doi.org/10.1111/j.1751-1097.2007.00226.x>.
- (14) Reed, K. B.; Brewer, J. D.; Lohse, C. M.; Bringe, K. E.; Pruitt, C. N.; Gibson, L. E. Increasing Incidence of Melanoma among Young Adults: An Epidemiological Study in Olmsted County, Minnesota. *Mayo Clin. Proc.* **2012**, *87* (4), 328–334. <https://doi.org/10.1016/j.mayocp.2012.01.010>.
- (15) Guy, G. P.; Zhang, Y.; Ekwueme, D. U.; Rim, S. H.; Watson, M. The Potential Impact of Reducing Indoor Tanning on Melanoma Prevention and Treatment Costs in the United States: An Economic Analysis. *J. Am. Acad. Dermatol.* **2017**, *76* (2), 226–233. <https://doi.org/10.1016/j.jaad.2016.09.029>.
- (16) Palmieri, G.; Colombino, M.; Casula, M.; Budroni, M.; Manca, A.; Sini, M. C.; Lissia, A.; Stanganelli, I.; Ascierto, P. A.; Cossu, A. Epidemiological and Genetic Factors Underlying Melanoma

Development in Italy. *Melanoma Manag.* **2015**, *2* (2), 149–163. <https://doi.org/10.2217/mmt.15.12>.

- (17) Wu, S.; Han, J.; Laden, F.; Qureshi, A. A. Long-Term Ultraviolet Flux, Other Potential Risk Factors, and Skin Cancer Risk: A Cohort Study. *Cancer Epidemiol. Biomarkers Prev.* **2014**, *23* (6), 1080–1089. <https://doi.org/10.1158/1055-9965.EPI-13-0821>.
- (18) Ribero, S.; Stucci, L. S.; Marra, E.; Marconcini, R.; Spagnolo, F.; Orgiano, L.; Picasso, V.; Queirolo, P.; Palmieri, G.; Quaglino, P.; Bataille, V. Effect of Age on Melanoma Risk, Prognosis and Treatment Response. *Acta Dermato-Venereologica. Medical Journals/Acta D-V* 2018, pp 624–629. <https://doi.org/10.2340/00015555-2944>.
- (19) Gupta, A. K.; Bharadwaj, M.; Mehrotra, R. Skin Cancer Concerns in People of Color: Risk Factors and Prevention. *Asian Pacific Journal of Cancer Prevention. Asian Pacific Organization for Cancer Prevention* 2016, pp 6157–6164. <https://doi.org/10.22034/APJCP.2016.17.12.6157>.
- (20) Chandra, P.; Wolfenden, L. L.; Ziegler, T. R.; Tian, J.; Luo, M.; Stecenko, A. A.; Chen, T. C.; Holick, M. G.; Tangpricha, V. Treatment of Vitamin D Deficiency with UV Light in Patients with Malabsorption Syndromes: A Case Series. *Photodermatol. Photoimmunol. Photomed.* **2007**, *23* (5), 179–185. <https://doi.org/10.1111/j.1600-0781.2007.00302.x>.
- (21) Diffey, B. L. Time and Place as Modifiers of Personal UV Exposure. *International Journal of Environmental Research and Public Health.* MDPI AG June 1, 2018. <https://doi.org/10.3390/ijerph15061112>.
- (22) Potrony, M.; Badenas, C.; Aguilera, P.; Puig-Butille, J. A.; Carrera, C.; Malveyh, J.; Puig, S. Update in Genetic Susceptibility in Melanoma. *Annals of Translational Medicine.* AME Publishing Company September 1, 2015. <https://doi.org/10.3978/j.issn.2305-5839.2015.08.11>.
- (23) Huang, J.; El-Gamil, M.; Dudley, M. E.; Li, Y. F.; Rosenberg, S. A.; Robbins, P. F. T Cells Associated with Tumor Regression Recognize

Frameshifted Products of the CDKN2A Tumor Suppressor Gene Locus and a Mutated HLA Class I Gene Product . *J. Immunol.* **2004**, *172* (10), 6057–6064. <https://doi.org/10.4049/jimmunol.172.10.6057>.

- (24) Latreille, J.; Ezzedine, K.; Elfakir, A.; Ambroisine, L.; Gardinier, S.; Galan, P.; Hercberg, S.; Gruber, F.; Rees, J.; Tschachler, E.; Guinot, C. MC1R Gene Polymorphism Affects Skin Color and Phenotypic Features Related to Sun Sensitivity in a Population of French Adult Women. *Photochem. Photobiol.* **2009**, *85* (6), 1451–1458. <https://doi.org/10.1111/j.1751-1097.2009.00594.x>.
- (25) Matichard, E.; Verpillat, P.; Meziani, R.; Gérard, B.; Descamps, V.; Legroux, E.; Burnouf, M.; Bertrand, G.; Bouscarat, F.; Archimbaud, A.; Picard, C.; Ollivaud, L.; Basset-Seguin, N.; Kerob, D.; Lanternier, G.; Lebbe, C.; Crickx, B.; Grandchamp, B.; Soufir, N. Melanocortin 1 Receptor (MC1R) Gene Variants May Increase the Risk of Melanoma in France Independently of Clinical Risk Factors and UV Exposure. *Journal of medical genetics.* February 2004. <https://doi.org/10.1136/jmg.2003.011536>.
- (26) Tagliabue, E.; Fargnoli, M. C.; Gandini, S.; Maisonneuve, P.; Liu, F.; Kayser, M.; Nijsten, T.; Han, J.; Kumar, R.; Gruis, N. A.; Ferrucci, L.; Branicki, W.; Dwyer, T.; Blizzard, L.; Helsing, P.; Autier, P.; García-Borrón, J. C.; Kanetsky, P. A.; Landi, M. T.; Little, J.; Newton-Bishop, J.; Sera, F.; Raimondi, S.; Autier, P.; García-Borrón, J. C.; Han, J.; Kanetsky, P. A.; Landi, M. T.; Little, J.; Caini, S.; Hofman, A.; Kayser, M.; Liu, F.; Nijsten, T.; Uitterlinden, A. G.; Kumar, R.; Scherer, D.; Nagore, E.; Hansson, J.; Hoiom, V.; Ghiorzo, P.; Pastorino, L.; Gruis, N. A.; Bavinck, J. N. B.; Aguilera, P.; Badenas, C.; Carrera, C.; Malvehy, J.; Mateu, M. P.; Puig, S.; Puig-Butille, J. A.; Tell, G.; Cochrane, J.; Fernandez-De-Misa, R.; Branicki, W.; Debniak, T.; Morling, N.; Johansen, P.; Mayne, S.; Bale, A.; Cartmel, B.; Ferrucci, L.; Pfeiffer, R.; Palmieri, G.; Ribas, G.; Stratigos, A.; Kypreou, K.; Bowcock, A.; Cornelius, L.; Council, M. L.; Motokawa, T.; Anno, S.; Helsing, P.; Andresen, P. A.; Wong, T. H.; Berwick, M.; Berwick, M.; Orlow, I.;

Mujumdar, U.; Hummer, A.; Busam, K.; Roy, P.; Canchola, R.; Clas, B.; Cotignola, J.; Monroe, Y.; Armstrong, B.; Kricker, A.; Litchfield, M.; Dwyer, T.; Tucker, P.; Stephens, N.; Gallagher, R.; Switzer, T.; Marrett, L.; Theis, B.; From, L.; Chowdhury, N.; Vanasse, L.; Purdue, M.; Northrup, D.; Zanetti, R.; Rosso, S.; Sacerdote, C.; Anton-Culver, H.; Leighton, N.; Gildea, M.; Gruber, S.; Bonner, J.; Jeter, J.; Klotz, J.; Wilcox, H.; Weiss, H.; Millikan, R.; Thomas, N.; Mattingly, D.; Player, J.; Tse, C. K.; Rebbeck, T.; Kanetsky, P. P.; Walker, A.; Panossian, S.; Mohrenweiser, H.; Setlow, R. MC1R Gene Variants and Non-Melanoma Skin Cancer: A Pooled-Analysis from the M-SKIP Project. *Br. J. Cancer* **2015**, *113* (2), 354–363. <https://doi.org/10.1038/bjc.2015.231>.

- (27) Herraiz, C.; Garcia-Borron, J. C.; Jiménez-Cervantes, C.; Olivares, C. MC1R Signaling. Intracellular Partners and Pathophysiological Implications. *Biochimica et Biophysica Acta - Molecular Basis of Disease*. Elsevier B.V. October 1, 2017, pp 2448–2461. <https://doi.org/10.1016/j.bbadis.2017.02.027>.
- (28) Potjer, T. P.; Bollen, S.; Grimbergen, A. J. E. M.; van Doorn, R.; Gruis, N. A.; van Asperen, C. J.; Hes, F. J.; van der Stoep, N. Multigene Panel Sequencing of Established and Candidate Melanoma Susceptibility Genes in a Large Cohort of Dutch Non-CDKN2A/CDK4 Melanoma Families. *Int. J. Cancer* **2019**, *144* (10), 2453–2464. <https://doi.org/10.1002/ijc.31984>.
- (29) Domingues, B.; Lopes, J.; Soares, P.; Populo, H. Melanoma Treatment in Review. *ImmunoTargets Ther.* **2018**, *Volume 7*, 35–49. <https://doi.org/10.2147/itt.s134842>.
- (30) Sladden, M. J.; Balch, C.; Barzilai, D. A.; Berg, D.; Freiman, A.; Handiside, T.; Hollis, S.; Lens, M. B.; Thompson, J. F. Surgical Excision Margins for Primary Cutaneous Melanoma. *Sao Paulo Medical Journal*. January 2011, p 56. <https://doi.org/10.1590/S1516-31802011000100014>.
- (31) Ott, P. A.; Hamilton, A.; Min, C.; Safarzadeh-Amiri, S.; Goldberg, L.;

- Yoon, J.; Yee, H.; Buckley, M.; Christos, P. J.; Wright, J. J.; Polsky, D.; Osman, I.; Liebes, L.; Pavlick, A. C. A Phase II Trial of Sorafenib in Metastatic Melanoma with Tissue Correlates. *PLoS One* **2010**. <https://doi.org/10.1371/journal.pone.0015588>.
- (32) Alcalá, A. M.; Flaherty, K. T. BRAF Inhibitors for the Treatment of Metastatic Melanoma: Clinical Trials and Mechanisms of Resistance. *Clinical Cancer Research*. January 1, 2012, pp 33–39. <https://doi.org/10.1158/1078-0432.CCR-11-0997>.
- (33) Shelledy, PharmD, L.; Roman, PharmD, BCOP, D. Vemurafenib: First-in-Class BRAF-Mutated Inhibitor for the Treatment of Unresectable or Metastatic Melanoma. *J. Adv. Pract. Oncol.* **2015**, *6* (4). <https://doi.org/10.6004/jadpro.2015.6.4.6>.
- (34) Ballantyne, A. D.; Garnock-Jones, K. P. Dabrafenib: First Global Approval. *Drugs* **2013**, *73* (12), 1367–1376. <https://doi.org/10.1007/s40265-013-0095-2>.
- (35) Dummer, R.; Ascierto, P. A.; Gogas, H. J.; Arance, A.; Mandala, M.; Liskay, G.; Garbe, C.; Schadendorf, D.; Krajsova, I.; Gutzmer, R.; Chiarion-Sileni, V.; Dutriaux, C.; de Groot, J. W. B.; Yamazaki, N.; Loquai, C.; Moutouh-de Parseval, L. A.; Pickard, M. D.; Sandor, V.; Robert, C.; Flaherty, K. T. Encorafenib plus Binimetinib versus Vemurafenib or Encorafenib in Patients with BRAF-Mutant Melanoma (COLUMBUS): A Multicentre, Open-Label, Randomised Phase 3 Trial. *Lancet Oncol.* **2018**, *19* (5), 603–615. [https://doi.org/10.1016/S1470-2045\(18\)30142-6](https://doi.org/10.1016/S1470-2045(18)30142-6).
- (36) Kakadia, S.; Yarlagadda, N.; Awad, R.; Kundranda, M.; Niu, J.; Naraev, B.; Mina, L.; Dragovich, T.; Gimbel, M.; Mahmoud, F. Mechanisms of Resistance to BRAF and MEK Inhibitors and Clinical Update of US Food and Drug Administration-Approved Targeted Therapy in Advanced Melanoma. *OncoTargets and Therapy*. Dove Medical Press Ltd. 2018, pp 7095–7107. <https://doi.org/10.2147/OTT.S182721>.

- (37) Griffin, D. E. Cytokines and Chemokines. In *Encyclopedia of Virology*; Elsevier Ltd, 2008; pp 620–624. <https://doi.org/10.1016/B978-012374410-4.00374-5>.
- (38) Lee, S.; Margolin, K. Cytokines in Cancer Immunotherapy. *Cancers*. December 2011, pp 3856–3893. <https://doi.org/10.3390/cancers3043856>.
- (39) Gadina, M.; Sudarshan, C.; O’Shea, J. J. IL-2, but Not IL-4 and Other Cytokines, Induces Phosphorylation of a 98-KDa Protein Associated with SHP-2, Phosphatidylinositol 3’-Kinase, and Grb2. *J. Immunol.* **1999**, *162* (4), 2081–2086.
- (40) Wargo, J. A.; Reuben, A.; Cooper, Z.; Amaria, R. Update on Use of Aldesleukin for Treatment of High-Risk Metastatic Melanoma. *ImmunoTargets Ther.* **2015**, *79*. <https://doi.org/10.2147/itt.s61590>.
- (41) Herndon, T. M.; Demko, S. G.; Jiang, X.; He, K.; Gootenberg, J. E.; Cohen, M. H.; Keegan, P.; Pazdur, R. U.S. Food and Drug Administration Approval: Peginterferon-Alfa-2b for the Adjuvant Treatment of Patients with Melanoma. *Oncologist* **2012**, *17* (10), 1323–1328. <https://doi.org/10.1634/theoncologist.2012-0123>.
- (42) Franco, S. Di; Turdo, A.; Todaro, M.; Stassi, G. Role of Type I and II Interferons in Colorectal Cancer and Melanoma. *Frontiers in Immunology*. Frontiers Media S.A. July 26, 2017. <https://doi.org/10.3389/fimmu.2017.00878>.
- (43) Salama, A. K. S.; Hodi, F. S. Cytotoxic T-Lymphocyte-Associated Antigen-4. *Clinical Cancer Research*. July 15, 2011, pp 4622–4628. <https://doi.org/10.1158/1078-0432.CCR-10-2232>.
- (44) Camacho, L. H. CTLA-4 Blockade with Ipilimumab: Biology, Safety, Efficacy, and Future Considerations. *Cancer Med.* **2015**, *4* (5), 661–672. <https://doi.org/10.1002/cam4.371>.
- (45) Latchman, Y.; Wood, C. R.; Chernova, T.; Chaudhary, D.; Borde, M.;

- Chernova, I.; Iwai, Y.; Long, A. J.; Brown, J. A.; Nunes, R.; Greenfield, E. A.; Bourque, K.; Boussiotis, V. A.; Carter, L. L.; Carreno, B. M.; Malenkovich, N.; Nishimura, H.; Okazaki, T.; Honjo, T.; Sharpe, A. H.; Freeman, G. J. PD-L2 Is a Second Ligand for PD-1 and Inhibits T Cell Activation. *Nat. Immunol.* **2001**, *2* (3), 261–268. <https://doi.org/10.1038/85330>.
- (46) Chemnitz, J. M.; Parry, R. V.; Nichols, K. E.; June, C. H.; Riley, J. L. SHP-1 and SHP-2 Associate with Immunoreceptor Tyrosine-Based Switch Motif of Programmed Death 1 upon Primary Human T Cell Stimulation, but Only Receptor Ligation Prevents T Cell Activation. *J. Immunol.* **2004**, *173* (2), 945–954. <https://doi.org/10.4049/jimmunol.173.2.945>.
- (47) Ward, W. H.; Farma, J. M. *Cutaneous Melanoma: Etiology and Therapy*.
- (48) Prasad, V.; Kaestner, V. Nivolumab and Pembrolizumab: Monoclonal Antibodies against Programmed Cell Death-1 (PD-1) That Are Interchangeable. *Seminars in Oncology*. W.B. Saunders April 1, 2017, pp 132–135. <https://doi.org/10.1053/j.seminoncol.2017.06.007>.
- (49) Homet Moreno, B.; Ribas, A. Anti-Programmed Cell Death Protein-1/Ligand-1 Therapy in Different Cancers. *Br. J. Cancer* **2015**, *112* (9), 1421–1427. <https://doi.org/10.1038/bjc.2015.124>.
- (50) Weber, J.; Mandala, M.; Del Vecchio, M.; Gogas, H. J.; Arance, A. M.; Cowey, C. L.; Dalle, S.; Schenker, M.; Chiarion-Sileni, V.; Marquez-Rodas, I.; Grob, J. J.; Butler, M. O.; Middleton, M. R.; Maio, M.; Atkinson, V.; Queirolo, P.; Gonzalez, R.; Kudchadkar, R. R.; Smylie, M.; Meyer, N.; Mortier, L.; Atkins, M. B.; Long, G. V.; Bhatia, S.; Lebbé, C.; Rutkowski, P.; Yokota, K.; Yamazaki, N.; Kim, T. M.; De Pril, V.; Sabater, J.; Qureshi, A.; Larkin, J.; Ascierto, P. A. Adjuvant Nivolumab versus Ipilimumab in Resected Stage III or IV Melanoma. *N. Engl. J. Med.* **2017**, *377* (19), 1824–1835. <https://doi.org/10.1056/NEJMoa1709030>.

- (51) Postow, M. A.; Chesney, J.; Pavlick, A. C.; Robert, C.; Grossmann, K.; McDermott, D.; Linette, G. P.; Meyer, N.; Giguere, J. K.; Agarwala, S. S.; Shaheen, M.; Ernstoff, M. S.; Minor, D.; Salama, A. K.; Taylor, M.; Ott, P. A.; Rollin, L. M.; Horak, C.; Gagnier, P.; Wolchok, J. D.; Hodi, F. S. Nivolumab and Ipilimumab versus Ipilimumab in Untreated Melanoma. *N. Engl. J. Med.* **2015**, *372* (21), 2006–2017. <https://doi.org/10.1056/NEJMoa1414428>.
- (52) Menshawy, A.; Eltonob, A. A.; Barkat, S. A.; Ghanem, A.; Mniesy, M. M.; Mohamed, I.; Abdel-Maboud, M.; Mattar, O. M.; Elfil, M.; Bahbah, E. I.; Elgebaly, A. Nivolumab Monotherapy or in Combination with Ipilimumab for Metastatic Melanoma: Systematic Review and Meta-Analysis of Randomized-Controlled Trials. *Melanoma Res.* **2018**, *28* (5), 371–379. <https://doi.org/10.1097/CMR.0000000000000467>.
- (53) Van Der Bruggen, P.; Traversari, C.; Chomez, P.; Lurquin, C.; De Plaen, E.; Van Den Eynde, B.; Knuth, A.; Boon, T. A Gene Encoding an Antigen Recognized by Cytolytic T Lymphocytes on a Human Melanoma. *Science* (80-.). **1991**, *254* (5038), 1643–1647. <https://doi.org/10.1126/science.1840703>.
- (54) Xiao, J.; Chen, H. S. Biological Functions of Melanoma-Associated Antigens. *World Journal of Gastroenterology*. WJG Press July 1, 2004, pp 1849–1853. <https://doi.org/10.3748/wjg.v10.i13.1849>.
- (55) Weon, J. L.; Potts, P. R. The MAGE Protein Family and Cancer. *Current Opinion in Cell Biology*. Elsevier Ltd December 1, 2015, pp 1–8. <https://doi.org/10.1016/j.ceb.2015.08.002>.
- (56) Brichard, V. G.; Godechal, Q. MAGE-A3-Specific Anticancer Immunotherapy in the Clinical Practice. *Oncoimmunology* **2013**, *2* (10). <https://doi.org/10.4161/onci.25995>.
- (57) Zajac, P.; Schultz-Thater, E.; Tornillo, L.; Sadowski, C.; Trella, E.; Mengus, C.; Iezzi, G.; Spagnoli, G. C. MAGE-A Antigens and Cancer Immunotherapy. *Front. Med.* **2017**, *4* (MAR).

<https://doi.org/10.3389/fmed.2017.00018>.

- (58) Perica, K.; Varela, J. C.; Oelke, M.; Schneck, J. Adoptive T Cell Immunotherapy For Cancer. *Rambam Maimonides Med. J.* **2015**, *6* (1), e0004. <https://doi.org/10.5041/rmmj.10179>.
- (59) Nguyen, L. T.; Saibil, S. D.; Sotov, V.; Le, M. X.; Khoja, L.; Ghazarian, D.; Bonilla, L.; Majeed, H.; Hogg, D.; Joshua, A. M.; Crump, M.; Franke, N.; Spreafico, A.; Hansen, A.; Al-Habeeb, A.; Leong, W.; Easson, A.; Reedijk, M.; Goldstein, D. P.; McCready, D.; Yasufuku, K.; Waddell, T.; Cypel, M.; Pierre, A.; Zhang, B.; Boross-Harmer, S.; Cipollone, J.; Nelles, M.; Scheid, E.; Fyrsta, M.; Lo, C. S.; Nie, J.; Yam, J. Y.; Yen, P. H.; Gray, D.; Motta, V.; Elford, A. R.; DeLuca, S.; Wang, L.; Effendi, S.; Ellenchery, R.; Hirano, N.; Ohashi, P. S.; Butler, M. O. Phase II Clinical Trial of Adoptive Cell Therapy for Patients with Metastatic Melanoma with Autologous Tumor-Infiltrating Lymphocytes and Low-Dose Interleukin-2. *Cancer Immunol. Immunother.* **2019**, *68* (5), 773–785. <https://doi.org/10.1007/s00262-019-02307-x>.
- (60) Gonzalez, H.; Hagerling, C.; Werb, Z. Roles of the Immune System in Cancer: From Tumor Initiation to Metastatic Progression. *Genes and Development*. Cold Spring Harbor Laboratory Press 2018, pp 1267–1284. <https://doi.org/10.1101/GAD.314617.118>.
- (61) Sharpe, M.; Mount, N. Genetically Modified T Cells in Cancer Therapy: Opportunities and Challenges. *DMM Disease Models and Mechanisms*. Company of Biologists Ltd April 1, 2015, pp 337–350. <https://doi.org/10.1242/dmm.018036>.
- (62) Khan, M. K.; Khan, N.; Almasan, A.; Macklis, R. Future of Radiation Therapy for Malignant Melanoma in an Era of Newer, More Effective Biological Agents. *Oncotargets and Therapy*. 2011, pp 137–148. <https://doi.org/10.2147/OTT.S20257>.
- (63) Luo, Y. M.; Xia, N. X.; Yang, L.; Li, Z.; Yang, H.; Yu, H. J.; Liu, Y.; Lei, H.; Zhou, F. X.; Xie, C. H.; Zhou, Y. F. CTC1 Increases the

Radioresistance of Human Melanoma Cells by Inhibiting Telomere Shortening and Apoptosis. *Int. J. Mol. Med.* **2014**, *33* (6), 1484–1490. <https://doi.org/10.3892/ijmm.2014.1721>.

- (64) Rogers, S. J.; Puric, E.; Eberle, B.; Datta, N. R.; Bodis, S. B. Radiotherapy for Melanoma: More than DNA Damage. *Dermatology Research and Practice*. Hindawi Limited 2019. <https://doi.org/10.1155/2019/9435389>.
- (65) Wilson, M. A.; Schuchter, L. M. Chemotherapy for Melanoma. In *Cancer Treatment and Research*; Kluwer Academic Publishers, 2016; Vol. 167, pp 209–229. https://doi.org/10.1007/978-3-319-22539-5_8.
- (66) Bhatia, S.; Tykodi, S. S.; Thompson, J. A. Treatment of Metastatic Melanoma: An Overview. *ONCOLOGY*. May 2009, pp 488–496.
- (67) Reid, J. M.; Kuffel, M. J.; Miller, J. K.; Rios, R.; Ames, M. M. Metabolic Activation of Dacarbazine by Human Cytochromes P450: The Role of CYP1A1, CYP1A2, and CYP2E1. *Clin. Cancer Res.* **1999**, *5* (8), 2192–2197.
- (68) Amatu, A.; Sartore-Bianchi, A.; Moutinho, C.; Belotti, A.; Bencardino, K.; Chirico, G.; Cassingena, A.; Rusconi, F.; Esposito, A.; Nichelatti, M.; Esteller, M.; Siena, S. Promoter CpG Island Hypermethylation of the DNA Repair Enzyme MGMT Predicts Clinical Response to Dacarbazine in a Phase II Study for Metastatic Colorectal Cancer. *Clin. Cancer Res.* **2013**, *19* (8), 2265–2272. <https://doi.org/10.1158/1078-0432.CCR-12-3518>.
- (69) Luke, J. J.; Schwartz, G. K. Chemotherapy in the Management of Advanced Cutaneous Malignant Melanoma. *Clin. Dermatol.* **2013**, *31* (3), 290–297. <https://doi.org/10.1016/j.clindermatol.2012.08.016>.
- (70) Chari, R. V. J.; Miller, M. L.; Widdison, W. C. Antibody-Drug Conjugates: An Emerging Concept in Cancer Therapy. *Angewandte Chemie - International Edition*. Wiley-VCH Verlag April 7, 2014, pp 3796–3827. <https://doi.org/10.1002/anie.201307628>.

- (71) Firer, M. A.; Gellerman, G. Targeted Drug Delivery for Cancer Therapy: The Other Side of Antibodies. *Journal of Hematology and Oncology*. 2012. <https://doi.org/10.1186/1756-8722-5-70>.
- (72) Thomas, A.; Teicher, B. A.; Hassan, R. Antibody–Drug Conjugates for Cancer Therapy. *The Lancet Oncology*. Lancet Publishing Group June 1, 2016, pp e254–e262. [https://doi.org/10.1016/S1470-2045\(16\)30030-4](https://doi.org/10.1016/S1470-2045(16)30030-4).
- (73) Bae, Y. H.; Park, K. Targeted Drug Delivery to Tumors: Myths, Reality and Possibility. *Journal of Controlled Release*. Elsevier B.V. August 10, 2011, pp 198–205. <https://doi.org/10.1016/j.jconrel.2011.06.001>.
- (74) Yan, L.; Hsu, K.; Beckman, R. A. Antibody-Based Therapy for Solid Tumors. *Cancer Journal*. May 2008, pp 178–183. <https://doi.org/10.1097/PPO.0b013e318172d71a>.
- (75) Pillay, V.; Gan, H. K.; Scott, A. M. Antibodies in Oncology. *New Biotechnology*. September 2011, pp 518–529. <https://doi.org/10.1016/j.nbt.2011.03.021>.
- (76) Attarwala, H. Role of Antibodies in Cancer Targeting. *J. Nat. Sci. Biol. Med.* **2010**, 1 (1), 53–56. <https://doi.org/10.4103/0976-9668.71675>.
- (77) Diamantis, N.; Banerji, U. Antibody-Drug Conjugates - An Emerging Class of Cancer Treatment. *British Journal of Cancer*. Nature Publishing Group February 1, 2016, pp 362–367. <https://doi.org/10.1038/bjc.2015.435>.
- (78) Ducry, L.; Stump, B. Antibody–Drug Conjugates: Linking Cytotoxic Payloads to Monoclonal Antibodies. *Bioconjug. Chem.* **2010**, 21 (1), 5–13. <https://doi.org/10.1021/bc9002019>.
- (79) Tsuchikama, K.; An, Z. Antibody-Drug Conjugates: Recent Advances in Conjugation and Linker Chemistries. *Protein and Cell*. Higher Education Press January 1, 2018, pp 33–46. <https://doi.org/10.1007/s13238-016-0323-0>.

- (80) Shefet-Carasso, L.; Benhar, I. Antibody-Targeted Drugs and Drug Resistance-Challenges and Solutions. *Drug Resist. Updat.* **2015**, *18*, 36–46. <https://doi.org/10.1016/j.drup.2014.11.001>.
- (81) Godwin, C. D.; Gale, R. P.; Walter, R. B. Gemtuzumab Ozogamicin in Acute Myeloid Leukemia. *Leukemia*. Nature Publishing Group September 1, 2017, pp 1855–1868. <https://doi.org/10.1038/leu.2017.187>.
- (82) Chalouni, C.; Doll, S. Fate of Antibody-Drug Conjugates in Cancer Cells. *Journal of Experimental and Clinical Cancer Research*. BioMed Central Ltd. February 6, 2018. <https://doi.org/10.1186/s13046-017-0667-1>.
- (83) Lu, J.; Jiang, F.; Lu, A.; Zhang, G. Linkers Having a Crucial Role in Antibody–Drug Conjugates. *International Journal of Molecular Sciences*. MDPI AG April 14, 2016. <https://doi.org/10.3390/ijms17040561>.
- (84) Carlson, B. *Antibody-Drug Conjugates – The New Frontier*; 2012.
- (85) Nejadmoghaddam, M.-R.; Minai-Tehrani, A.; Ghahremanzadeh, R.; Mahmoudi, M.; Dinarvand, R.; Zarnani, A.-H. *Antibody-Drug Conjugates: Possibilities and Challenges*; Vol. 11.
- (86) Tolcher, A. W. Antibody Drug Conjugates: Lessons from 20 Years of Clinical Experience. *Annals of oncology: official journal of the European Society for Medical Oncology*. December 1, 2016, pp 2168–2172. <https://doi.org/10.1093/annonc/mdw424>.
- (87) Anami, Y.; Yamazaki, C. M.; Xiong, W.; Gui, X.; Zhang, N.; An, Z.; Tsuchikama, K. Glutamic Acid-Valine-Citrulline Linkers Ensure Stability and Efficacy of Antibody-Drug Conjugates in Mice. *Nat. Commun.* **2018**, *9* (1). <https://doi.org/10.1038/s41467-018-04982-3>.
- (88) Erickson, H. K.; Park, P. U.; Widdison, W. C.; Kovtun, Y. V.; Garrett, L. M.; Hoffman, K.; Lutz, R. J.; Goldmacher, V. S.; Blättler, W. A. Antibody-Maytansinoid Conjugates Are Activated in Targeted Cancer

Cells by Lysosomal Degradation and Linker-Dependent Intracellular Processing. *Cancer Res.* **2006**, *66* (8), 4426–4433. <https://doi.org/10.1158/0008-5472.CAN-05-4489>.

- (89) Kim, E. G.; Kim, K. M. Strategies and Advancement in Antibody-Drug Conjugate Optimization for Targeted Cancer Therapeutics. *Biomolecules and Therapeutics*. Korean Society of Applied Pharmacology November 1, 2015, pp 493–509. <https://doi.org/10.4062/biomolther.2015.116>.
- (90) Bargh, J. D.; Isidro-Llobet, A.; Parker, J. S.; Spring, D. R. Cleavable Linkers in Antibody-Drug Conjugates. *Chemical Society Reviews*. Royal Society of Chemistry August 21, 2019, pp 4361–4374. <https://doi.org/10.1039/c8cs00676h>.
- (91) Maass, K. F.; Kulkarni, C.; Betts, A. M.; Wittrup, K. D. Determination of Cellular Processing Rates for a Trastuzumab-Maytansinoid Antibody-Drug Conjugate (ADC) Highlights Key Parameters for ADC Design. *AAPS J.* **2016**, *18* (3), 635–646. <https://doi.org/10.1208/s12248-016-9892-3>.
- (92) Tang, H.; Liu, Y.; Yu, Z.; Sun, M.; Lin, L.; Liu, W.; Han, Q.; Wei, M.; Jin, Y. The Analysis of Key Factors Related to ADCS Structural Design. *Frontiers in Pharmacology*. 2019. <https://doi.org/10.3389/fphar.2019.00373>.
- (93) Chen, L.; Wang, L.; Shion, H.; Yu, C.; Yu, Y. Q.; Zhu, L.; Li, M.; Chen, W.; Gao, K. In-Depth Structural Characterization of Kadcyla® (Ado-Trastuzumab Emtansine) and Its Biosimilar Candidate. *MABs* **2016**, *8* (7), 1210–1223. <https://doi.org/10.1080/19420862.2016.1204502>.
- (94) Li, W.; Prabakaran, P.; Chen, W.; Zhu, Z.; Feng, Y.; Dimitrov, D. Antibody Aggregation: Insights from Sequence and Structure. *Antibodies* **2016**, *5* (3), 19. <https://doi.org/10.3390/antib5030019>.
- (95) Liu, H.; Chumsae, C.; Gaza-Bulseco, G.; Hurkmans, K.; Radziejewski, C. H. Ranking the Susceptibility of Disulfide Bonds in Human IgG1

Antibodies by Reduction, Differential Alkylation, and LC-MS Analysis. *Anal. Chem.* **2010**. <https://doi.org/10.1021/ac100575n>.

- (96) McCombs, J. R.; Owen, S. C. Antibody Drug Conjugates: Design and Selection of Linker, Payload and Conjugation Chemistry. *AAPS J.* **2015**, *17* (2), 339–351. <https://doi.org/10.1208/s12248-014-9710-8>.
- (97) Zhao, R. Y.; Wilhelm, S. D.; Audette, C.; Jones, G.; Leece, B. A.; Lazar, A. C.; Goldmacher, V. S.; Singh, R.; Kovtun, Y.; Widdison, W. C.; Lambert, J. M.; Chari, R. V. J. Synthesis and Evaluation of Hydrophilic Linkers for Antibody-Maytansinoid Conjugates. *J. Med. Chem.* **2011**, *54* (10), 3606–3623. <https://doi.org/10.1021/jm2002958>.
- (98) Dan, N.; Setua, S.; Kashyap, V. K.; Khan, S.; Jaggi, M.; Yallapu, M. M.; Chauhan, S. C. Antibody-Drug Conjugates for Cancer Therapy: Chemistry to Clinical Implications. *Pharmaceuticals*. MDPI AG June 1, 2018. <https://doi.org/10.3390/ph11020032>.
- (99) Deonarain, M.; Yahioğlu, G.; Stamati, I.; Pomowski, A.; Clarke, J.; Edwards, B.; Diez-Posada, S.; Stewart, A. Small-Format Drug Conjugates: A Viable Alternative to ADCs for Solid Tumours? *Antibodies* **2018**, *7* (2), 16. <https://doi.org/10.3390/antib7020016>.
- (100) Chari, R. V. J.; Jacket, K. A.; Bourret, L. A.; Derr, S. M.; Tadayoni, B. M.; Mattocks, K. M.; Liu, C.; Blattler, W. A.; Goldmacher, V. S.; Shah, S. A. Enhancement of the Selectivity and Antitumor Efficacy of a CC-1065 Analogue through Immunoconjugate Formation. *Cancer Res.* **1995**, *55* (18).
- (101) Ghosh, N.; Sheldrake, H.; Searcey, M.; Pors, K. Chemical and Biological Explorations of the Family of CC-1065 and the Duocarmycin Natural Products. *Curr. Top. Med. Chem.* **2009**, *9* (16), 1494–1524. <https://doi.org/10.2174/156802609789909812>.
- (102) Ghosh, N.; Sheldrake, H.; Searcey, M.; Pors, K. Chemical and Biological Explorations of the Family of CC-1065 and the Duocarmycin Natural Products. *Curr. Top. Med. Chem.* **2009**, *9* (16), 1494–1524.

<https://doi.org/10.2174/156802609789909812>.

- (103) Mohamadi, F.; Spees, M. M.; Staten, G. S.; Marder, P.; Kipka, J. K.; Johnson, D. A.; Boger, D. L.; Zarrinmayeh, H. Total Synthesis and Biological Properties of Novel Antineoplastic (Chloromethyl)Furanoidolines: An Asymmetric Hydroboration Mediated Synthesis of the Alkylation Subunits. *J. Med. Chem.* **1994**, *37* (2), 232–239. <https://doi.org/10.1021/jm00028a005>.
- (104) Li, L. H.; Swenson, D. H.; Schpok, S. L. F.; Kuentzel, S. L.; Dayton, B. D.; Krueger, W. C. CC-1065 (NSC 298223), a Novel Antitumor Agent That Interacts Strongly with Double-Stranded DNA. *Cancer Res.* **1982**, *42* (3), 999–1004.
- (105) Bhuyan, B. K.; Newell, K. A.; Adams, E. G. CC-1065 (NSC 298223), a Most Potent Antitumor Agent: Biological Activity, Cell-Kill and DNA Synthesis Inhibition Kinetics. *Proc. Am. Assoc. Cancer Res.* **1981**, *Vol. 22*, 889.
- (106) Wrasidlo, W.; Johnson, D. S.; Boger, D. L. Induction of Endonucleolytic DNA Fragmentation and Apoptosis by the Duocarmycins. *Bioorganic Med. Chem. Lett.* **1994**, *4* (4), 631–636. [https://doi.org/10.1016/S0960-894X\(01\)80168-2](https://doi.org/10.1016/S0960-894X(01)80168-2).
- (107) Tada-Oikawa, S.; Oikawa, S.; Kawanishi, M.; Yamada, M.; Kawanishi, S. Generation of Hydrogen Peroxide Precedes Loss of Mitochondrial Membrane Potential during DNA Alkylation-Induced Apoptosis. *FEBS Lett.* **1999**, *442* (1), 65–69. [https://doi.org/10.1016/S0014-5793\(98\)01618-4](https://doi.org/10.1016/S0014-5793(98)01618-4).
- (108) Boger, D. L.; Santillán, A.; Searcey, M.; Jin, Q. Critical Role of the Linking Amide in CC-1065 and the Duocarmycins: Implications on the Source of DNA Alkylation Catalysis. *J. Am. Chem. Soc.* **1998**, *120* (45), 11554–11557. <https://doi.org/10.1021/ja9818093>.
- (109) Boger, D. L.; Santillán, A.; Searcey, M.; Jin, Q. Synthesis and Evaluation of Duocarmycin and CC-1065 Analogues Containing Modifications in

the Subunit Linking Amide. *J. Org. Chem.* **1999**, *64* (14), 5241–5244.
<https://doi.org/10.1021/jo990452y>.

- (110) Boger, D. L.; Johnson, D. S. CC-1065 and the Duocarmycins: Unraveling the Keys to a New Class of Naturally Derived DNA Alkylating Agents. *Proceedings of the National Academy of Sciences of the United States of America*. National Academy of Sciences April 25, 1995, pp 3642–3649. <https://doi.org/10.1073/pnas.92.9.3642>.
- (111) Harbach, P. R.; Zimmer, D. M.; Mazurek, J. H.; Bhuyan, B. K. Mutagenicity of the Antitumor Antibiotic CC-1065 and Its Analogues in Mammalian (V79) Cells and Bacteria. *Cancer Res.* **1988**, *48* (1), 32–36.
- (112) Searcey, M. Duocarmycins--Natures Prodrugs? *Curr. Pharm. Des.* **2002**, *8* (15), 1375–1389.
- (113) van der Lee, M. M. C.; Groothuis, P. G.; Ubink, R.; van der Vleuten, M. A. J.; van Achterberg, T. A.; Loosveld, E. M.; Damming, D.; Jacobs, D. C. H.; Rouwette, M.; Egging, D. F.; van den Dobbelen, D.; Beusker, P. H.; Goedings, P.; Verheijden, G. F. M.; Lemmens, J. M.; Timmers, M.; Dokter, W. H. A. The Preclinical Profile of the Duocarmycin-Based HER2-Targeting ADC SYD985 Predicts for Clinical Benefit in Low HER2-Expressing Breast Cancers. *Mol. Cancer Ther.* **2015**, *14* (3), 692–703. <https://doi.org/10.1158/1535-7163.MCT-14-0881-T>.
- (114) Elgersma, R. C.; Coumans, R. G. E.; Huijbregts, T.; Menge, W. M. P. B.; Joosten, J. A. F.; Spijker, H. J.; De Groot, F. M. H.; Van Der Lee, M. M. C.; Ubink, R.; Van Den Dobbelen, D. J.; Egging, D. F.; Dokter, W. H. A.; Verheijden, G. F. M.; Lemmens, J. M.; Timmers, C. M.; Beusker, P. H. Design, Synthesis, and Evaluation of Linker-Duocarmycin Payloads: Toward Selection of HER2-Targeting Antibody-Drug Conjugate SYD985. *Mol. Pharm.* **2015**, *12* (6), 1813–1835. <https://doi.org/10.1021/mp500781a>.
- (115) Baig, M. H.; Ahmad, K.; Saeed, M.; Alharbi, A. M.; Barreto, G. E.; Ashraf, G. M.; Choi, I. Peptide Based Therapeutics and Their Use for the

- Treatment of Neurodegenerative and Other Diseases. *Biomedicine and Pharmacotherapy*. 2018.
<https://doi.org/10.1016/j.biopha.2018.04.025>.
- (116) Ma, L.; Wang, C.; He, Z.; Cheng, B.; Zheng, L.; Huang, K. Peptide-Drug Conjugate: A Novel Drug Design Approach. *Curr. Med. Chem.* **2017**.
<https://doi.org/10.2174/0929867324666170404142840>.
- (117) Habault, J.; Poyet, J. L. Recent Advances in Cell Penetrating Peptide-Based Anticancer Therapies. *Molecules* **2019**.
<https://doi.org/10.3390/molecules24050927>.
- (118) Imesch, P.; Scheiner, D.; Szabo, E.; Fink, D.; Fedier, A. Conjugates of Cytochrome c and Antennapedia Peptide Activate Apoptosis and Inhibit Proliferation of HeLa Cancer Cells. *Exp. Ther. Med.* **2013**.
<https://doi.org/10.3892/etm.2013.1205>.
- (119) Yandek, L. E.; Pokorny, A.; Florén, A.; Knoelke, K.; Langel, Ü.; Almeida, P. F. F. Mechanism of the Cell-Penetrating Peptide Transportan 10 Permeation of Lipid Bilayers. *Biophys. J.* **2007**, *92* (7), 2434–2444.
<https://doi.org/10.1529/biophysj.106.100198>.
- (120) Tang, H.; Yin, L.; Kim, K. H.; Cheng, J. Helical Poly(Arginine) Mimics with Superior Cell-Penetrating and Molecular Transporting Properties. *Chem. Sci.* **2013**. <https://doi.org/10.1039/c3sc51328a>.
- (121) Mo, Robert H. Mo, R. H., Zaro, J. L., & Shen, W. C. (2012). C. of cationic and amphipathic cell penetrating peptides for siRNA delivery and efficacy. M. P. <https://doi.org/10.1021/mp200481g>; Zaro, J. L.; Shen, W. C. Comparison of Cationic and Amphipathic Cell Penetrating Peptides for SiRNA Delivery and Efficacy. *Mol. Pharm.* **2012**.
<https://doi.org/10.1021/mp200481g>.
- (122) Ruseska, I.; Zimmer, A. Internalization Mechanisms of Cell-Penetrating Peptides. *Beilstein J. Nanotechnol.* **2020**, *11*, 101–123.
<https://doi.org/10.3762/bjnano.11.10>.

- (123) Liang, J. F.; Yang, V. C. Synthesis of Doxorubicin-Peptide Conjugate with Multidrug Resistant Tumor Cell Killing Activity. *Bioorganic Med. Chem. Lett.* **2005**. <https://doi.org/10.1016/j.bmcl.2005.07.087>.
- (124) Gräslund, A.; Madani, F.; Lindberg, S.; Langel, Ü.; Futaki, S. Mechanisms of Cellular Uptake of Cell-Penetrating Peptides. *Journal of Biophysics*. 2011. <https://doi.org/10.1155/2011/414729>.
- (125) Hillaireau, H.; Couvreur, P. Nanocarriers' Entry into the Cell: Relevance to Drug Delivery. *Cellular and Molecular Life Sciences*. 2009. <https://doi.org/10.1007/s00018-009-0053-z>.
- (126) Moreno, P.; Ramos-Álvarez, I.; Moody, T. W.; Jensen, R. T. Bombesin Related Peptides/Receptors and Their Promising Therapeutic Roles in Cancer Imaging, Targeting and Treatment. *Expert Opinion on Therapeutic Targets*. 2016. <https://doi.org/10.1517/14728222.2016.1164694>.
- (127) McCann, S. M.; Kimura, M.; Walczewska, A.; Karanth, S.; Rettori, V.; Yu, W. H. Hypothalamic Control of FSH and LH by FSH-RF, LHRH, Cytokines, Leptin and Nitric Oxide. *NeuroImmunoModulation*. 1998. <https://doi.org/10.1159/000026337>.
- (128) Dharap, S. S.; Qiu, B.; Williams, G. C.; Sinko, P.; Stein, S.; Minko, T. Molecular Targeting of Drug Delivery Systems to Ovarian Cancer by BH3 and LHRH Peptides. In *Journal of Controlled Release*; 2003; Vol. 91. [https://doi.org/10.1016/S0168-3659\(03\)00209-8](https://doi.org/10.1016/S0168-3659(03)00209-8).
- (129) He, R.; Finan, B.; Mayer, J. P.; DiMarchi, R. D. Peptide Conjugates with Small Molecules Designed to Enhance Efficacy and Safety. *Molecules*. 2019. <https://doi.org/10.3390/molecules24101855>.
- (130) Fodor, K.; Dobos, N.; Schally, A.; Steiber, Z.; Olah, G.; Sipos, E.; Szekvolgyi, L.; Halmos, G. The Targeted LHRH Analog AEZS-108 Alters Expression of Genes Related to Angiogenesis and Development of Metastasis in Uveal Melanoma. *Oncotarget* **2020**. <https://doi.org/10.18632/oncotarget.27431>.

- (131) Ruoslahti, E.; Pierschbacher, M. D. New Perspectives in Cell Adhesion: RGD and Integrins. *Science* (80-.). **1987**, *238* (4826), 491–497. <https://doi.org/10.1126/science.2821619>.
- (132) Nieberler, M.; Reuning, U.; Reichart, F.; Notni, J.; Wester, H. J.; Schwaiger, M.; Weinmüller, M.; Räder, A.; Steiger, K.; Kessler, H. Exploring the Role of RGD-Recognizing Integrins in Cancer. *Cancers*. 2017. <https://doi.org/10.3390/cancers9090116>.
- (133) Zuo, H. IRGD: A Promising Peptide for Cancer Imaging and a Potential Therapeutic Agent for Various Cancers. *J. Oncol.* **2019**, *2019*. <https://doi.org/10.1155/2019/9367845>.
- (134) Tian, Y.; Li, S.; Song, J.; Ji, T.; Zhu, M.; Anderson, G. J.; Wei, J.; Nie, G. A Doxorubicin Delivery Platform Using Engineered Natural Membrane Vesicle Exosomes for Targeted Tumor Therapy. *Biomaterials* **2014**, *35* (7), 2383–2390. <https://doi.org/10.1016/j.biomaterials.2013.11.083>.
- (135) Yu, K. F.; Zhang, W. Q.; Luo, L. M.; Song, P.; Li, D.; Du, R.; Ren, W.; Huang, D.; Lu, W. L.; Zhang, X.; Zhang, Q. The Antitumor Activity of a Doxorubicin Loaded, IRGD-Modified Sterically-Stabilized Liposome on B16-F10 Melanoma Cells: In Vitro and in Vivo Evaluation. *Int. J. Nanomedicine* **2013**, *8*, 2473–2485. <https://doi.org/10.2147/IJN.S46962>.
- (136) Liu, X.; Jiang, J.; Ji, Y.; Lu, J.; Chan, R.; Meng, H. Targeted Drug Delivery Using IRGD Peptide for Solid Cancer Treatment. *Molecular Systems Design and Engineering*. Royal Society of Chemistry 2017, pp 370–379. <https://doi.org/10.1039/c7me00050b>.
- (137) Boger, D. L.; McKie, J. A. An Efficient Synthesis of 1, 2, 9, 9a-Tetrahydrocyclopropa[c]Benz[e]Indol-4-One (CBI): An Enhanced and Simplified Analog of the CC-1065 and Duocarmycin Alkylation Subunits. *J. Org. Chem.* **1995**, *60* (5), 1271–1275. <https://doi.org/10.1021/jo00110a034>.
- (138) L. Boger, D.; Ishizaki, T.; A. Kitos, P.; Suntornwat, O. Synthesis of N-

- (Tert-Butyloxycarbonyl)-CBI, CBI, CBI-CDPI1, and CBI-CDPI2: Enhanced Functional Analogs of CC-1065 Incorporating the 1,2,9,9a-Tetrahydrocyclopropa[c]Benz[e]Indol-4-One (CBI) Left-Hand Subunit. *J. Org. Chem.* **2002**, *55* (23), 5823–5832. <https://doi.org/10.1021/jo00310a013>.
- (139) Tietze, L. F.; Von Hof, J. M.; Krewer, B.; Müller, M.; Major, F.; Schuster, H. J.; Schuberth, I.; Alves, F. Asymmetric Synthesis and Biological Evaluation of Glycosidic Prodrugs for a Selective Cancer Therapy. *ChemMedChem* **2008**, *3* (12). <https://doi.org/10.1002/cmdc.200800250>.
- (140) Tietze, L. F.; Liu, D. Continuous-Flow Microreactor Multi-Step Synthesis of an Aminonaphthalene Derivative as Starting Material for the Preparation of Novel Anticancer Agents. *Arkivoc* **2008**, *2008* (8). <https://doi.org/10.3998/ark.5550190.0009.816>.
- (141) Johnson, W. S.; McCloskey, A. L.; Dunnigan, D. A. The Mechanism of the Stobbe Condensation. *J. Am. Chem. Soc.* **1950**, *72* (1). <https://doi.org/10.1021/ja01157a133>.
- (142) Zhang, Y. Facile Syntheses of Isotope-Labeled Chiral Octahydroindole-2carboxylic Acid and Its N-Methyl Analog. *J. Radioanal. Nucl. Chem.* **2012**, *291* (3), 1371–1376. <https://doi.org/10.1007/s10967-012-1619-z>.
- (143) L. Boger, D.; Yun, W.; R. Teegarden, B. An Improved Synthesis of 1,2,9,9a-Tetrahydrocyclopropa[c]Benz[e]Indol-4-One (CBI): A Simplified Analog of the CC-1065 Alkylation Subunit. *J. Org. Chem.* **2002**, *57* (10), 2873–2876. <https://doi.org/10.1021/jo00036a023>.
- (144) Lajiness, J. P.; Boger, D. L. Asymmetric Synthesis of 1,2,9,9a-Tetrahydrocyclopropa[c]Benzo[e]Indol-4-One (CBI). *J. Org. Chem.* **2010**, *76* (2), 583–587.
- (145) Powers, J. C.; Seidner, R.; Parsons, T. G. The Cleavage of Formyl Groups by Sodium Hydride. *Tetrahedron Lett.* **1965**, *6* (22). [https://doi.org/10.1016/S0040-4039\(00\)90114-X](https://doi.org/10.1016/S0040-4039(00)90114-X).

- (146) Yang, Q.; Sheng, M.; Henkelis, J. J.; Tu, S.; Wiensch, E.; Zhang, H.; Zhang, Y.; Tucker, C.; Ejeh, D. E. Explosion Hazards of Sodium Hydride in Dimethyl Sulfoxide, N, N-Dimethylformamide, and N, N-Dimethylacetamide. *Org. Process Res. Dev.* **2019**, *23* (10). <https://doi.org/10.1021/acs.oprd.9b00276>.
- (147) Carpino, L. A.; Imazumi, H.; Foxman, B. M.; Vela, M. J.; Henklein, P.; El-Faham, A.; Klose, J.; Bienert, M. Comparison of the Effects of 5- and 6-HOAt on Model Peptide Coupling Reactions Relative to the Cases for the 4- and 7-Isomers. *Org. Lett.* **2000**, *2* (15). <https://doi.org/10.1021/ol006013z>.
- (148) Wu, X.; Fu, S.; Liu, Y.; Luo, H.; Li, F.; Wang, Y.; Gao, M.; Cheng, Y.; Xie, Z. NDP-MSH Binding Melanocortin-1 Receptor Ameliorates Neuroinflammation and BBB Disruption through CREB/Nr4a1/NF-KB Pathway after Intracerebral Hemorrhage in Mice. *J. Neuroinflammation* **2019**, *16* (1). <https://doi.org/10.1186/s12974-019-1591-4>.
- (149) Brzoska, T.; Luger, T. A.; Maaser, C.; Abels, C.; Böhm, M. α -Melanocyte-Stimulating Hormone and Related Tripeptides: Biochemistry, Antiinflammatory and Protective Effects in Vitro and in Vivo, and Future Perspectives for the Treatment of Immune-Mediated Inflammatory Diseases. *Endocrine Reviews.* **2008**. <https://doi.org/10.1210/er.2007-0027>.
- (150) O'Donohue, T. L.; Jacobowitz, D. M. Studies of Alpha-MSH-Containing Nerves in the Brain. *Prog. Biochem. Pharmacol.* **1980**, *16*.
- (151) Vehapoğlu, A.; Türkmen, S.; Terzioğlu, Ş. Alpha-Melanocyte-Stimulating Hormone and Agouti-Related Protein: Do They Play a Role in Appetite Regulation in Childhood Obesity? *JCRPE J. Clin. Res. Pediatr. Endocrinol.* **2016**, *8* (1). <https://doi.org/10.4274/jcrpe.2136>.
- (152) Ghanem, G. E.; Comunale, G.; Libert, A.; Vercammen-Grandjean, A.; Lejeune, F. J. Evidence for Alpha-melanocyte-stimulating Hormone (A-

- MSH) Receptors on Human Malignant Melanoma Cells. *Int. J. Cancer* **1988**, *41* (2). <https://doi.org/10.1002/ijc.2910410216>.
- (153) Sawyer, T. K.; Sanfilippo, P. J.; Hruby, V. J.; Engel, M. H.; Heward, C. B.; Burnett, J. B.; Hadley, M. E. 4-Norleucine, 7-d-Phenylalanine- α -Melanocyte-Stimulating Hormone: A Highly Potent α -Melanotropin with Ultralong Biological Activity. *Proc. Natl. Acad. Sci. U. S. A.* **1980**, *77* (10 II). <https://doi.org/10.1073/pnas.77.10.5754>.
- (154) Castrucci, A. M. de L.; Hadley, M. E.; Sawyer, T. K.; Hruby, V. J. Enzymological Studies of Melanotropins. *Comp. Biochem. Physiol. -- Part B Biochem.* **1984**, *78* (3). [https://doi.org/10.1016/0305-0491\(84\)90090-7](https://doi.org/10.1016/0305-0491(84)90090-7).
- (155) Yang, J.; Xu, J.; Gonzales, R.; Lindne, T.; Kratochwil, C.; Miao, Y. Evaluation of Ga-68-DOTA-GGNle-CycMSHhex for Melanoma Imaging. *Nucl. Med. Biol.* **2019**, *72–73*. [https://doi.org/10.1016/s0969-8051\(19\)30285-9](https://doi.org/10.1016/s0969-8051(19)30285-9).
- (156) Xu, J.; Yang, J.; Gonzalez, R.; Fisher, D. R.; Miao, Y. Melanoma-Targeting Property of Y-90-Labeled Lactam-Cyclized α -Melanocyte-Stimulating Hormone Peptide. *Cancer Biother. Radiopharm.* **2019**, *34* (9). <https://doi.org/10.1089/cbr.2019.3049>.
- (157) Merrifield, R. B. Solid Phase Peptide Synthesis. I. The Synthesis of a Tetrapeptide. *J. Am. Chem. Soc.* **1963**, *85* (14). <https://doi.org/10.1021/ja00897a025>.
- (158) Mäde, V.; Els-Heindl, S.; Beck-Sickinger, A. G. Automated Solid-Phase Peptide Synthesis to Obtain Therapeutic Peptides. *Beilstein J. Org. Chem.* **2014**, *10*. <https://doi.org/10.3762/bjoc.10.118>.
- (159) Jaradat, D. M. M. Thirteen Decades of Peptide Synthesis: Key Developments in Solid Phase Peptide Synthesis and Amide Bond Formation Utilized in Peptide Ligation. *Amino Acids.* **2018**. <https://doi.org/10.1007/s00726-017-2516-0>.

- (160) BODANSZKY, M.; DESHMANE, S. S.; MARTINEZ, J. ChemInform Abstract: SIDE REACTIONS IN PEPTIDE SYNTHESIS. 11. POSSIBLE REMOVAL OF THE 9-FLUORENYLMETHYLOXYCARBONYL GROUP BY THE AMINO COMPONENTS DURING COUPLING. *Chem. Informationsd.* **1979**, *10* (37). <https://doi.org/10.1002/chin.197937115>.
- (161) Di Gioia, M. L.; Costanzo, P.; De Nino, A.; Maiuolo, L.; Nardi, M.; Olivito, F.; Procopio, A. Simple and Efficient Fmoc Removal in Ionic Liquid. *RSC Adv.* **2017**, *7* (58). <https://doi.org/10.1039/c7ra04425a>.
- (162) Vrettos, E. I.; Sayyad, N.; Mavrogiannaki, E. M.; Stylos, E.; Kostagianni, A. D.; Papas, S.; Mavromoustakos, T.; Theodorou, V.; Tzakos, A. G. Unveiling and Tackling Guanidinium Peptide Coupling Reagent Side Reactions towards the Development of Peptide-Drug Conjugates. *RSC Adv.* **2017**, *7* (80). <https://doi.org/10.1039/c7ra06655d>.
- (163) Hwang, J. W.; Choi, D. H.; Jeon, J. H.; Kim, J. K.; Jun, J. G. Facile Preparation of 2-Arylbenzo[b]Furan Molecules and Their Anti-Inflammatory Effects. *Bull. Korean Chem. Soc.* **2010**, *31* (4). <https://doi.org/10.5012/bkcs.2010.31.04.965>.
- (164) Sousa, C.; Silva, P. J. BBr₃-Assisted Cleavage of Most Ethers Does Not Follow the Commonly Assumed Mechanism. *European J. Org. Chem.* **2013**, No. 23. <https://doi.org/10.1002/ejoc.201300337>.
- (165) Davis, P. E.; Wilkinson, E. C.; Dores, R. M. Identifying Common Features in the Activation of Melanocortin-2 Receptors: Studies on the *Xenopus Tropicalis* Melanocortin-2 Receptor. *Int. J. Mol. Sci.* **2019**, *20* (17). <https://doi.org/10.3390/ijms20174166>.
- (166) Kalepu, S.; Nekkanti, V. Insoluble Drug Delivery Strategies: Review of Recent Advances and Business Prospects. *Acta Pharmaceutica Sinica B.* **2015**. <https://doi.org/10.1016/j.apsb.2015.07.003>.
- (167) Connelly, P. R.; Snyder, P. W.; Zhang, Y.; McClain, B.; Quinn, B. P.; Johnston, S.; Medek, A.; Tanoury, J.; Griffith, J.; Patrick Walters, W.; Dokou, E.; Knezic, D.; Bransford, P. The Potency-Insolubility

- Conundrum in Pharmaceuticals: Mechanism and Solution for Hepatitis C Protease Inhibitors. *Biophys. Chem.* **2015**, *196*. <https://doi.org/10.1016/j.bpc.2014.08.008>.
- (168) Paraskevopoulou, V.; Falcone, F. Polyionic Tags as Enhancers of Protein Solubility in Recombinant Protein Expression. *Microorganisms* **2018**, *6* (2). <https://doi.org/10.3390/microorganisms6020047>.
- (169) Lemke, T. L. *Review of Organic Functional Groups : Introduction to Medicinal Organic Chemistry*, 5th ed.; Wolters Kluwer: Philadelphia, 2012.
- (170) Boger, D. L.; Hertzog, D. L.; Bollinger, B.; Johnson, D. S.; Cai, H.; Goldberg, J.; Turnbull, P. Duocarmycin SA Shortened, Simplified, and Extended Agents: A Systematic Examination of the Role of the DNA Binding Subunit. *J. Am. Chem. Soc.* **1997**, *119* (21). <https://doi.org/10.1021/ja9637208>.
- (171) Tichenor, M. S.; Trzuppek, J. D.; Kastrinsky, D. B.; Shiga, F.; Hwang, I.; Boger, D. L. Asymmetric Total Synthesis of (+)- and Ent(-)-Yatakemycin and Duocarmycin SA: Evaluation of Yatakemycin Key Partial Structures and Its Unnatural Enantiomer. *J. Am. Chem. Soc.* **2006**, *128* (49). <https://doi.org/10.1021/ja064228j>.
- (172) The Human Protein Atlas. <https://www.proteinatlas.org/ENSG00000258839-MC1R/cell>.
- (173) Wolf Horrell, E. M.; Boulanger, M. C.; D'Orazio, J. A. Melanocortin 1 Receptor: Structure, Function, and Regulation. *Frontiers in Genetics*. Frontiers Media S.A. May 31, 2016. <https://doi.org/10.3389/fgene.2016.00095>.
- (174) Roberts, D. W.; Newton, R. A.; Beaumont, K. A.; Helen Leonard, J.; Sturm, R. A. Quantitative Analysis of MC1R Gene Expression in Human Skin Cell Cultures. *Pigment Cell Res.* **2006**, *19* (1). <https://doi.org/10.1111/j.1600-0749.2005.00286.x>.

- (175) Rosenkranz, A. A.; Slastnikova, T. A.; Durymanov, M. O.; Sobolev, A. S. Malignant Melanoma and Melanocortin 1 Receptor. *Biochemistry (Moscow)*. November 2013, pp 1228–1237. <https://doi.org/10.1134/S0006297913110035>.
- (176) Scudiero, D. A.; Shoemaker, R. H.; Paull, K. D.; Monks, A.; Tierney, S.; Nofziger, T. H.; Currens, M. J.; Seniff, D.; Boyd, M. R. Evaluation of a Soluble Tetrazolium/Formazan Assay for Cell Growth and Drug Sensitivity in Culture Using Human and Other Tumor Cell Lines. *Cancer Res.* **1988**, *48* (17).
- (177) Riss, T. L.; Moravec, R. A.; Niles, A. L. *Cell Viability Assays*; 2013.
- (178) Corporation, P. *CellTiter 96 Aqueous Non-Radioactive Cell Proliferation Assay Technical Bulletin #TB169*.
- (179) Corporation, P. *CellTiter-Glo® Luminescent Cell Viability Assay Instructions for Use of Products G7570, G7571, G7572 and G7573*.
- (180) Martinez-Serra, J.; Gguterrez, A.; Muñoz-Ccapó, S.; Nnavarro-Palou, M.; Rros, T.; Aamat, J. C.; Lopez, B.; Marcus, T. F.; Fueyo, L.; Suquia, A. G.; Gines, J.; Rrubio, F.; Rramos, R.; Besalduch, J. XCELLcelligence System for Real-Time Label-Free Monitoring of Growth and Viability of Cell Lines from Hematological Malignancies. *Onco. Targets. Ther.* **2014**, *7*. <https://doi.org/10.2147/OTT.S62887>.
- (181) Xi, B.; Ye, P.; Golubovskaya, V.; Abassi, Y. In Vitro Functional Assay Using Real-Time Cell Analysis for Assessing Cancer Immunotherapeutic Agents. In *Methods in Pharmacology and Toxicology*; 2020. https://doi.org/10.1007/978-1-0716-0171-6_3.
- (182) Waller, A.; Simons, P. C.; Biggs, S. M.; Edwards, B. S.; Prossnitz, E. R.; Sklar, L. A. Techniques: GPCR Assembly, Pharmacology and Screening by Flow Cytometry. *Trends in Pharmacological Sciences*. 2004. <https://doi.org/10.1016/j.tips.2004.10.009>.
- (183) Sklar, L. A.; Edwards, B. S.; Graves, S. W.; Nolan, J. P.; Prossnitz, E. R.

Flow Cytometric Analysis of Ligand-Receptor Interactions and Molecular Assemblies. *Annual Review of Biophysics and Biomolecular Structure*. 2002.
<https://doi.org/10.1146/annurev.biophys.31.082901.134406>.

- (184) Wu, Y. K.; Tu, Y. K.; Yu, J.; Cheng, N. C. The Influence of Cell Culture Density on the Cytotoxicity of Adipose-Derived Stem Cells Induced by L-Ascorbic Acid-2-Phosphate. *Sci. Rep.* **2020**, *10* (1).
<https://doi.org/10.1038/s41598-019-56875-0>.
- (185) Single, A.; Beetham, H.; Telford, B. J.; Guilford, P.; Chen, A. A Comparison of Real-Time and Endpoint Cell Viability Assays for Improved Synthetic Lethal Drug Validation. *J. Biomol. Screen.* **2015**, *20* (10). <https://doi.org/10.1177/1087057115605765>.
- (186) Pasini, L.; Re, A.; Tebaldi, T.; Ricci, G.; Boi, S.; Adami, V.; Barbareschi, M.; Quattrone, A. TrkA Is Amplified in Malignant Melanoma Patients and Induces an Anti-Proliferative Response in Cell Lines. *BMC Cancer* **2015**, *15* (1). <https://doi.org/10.1186/s12885-015-1791-y>.
- (187) Riss, T.; O'Brien, M.; Moravec, R. Choosing the Right Cell-Based Assay For Your Research. *Cell Notes* **2003**, No. 6.
- (188) Wang, P.; Henning, S. M.; Heber, D. Limitations of MTT and MTS-Based Assays for Measurement of Antiproliferative Activity of Green Tea Polyphenols. *PLoS One* **2010**, *5* (4).
<https://doi.org/10.1371/journal.pone.0010202>.
- (189) Liang, J. L.; Javed, U.; Lee, S. H.; Park, J. G.; Jahng, Y. Synthesis of 6-Deoxymollugin and Their Inhibitory Activities on Tyrosinase. *Arch. Pharm. Res.* **2014**, *37* (7). <https://doi.org/10.1007/s12272-013-0240-1>.
- (190) Hong, W. P.; Lim, H. N.; Park, H. W.; Lee, K. J. Synthesis of Methyl (E)-2-Cyanomethylcinnamates Derived from Baylis-Hillman Acetates and Conversion into Several 4-Hydroxy-2-Naphthoic Acids and Benzylidenesuccinimides. *Bull. Korean Chem. Soc.* **2005**, *26* (4).
<https://doi.org/10.5012/bkcs.2005.26.4.655>.

- (191) Wang, Y.; Mowla, R.; Ji, S.; Guo, L.; De Barros Lopes, M. A.; Jin, C.; Song, D.; Ma, S.; Venter, H. Design, Synthesis and Biological Activity Evaluation of Novel 4-Substituted 2-Naphthamide Derivatives as AcrB Inhibitors. *Eur. J. Med. Chem.* **2018**, *143*. <https://doi.org/10.1016/j.ejmech.2017.11.102>.
- (192) Stephenson, M. J.; Howell, L. A.; O'Connell, M. A.; Fox, K. R.; Adcock, C.; Kingston, J.; Sheldrake, H.; Pors, K.; Collingwood, S. P.; Searcey, M. Solid-Phase Synthesis of Duocarmycin Analogues and the Effect of C-Terminal Substitution on Biological Activity. *J. Org. Chem.* **2015**, *80* (19). <https://doi.org/10.1021/acs.joc.5b01373>.